CONTRIBUTION OF STROMAL CELLS TO THE FORMATION AND STABILISATION OF BLOOD MICROVESSELS

A THESIS SUBMITTED TO

UNIVERSITY COLLEGE LONDON

FOR THE DEGREE OF

DOCTOR OF PHILOSOPHY

BY

SOMAYEH SHAHREZAGAMASAEI

DEPARTMENT OF MECHANICAL ENGINEERING

UNIVERSITY COLLEGE LONDON

ROBERTS BUILDING

LONDON WC1E 7JE

2021

A few words to my mother;

Mum, I clearly remember your passion for study, the painful regret in your beautiful kind eyes whenever you talk about your unfinished education. You wanted to pursue your study further with a PhD, but unfortunately, you never got a chance to make your dream come true. You sacrificed everything for us.

In addition to my insatiable desire to keep learning and my endless love for science, I did it for you, mum.

I can't thank you enough for even one of your sacrifices.

This is the least I can do;

to you and dad,

Mrs Mahin Shahreza and Mr Hekmat Shahreza

who have dedicated your lives to your children and made many sacrifices without any expectations.

with eternal love,

Negar

Declaration

I hereby declare that except where specific reference is made to the work of others, the contents of this dissertation are original and have not been submitted in whole or in part for consideration for any other degree or qualification in this, or any other university. This dissertation is my own work and contains nothing which is the outcome of work done in collaboration with others, except the microfluidics platform developed in Kamm's lab at MIT.

Somayeh Shahrezagamasaei

04/03/2021

Abstract

Vasculogenesis, the creation of new blood vessels, occurs due to an inherent ability of endothelial cells (ECs) to self-assemble and form tubules. Additionally, many studies have shown that stromal cells, connective tissue cells of any organ, including fibroblasts (FBs), play a vital role in the formation and stabilisation of new vessels, mostly chemically by producing and secreting growth factors. However, still we lack ground understanding of the mechanical contribution of FBs to vasculogenesis. In this study, employing microfluidic platforms, we aimed to address the mechanical role of FBs in vascularisation.

Applying a 7-channel microfluidic platform, we encapsulated ECs with 3 different conditions: mono-cultured (MC, embedding only ECs within a hydrogel), paracrine co-cultured (PCC, embedding ECs and FBs separately in two hydrogels) and juxtacrine co-cultured (JCC, embedding ECs mixed with FBs in a hydrogel) to investigate the impact of FB presence on formation of functional microvessels. Imaging techniques and dextran perfusion revealed that the cluster-like structures formed in the device seeded with MC and PCC conditions were not functional in terms of perfusability and permeability and deteriorated within a week while the microvessels developed in the device seeded with JCC condition were functional, well-interconnected and survived much longer (~3 weeks), indicating that the direct physical interaction between FBs and ECs is crucial for the formation of functional blood microvessels.

Also, chemical perturbation of mechanotransduction genes, YAP, Src, Wnt/β-catenin, RhoA, and FAK, in both ECs and FBs, resulted in either the inhibition of microvessel formation or the development of microvessels which were significantly different in morphology, perfusability, vessel length, diameter, and coverage area compared to control microvessels, demonstrating that mechanotransduction pathways play key roles in vascularisation.

Additionally, using siRNA approach, we inhibited the same genes only in FBs to examine the mechanical contribution of FBs to vascularisation. This revealed that ECs co-cultured with siRNA-inhibited FBs (excluding RhoA) retained their ability to form microvessels. However, further characterisations demonstrated that the microvessels did not resemble control microvessels in terms of permeability, perfusability, tissue stiffness, barrier function, morphology, and vessel topology.

Together, these results highlight the mechanical contribution of FBs to the formation, morphogenesis and function of microvessels and suggests that FBs are intrinsic mechanical promoters and stabilisers of microvessels. Such knowledge on the mechanisms underlying the vascularisation, will be useful in further developing vascularisation strategies for organ-specific, disease-specific, and cancer-specific tissue engineering and regenerative medicine applications.

Impact Statement

Without a doubt, owing to their inherent ability to self-assemble and form lumens/tubules, endothelial cells (ECs) are the key players in vascularisation. In addition to ECs, supporting cells such as fibroblasts (FBs) contribute to vascularisation. To date, majority of studies have investigated the chemical roles of FBs in vascularisation. A few have studied the role of external mechanical cues such as shear stress or ECM stiffness on vascularisation. However, there is a gap in the knowledge of the internal mechanical contribution of FBs to vascularisation and the molecular mechanisms underlying this role of FBs in microvessel formation.

This study revealed that direct physical interaction between FBs and ECs is essential for forming functional microvessels. Besides, by applying small molecule inhibitors against mechanotransduction genes, we showed that mechanotransduction pathways play key roles in the formation, stabilisation, characteristics, topology, and function of blood microvessels. Finally, by perturbing mechanotransduction genes in FBs, we showed that FBs mechanically contribute to vascularisation through mechanotransduction pathways.

In short, recent work has opened new avenues in microvascular research. We showed that the emergence of the unique microvessel mechanical features and phenotypes is tightly interlinked with FBs mechanotransduction programs, thus suggesting FBs are an intrinsic mechanical promoter and stabiliser of microvascular networks. It sheds light on the molecular mechanisms underlying microvessel formation, morphogenesis, stabilisation, and function. This can be used to develop *in vivo*-like engineered microvascular models which not only help us understand the fundamentals of vasculogenesis but also help us study diseases, develop treatments, screen drugs, and vascularise engineered constructs to replace damaged tissues/organs.

Publications

- **Shahreza N**, Whisler J, Malandrino A, Javanmardi Y, Fantin A, Szita N, Sheridan G, Calvo F, Ruhrberg C, Sahai E, Kamm R, Moeendarbary E. Intrinsic mechanical control of vascular morphology. (**Journal of Nature**. 2021. Submitted.)

- Eames I, D'Aiuto F, **Shahreza N**, Balachandran R, Hyde M, Yuan-Ling Ng, Gulabivala K, Javanmardi Y, Watson S, Davies H, Khajeh J, Suvan j, Moeendarbary E. Dispersion of Infectious Agents by Medical Devices. (**Journal of iScience**. 2021. Under review.)

- **Shahreza N**, Moeendarbary E. Fibroblasts contributions to vascularisation – a mechanical perspective. (In preparation.)

- **Shahreza N**, Moeendarbary E. EED; a neglected key player in vasculogenesis. (In preparation.)

- **Shahreza N**, Moeendarbary. Fibroblasts serve newly-formed vasculature both chemically and mechanically. (In preparation.)

- **Shahreza N**, Agrawal A, Raimes W, Moeendarbary E. NHLFs and HDFs in vascularisation. (In preparation.)

- Schlegelmilch K, Ege Nil, **Shahreza N**, Moeendarbary E, Sahai E. Yap's function in fibroblasts (In preparation.)

Conferences

Oral presentation:

- **Negar Shahreza**, Emad Moeendarbary. Contribution of stromal cells to the formation and stabilisation of blood microvessels. 2022. BIOMATMEET2022. Tokyo, Japan.

- **Negar Shahreza**, Yousef Javanmardi, Jordan Whisler, Roger Kamm, Emad Moeendarbary. Contribution of stromal cells to the formation and stabilisation of

vascular networks. 2020. EMBL.IBEC Winter Conference Engineering Multicellular Systems. Barcelona. Spain.

- **Negar Shahreza**, Yousef Javanmardi, Jordan Whisler, Roger Kamm, Emad Moeendarbary. The role of stromal cells in the formation and stabilisation of vascular networks. 2019. ESB. Vienna. Austria.

- **Negar Shahreza**, Yousef Javanmardi, Jordan Whisler, Roger Kamm, Emad Moeendarbary. Mechanical roles of stromal cells in the formation and stabilisation of human vasculature. 2020. 24th European Biotechnology Congress. London, UK.

- **Negar Shahreza**, Yousef Javanmardi, Emad Moeendarbary. Intrinsic mechanical control of vascular morphology. 2020. International Biomedical & Tissue Engineering Conference. Valencia, Spain.

Poster presentations:

- **Negar Shahreza**, Yousef Javanmardi, Jordan Whisler, Roger Kamm, Emad Moeendarbary. Role of stromal cells in formation of functional human microvascular networks - an *in vitro* assay. 2019. CRUK - AACR Joint Conference on Engineering and Physical Sciences in Oncology. London. UK.

- **Negar Shahreza**, Yousef Javanmardi, Emad Moeendarbary. Generation of large scale functional human microvascular networks using *in vitro* microfluidic assay. 2019. Physics of Living Matter (PLM 14). Cambridge. UK.

- **Negar Shahreza**, Yousef Javanmardi, Jordan Whisler, Roger Kamm, Emad Moeendarbary. Mechanobiology of vascular morphogenesis. 2019. CellMech. Milan, Italy.

- Sebastian G Gilbert, **Negar Shahreza**, Emad Moeedenbrary, Fabian Spill. Automated image analysis for tissue engineered by self-assembly from confocal microscopy. 2020. 3D bioNet. London, UK.

Acknowledgement

Table of Content

List of Figures

XXIV

XXXI

List of Tables

List of Abbreviations

aFGF   Acidic Fibroblast Growth Factor

AFM   Atomic Force Microscopy

Ang1   Angiopoietin1

Ang2   Angiopoietin2

Ang3   Angiopoietin3

Ang4   Angiopoietin4

AO   Acridine Orange

BBB   Blood-Brain Barrier

bFGF   basic fibroblast growth factor

CAF   Cancer Associated Fibroblasts

CNS   Central Nervous System

DAPI   4′,6-diamidino-2-phenylindole

DI water   Deionised water

DLL4   Delta Like Ligand 4

DMSO   Dimethyl Sulfoxide

ECM   Extra Cellular Matrix

ECs   Endothelial Cells

EED   Embryonic Ectoderm Development

FAs   Focal Adhesions

FAK   Focal Adhesion Kinase

FAP   Fibroblast Activation Protein

FBCM	Fibroblast Conditioned Medium
FBs	Fibroblasts
FGF	Fibroblast Growth Factor
FGFs	Fibroblast Growth Factors
FSP1	Fibroblast-Specific Protein 1
GFP-HUVECs	Green Fluorescent Protein expressing Human Umbilical Vein Endothelial Cells
GPI	Glycosylphosphatidylinositol
HDFs	Human Dermal Fibroblasts
HGF/SF	Hepatocyte Growth Factor or Scatter Factor
HLCAFs	Human Lung Cancer Associated Fibroblasts
HMVECs	Human Microvascular Endothelial Cells
HSFs	Human Skin Fibroblasts
HUVECs	Human Umbilical Vein Endothelia Cells
IGF-1	Insulin-like Growth factor-1
ITS	Insulin Transferrin Selenium
JCC	Juxtacrine Mixed Co-Cultured
JCCCM	Juxtacrine Co-Culture Conditioned Medium
Lrg1	leucine-rich alpha-2-glycoprotein 1
MC	Mono-Cultured
mRNA	messenger RiboNucleic Acid
MSC	Mesenchymal Stem Cells
NHLFs	Normal Human Lung Fibroblasts

PCC-1	Paracrine Co-Cultured with FBs-1
PCC-2	Paracrine Co-Culture with Mixed Co-Culture of FBs and ECs-2
PDGF	Platelet-Derived Growth Factor
PDMS	Polydimethylsiloxane
PECAM-1	Platelet Endothelial Cell Adhesion Molecule-1
PLGF	Placental Growth Factor
PPP	Picropodophyllotoxin
PRC2	Polycomb repressive complex 2
RFP	Red Fluorescent Protein
ROIs	Region Of Interests
SDS	Sodium Dodecyl Sulfate
SDS-PAGE	Sodium Dodecyl Sulfate–PolyAcrylamide Gel Electrophoresis
siRNA	small interfering RiboNucleic Acid
SMMHH	Smooth Muscle Myosin Heavy Chain
TBS	Tris Buffered Saline
TG 10X	Tris Glycine 10X
TGFα	Transforming Growth Factor α
TGFβ	Transforming Growth Factor β
TGS	Tris/Glycine/SDS
VEGF	Vascular Endothelial Growth Factor
VEGF-A	Vascular Endothelial Growth Factor-A

VEGF-R1	Vascular Endothelial Growth Factor-Receptor1
VEGF-R2	Vascular Endothelial Growth Factor-Receptor2
VEGF-R3	Vascular Endothelial Growth Factor-Receptor3
vSMCs	vascular Smooth Muscle Cells
vWF	von Willebrand Factor
WB	Western Blot
YAP	Yes Associated Protein
α-SMA	α-Smooth Muscle Actin

Introduction

Blood vessels supply nutrients and oxygen to tissues and remove CO_2 and wastes from them. Leucocytes and hormones also travel through blood vessels to their target sites[1,2]. In the human body during embryonic development and adulthood, the creation of blood vessels occurs via two distinct mechanisms: vasculogenesis and angiogenesis. The former is forming new blood vessels from endothelial cells (ECs), and the latter is defined as the growth of new blood vessels from pre-existing vessels[3–5]. Both processes are involved in wound healing, growth, tissue repair, and female reproductive cycle[1,3,4,6–8]. Additionally, angiogenesis is evolved in vascularisation as a response to ischemic and malignant tissues[3] as well as in diseases such as solid tumour angiogenesis[9], arteriovenous malformations[10], blindness, also age-related diseases including macular degeneration, proliferative diabetic retinopathy (PDR), atherosclerosis, and rheumatoid arthritis[11]. In both vasculogenesis and angiogenesis, ECs are the most important players due to their inherent ability to self-assemble and form lumens[3–5]. In addition to ECs, another group of cells named stromal cells, including fibroblasts (FBs), are believed to play a key role in vessel formation.

Many studies have shown that FBs support blood vessel formation chemically by producing and secreting growth factors[12–17]. Unlike the chemical contribution of FBs to the formation and stabilisation of blood vessels that has been extensively studied, the mechanical role of these cells has been poorly understood.

Today, there is an increasing need to develop *in vitro* vascular models to study vascularisation fundamentals, develop drugs, study intravasation and extravasation of cancer cells, vascularise engineered tissues/organs, and study angiotherapy and anti-angiotherapy[18]. However, to create a physiologically more relevant *in vitro* vascular models which resemble *in vivo*, it is crucial to consider the role of mechanical cues along with chemical determinants. Also, the enhanced understanding of fibroblast-mediated

microvessel formation could potentially provide alternative therapeutic strategies that focus on modulating the mechanobiology of FBs. Over the past few years, the mechanical role of FBs has gained increasing attention. However, most of the studies about the mechanical role of FBs refer to ECM deposition and ECM stiffness and the molecular mechanism underlying it has not been fully understood. We hypothesised that this process is mediated via mechanotransduction pathways including RhoA, YAP, SRC, Wnt7b and FAK. Hence, employing an *in vitro* system which tries to model vasculogenesis this thesis aims to shed light on the mechanical contribution of FBs via mechanotransduction pathways to vascularisation.

Project Objectives

The ultimate goal of this thesis is to shed light on the neglected mechanical role(s) of FBs in the formation and stabilisation of blood microvessels. The specific aims of this project are listed below;

Impact of *FBs presence* on the formation and stabilisation of blood microvessels via 3D *in vitro* assay of vasculogenesis

- Assessment of *FBs-ECs physical interaction* on the formation, morphogenesis, function, and stabilisation of blood microvessels
- Assessment of the role of *mechanotransduction pathways* in the formation and stabilisation of blood microvessels
- Assessment of *the mechanical contribution of FBs* to the formation and stabilisation of microvessels
- Assessment of *FBs-ECs colocalisation* in a 3D microenvironment

The thesis is composed of five main chapters;

Chapter 1 reviews the natural methods employed by the body to form vasculature *in vivo,* such as angiogenesis and vasculogenesis, and the relevant biological background information on solute factors and cells involved

in vascularisation. It also briefly describes different mechanotransduction genes/pathways involved in vascularisation. The chapter is closed by briefly mentioning different *in vitro* microvessel models.

Chapter 2 presents the methods utilised to address the first two aims of the current thesis in detail. The chapter begins by explaining the microfluidic platforms design, mould and device fabrication. It continues by describing different cell seeding conditions to assess the importance of FB presence in vascularisation, followed by investigating the impact of solute factors on vascularisation. In the following, the chapter describes microvessel characterisation (microvessel diameter, coverage area, topology, and function) and ends by assessing the impact of a lower density of FBs on vascularisation.

Chapter 3 describes experimental work directed at the contribution of mechanotransduction/chemotransduction pathways to the microvessel formation, stabilisation, characteristics, topology, function and subsequent characterisation studies by inhibiting our interest genes in both FBs and ECs using small molecule inhibitors (chemical inhibition).

Chapter 4 covers experimental work and results used to address the mechanical role of FBs in vascularisation. It describes how perturbation of the genes of interest was experimentally achieved by transfection of siRNAs to the FBs followed by co-culturing them with ECs. In addition to the characterisation of the microvessels, including barrier function and elastic modulus of the hydrogels, the chapter describes ECs' physical interaction (colocalisation) with FBs and RhoA-deficit FBs.

Chapter 5 offers a general conclusion for the present work, preliminary developments, and future studies.

1 Background

1.1 Blood Vessels Function and Structure

Blood vessels play a conventional and crucial role in the transportation of nutrients, oxygen, signals, and blood cells to the body's tissues and in taking the waste and CO_2 away from them[1,2]. Leonardo da Vinci was the first one speculating about the heart and circulatory system. He likened it to a tree formed from a seed, the heart, by sprouting roots, blood vessels, which its trunk and main branches were the arteries and veins, and its tiny components were capillaries[6].

The vessel walls consist of three layers, tunica intima, tunica media, and tunica externa (**Fig 1.1**). The thinnest layer, tunica intima, is a single layer of endothelial cells covering the vessels' inner surface and lies on a basement membrane. The tunica media is the thickest layer in arteries that consists of circularly arranged elastic fibres, connective tissue, and polysaccharide substances. This layer is rich in vascular smooth muscle cells (SMCs). The third layer, tunica externa, is the thickest in veins and is made of connective tissue containing stromal cells, including fibroblasts. Capillaries form the smallest vessels of the microvasculature, consisting of only the tunica intima. These are surrounded by mural cells, pericytes, and SMCs[19].
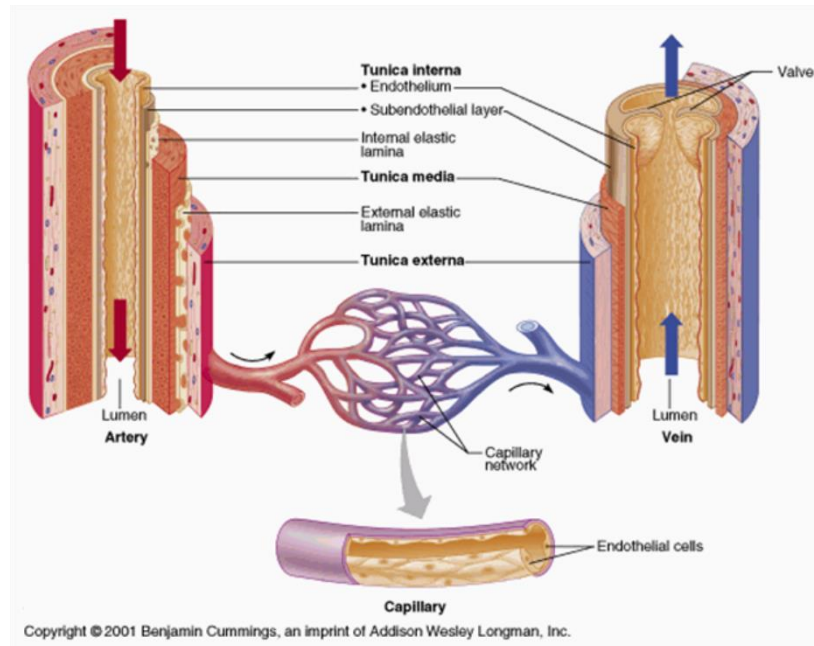
Fig 1.1: Vessels structure. Schematic overview of the structure of arteries, veins and capillaries. Reprinted from https://ckgfendi.blogspot.com/2011/12/biology-form-5-lesson-1.html.

1.2   Formation of Blood Vessels

In general, there are two distinct processes, vasculogenesis and angiogenesis, through which new blood vessels are developed[20].

1.2.1   Vasculogenesis

During embryonic development and adulthood, as a response to ischemic and malignant tissues, blood vessel formation occurs via vasculogenesis. The process is defined as creating new blood vessels from collective self-assembly of endothelial cells[3,4] (**Fig 1.2**). In such a way, from the mesoderm, the middle layer of an embryo, it takes only a few cells to differentiate into a type of cells known as haemangioblasts. These cells are bi-potential, which can differentiate into either hematopoietic stem cells or angioblasts[6]. The former produces white blood cells, red blood cells, and platelets, and the latter contributes to vasculogenesis by differentiating into endothelial cells[6,21].

6
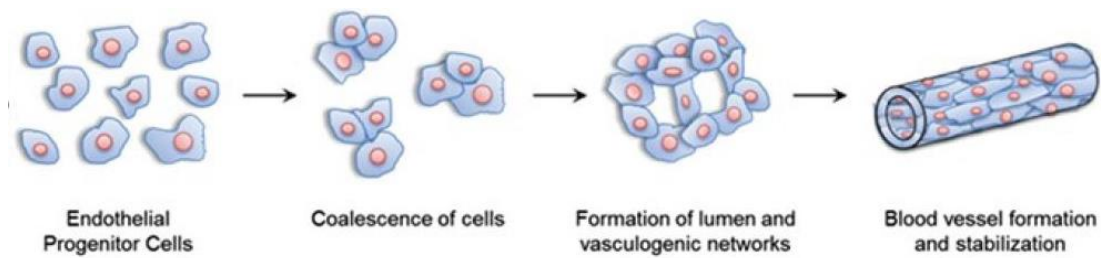
Fig 1.2: Vasculogenesis. *Schematic representing formation of new blood vessels through vasculogenesis which occurs due to inherent ability of endothelial cells to self-assemble into functional blood vessels*[22].

1.2.2 Angiogenesis

Whereas vasculogenesis is considered the formation of new blood vessels from endothelial cells, the construction of new blood vessels from pre-existing blood vessels is known as angiogenesis, which occurs in both embryos and adults' bodies in direct response to tissue demands[5]. Angiogenesis plays a crucial role in physiological conditions such as wound healing, growth, hypoxia, tissue repair, and female reproductive cycle[1,6–8]. Essentially, there are two different types of angiogenesis: 1) sprouting angiogenesis which was the basis of Leonardo da Vinci view and proposed since long time ago, 2) splitting angiogenesis that was discovered more recently in 1986. Splitting angiogenesis is also known as intussusceptive or non-sprouting angiogenesis[6]. Since both sprouting and splitting angiogenesis are triggered by hypoxic conditions, they are also known as hypoxia-induced angiogenesis. It is worth mentioning that both splitting and sprouting angiogenesis affect mainly capillaries, in particular sprouting angiogenesis. However, splitting angiogenesis can also occur in arteries and veins.

1.2.2.1 Sprouting Angiogenesis

In sprouting angiogenesis, the leading players are endothelial cells. Releasing proangiogenic molecules by the angiogenic centre triggers angiogenesis. Angiogenic centres could be cells in a tissue that are hypoxic or immune cells such as macrophages at a wound's site[1,23]. Two capillaries are involved in

7

sprouting angiogenesis, where both capillaries give of little sprouts. These tiny sprouts migrate towards the angiogenic centre, and finally, they will meet at the angiogenic centre and fuse together. This fusion leads to create a connection between two capillaries sending the sprouts[2].

The first step to produce such sprouts is known as tip cell selection. The very specialised tip cell exists at the tip of a shoot, and there is only one. All endothelial cells have a unique receptor, VEGF-R2, on their surface. VEGF-A, one of the chief angiogenic molecules, binds to this receptor. The cells that receive the most significant dose of VEGF-A differentiate into tip cells. The tip cells can produce a unique structure, which is called filopodia. One of VEGF-A functions on endothelial cells is that the tip cells will have these filopodia by which the sprouts migrate towards the angiogenic centre[24]. In addition to generating filopodia, the tip cells can also break down the capillaries' basement membrane by releasing proteolytic enzymes. The tip cells will then be free and pass the basement membrane, moving towards the angiogenic centre[25].

Apart from producing filopodia and releasing proteolytic enzymes, the tip cells stop their neighbouring cells from becoming tip cells by expressing Delta Like Ligand 4 (DLL4) on their surface. The adjacent cells have special receptors called notch receptors for DLL4. Binding DLL4 to its receptor on the surface of neighbouring cells causes these cells to stop expressing VEGF-R2, leading to receiving no VEGF-A so that the adjacent cells will not differentiate into tip cells[24].

The next step is the stalk elongation. The tip cell leaves a hole behind, migrating towards the angiogenic centre, but the neighbouring cells right next to the hole will not move and chase the tip cells. Instead, they begin to proliferate, and the newly produced cells will track the tip cell as it migrates towards the angiogenic centre. Therefore, there will no longer be a hole at the site of the capillary. The adjacent cells keep proliferating, and the newly produced cells, also known as stalk cells, go with the tip cells, forming a

structure called a sprout[1]. At this point, the shoot, which consists of a tip cell and a stalk (the proliferated cells), still does not contain a lumen. By proliferation of the stalk cells, the sprout gets longer and longer. As the stem grows and navigates towards the angiogenic centre, there is no basement membrane surrounding it.

The third step is called tubulogenesis, during which the stalks turn into tubes. In tubulogenesis, first, the stalk cells press up against each other to form a few little holes. These small air packages called vacuoles then fuse and form a tube or lumen[26].

The next step after tubulogenesis is when the two sprouts meet and fuse[1]. The capillary is still not complete in this step since there is no basement membrane and pericytes and fibroblasts around it. The last step is forming the basement membrane surrounding the newly formed capillary, following by recruiting pericytes and fibroblasts. Being surrounded by pericytes is a process known as pericytes stabilisation[27].

Once the capillary formed, the blood flows down, providing the tissue with oxygen. Therefore, if the angiogenic centre produces VEGF-A due to hypoxia, it will stop releasing this angiogenic molecule. As a result, sprouting will stop additionally[1]. **Fig 1.3** schematically depicts the process of sprouting angiogenesis.
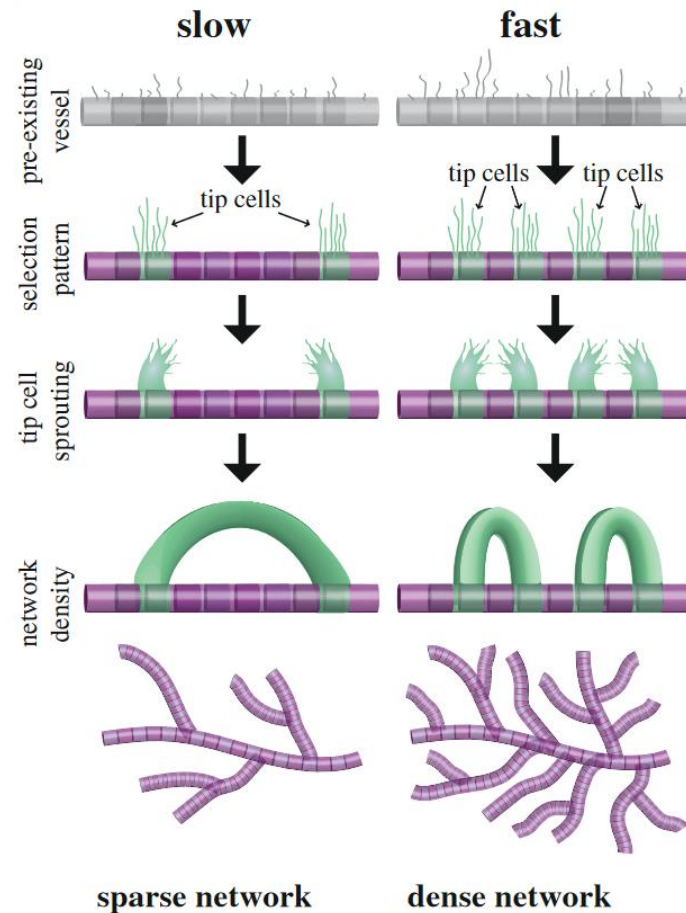
Fig 1.3: Sprouting angiogenesis. *Schematic overview of the process of sprouting angiogenesis*[28].

1.2.2.2 Splitting Angiogenesis

Intussusception or vascular splitting is an alternative process for angiogenesis[29]. This type of angiogenesis, like sprouting angiogenesis, occurs in response to VEGF-A. The difference is that one blood vessel divides into two separate blood vessels in splitting angiogenesis. In such a way that two endothelial cells forming a vessel start folding back into the lumen, producing protrusions and continue folding so that they reach the centre of the lumen and close off the wall. While endothelial cells are folding back to form two vessels, fibroblasts will follow the endothelial cells migrating towards the lumen's centre. When the wall is completed, fibroblasts push the newly formed blood vessels away from each other. Once the vessels are separated,

fibroblasts and pericytes surrounding them begin to produce and release a considerable amount of collagen to separate them and help them establish more. In other words, it is fibroblasts' function to detach these newly formed blood vessels[29,30]. **Fig 1.4** schematically depicts the process of splitting angiogenesis.
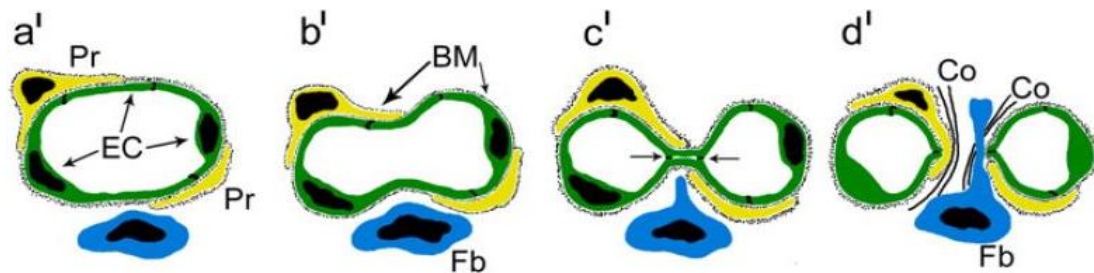
Fig 1.4: Splitting angiogenesis. Schematic overview of the process of splitting angiogenesis. Endothelial cells (EC in green) on the opposite sides of a capillary begin to migrate towards the centre of its lumen until they meet each other. Fibroblasts (Fb in blue) and pericytes (Pr in yellow) help with the stabilisation of these newly formed vessels by producing and releasing collagen (Co) fibrils[30].

1.3   Vascular Growth Factors

Many gene products, including different growth factors, play crucial roles in forming blood vessels. Among these products, vascular growth factors have recently received much attention. These growth factors are categorised based on their functionality on endothelial cells. VEGF family (5 members), angiopoietin (4 members), and ephrin family (1 member) are considered vascular endothelium-specific growth factors. In contrast, fibroblast growth factors (FGFs), transforming growth factor β (TGF β), and platelet-derived growth factor (PDGF) are considered vascular non-specific growth factors because they can act on many other cell types[21]. Here we briefly mention these two types of growth factors and their function in vascularisation.

1.3.1 Vascular-Specific Growth Factors

As mentioned earlier, five VEGF family members, four angiopoietin family members, and one member of the ephrin family are known as vascular-specific growth factors because they act only on endothelial cells[21].

1.3.1.1 VEGF

In adults and during the development of embryos, vasculogenesis, angiogenesis, and vascular maintenance are regulated by Vascular Endothelial Growth Factor (VEGF) family[31]. Hence, VEGF is considered the master regulator of vascularisation in embryonic, adulthood, physiological development, and diseases[29]. VEGF is produced and released by a cell that is not supplied with enough oxygen or a cell at a wound's site[1,23]. Once released, VEGF binds to its receptor, VEGF-R2, on endothelial cells' surface, leading them to proliferate, elongate and self-assemble to form new blood vessels[32]. In addition to inducing endothelial cells to proliferate and migrate, VEGF regulates vascular diameter[33].

VEGF gene has eight exons and seven introns and locates on the short arm of chromosome 6. Hypoxia-mediated control of gene transcription controls the transcription of the VEGF gene, and alternative mRNA splicing and proteolytic processing control the production of different types of VEGF isoforms. VEGF189, VEGF165, VEGF121, and VEGF205 are the main isoforms of VEGF[34]. There are different VEGFs classified by their structure, including VEGF-A, VEGF-B, VEGF-C, VEGF-D, VEGF-E, VEGF-F, and Placental Growth Factor (PLGF). The main type, VEGF-A, cloned in 1989[31,35], plays several functions in endothelial cells, such as regulating angiogenesis, mitogenesis, vascular permeability, vascular tone, and the production of vasoactive molecules[31,34]. Three receptor tyrosine kinases, VEGF-R1 (Flt-1), VEGF-R2 (KDR/Flk-1), and VEGF-R3 (Flt-4), mediate the activity of VEGF[32,35,36]. Cell motility is mediated by VEFG-R1, which is expressed on endothelial cells and monocytes[32,37]. VEGF-R2 mediates the proliferative and

mitogenic actions of VEGF, as well as vascular permeability. Also, it is believed that VEGF-R3, so-called Flt-1, mediates lymphangiogenesis, the growth of lymphatic vessels[21,32,38,39]. **Fig 1.5** represents the signalling pathways activated by VEGF, which result in angiogenesis.
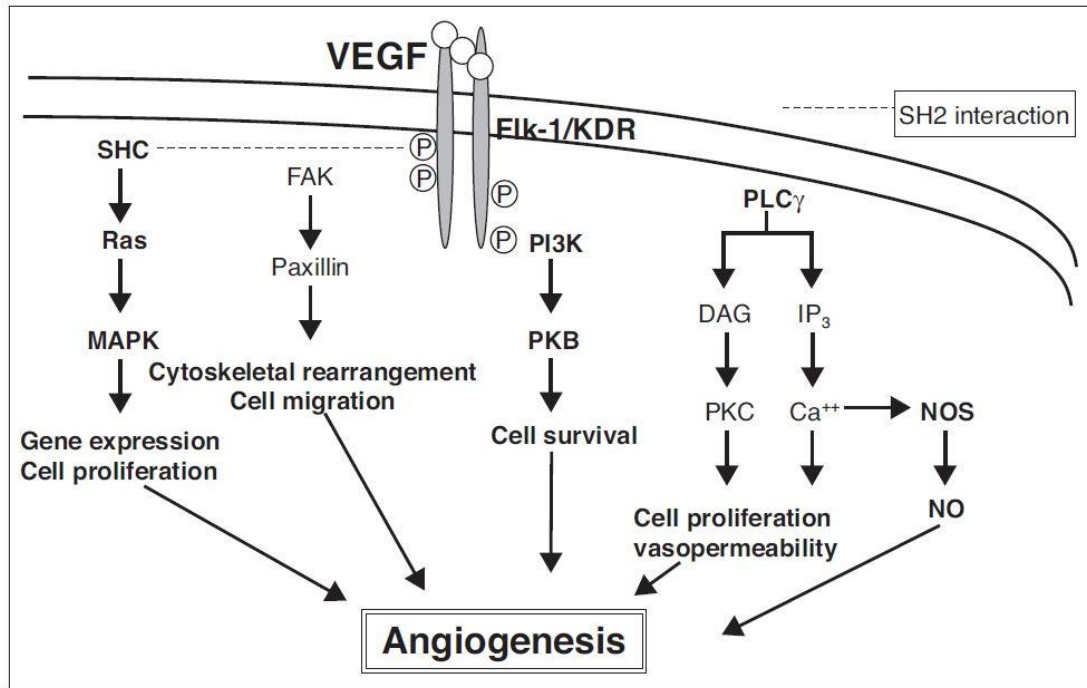
Fig 1.5: Signalling pathways activated by VEGF. Activity of VEGF is mediated through three receptor tyrosine kinases[34].

1.3.1.2 Angiopoietins

Angiopoietins are 70 kDa glycoproteins that act primarily on the vascular networks to regulate blood vessel development and stability[40]. Angiopoietins are considered vascular-specific growth factors because Tie-1 and Tie-2 tyrosine kinases, receptors for angiopoietins, are explicitly expressed in vascular endothelial cells[21,41]. Studies indicate that the Ang/Tie signalling is crucial for vessel remodelling, also for recruitment of mural cells and vessel maturation during the development of embryo and adult vessel homeostasis[42]. Four members of the angiopoietin family, Ang-1, Ang-2, Ang-3, and Ang-4,

have been identified as the most important partners of VEGFs. They work in concert with the VEGF family to form vascular networks[21]. Ang-1, expressed by pericytes, SMCs and fibroblasts, is the regulator of Endothelial cells' phenotype. Park *et al.* and Nishishita *et al.* reported that expression of Ang-1 is elevated in pericytes and SMCs by hypoxia, VEGF-A and PDGF-B[43,44]. Ang-1 is a critical growth factor for vessel maturation, adhesion, migration, and survival[45,25-27]. Ang-2 is produced by endothelial cells where various growth factors and physiological conditions such as VEGF-A and hypoxia regulate its production at the transcriptional level[46,30]. This member of the angiopoietin family expressed by endothelial cells at the angiogenesis sites promotes cell death and disrupts blood vessel formation. Ang-2 also disturbs the connection between endothelial cells and perivascular cells. However, when in conjunction with VEGF, Ang-2 can promote neo-vascularisation[41,23].

1.3.1.3 Ephrin

Ephrins, also known as ephrin ligands, are cell membrane-associated signalling proteins that act as the ligands for Eph receptors. These growth factors are considered the largest receptor protein tyrosine kinases with 14 members. Based on their structure and linkage to the membrane, ephrins are categorised into two subclasses, A-subclass and B-subclass. Ephrin-As consisting of ephrin-A1 – ephrin-A5 are linked to cell membrane by a glycosylphosphatidylinositol (GPI). This subclass of ephrins has no cytoplasmic domain. In contrast with ephrin-As, ephrin-Bs are anchored to cell membrane by a single transmembrane domain which comprises a short cytoplasmic domain. Ephrin-B contains three members, ephrin-B1 – ephrin-B3[47–49].

Ephrins have essential functions during development and adulthood. They are associated with axon guidance[50], cell proliferation and retinotopic mapping[48], reverse signalling[49] and angiogenesis[47].

Ephrin-B2 and its receptor, EphB4, carry out important functions during blood vessel formation. Ephrin-B2 labels arterial endothelial cells where its receptor, EphB4, marks venous endothelial cells. In other words, the arterial and venous fate of endothelial cells is determined by Ephrin-B2 and EphB4[47].

1.3.2 Vascular-Nonspecific Growth Factors

Fibroblast growth factor (FGF), transforming growth factors (TGFs), and platelet-derived growth factor (PDGF) are considered vascular non-specific growth factors because they can act on the function of not only endothelial cells but also many other cell types[21].

1.3.2.1 FGF

FGF family comprises nine members, which are multifunctional regulatory peptides. Their effects have been significantly studied on tumorigenesis, cardiovascular disease, repair of tissue injury, neurobiology, and embryonic development[51]. FGFs are potent mitogens and chemo-attractants for endothelial cells and various mesenchymal cells, including fibroblasts, osteoblasts, chondrocytes, smooth muscle cells, skeletal myoblasts, and cells of neuro-ectodermal origin. FGFs not only have growth-promoting effects on most fibroblastic cell types also stimulates angiogenesis, neovascularisation, wound healing, and cell migration[51].

FGF-2, or simply FGF, an FGF family member, is a 13.3 kDa polypeptide that was first purified from the bovine pituitary gland in 1975[52]. Acidic fibroblast growth factor (aFGF) and basic fibroblast growth factor (bFGF) were the first members of this family, which were purified on the basis of their mitogenicity toward fibroblasts[53]. This growth factor is a potent angiogenic molecule *in vivo* and *in vitro* capable of promoting all phases necessary for new blood vessel formation[51,54]. FGF-2 induces EC proliferation, migration, and angiogenesis *in vitro*. It also regulates several molecules' expression thought to mediate critical steps during angiogenesis. FGF-2 also plays a crucial role in developing and differentiation of vessel walls by stimulating smooth muscle cell

proliferation[51,54]. Besides, it regulates collagen type I production and laminin production, one of the most important biological substances both participate in angiogenesis by the periodontal ligament-derived cell. Applying FGF-2 at the early phase of the wound healing process leads to many new capillaries[51].

1.3.2.2 TGFs

Transforming growth factors (TGFs) and platelet-derived growth factor (PDGF) are produced by platelets, fibroblasts, and transformed cells [55,56]. The name of TGF comes from their ability to alter the phenotype of the cells in their presence[56]. TGFβ with 25 kDa molecular weight can be found in tumours and normal cells such as kidney, placenta, and platelets[56]. A low concentration of TGFβ triggers microvascular endothelial cells' proliferation and angiogenesis, whereas its high concentration inhibits these processes *in vitro*[57].

TGFβ is considered the major modulator of angiogenesis in wound healing as it regulates cell proliferation, migration, capillary tubule formation, and ECM deposition. Three TGFβ isoforms, TGFβ1, β2, and β3, are expressed in the mammalian system and bind to the same receptors and elicit similar biological responses when tested on most cell cultures[58]. Yang *et al.* showed that TGFβ promotes angiogenesis through stimulating EC migration, differentiation, and tubule formation[59]. Some other studies indicated that TGFβ stimulates angiogenesis by deposing ECM and upregulating their integrin receptors[60–62]. Roberts *et al.* showed that TGFβ injection into the nape of the neck in neonate mice led to an increase in macrophages, fibroblasts, collagen production, and new capillaries formation[63].

1.3.2.3 PDGF

Platelet-derived growth factor (PDGF)-BB is another key chemoattractant for migrating mural cells that express PDGF receptor-β. This chemoattractant is among the signalling pathways involved in smooth muscle development and differentiation[64]. By secreting PDGF-β, endothelial cells recruit mural cells[52].

1.4 Cells Involved in Vascular Formation

Three groups of cells, endothelial cells, mural cells, and stromal cells, are involved in the formation and stabilisation of blood vessels. **Table 1.1** summarises these cells, their function and markers.

Table 1.1: Cells involved in vascularisation and their markers. As, there is no pericyte-specific and fibroblast-specific marker, a combination of markers is used to identify them.

Cell Type		Common Marker(s)	Ref
Endothelial Cells	-	PECAM-1	65
Mural Cells	Pericytes	PDGF$^+$/FSP1$^-$	66
	vascular Smooth Muscle Cell (vSMCs)	α-SMA, SM22a	67
Stromal Cells	Mesenchymal Stem Cells (MSCs)	Stro-1, SSEA-4, CD271, CD146	68
	Fibroblasts	PDGF$^+$/FSP1$^+$	66

1.4.1 Endothelial Cells

Based on their structure and functions, blood vessels can be divided into three major groups, arteries, veins and capillaries. Regardless of what layers these vessels could comprise, the inner surface of all of them is covered with a very thin mono-layer of endothelial cells, called the endothelium.

Endothelial cells are given rise by mesoderm, the second layer of an embryo sandwiched between ectoderm and endoderm[69]. Originated from their common precursor called angioblasts in the mesoderm, endothelial cells differentiate into specialised endothelial cells of arteries, veins, and capillaries. To develop organ-specific phenotypes, endothelial cells forming capillaries then differentiate further[70,71]. The vessels are different in their functions such

as permeability, response to cytokine exposure, ability to attract immune cells, and tumour cells adhesion affinity owing to the different phenotypes[72].

Apart from the Platelet Endothelial Cell Adhesion Molecule-1 (PECAM-1), also known as CD31/endo-CAM, which is a universal and particular marker of the endothelium, endothelial cells are identified by expression of von Willebrand Factor (vWF) and specific receptors for VEGF such as VEGF-R1 (Flt-1) and VEGF-R2 (Flk-1)[65,71,73,74].

Owing to their relative ease of procurement and extensive characterisation, Human Umbilical Vein Endothelial Cells (HUVECs), the first endothelial cells successfully cultured[73], have been commonly used in microfluidic microvascular models. When removed from their native environment and cultured *in vitro*, vessel-specific endothelial cells partially dedifferentiate because they owe their specification to both inherited epigenetic modifications and local environmental cues. However, by adequately providing the biochemical, mechanical, and physical environment, endothelial cells' phenotype can be maintained in microfluidic microvascular models.

1.4.2 Mural Cells

Mural cells generally refer to cells surrounding and wrapping around blood vessels. They are in close contact with endothelial cells. Among the most well-known mural cells are pericytes that wrap around capillaries and vascular smooth muscle cells (vSMCs) surrounding larger vessels[1].

1.4.2.1 Pericytes

A population of contractile cells laid on capillaries was first described by a French scientist named Charles-Marie Benjamin Rouget in the late 1800s. Initially, this population of cells was named Rouget cells, but they were renamed pericytes because they were in peri-capillaries area[60]. For more than 100 years post-describing by Rouget, due to their low numbers and lack of specific cell markers, pericytes have not been isolated. Duffy *et al.* could

recently isolate them from transgenic mice, and Crisan *et al.* isolated them from human fetal tissue[75,76]. Since there is no pericyte-specific marker, a combination of marker expression and their anatomical location in a very close relationship between blood vessel endothelial cells is the strategy used to identify pericytes. For instance, both fibroblasts and pericytes express PDGF receptor-β (PDGFRβ), but in contrast with pericytes, fibroblasts express fibroblast-specific protein 1 (FSP1) as well. Therefore, a population of cells expressing PDGFRβ that does not express FSP1 is considered pericytes[66].

Pericytes are polymorphic, elongated, multi-branched peri-endothelial cells covered by the basement membrane. Based on their location and histological characteristics, there are at least three types: pre-endothelial cell capillary pericytes, capillary pericytes, and post-capillary venule pericytes[77]. Microvascular pericytes wrap around the capillaries and crosstalk with endothelial cells by physical contact and paracrine signalling[66], essential for normal blood vessel development[77].

Pericytes play essential roles in physically stabilising vessels, blood flow regulation[78], vascular development[79], vascular morphogenesis and stability[45,80], and microvascular remodelling. Both endothelial cells and pericytes produce a basement membrane indicating the importance of pericytes-endothelial cells interaction in the formation, maintenance, and remodelling of the basal lamina. They are also associated with allowing endothelial cells to differentiate, proliferate, and develop vessel branches (angiogenesis). TGF-1 expression by endothelial cells and pericytes sustains endothelial cell-pericyte interaction. This interaction is essential to inhibit the proliferation of endothelial cells[45]. Owing to their contractile properties, pericytes play a solid role in the regulation of capillary blood flow and diameter[81]. Stimulating retinal pericytes electrically, Peppiatt *et al.* showed that pericytes control capillary diameter in whole retina and cerebellar slices. Their findings indicate that pericytes are likely regulators of capillary diameter because the changes in diameter of capillaries occur where the capillaries are

wrapped by pericytes not in pericyte-free regions[82]. Through specialised junctions, pericytes also produce focal contacts with endothelial cells. In organs, including the central nervous system where pericytes are found frequently, these cells may play a role in microvasculature's mechanical stability. They stabilise the vessels by Extra Cellular Matrix (ECM) deposition and/or by secreting and activating signals that induce differentiation and quiescence of endothelial cells[83]. Armulik *et al.* showed that pericytes deficiency increases the blood-brain barrier (BBB) permeability to a range of low-molecular-mass and high-molecular-mass components[84]. Although endothelial cell sprouts may initially form without pericytes involvement, pericytes are among the first cells to invade newly vascularised tissues through paracrine PDGF-β signalling, indicating their essential role in vasculogenesis[77]. The quiescence of blood vessels in adults can be disturbed by pericytes during wound healing and tumour growth, making pericytes a promising target in pharmacological therapy[85,86].

1.4.2.2 Vascular Smooth Muscle Cells (vSMCs)

In contrast to pericytes that surround capillaries, vascular Smooth Muscle Cells (vSMCs) are another type of mural cells that wrap around larger vessels. vSMCs are found in tunica media[87]. In small vessels like arterials, where pressures are not so significant, 1-2 layers of vSMCs are adequate. In larger vessels such as arteries, up to 40 layers are necessary since forces are considerable[88]. The main function of vSMCs is contraction, by which they regulate vessel diameter. Besides, the cells remodel the vessels' walls and thereby provide vessel integrity by regulation of vascular tone and synthesis and decomposition of the matrix[89]. To accomplish these functions, normal adult vSMCs are identified by the expression of a profile of specific contractile proteins such as α-Smooth Muscle Actin (α-SMA), Smooth Muscle Myosin Heavy Chain (SMHHC), SM22α and smoothelin[64], ion channels, calcium handling proteins, and cell surface receptors that serve to regulate contraction of the cell[90]. Although fully differentiated or mature vSMCs barely proliferate,

during vasculogenesis, endothelial cell dysfunction, and at the site of a wound, they may dedifferentiate and, by changing their phenotype begin to produce and release ECM[64,91]. It was demonstrated by Orlidge *et al.* that pericytes and vSMCs inhibit endothelial cell growth by a mechanism that requires contact or proximity[92].

Through a variation of the coated channel technique, vSMCs have been applied to microfluidic microvascular models. For instance, using an orthogonally micro-patterned circular microfluidic channel, Choi *et al.* formed an *in vivo*-like smooth muscle cell layer[19]. In another example, perfusable multilayer vessels were created in a microfluidic device made of PDMS by sequentially seeding cell-laden GelMa hydrogels around concentric needles[93].

1.4.3 Stromal Cells

Connective tissue cells of any organ are known as stromal cells that support the function of the organ's parenchymal cells. Fibroblasts are the most common stromal cells, and mesenchymal stem cells are another group of stromal cells.

1.4.3.1 Mesenchymal Stem Cells (MSCs)

Mesenchymal stem cells, first introduced by Friedenstein, are multipotent stromal cells that can differentiate into and give rise to osteoblasts (bone cells), chondrocytes (cartilage cells), myocytes (muscle cells), and adipocytes (fat cells). Pericytes and MSCs have some properties in common as it is thought that after activation, pericytes leave the vessels and differentiate into MSCs, though this has not been proved[94]. Studies also show that fibroblasts are also able to differentiate into MSCs[69]. Sobrino *et al.* and Ghajar *et al.* have shown that Normal Human Lung Fibroblasts (NHLFs) play the role of both stromal cells and mural cells in microfluidic microvascular models[95,96]. Their findings proved the phenomenon observed by Jeon *et al.* They could generate a 3D functional microvascular network recruiting human MSCs in microfluidic

systems in which bone marrow-derived MSCs formed vascular networks and initiated to express α-SMA[97].

1.4.3.2 Fibroblasts

Fibroblasts, the most common stromal cells, were first reported over 100 years ago. These spindle-like shape cells are characterised by other cells by their morphology, ability to adhere to plastic, and lack of markers that indicate other cell lineages. Although there are several well-established indicators of fibroblast phenotype, none is exclusive to a particular group of fibroblasts and can be found in all different types of fibroblasts. However, FSP1 seems to provide the best specificity for detecting fibroblasts *in vivo*. Besides, several markers can be considered site-specific indicators (**Table 1.2**). For example, desmin is a specific marker for fibroblasts in the skin, whereas it is strongly expressed in muscle cells in other sites[98,99]. These non-vascular, non-epithelial, and non-inflammatory cells synthesise and secrete various important extracellular matrix components such as collagen type I, III, V, and also fibronectin when embedded within the fibrillar matrix[98,100]. Fibroblasts are significantly involved in ECM deposition, epithelial differentiation, inflammation regulation, and wound healing[101,102]. By producing collagen type IV and laminin, fibroblasts contribute to basement membrane formation[103]. Another vital function of fibroblasts is the maintenance of ECM homeostasis by producing and releasing ECM-degrading proteases such as matrix metalloproteinases (MMPs)[103,104]. Like endothelial cells, fibroblasts are also involved in angiogenesis[98].

Table 1.2: Fibroblasts site-specific indicators. *No marker is exclusive to fibroblasts and can be found in all fibroblasts, but some indicators can be considered site-specific markers for the fibroblasts of that organ[98].*

Marker	Function	Fibroblast types in which it is found	Other cell types in which it is found
Vimentin	Intermediate-filament-associated protein	Miscellaneous	Endothelial cells, myoepithelial cells and neurons
α-Smooth-muscle-actin	Intermediate-filament-associated protein	Myofibroblasts	Vascular smooth muscle cells, pericytes and myoepithelial cells
Desmin	Intermediate-filament-associated protein	Skin fibroblasts	Muscle cells and vascular smooth muscle cells
FSP1	Intermediate-filament-associated protein	Miscellaneous	Invasive carcinoma cells
Discoidin-domain receptor 2	Collagen receptor	Cardiac fibroblasts	Endothelial cells
Fibroblast-activation protein (FAP)	Serine protease	Activated fibroblasts	Activated melanocytes
$\alpha_1\beta_1$ integrin	Collagen receptor	Miscellaneous	Monocytes and endothelial cells
Prolyl 4-hydroxylase	Collagen biosynthesis	Miscellaneous	Endothelial cells, cancer cells and epithelial cells
Pro-collagen I α2	Collagen-I biosynthesis	Miscellaneous	Osteoblasts and chondroblasts

1.5 Roles of Fibroblast in Vascularisation

As mentioned above, fibroblasts are the most common stromal cells of connective tissue in the human body. These cells are different, based on which organ they originate[99]. Many studies have shown their critical roles in the formation of blood vessels. For example, although endothelial cells seeded onto Matrigel and supplied with adequate growth factors rapidly migrate, proliferate, elongate, and form capillary-like tubes, these constructs deteriorate within 1-2 days. In contrast, in the absence of exogenous growth factors, fibroblasts can promote endothelial cell differentiation and stabilise

capillary-like tubes for several weeks, indicating the importance of these cells in vasculogenesis and angiogenesis[12,13].

The findings of another study performed by Velazquez *et al.* proved the previously mentioned results. They plated human microvascular endothelial cells (HMVECs) monolayer and induced them to form 3D, capillary-like microvessels by covering them with a collagen layer followed by another layer of collagen with embedded fibroblasts. Detachment and migration of endothelial cells toward the collagen layer happened within the first few hours, and the formation of tube-like structures occurred over the next 4-5 days. Their results showed that the differentiation into branching capillary-like structures depended on direct interaction between fibroblast-endothelial cell contact owing to the fact that such a differentiation did not occur when fibroblasts were replaced by other cells[14].

It is well known that the transplantation of fibroblasts accelerates angiogenesis around wounds by stimulating the secretion of various growth factors. It has been shown that dermal fibroblasts play important roles in the deposition and destruction of the matrices in a wound and control angiogenesis in the tissue through cytokines such as VEGF, bFGF, and others[15]. Martin *et al.* showed that matrix-bound fibroblasts increase angiogenesis and migration of endothelial cells by producing and secreting factors such as VEGF and hepatocyte growth factor or scatter factor (HGF/SF)[16]. In another study, applying a monoclonal antibody against VE-cadherin showed that the formation of tubule stimulated by fibroblast-derived growth factor is prevented, indicating that fibroblasts may regulate angiogenesis by changing VE-cadherin expression of endothelial cells[17].

By culturing microvessels with and without fibroblasts, Villaschi *et al.* demonstrated that fibroblasts' presence promotes angiogenesis and stabilise neovascular endothelium. Microvessels cultured without fibroblasts deteriorated within 3 to 4 days, while the microvessels cultured with fibroblasts were significantly prolonged. This was associated with ECM deposition by

fibroblasts that stabilised newly formed vessels. Their results showed that both fibroblasts and fibroblast-conditioned medium promoted angiogenesis in the rat aorta assay[105].

The formation of collagen, the most common ECM protein, depends on ascorbate[106,107]. By culturing their model of endothelialised-reconstructed connective tissue without ascorbate, Berthod *et al.* decreased the amount of ECM surrounding fibroblasts to prove the importance of these cells to promote the formation of capillary-like tubes by endothelial cells through deposition of ECM. ECM deposited may help the cells trap growth factors secreted by fibroblasts and increase 3D cell organisation[106]. Recruiting two types of human dermal fibroblasts, Costa-Almeida *et al.* showed that different fibroblasts are of various abilities to promote vascularisation, probably due to the expression of varying levels of α-SMA and podoplanin, a small mucin-like protein, and production of ECM[107]. Fibroblast-endothelial cell interaction, the formation and long-term stabilisation of capillary-like tubes in fibroblast-endothelial cell co-culture depend on nonsoluble factors, HGF/SF, in the ECM[108].

Fibroblasts support both vessel sprouting and lumen formation by producing and releasing two different classes of proteins. A combination of angiopoietin-1, angiogenin, hepatocyte growth factor, transforming growth factor-α, and tumour necrosis factor is necessary for endothelial cell sprouting. In contrast, a combination of collagen I, procollagen C endopeptidase enhancer 1, secreted protein acidic and rich in cysteine, transforming growth factor-β–induced protein ig-h3, and insulin growth factor–binding protein 7, all of ECM and produced by fibroblasts are essential for endothelial cell lumen formation[109]. In a study performed by Nakatsu *et al.* endothelial cell-coated beads were embedded in a fibrin gel with and without dermal fibroblasts seeded on top of the gel. Over seven days post-seeding, many thin vessels were formed from the beads in the presence of skin fibroblasts. At the same time, endothelial cells began to detach and migrate from the beads in the absence of fibroblasts without forming any vessels, indicating the importance

of fibroblasts in vessel formation[110]. In a fascinating study, a 3D tissue-like stromal environment (fibroblast-endothelial cells spheroids) was applied to verify that fibroblasts support and modulate endothelial cells migration, viability, and network formation[111].

Apart from mediating angiogenesis chemically via producing growth factors, fibroblasts also regulate angiogenesis mechanically via cell-mediated scaffold disruption, extracellular matrix deposition, and ECM remodelling. Hurley *et al.* demonstrated that interaction between fibroblasts and endothelial cells results in greater construct stiffness via decreased expression of fibroblast matrix metalloproteinase-2 and increased collagen I deposition when endothelial cells are co-embedded with fibroblasts. In other words, fibroblasts regulate capillary morphogenesis chemically, via secretion of growth factors and mechanically via cell-mediated scaffold disruption, ECM deposition, and ECM remodelling[112]. Other studies also showed that fibroblasts regulate angiogenesis by altering the mechanical properties of ECM via deposition of matrix and metalloproteinase-mediated extracellular matrix remodelling[113,114].

Apart from matrix deposition, Cancer-Associated Fibroblasts (CAFs) support vessel formation mechanically. In such a way, the inhibition of mechanotransduction pathways, including Rock, YAP, and Snail1 in CAFs co-cultured with endothelial cells, attenuated vascular growth. Utilising magnetic microbeads to induce mechanically-inhibited CAFs mechanically and overexpressing Rho in normal breast fibroblasts increased vascular growth, indicating the importance of mechanical support of fibroblasts in the formation of microvessels[115].

1.6   Mechanotransduction Pathway

Living cells constantly receive mechanical cues from ECM as well as from their adjacent cells. Such stimuli are transformed into biological responses through the intracellular molecular processes, called mechanotransduction. This helps the cells adapt to the continuous dynamic changes of the surrounding

microenvironment. A variety of mechanosensitive molecules such as integrins, Focal Adhesions, ion channels, G protein coupled-receptors, growth factor receptors receive and transfer mechanical signals to cells by activating different mechanotransduction pathways[116,117]. Of all, we will mention FAK, RhoA, YAP, Src, and Wnt/β-catenin in greater detail.

1.6.1 FAK

Plasma membrane is the primary site of force transmission to cells because it enables direct contact between the cells and ECM. Focal Adhesions (FAs) are developed beneath the plasma membrane when cells contact stiff microenvironments. These large multiprotein structures are the leading centres for cell-matrix interaction. FAs are responsible for receiving mechanical stimuli from ECM, transferring them to the cellular cytoskeleton as well as transmitting the forces generated by the cells to ECM. Their construction makes their mission possible as FAs compose two parts, transmembrane and intracellular parts. The former is in direct contact with ECM components, namely integrins, fibronectin, vitronectin, collagens, and laminins, while the latter serves as the intermediate part between the transmembrane part and ECM. FAs compose 200 different proteins, including focal adhesion kinase, Talin, Paxillin, Vinculin, Zyxilin, p130[Cas], and Actinin[118]. Of all, we mention focal adhesion kinase (FAK) in greater detail. **Fig 1.6** illustrates FAs members.
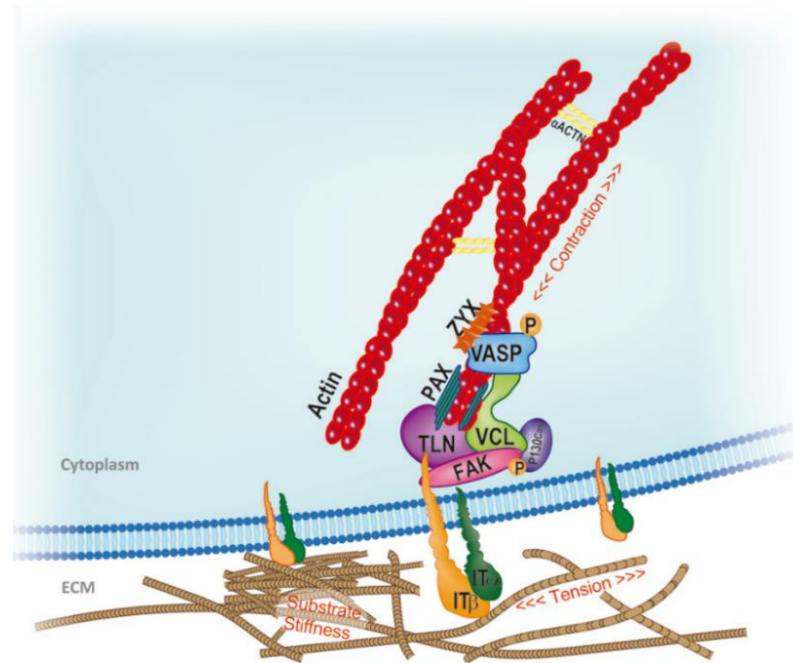
Fig 1.6: Schematic illustrating focal adhesion's members[116].

FAK is one of the first proteins recruited to forming FAs. It is activated by autophosphorylation. When activated, FAK triggers intracellular mechanotransduction by activating downstream mechanotransducers, particularly SH-2-domain containing proteins such as the Src family within the given cell, resulting in full FAK activation[116,119]. By transferring physical stimuli produced by integrins to the cytoskeleton, FAK plays a key role in cell growth, proliferation, survival, adhesion, migration (by stimulating metalloproteinase secretion), and differentiation[118–120]. Unlike FAK-expressing fibroblasts that can respond to exerted forces by adjusting their movement direction and forming FAs, FAK-inhibited ones fail to respond to such stimuli[120]. Llic *et al.* also showed that FAK-deficient fibroblasts lost their ability to migrate, indicating this mechanotransducer's pivotal role in cell migration[121]. The study by Mitra *et al.* showed that the inhibition of FAK led to a decrease in VEGF, subsequently, lack of angiogenesis[122]. This finding is consistent with another study done by the same research group indicating that FAK promotes neo-

28

vascularisation. This occurs due to the FAK ability to upregulate angiogenic factors such as VEGF[123].

1.6.2 RhoA

Cytoskeleton provides cells with mechanical support and plays a vital role in cell shape, protrusion formation, cell proliferation, migration, etc. It comprises three components; actin fibres, intermediate filaments, and microtubules[117]. RhoA family contributes to cell responses to mechanical forces. Of 20 members of the Rho GTPase family, three members, including RhoA, Cdc42, and Rac1, are ubiquitous and widely-studied. RhoA is the key regulator of the actin cytoskeleton[117]. It regulates α-actin stabilisation, α-actin-myosin interaction necessary for cell contractility, and α-actin polymerisation in response to mechanical signals[116] (**Fig 1.7**). Overexpressing RhoA in normal breast fibroblasts co-cultured with endothelial cells increases endothelial cells' ability to form microvessels[115]. Several studies have also shown that RhoA is involved in endothelial cell permeability[124] and junction assembly of epithelial cells[125]. Uchida *et al.* showed that the formation of tube-like structures was arrested both *in vitro* and *in vivo* when RhoA was inhibited by either an exoenzyme, *Clostridium botulinum* C3 transferase, or Y-27632, suggesting that RhoA contributes to angiogenesis[126]. This finding is consistent with another study that showed the inhibition of RhoA by alendronate in HUVECs resulted in arresting the cell's ability to migrate and form capillary-like structures[127].
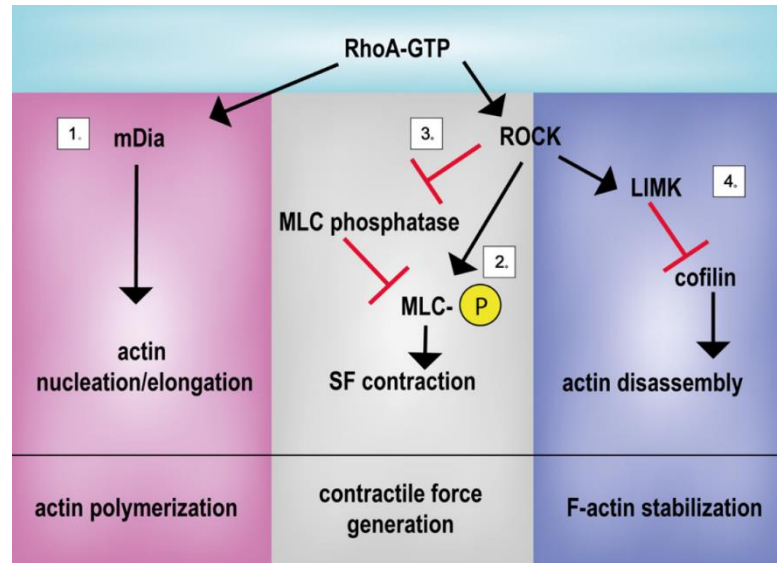
Fig 1.7: RhoA controls mechanical signals propagation. RhoA regulates 1) acting polymerisation by binding to mDia, generating contractile force either by 2) phosphorylation of light myosin chain (MLC) or 3) inhibition of MLC phosphatase via ROCK, as well as 4) stabilising F-actin fibres by activating LIM kinase (LIMK)[116].

1.6.3 YAP

In 1994, Yes Associated Protein (YAP) was discovered as a nuclear receptor of the inhibitory Hippo pathway. As a transcriptional coactivator, YAP mainly functions as the regulator of tissues and organs' size by modulating cell proliferation and apoptosis[128,129]. Depending on the Hippo pathway being on or off, YAP can be found in the cytoplasm or nucleus. When the pathway is on, YAP is phosphorylated by LATS kinases (members of Hippo kinase cascade), retains to the cytoplasm (inactive form), and gets degraded. In contrast, when the pathway is off, YAP is dephosphorylated, relocated into the nucleus (active form), and activates the target genes by binding to TEAD (a transcription factor), triggering cell proliferation[128–131]. Being a nuclear receptor that identifies and transmits intracellular and extracellular mechanical stimuli, YAP is translocated from the cytoplasm into the nucleus in response to ECM stiffness and cellular stretching changes. This happens through ROCK/RhoA GTPase[132,133]. From a mechanical point of view, Wang *et al.* showed that YAP and TAZ, another Hippo pathway effector, play a pivotal role in angiogenesis

via mediating VEGF-VEGF-R2 signalling. They demonstrated that VEGF induces YAP/TAZ by acting on the actin cytoskeleton. Activation of YAP/TAZ results in inducing a transcriptional program to remodel the cytoskeleton and trigger a feedforward loop that guarantees a proper angiogenic response. By deleting YAP/TAZ, they also showed that lack of the proteins alters VEGF-R2 distribution on the cell membrane caused by trafficking deficiency from the Golgi apparatus to the plasma membrane[130]. **Fig 1.8** represents YAP activation and deactivation in the presence and absence of mechanical cues.
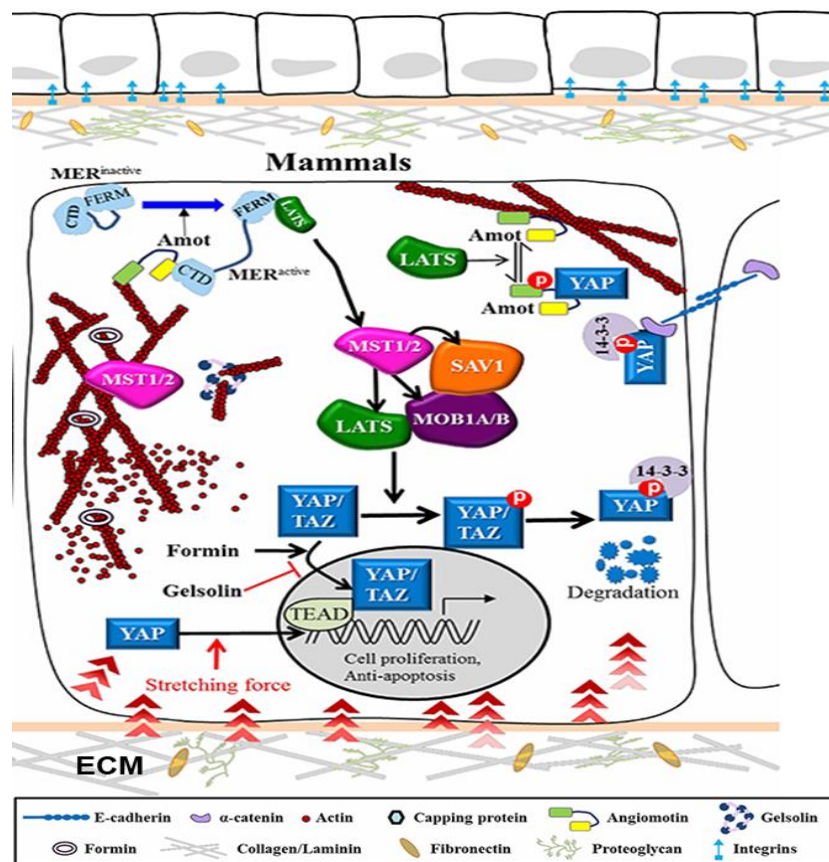
Fig 1.8: YAP activation and deactivation due to mechanical stimuli. When activated in response to mechanical cues, dephosphorylated YAP is translocated to the nucleus where its binding to TEAD turns on the target genes resulting in cell proliferation. When deactivated (phosphorylated), YAP is re-disturbed to cytoplasm and undergoes degradation[131].

1.6.4 Wnt/β-catenin

Wnt signalling is a pathway comprising 19 genes that regulates proliferation, survival, polarity, migration, cell repair, embryogenesis, tissue homeostasis, and tissue differentiation[134,135]. The genes code for glycoproteins rich in cysteine, which function as extracellular signalling factors by binding to their receptors, Fzd. Fzd receptor is of 10 isoforms that capable Wnt proteins to signal through three different pathways; canonical Wnt/β-catenin pathway, planar cell polarity pathway, and Wnt/Ca^{+2} pathway, also known as noncanonical pathway of which we will mention the first one that is known to contribute to angiogenesis, vascular remodelling, and differentiation[135,136]. **Fig 1.9** illustrates the key members of each Wnt pathway.
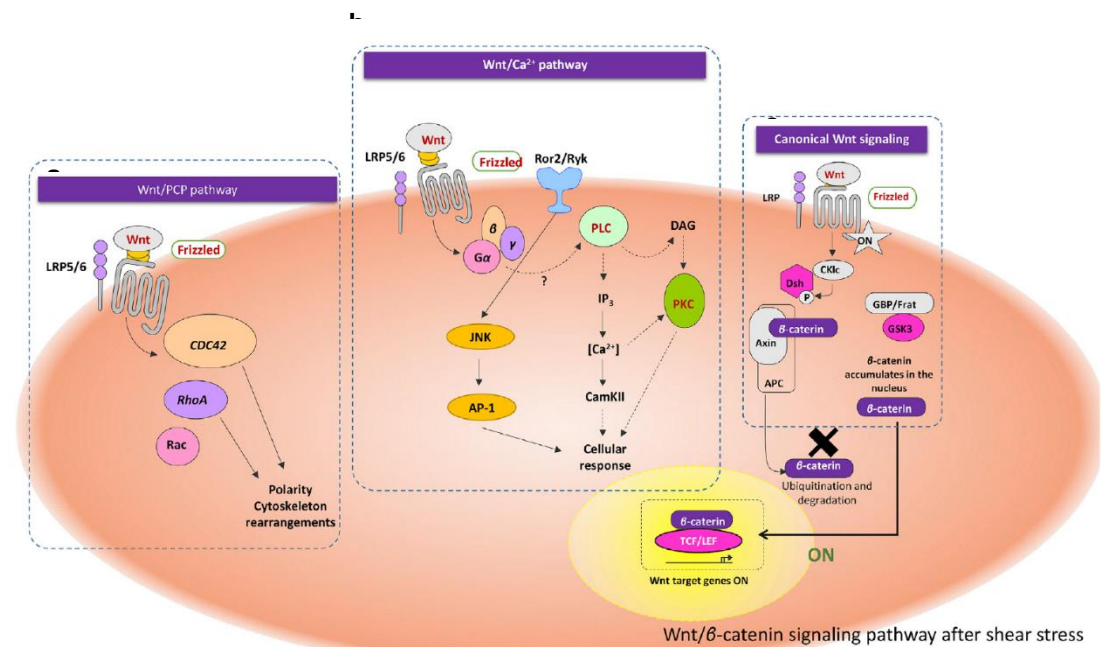
Fig 1.9: The schematic illustrating the key members of three Wnt signalling pathways.
a) planar cell polarity pathway b) Wnt/Ca^{+2} pathway c) Canonical Wnt/β-catenin pathway[134].

The Wnt/β-catenin pathway is the most studied Wnt signalling pathway, triggered by binding a Wnt family's glycoprotein to their receptor, Fzd, and their co-receptor, LRP5. Activation of Dsh protein as a result of the ligand and the receptors binding leads to dephosphorylation of β-catenin, a transcriptional

activator, and its shift from the cytoplasm to the nucleus, where it activates the TCF/LEF-1 family of DNA binding proteins. One of the target genes is VEGF, indicating the contribution of Wnt/β-catenin to vascularisation[135]. Using cell-based approaches and mouse models, Cha *et al.* demonstrated that Wnt/β-catenin contributes to lymphatic vascular morphogenesis, forming lymphatic and lymphovenous valves, and lymphatic vessel patterning. They also found that oscillatory shear stress activates the Wnt/β-catenin pathway in lymphatic endothelial cells, which sequentially regulates the expression of the lymphedema-associated transcription factor FOXC2. FOXC2 rescues the lymphatic vessel patterning deficiencies in β-catenin-defected mice. Altogether their findings demonstrate that Wnt/β-catenin signalling regulates lymphatic vascular development via sensing oscillatory shear stress[137].

1.6.5 Src

Src is one of the nine members of the Src family kinases. Interacting with multiple proteins and protein complexes, Src mediates signal transductions. It regulates various cell biological processes such as proliferation, survival, adhesion, and motility by interrupting FAK. Phosphorylating integrins' subunits, Src suppresses the attachment of integrins to ECM. Src also can inhibit actin filament assembly and stabilisation of FAs by interrupting RhoA. Besides, Src plays a key role in angiogenesis by regulating the gene expression of angiogenic growth factors, such as FGF, VEGF, and interleukin 8[138]. **Fig 1.10** illustrates Src signalling pathways and function.
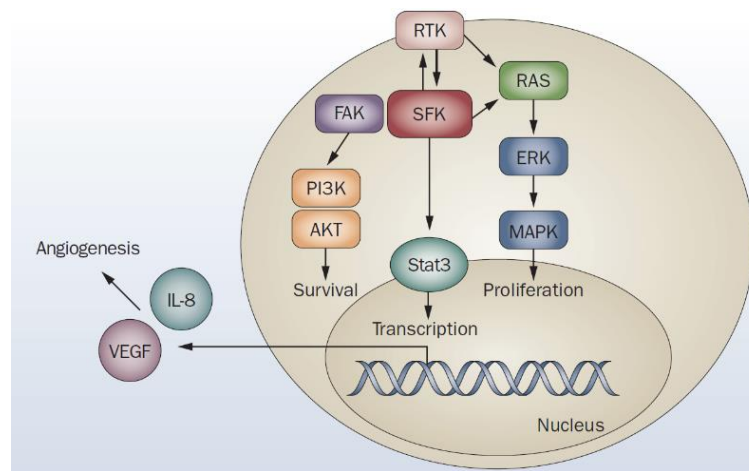
Fig 1.10: SFK signalling pathways and functions. *Src regulates several cell functions such as proliferation, survival and angiogenesis through interacting with different proteins*[138].

Using a combination of molecular and pharmacologic techniques, Mukhopadhyay *et al.* were the first research group that showed Src-inhibited fibroblasts fail to upregulate VEGF in hypoxia conditions, indicating the role of Src in VEGF regulation and subsequently vascularisation[139]. The findings of Eliceiri *et al.* highlighted that Src perturbation in tumour-associated blood vessels resulted in suppressing tumour angiogenesis[140]. Another study by Pyun *et al.* revealed that Src inhibitor, Capsiate, inhibits tubule formation by endothelial cells, *in vitro* and sprouting of rat aorta as well as the formation of new blood vessels in the mouse Matrigel plug assay, *in vivo*, demonstrating the contribution of Src to the vascularisation[141]. Being localised to FAs Src also acts as a mechanotransducer. Therefore its functions can be regulated by mechanical signals[142]. Locally applied force and cyclic cell stretch result in the activation of Src, indicating the contribution of the protein to mechanosensing[143,144]. Shimizu *et al.* showed that difference in the elasticity of polyacrylamide gels results in different morphology of fibroblasts and mouse embryonic stem cells involving the Src-ShcA-MAP kinase pathway demonstrating the mechanical role of Src[145]. They also showed that the differentiation of mouse embryonic stem cells changes depending on the substrate stiffness. In such a way, they observed a decrease in the expression

of the pluripotency markers on the softer gel (7.5 kPa) compared to the stiffer one (76 kPa)[145].

1.7 Microfluidic Based Methods of Microvessels Formation

There are different *in vivo* and *in vitro* methods to study vascular phenomena. Injection of Matrigel or implantable tumours into mice[146], the corneal pocket assay[147], and the chick CAM assay[148] are different types of *in vivo* assays which have their advantages such as having greater physiological relevance and limitations, for instance; 1) difficulty in independent control of experimental variable, 2) difficulty in manipulating gene expression in cells, and 3) difficulty in purifying cells for biochemical and gene expression analysis. To address the limitations of *in vivo* methods, *in vitro* microvessel models have been developed which offer the advantage of 1) study of the structure and function of the endothelium in response to a wide range of biochemical and physical stimuli, 2) study of angiogenesis and vessel formation mechanism, 3) study of endothelium dysfunction and shedding light on the molecular mechanism of disease, 4) study of drug transportation, uptake, and efficiency, 5) development of design rules for vascularising tissues and organs, 6) independent control of experimental variables[149]. Four broad fabrication methods, microfluidics, templating, 3D printing, and self-organisation, are used in *in vitro* microvessel models. Of all, microfluidics technologies offer the advantage of being relatively quick, recovering pure populations of cells, and easily transfecting the cells of interest, as well as the possibility of high resolution and live imaging[110]. In addition, employing microfluidics platforms need fewer cells and reagents[150]. It enables applying physiological forces and flows[151], introducing known concentrations of individual molecules, controlling ECM hydrogels' mechanical and biochemical properties, and culturing vascular cells in well-defined 3D environments.

Microfluidic-based microvascular formation methods can be divided into two main groups, 1) engineered methods and 2) natural methods. A coated channel is an engineered method in which endothelial cells are seeded onto

the ECM-coated walls of microfabricated vascular channels. Inorganic walls of such channels are covered with ECM proteins such as collagen, fibronectin, or gelatins to ensure a confluent endothelial monolayer's formation. The natural method is subdivided into two groups, sprouting and self-assembly. In the sprouting method, employing a three-channel microfluidic device with a hydrogel channel in the middle, endothelial cells seeded onto the wall form sprouts toward the hydrogel channel in response to the gradient of angiogenic growth factors. Alternatively, spheroids of endothelial cells or endothelial cell-coated microbeads can be encapsulated within a hydrogel matrix and be induced to form sprouts. The self-assembly method resembles the *in vivo* process of vasculogenesis in which endothelial cells are embedded homogeneously within a hydrogel channel. The cells embedded are fed with growth medium containing soluble and insoluble signalling components necessary to activate endothelial cells' inherent ability to elongate, connect, and form intracellular vacuoles that coalesce to form vascular lumens[152]. **Fig 1.11** illustrates the different microvascular formation methods applying microfluidic platforms.
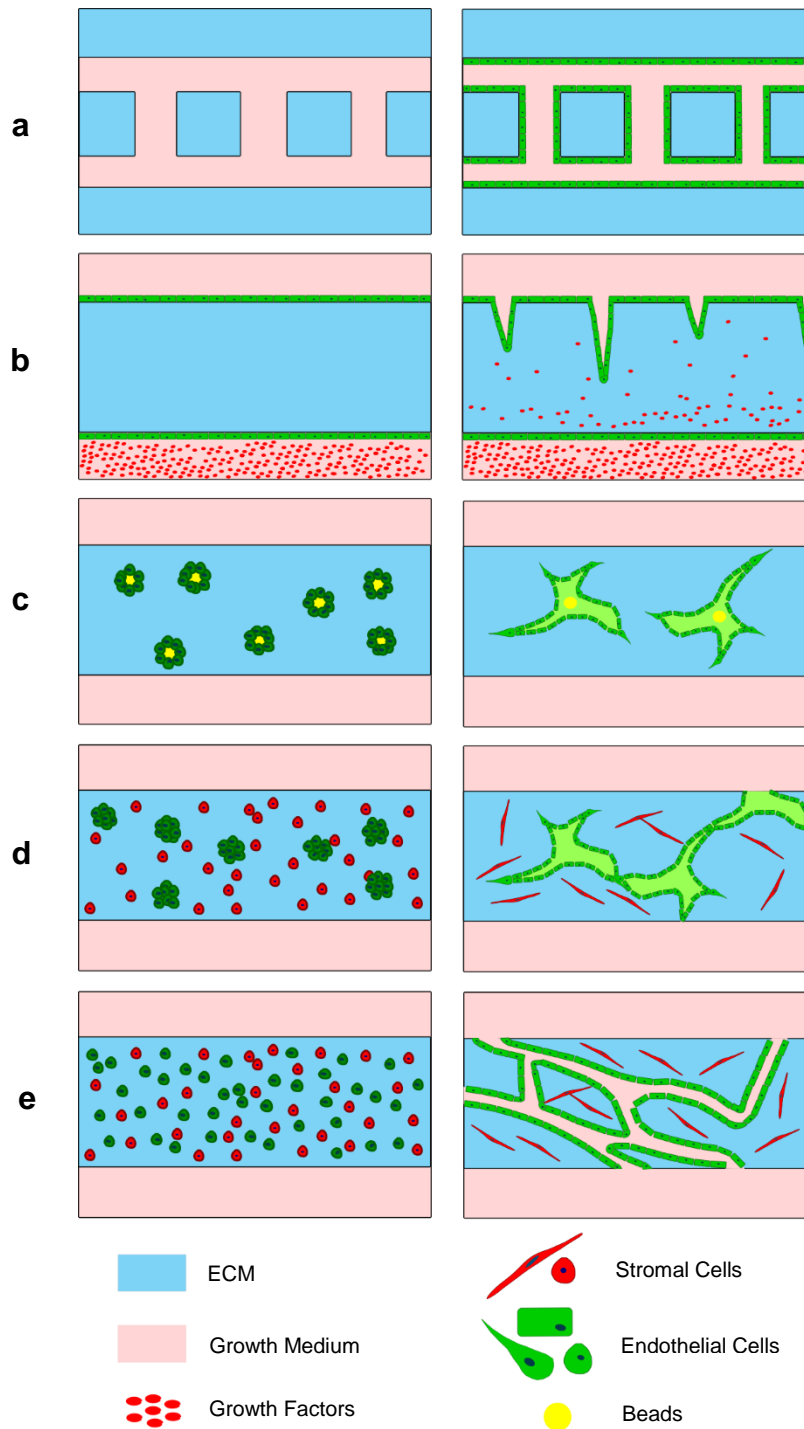
Fig 1.11: Schematics illustrating different methods of microfluidic microvasculature formation. *a) coated-channel method. b) angiogenic sprouting with a growth factor gradient. c) sprouting from endothelial cell-coated beads. d) Sprouting from endothelial cell spheroids. e) self-assembly.*

2 Role of FB-EC Physical Interaction in Vascularisation

2.1 Introduction

Many studies have shown that fibroblasts assist endothelial cells in the formation and stabilisation of blood microvessels[12–15]. However, there is some disagreement in the literature over whether paracrine signalling between endothelial cells and fibroblasts is sufficient to form functional blood microvessels or direct physical interaction between two cell types is required.

To elucidate the discrepancy above, we employed a microfluidic platform developed in Kamm's Lab. The platform consisted of 7 channels comprising three hydrogel channels (one EC channel and two FB channels) and four medium channels (two inside and two outside medium channels), which enabled the separate culture of the two cell types (**Fig 2.1**). We changed the design slightly by narrowing the two inside medium channels to address the impact of paracrine signalling. The impact of the presence of fibroblasts, paracrine signalling, and direct interaction was respectively studied over one week by three conditions:

- **Mono-Cultured (MC) condition:** endothelial cells embedded in the EC channel and a cell-free hydrogel in FB channels.
- **Paracrine Co-Cultured-1 condition (PCC-1):** endothelial cells embedded in the EC channel and fibroblasts in FB channels,
- **Juxtacrine Co-Cultured (JCC) condition:** endothelial cells embedded along with fibroblasts in EC channel and a cell-free hydrogel in FB channels

We also investigated the sufficiency of solute factors to support ECs to form blood microvessels by treating MC ECs with conditioned media.

Then, we characterised and stained JCC microvessels and assessed the impact of reducing FB concentration on microvessels formation, morphogenesis, and function.

2.2 Method

In this section, the materials and methods used to address the current chapter's aim are described.

2.2.1 Device Design

To fulfil the chapter's objective and the thesis, two different microfluidic platforms, a 7-channel device and a 3-channel device, were employed. The following sections describe the designs, mould fabrications, device fabrication, sterilisation and assembly.

2.2.1.1 Microfluidic Platforms (7-channel devices)

A 7-channel microfluidic device with dimensions mentioned in **Table 2.1** was employed to study the impact(s) of fibroblasts' presence in the formation of functional blood microvessels. The platform enables (1) high-resolution real-time imaging of the cells and (2) vascular perfusion for functional study. The device consisted of seven adjacent, parallel, rectangular channels comprising three hydrogel channels plus four medium channels (**Fig 2.1 a**). The middle hydrogel channel where endothelial cells (ECs) were embedded was called EC channel. Two side hydrogel channels where fibroblasts (FBs) were encapsulated in a fibrin matrix were named FB channels. These hydrogel channels were separated by two medium channels called inside medium channels, which were designed narrow enough to keep chemical interaction steady between FBs and ECs. Two outside medium channels were designed large enough to supply sufficient medium for the cells to grow (**Fig 2.1 b**). Microposts (250 μm diameter and 1 mm height) were designed to partition the adjacent channels and prevent the solution from leaking into the neighbouring channels. Ports of 2 mm and 4 mm diameter were considered to enable hydrogel and medium injection through the respective channels (**Fig 2.1 c**).

Table 2.1: Dimensions of a 7-channel device.

Dimensions (mm)								
Hydrogel Channels			Medium Channels					
			Inside Medium Channels			Outside Medium Channels		
Width	Length	Height	Width	Length	Height	Width	Length	Height
3.2	10	1	0.8	10	1	3.2	10	1

a

b

(Fig 2.1 continued on next page. Legend follows)

c

Medium Filling Port   Gel Filling Port

1 mm

Micropost

250 µm   190 µm
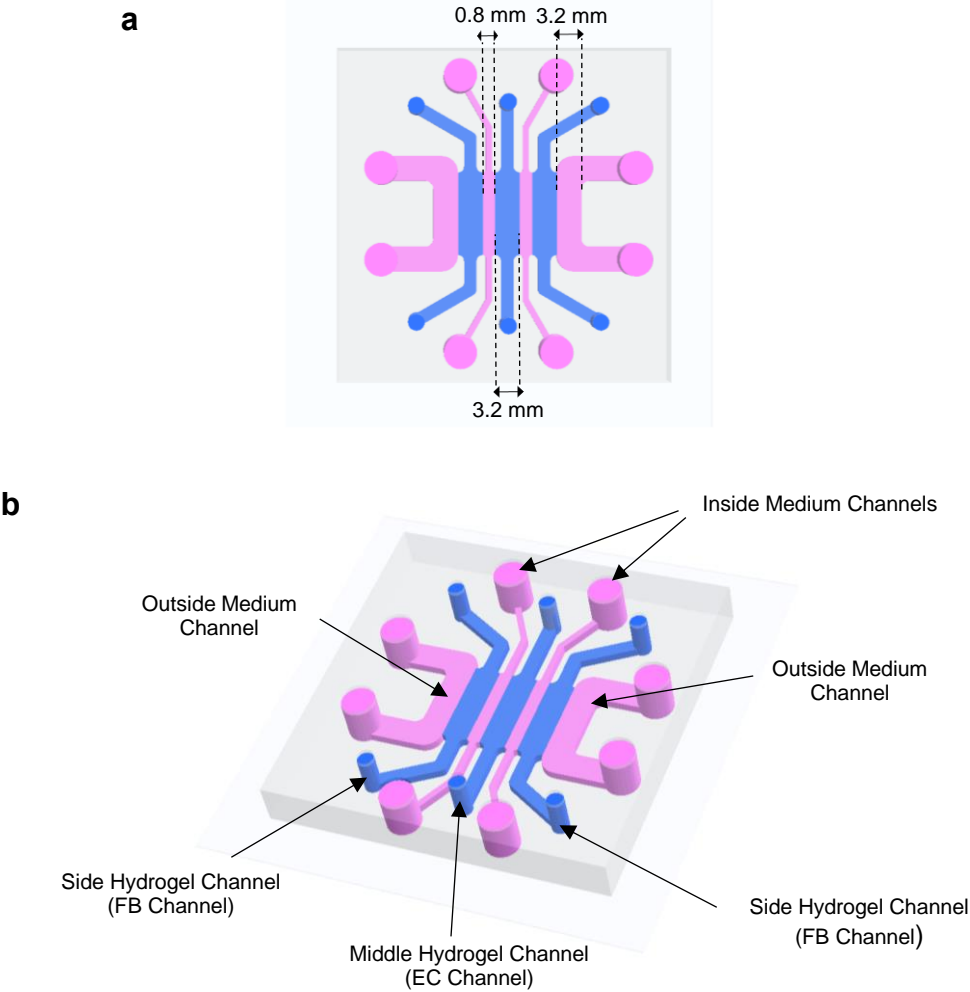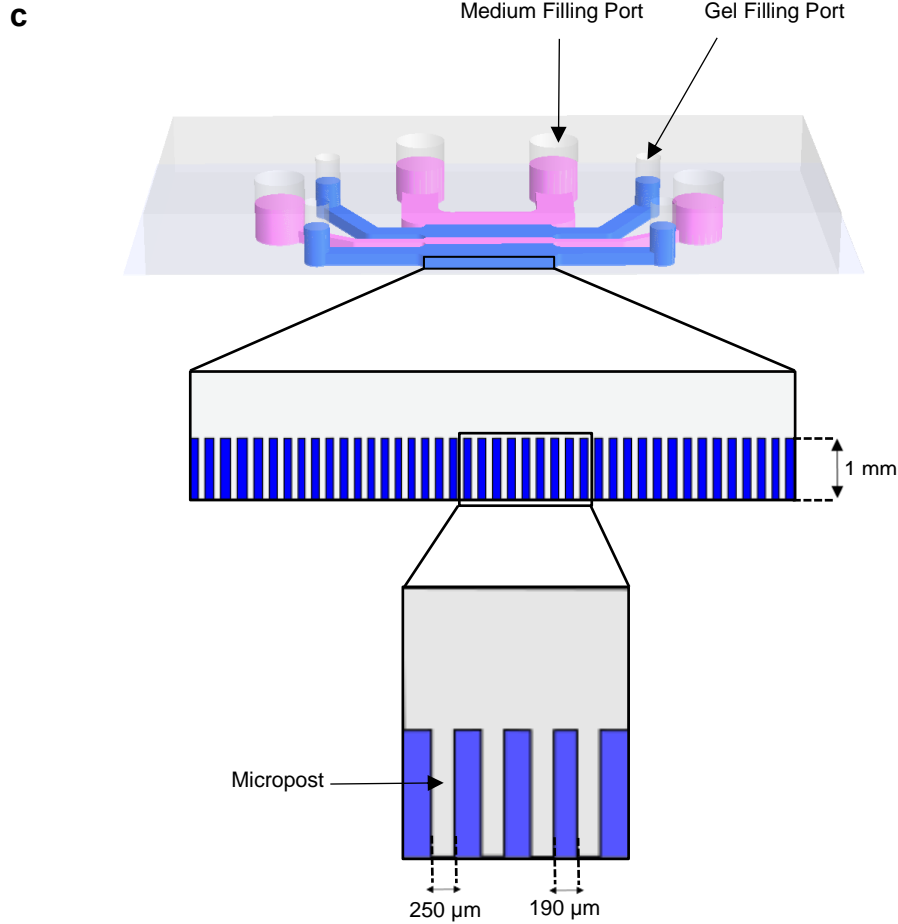
Fig 2.1: 7-channel fluidic device. *a) Top view of a 7-channel device showing dimensions of channels. b) Schematic of the device representing hydrogel and medium channels. c) Microposts partitioning adjacent channels.*

2.2.1.2 Acrylic Moulds Fabrication

Poly-methyl methacrylate (PMMA, Sheet Plastics/UK) moulds, also known as acrylic moulds, were used to make polydimethylsiloxane (PDMS, Ellsworth Adhesives/US) microfluidic devices. To construct the moulds, 2D drawing of the microfluidic devices were generated using AutoCAD 2018 (Autodesk/US). The drawings were then used to laser-cut a piece of an acrylic sheet (1 mm thick, **Fig 2.2 a**). To separate individual microfluidic channels, rows of microposts (height of 1mm, diameter of 250 µm, and edge to edge distance of 190 µm) were etched into the top of the moulds (**Fig 2.2 b**). Finally, 30 psi at

42

85°C was applied for 30 minutes to bond the bottom of the moulds to acrylic bases (**Fig 2.2 c**).
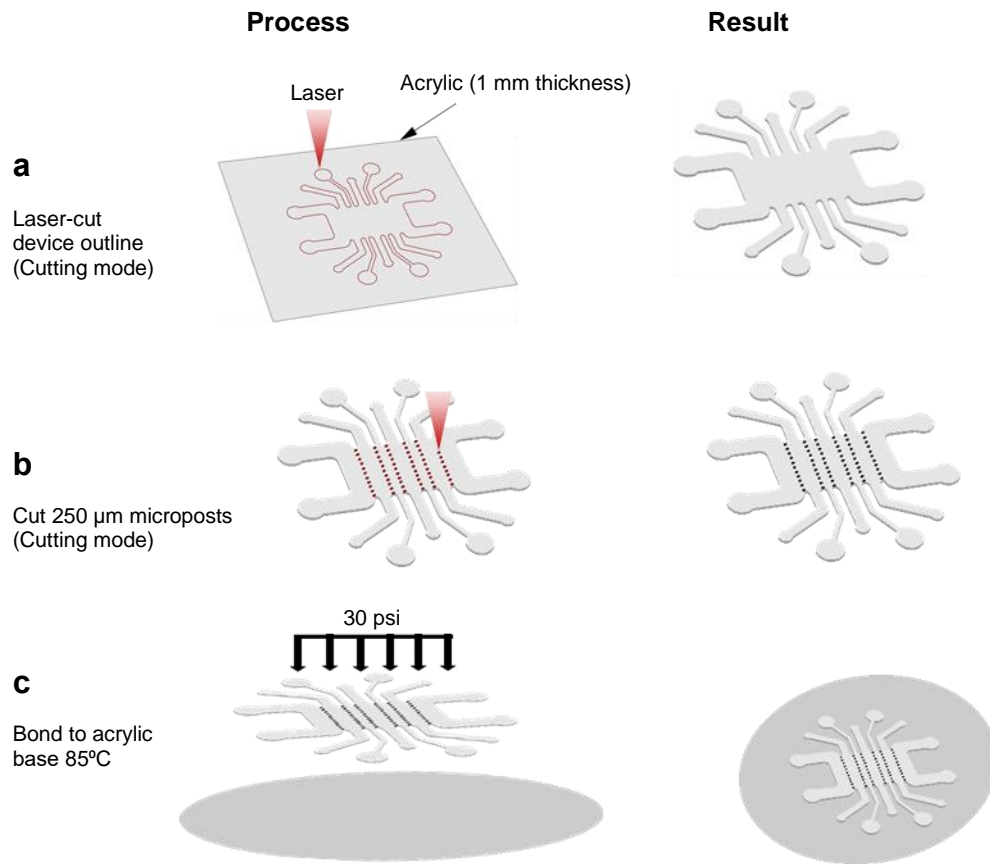
Fig 2.2: Acrylic mould fabrication. A process of 3 steps; a) outline of mould was cut out of a piece of 1-mm acrylic sheet, b) microposts of 1 mm height were cut at boundaries between the adjacent channels, c) the bottom of the mould was bonded to an acrylic base.

2.2.1.3 Device Fabrication

Microfluidic devices were fabricated as described below:

PDMS moulding: To fabricate devices, PDMS and curing agent were mixed in a ratio of 10:1. After stirring, the mixture was degassed using a desiccator for 30 minutes. The mixture was poured onto the moulds and rest for 30 minutes to let the trapped bubbles rise to the top. Then, the moulds with the mixture were put in a pre-warmed oven (80°C) for 1 hr and 30 min. Using a

razor, the cured PDMS (device) was detached and peeled off carefully to avoid ripping. Ports of diameter 2 mm and 4 mm were poked using biopsy punches for the hydrogel and medium channels.

Device sterilisation: Before sterilisation, debris was removed from the surface of the devices by applying a piece of scotch tape. The baked devices were then submerged in a beaker filled with Deionised (DI) water, and the top of the beaker was covered using aluminium foil. After wet autoclaving (20 minutes, 121°C), DI water was discarded. The devices, along with glass coverslips (Electron Microscopy Science/US), were transferred onto sterile boxes using a pair of sterile tweezers and were dry autoclaved (20 minutes, 121°C). Both the devices and coverslips were placed in an oven (80°C) to dry overnight.

Device assembly: The channel side of the device was plasma-bonded (Blackhole.Lab/France) onto a glass coverslip. Gentle pressure was applied to bond two sides and to avoid air gaps between the device surface and the glass coverslip (**Fig 2.3**). The bonded devices were placed inside an oven (80°C) overnight to restore the hydrophobicity of the PDMS and to ensure the formation of an irreversible bond.
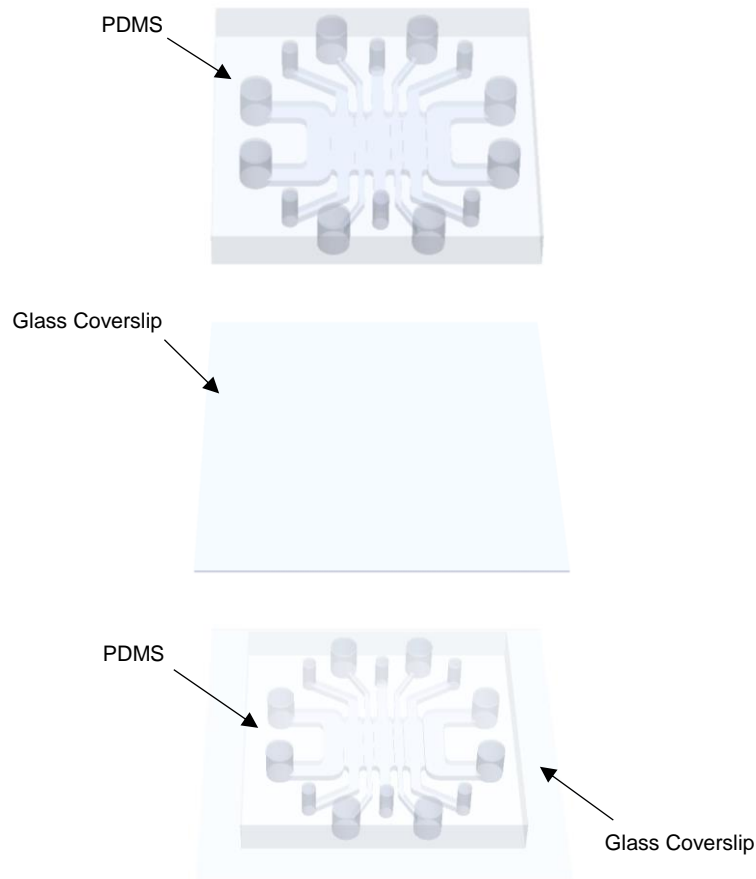
Fig 2.3: Device assembly. *Applying plasma, a glass coverslip was bonded to PDMS device.*

2.2.2 Cell Culture

Two types of cells, Normal Human Lung Fibroblasts (NHLFs) and Green Fluorescent Protein expressing Human Umbilical Vein Endothelial Cells (GFP-HUVECs), were recruited in this project.

NHLFs: NHLFs (FBs) and FGM-2, the growth medium used to grow the cells, were purchased from Lonza/Switzerland. The cells were frozen down and stored in a liquid nitrogen tank (-192ºC). Herein, these cells have been referred to as FBs.

GFP-HUVECs: GFP-HUVECs (ECs) were purchased from 2B Scientific/UK and were cultured in EGM-2MV medium (Lonza/Switzerland). To help ECs

45

attach, grow, and survive, the cells were cultured in rat tail Collagen-I-coated flasks. The cells were frozen down and stored in a liquid nitrogen tank. Herein, these cells have been referred to as ECs.

Rat tail collagen-I-coated flasks preparation: A working solution was prepared by mixing 14 µL of acetic acid (Lonza/Switzerland), 50 µg/mL of rat tail collagen I (VWR/US), and 10 mL of PBS 1X (Fisher Scientific Ltd/UK). The working solution was added to cell culture flasks as 1 mL working solution per 25 m^2 flask area. Then, the treated flasks were incubated at room temperature for 2 hours inside a biosafety cabinet before being washed four times with PBS. The flasks were either used immediately or stored at 4°C for up to one month.

2.2.3 Impact of FBs presence on Microvessels Formation – 7– Channel Platforms

ECs and FBs were used in all experiments between passages 6-8 and passages 5-10, respectively.

Thrombin solution, fibrinogen solution, re-suspension medium and Humidified boxes needed to encapsulate the cells were prepared as described below:

Thrombin stock 100U/mL: Thrombin powder was resuspended with PBS$^{-/-}$ (Calcium/Magnesium-Free PBS, Thermo Fisher Scientific/US) to a final concentration of 100 U/mL. Thrombin stock was then aliquoted, and the aliquots were stored at -20°C until use.

Fibrinogen solution (6 mg/mL): Fibrinogen flakes (6 mg) from bovine plasma (Sigma-Aldrich/US) were dissolved in 1 mL of PBS$^{-/-}$. The mixture was incubated in a water bath (37°C) and was gently agitated every 30 minutes. After 2 hours of incubation, the solution was filtered through 0.22 µm filters and was kept at 4°C for up to 1 week.

Re-suspension medium (4 U/mL): Prior to device seeding, 40 µL of thrombin stock was added to 1 mL of cold EGM-2MV to make 4U/mL re-suspension medium.

Humidified boxes: The racks of tip boxes were removed. Empty tip boxes were then filled halfway with water, the racks were put back, autoclaved, and set aside to cool. When cooled enough, the boxes were transferred to an incubator (37°C).

Notes: In all experiments;

- ECs and FBs were seeded at 4×10^6/mL and 2×10^6/mL final concentrations, respectively.
- Growth medium was replenished every 24 hours.
- The final fibrin gel concentration was 3 mg/mL in all hydrogel channels.
- All the cells encapsulated in the devices were fed with EGM-2MV.
- All images (z-stacks containing 21 slides, 10 µm z-step, 10X objective) were taken by a confocal microscope (Olympus FV1000/Japan) unless otherwise stated in the text.
- For all experiments, n=5 unless otherwise stated in the text.

The 7-channel devices were seeded with three different conditions described below to investigate the impact of FBs presence on blood microvessel formation.

Fibrin is a biopolymer of the monomer fibrinogen. The fibrinogen molecule is composed of two sets of three polypeptide chains named Aα, Bβ, and γ, which are joined together by six disulfide bridges. Fibrin is formed after thrombin-mediated cleavage of fibrinopeptide A from the Aα chains and fibrinopeptide B from the Bβ chains, with subsequent conformational changes and exposure of polymerisation sites. This generates the fibrin monomer that has a great tendency to self-associate and form insoluble fibrin[143,153,154]. As the most

widely used scaffolds, fibrin gels are of some important advantages such as 1) high seeding efficiency, 2) uniform cell distribution 3) adhesion capabilities, 4) being easy to adjust the concentration of interest and 5) having a key role in cellular and matrix interactions[153,154] which make fibrin gels a good choice for the current project.

Owing to their relative ease of procurement and extensive characterisation, HUVECs, the first endothelial cells successfully cultured[73], have been commonly used in microfluidic microvascular models. When removed from their native environment and cultured *in vitro*, vessel-specific endothelial cells partially dedifferentiate because they owe their specification to both inherited epigenetic modifications and local environmental cues. However, by adequately providing the biochemical, mechanical, and physical environment, endothelial cells' phenotype can be maintained in microfluidic microvascular models. For these reasons HUVECs were employed to as the source of ECs in this project. NHLFs were used as the population of stromal cells based on their known ability to stimulate capillary sprouting in a similar in vitro models of vascularisations.

ECs Mono-Cultured (MC): ECs were trypsinised, spun down, counted, and re-suspended in re-suspension medium. Equal parts (30 µL) of the cell re-suspension and fibrinogen solution (30 µL) were mixed over ice to avoid premature polymerisation. Then, the mixture was introduced to the EC channel of a 7-channel device gently. FB channels were filled with cell-free hydrogel solution (**Fig 2.4 a**). The seeded device was immediately placed in a Humidified box and incubated at room temperature for 30 minutes, followed by filling the medium channels with pre-warmed growth medium. Finally, the device was set in an incubator (37°C, 5% CO_2).

ECs Paracrine Co-Cultured with FBs-1 (PCC-1): Following trypsinising, spinning down, counting, and re-suspending ECs and FBs in resuspension medium, ECs were introduced in the EC channel once mixed with an equal amount of fibrinogen solution. Thirty µL of FBs suspension was mixed with an

equal fibrinogen solution. The mixture was immediately introduced in the FB channel. We did so to fill the other FB channel (**Fig 2.4 b**). The device was placed in a Humidified box to get the solutions gelled. After half an hour, following filling the medium channels with pre-warmed growth medium, the device was placed in an incubator.

ECs Juxtacrine Mixed Co-Cultured with FBs (JCC): ECs and FBs were dissociated, counted, pelleted, and re-suspended in re-suspension medium. Two cell suspensions were combined and mixed in equal parts. Thirty µL of the combined cell suspension was mixed with 30 µL of fibrinogen solution, pipetting up and down over ice to mix them homogenously. The mixture was then pipetted into the EC channel gently. FB channels were filled with cell-free hydrogel solution (**Fig 2.4 c**). The seeded device was immediately placed in a Humidified box and incubated at room temperature for 30 minutes. Finally, medium channels were filled with pre-warmed growth medium.
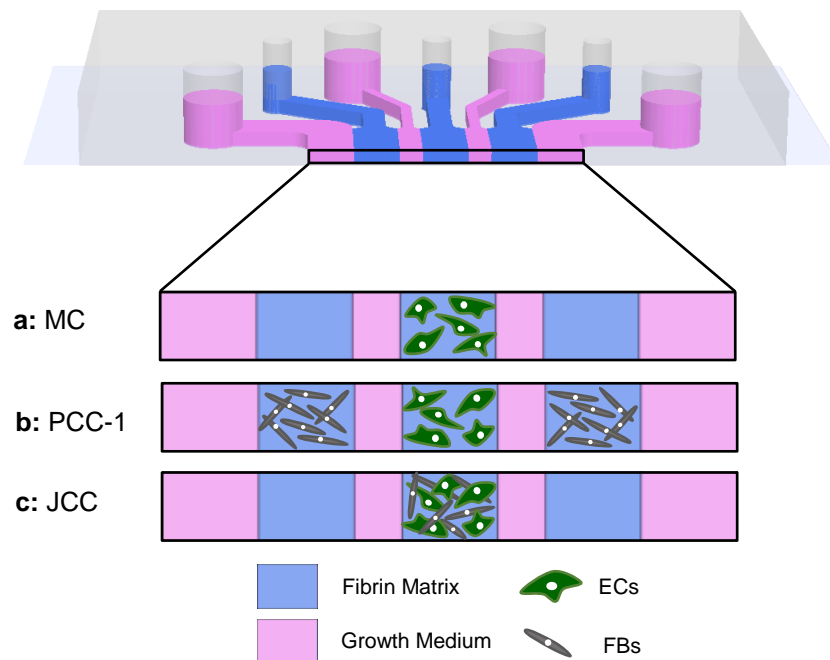
Fig 2.4: Cell seeding. *a) Schematic representing ECs mono-cultured in fibrin matrix (MC), b) ECs paracrine co-cultured with FBs-1 (PCC-1), c) ECs mixed co-cultured with FBs (JCC).*

On days 1, 4, and 7 post-seeding, the devices were imaged by a confocal microscope to assess vessel formation.

Investigation of Microvessels Function (Perfusability): We measured microvessels perfusability to a fluorescent tracer dye (dextran 70 kDa) as described below:

Dextran stock preparation: Texas red fluorescent dextran 70 kDa (Thermo Fisher Scientific/US) was prepared by dissolving 10 mg of dextran flakes in 10 mL PBS$^{-/-}$. The solution was then divided into aliquots and kept in a freezer (-20°C) until use.

Working solution preparation: Prior to perfusability measurement, 10 μL of dextran stock was diluted with 400 μL of pre-warmed growth medium.

On day 7 of culture, the growth medium in upstream inside medium channel was removed. To create a head pressure, ports of downstream medium channels were emptied, followed by re-filling upstream inside medium channel with the fluorescent tracer dye (**Fig 2.5**). EC channel was imaged immediately to assess the perfusion of the dextran.

a

Upstream Inside Medium Channel

Downstream Medium Channels

1) Upstream inside medium channel was fully emptied.

2) Ports of downstream medium channels were emptied.

3) Upstream inside medium channel was fully filled with a dye tracer.

b

4 mm

Direction of Dextran Flow
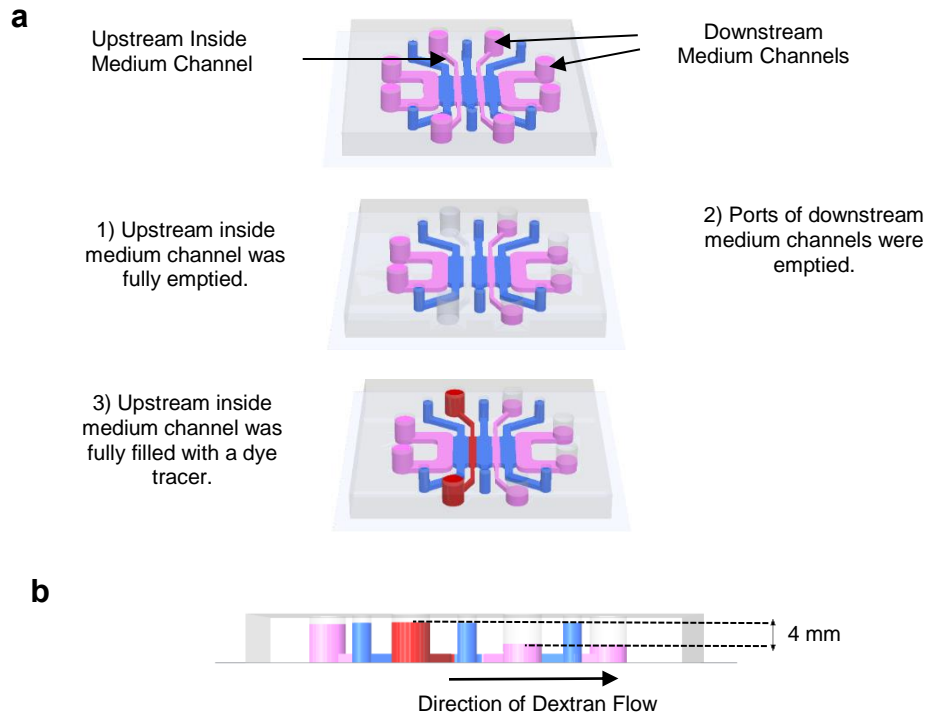
Fig 2.5: Perfusability visualisation. a) Experiment set-up. b) Head pressure initiates dextran perfusion through EC channel.

Data analysis: An image processing program, ImageJ (National Institutes of Health/US), was used to analyse data. Perfusability, percentage of microvessel lumens containing tracer dye (dextran) after perfusion, was assessed by re-slicing confocal stacks in the x-z plane. After binarising both the ECs channel (green) and dextran channel (red), the EC channel was used to identify vessel outlines. Overlaying outlines of the EC channel with the dextran channel, perfused vessels were identified (**Fig 2.6**). All microvessel cross-sections contained dextran within them were added to the total perfused area. The total perfused volume was divided by the total vascular volume to calculate perfusability (Appendix 1).

51

	EC Channel	Dextran Channel
1) Re-slicing confocal stacks in x-z plane.		
2) Binarising and identifying vessels' outlines.		
3) overlay		
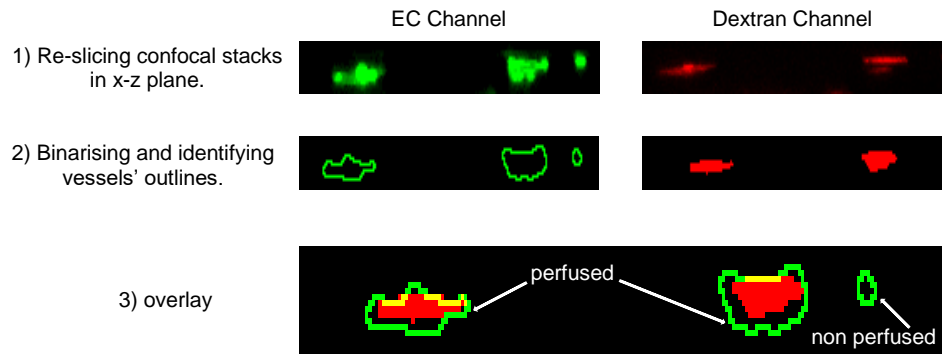
Fig 2.6: Visualisation of perfusability analysis.

2.2.4 Diffusion

Dextran 10 kDa stock preparation: Texas Red Fluorescent Dextran 10 kDa (Thermo Fisher Scientific/US) was prepared by dissolving 25 mg of dextran flakes in 2.5 mL PBS $^{-/-}$. Then, the solution was divided into aliquots that were kept at -20ºC until use.

Working solution preparation: Prior to experiment conduction, 20 µL of dextran stock was diluted with 400 µL of pre-warmed medium.

Experiment performing: Hydrogel channels were filled with cell-free hydrogel solution. Once gelled, three medium channels were filled with pre-warmed growth medium, whereas one of the outside medium channels was filled with fluorescent dextran (**Fig 2.7**). EC channel was imaged by an epi-fluorescent microscope (Leica/Germany) every five minutes to track the tracer dynamics.

Data analysis: Region Of Interests (ROIs), 0.75 x 0.75 mm, were defined in the middle of the EC channel, and the intensity of dextran was read out within it over time. The measured numbers were normalised with respect to maximum intensity (Appendix 2).

a

Upstream Outside
Medium Channel

Downstream Channels

1) Upstream outside
medium channel
was emptied.

2) Downstream channels
were left fully filled with
growth medium.

3) Upstream outside
medium channel was
fully filled with the tracer
dye (Dextran).

b

4 mm

Direction of Dextran Flow
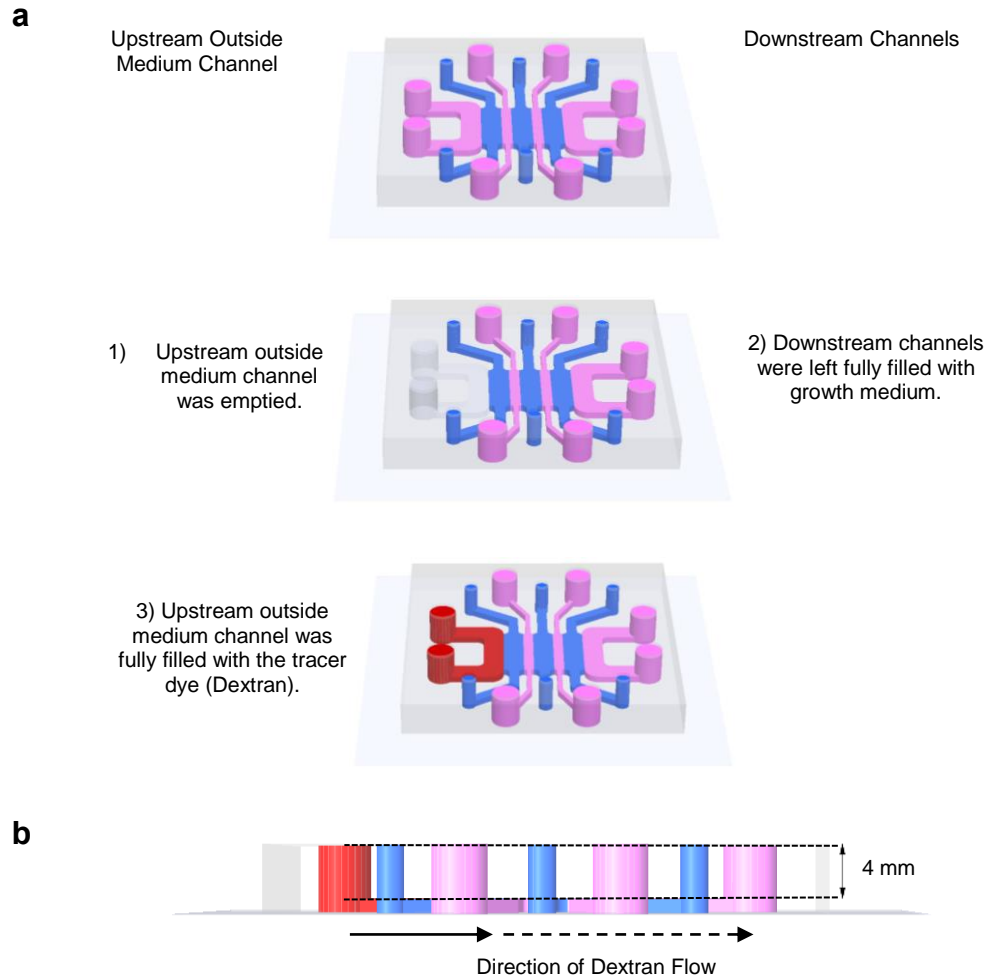
*Fig 2.7: Diffusion visualisation. a) Procedure of replacing growth medium
with the tracer dye to assess diffusion. b) Side view of the channels after
injecting dextran. No head pressure was applied to help dextran diffusion
initiate.*

2.2.5 Impact of FBs on Microvessel Formation – 3-Channel Platforms

When functional microvessels formed in the JCC device (please see **Fig 2.4
c** and **Fig 2.15 b**), we shifted from 7-channel devices to 3-channel devices as
described below. That was because we no longer needed 3 hydrogel channels
to form microvessels. We continued the project with 3-channel devices unless
otherwise explicitly stated in the text.

53

The 3-channel microfluidic device employed systematically to study microvessel formation properties, function, and morphogenesis met the same criteria mentioned in part **2.2.1.1**. The device consisted of three adjacent, parallel rectangular channels (each 3 mm width, 23 mm length, and 1 mm height) (**Fig 2.8 a**). The middle channel in which vascular cells were embedded within a 3D hydrogel was known as vascularisation or hydrogel channel. Two side channels through where the cells were fed with growth medium were known as perfusion or medium channels (**Fig 2.8 b**). Two PDMS lips (0.3 mm) extending from the top surface separated the individual channels. These lips enabled filling each channel without any leakage to the adjacent channel. The direct interaction between adjacent channels was provided by the remaining 0.7 mm height of the channel interfaces. Two-millimeter and four-millimeter ports were considered to enable hydrogel and medium injection through the respective channels (**Fig 2.8 c**).
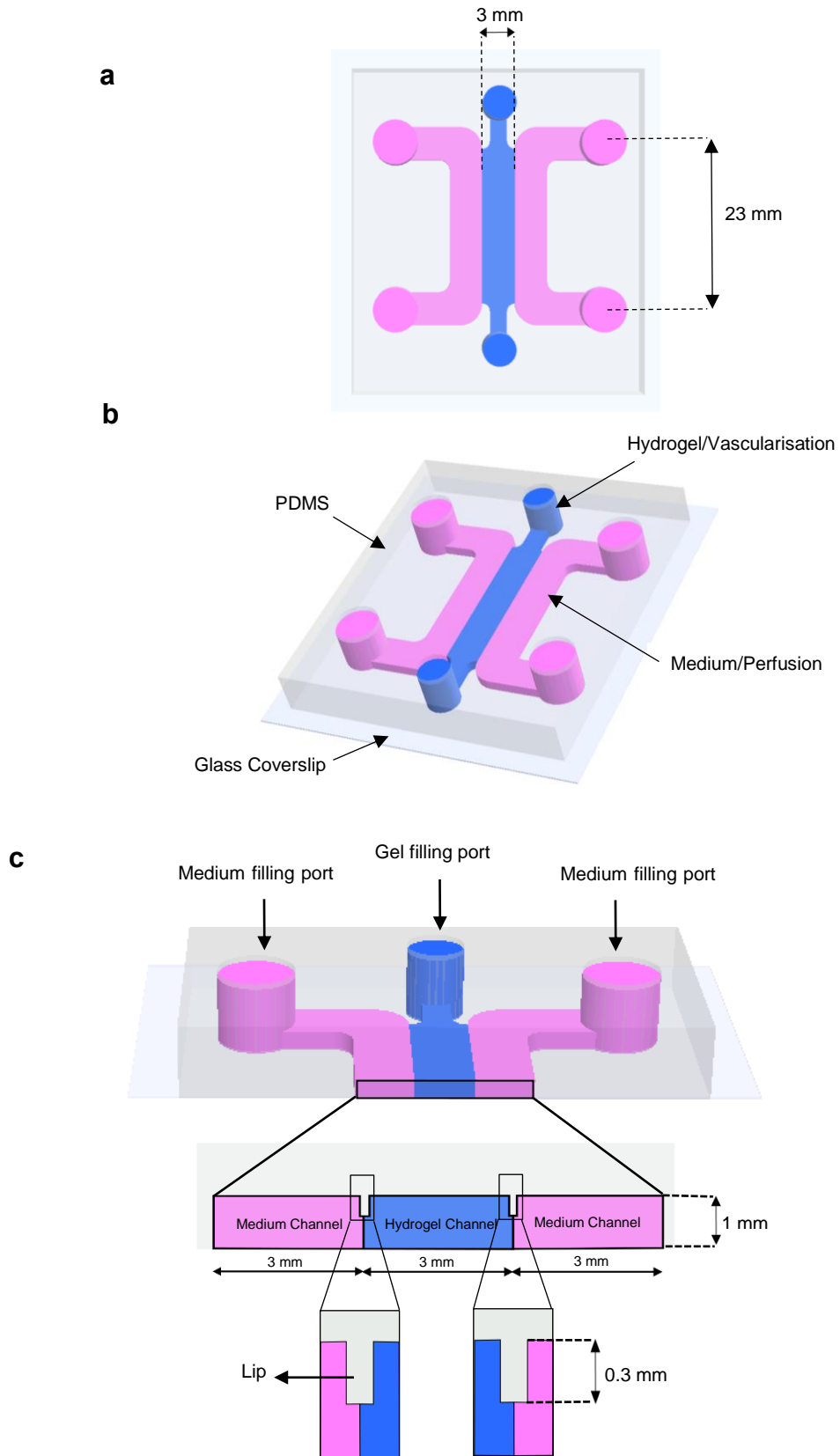
Fig 2.8: 3-channel device. *a) Top view of the device showing the dimensions. b) 3D Schematic of the device representing vascularisation and medium channels. c) Ports were poked to enable gel and medium injection. Two 0.3 mm lips separating the adjacent channels.*

To fabricate 3-channel acrylic moulds and to make, sterilise, and assemble the devices, the same procedures mentioned in section **2.2.1.3** were followed. The devices were juxtacrine co-cultured as described in section **2.2.3.3** (Also, see **Fig 2.4 c**). **Fig 2.9** represents a 3-channel device seeded with JCC condition.
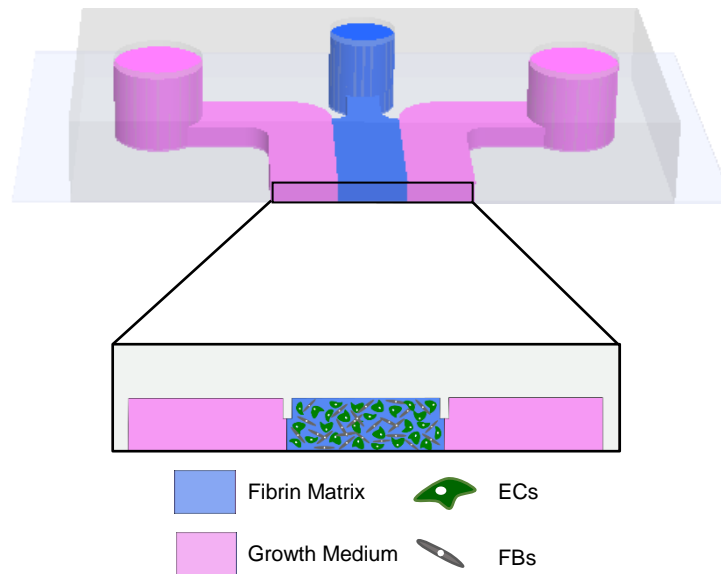
Fig 2.9: JCC in a 3-channel microfluidic device. ECs and FBs were mixed juxtacrine co-cultured in the vascularisation channel.

2.2.6 Conditioned Medium Experiment

We employed both 3-channel and 7-channel platforms to perform conditioned medium experiments. It is worth mentioning that all the seeded devices were fed with growth medium for the first 24 hours.

Seeding 3-channel microfluidic devices: 3-channel microfluidic devices were seeded with MC condition as described in sections **2.2.3** and JCC conditions (**Fig 2.10 a i, ii**). One device was seeded only with FBs named FB-seeded device (**Fig 2.10 a iii**).

Seeding 7-channel microfluidic device: One 7-channel microfluidic device was seeded as *ECs Paracrine Co-Culture with Mixed Co-Culture of FBs and*

ECs-2 (PPC-2). To that end, the EC channel was seeded with MC condition followed by seeding FB channels with both ECs and FBs (**Fig 2.10 b**). Once the cell/gel solutions got polymerised in a Humidified box, the medium channels were filled with pre-warmed growth medium, and the device was kept in an incubator.
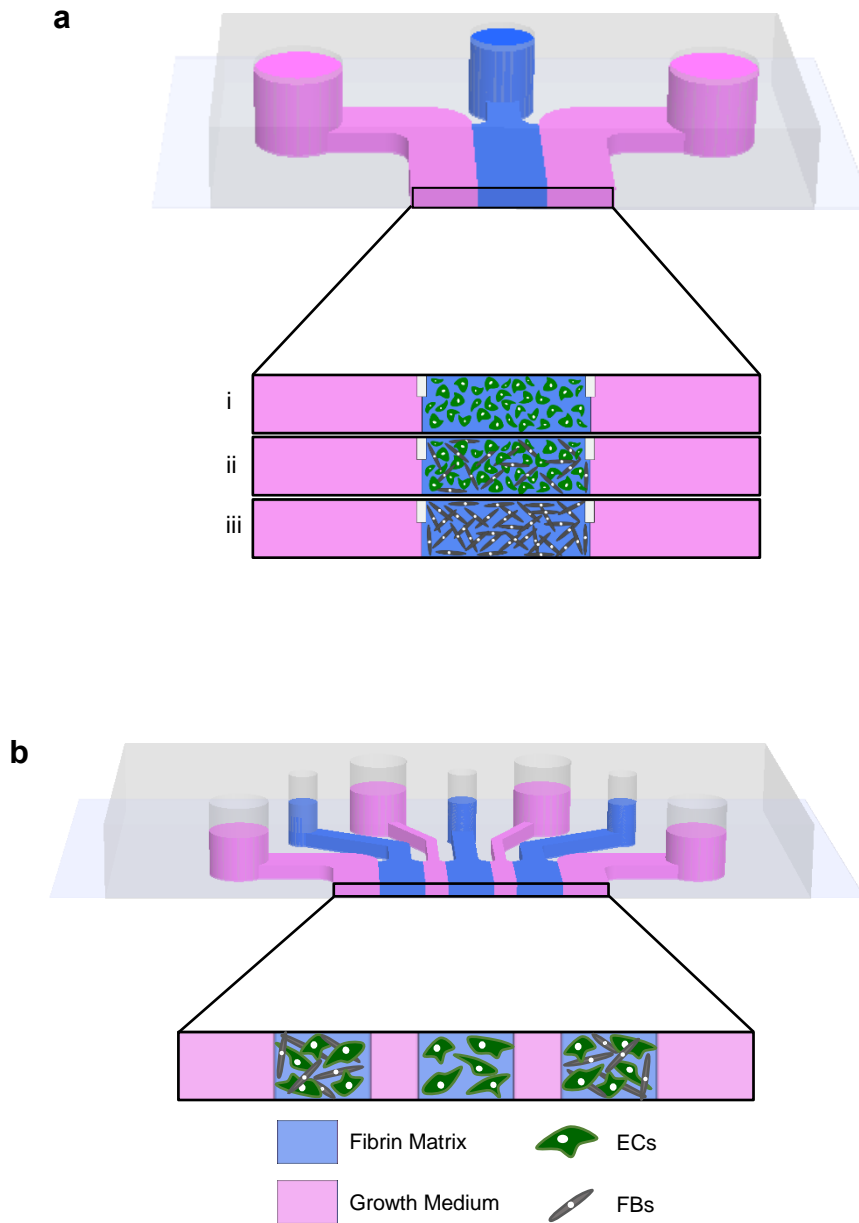
2.10: Cell seeding for conditioned medium experiment. *a) 3-channel device seeded with (i) MC, ii) JCC and iii) FBs. b) Schematic of a 7-channel device seeded with PCC-2 condition.*

To prepare conditioned medium, growth medium was harvested from medium channels every 24 hours after culture and diluted 1:1 with fresh growth medium to replenish nutrients depleted over the interval. Conditioned medium from JCC devices was called *Juxtacrine Co-Culture Conditioned Medium (JCCCM),* and conditioned medium from FB-seeded devices was called *Fibroblast Conditioned Medium (FBCM).*

To fulfil the conditioned medium experiment, three MC devices were fed with EGM-2MV, JCCCM, and FBCM, respectively, for one week. One JCC device was fed with JCCCM to ensure that the difference in microvessels formation was not due to a shortage of nutrients. PCC-2 was fed with growth medium. Z-stacks taken on days 1, 4, and 7 were used to investigate microvessels formation. Perfusability was assessed as described in section 2.2.3 (**Fig 2.5** and **Fig 2.6**). The experiment is summarised in **Table 2.2**.

Table 2.2: Conditioned medium experiment summary.

Condition	Type of Platform	Device Seeding Conditions	Number of Seeded Devices	Fed with
Controls	3-Channel Microfluidic Platform	Juxtacrine Co-Culture (JCC)	2	Growth Medium
				Juxtacrine Co-Cultured Conditioned Medium (JCCCM)
	7-Channel Microfluidic Platform	Paracrine Co-Culture-2 (PCC-2)	1	Growth Medium
Conditioned Medium Treated Devices	3-Channel Microfluidic Platform	Mono-Culture (MC)	3	Growth Medium
				Juxtacrine Co-Cultured Conditioned Medium (JCCCM)
				Fibroblast Conditioned Medium (FBCM)

2.2.7 3D Functional and Morphological Characterisation

We then characterised JCC microvessels for some features such as perfusability, permeability, length, diameter, coverage area, and topology.

2.2.7.1 Perfusability

Growth medium was removed from the upstream medium channel and the downstream medium channel ports on days 1, 4, and 7 after seeding, followed by perfusion of the fluorescent tracer dye in the upstream medium channel (**Fig 2.11**). The vascularisation channel was imaged immediately. Data analysis was performed as described in part **2.2.3**.

a

Upstream Medium Channel

Downstream Medium Channel

1) Upstream medium channel was fully emptied.

2) Ports of downstream inside medium channel were emptied.

3) Upstream medium channel was fully filled with the tracer dye.

b

4 mm

Direction of Dextran Flow
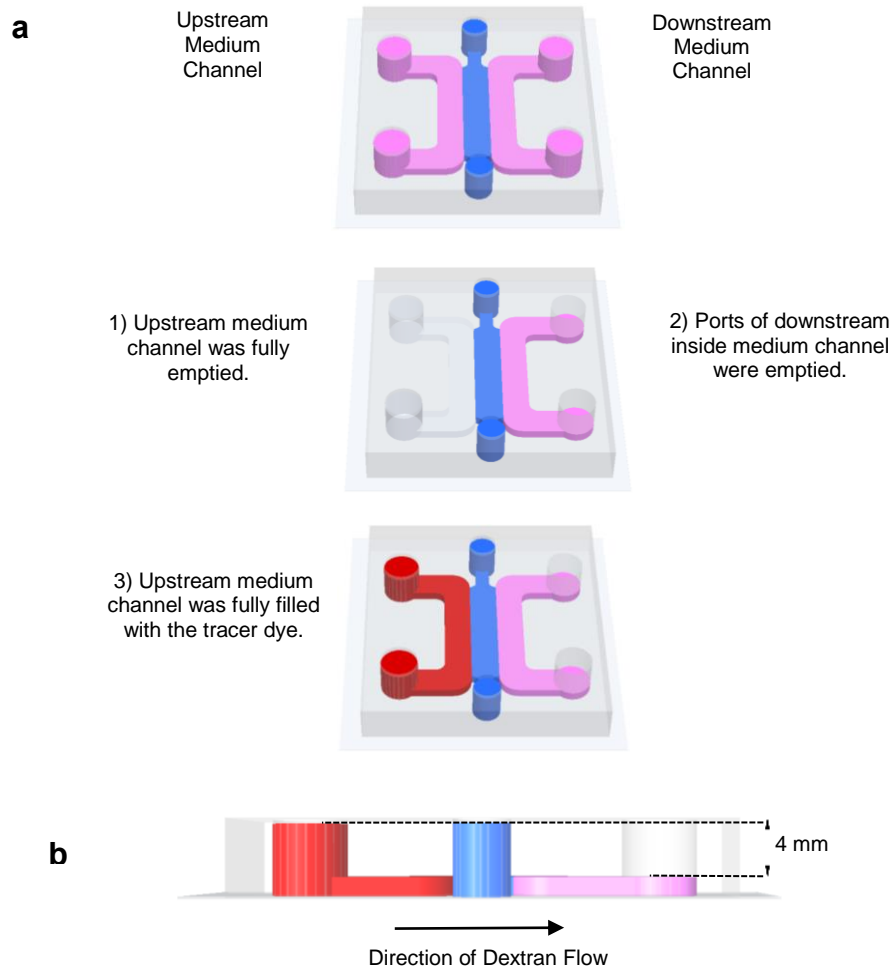
Fig 2.11: Perfusability visualisation. a) Schematic representing perfusability experiment set-up. b) Head pressure initiates dextran perfusion through vascularisation channel.

2.2.7.2 Permeability

Permeability, crossing plasma and its solutes through the vascular barrier[155], was measured to a fluorescent tracer dye, 10kDa dextran.

3-channel devices were seeded with JCC condition. On day 4, 1.5×10^6/mL ECs were seeded on both medium channels to form a monolayer within the next 3 days (**Fig 2.12**). This was to stop dextran perfusing into the vascularisation channel via the gel.
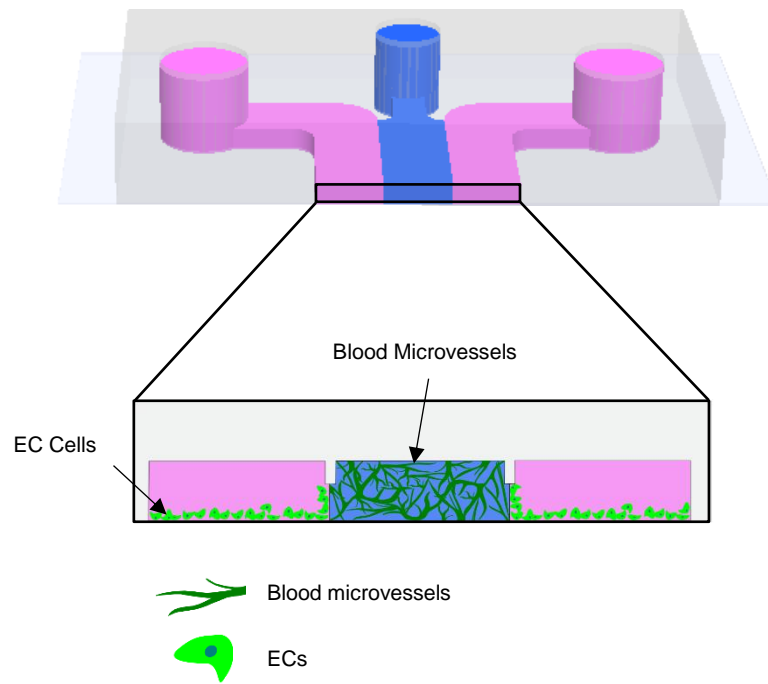
Fig 2.12: ECs seeding. *ECs were seeded in both medium channels on day 4 of culture to form a monolayer within the next 3 days.*

On day 7, growth medium in both upstream and downstream medium channels was removed, followed by being filled with the tracer dye. To create a head pressure, ports of downstream medium channel left empty (**Fig 2.13**). The vascularisation channel was imaged immediately after introducing the tracer (Time 0 - T_0), followed by imaging the same spot of the device every 20 minutes for 1 hour with a confocal microscope (10X objective - 11 slices - 15 µm z-step) named as T_1, T_2, and T_3.
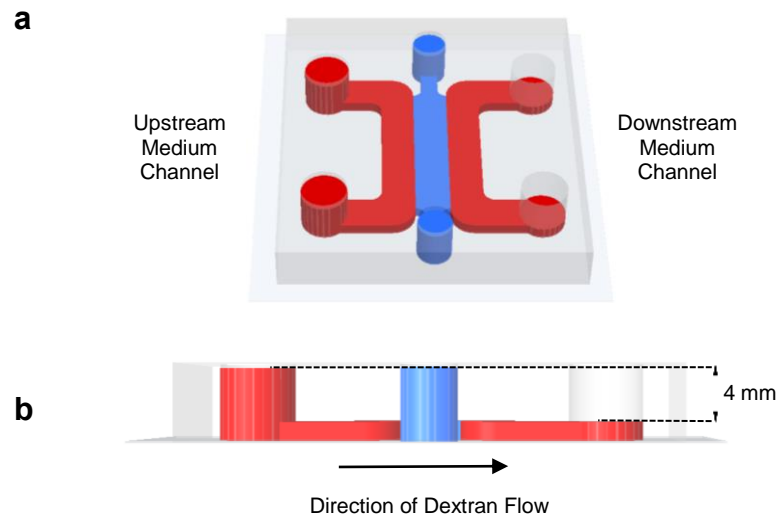
Fig 2.13: Permeability visualisation. a) Dextran was transduced into both upstream and downstream medium channels. b) Head pressure initiated dextran perfusion through vascularisation channel.

Data analysis: To calculate permeability, the average tracer intensity in both microvessels and interstitial spaces, was calculated by comparing T_0 with T_1, T_0 with T_2, and T_0 with T_3. The permeability coefficient was measured by comparing interstitial intensity at different times.

2.2.7.3 Microvessel Length

Epifluorescent 2D images were analysed using ImageJ to calculate microvessel lengths. The software produced a 3D skeleton by performing a thinning algorithm. The skeleton segment lengths were directly used to determine vessel lengths (See appendix 3 for macro script).

2.2.7.4 Microvessels Diameter

To measure microvessels diameter, 3D confocal images were collapsed in a z direction. The diameters were then measured by drawing a line from one edge of a microvessel to another edge. The length of these lines was measured using ImageJ.

62

2.2.7.5 Microvessels Coverage Area

To quantify the microvessel coverage area, the EC channel was processed using ImageJ. In such a way that background and noise of 3D confocal images were removed, followed by applying a Gaussian blur. The images were then thresholded and binarised. The area of the microvessels was measured using "Analyse Particle" plugin. Finally, to calculate the microvessels coverage area per cross-section, the number obtained was divided by the cross-sectional area (See appendix 4 for macro script).

2.2.7.6 Microvessels Topology

The topology of the microvessels, including the number of branches, the number of junctions, average branch length, and maximum branch length, were assessed by the projection of 3D confocal images (4 slides) in the z direction. The z-projected stacks were segmented into vessels and interstitial regions (voids) using the "Trainable Weka Segmentation" plugin (ImageJ). Then, the images were skeletonised to measure vascular branching, the number of junctions, average and maximum branch length using "Analyse Skeleton" plugin. **Fig 2.14** illustrates the procedure of assessing microvessels topology.

1) Confocal z-stack images, dextran channel (4 slices) were projected (average intensity) in the z direction.
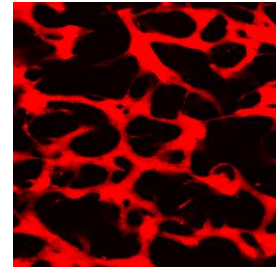
2) Vessels and voids were defined by drawing outlines.

<table>
<tr><td>■ Vessel</td><td>■ Void</td></tr>
</table>
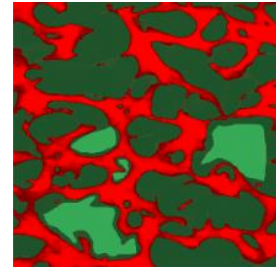
3) Vessels and voids were classified by Trainable Weka segmentation plugin.

<table>
<tr><td>■ Vessel</td><td>■ Void</td></tr>
</table>
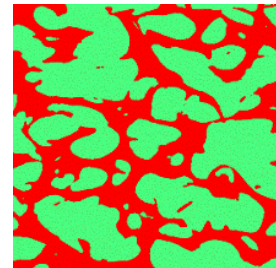
4) Microvessels were skeletonised using Skeletonised (2D/3D) plugin.
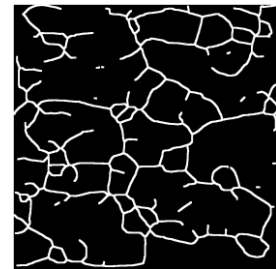
5) Overlaid.
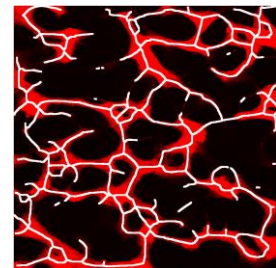
Fig 2.14: Procedure of evaluating microvessel topology.

2.2.7.7 Staining

Hoechst (New England Biolabs/US), Hu CD31 Alexa 647 (BD BioScience/US), anti-human CD144 (VE-Cadherin) antibody (BioLegend, US), and CellMask plasma membrane stain (Thermo Fisher Scientific/US) were applied to stain blood microvessels for nuclei, PECAM-1, and cell membrane, respectively.

Hoechst stock preparation: The Hoechst dye stock solution (10 mg/mL, 16.23 mM) was prepared by dissolving 100 mg of the dye powder in 10 mL of deionised water. The stock was then divided into aliquots and stored at -20ºC.

Nuclei staining: A fresh staining solution was prepared by diluting 1 µL of the dye stock with 2 mL of pre-warmed growth medium. To stain the nuclei, both medium channels were emptied. The nuclei were stained by introducing 200 µL of the staining solution to one of the medium channels. The staining solution was removed after 5 minutes of incubation at room temperature. The remaining staining solution was washed away by rinsing the device with PBS (3 times, 5 minutes each). The device was then used to stain the plasma membrane of the microvessels as follows;

Membrane staining: To prepare a staining solution (1X), 1 µL of the provided 1000X concentrated stain solution was diluted with 1 mL of pre-warmed growth medium. The staining solution (200 µL) was introduced to one of the medium channels, followed by incubation of the device at room temperature. After 5 minutes of incubation, the working solution was removed, and the device was washed three times with PBS (5 minutes each.) The microvessels were, then, stained with Hu CD31 Alexa 647 as follows;

PECAM-1 and VE-Cadherin staining: A fresh staining solution was prepared by mixing 5 µL of the pre-diluted reagent and 100 µL of pre-warmed growth medium. The solution was injected into one of the medium channels. The device, covered by a piece of aluminium foil to be protected from light, was then incubated at room temperature. After 5 minutes of incubating, the solution was removed, and the device was rinsed three times (5 minutes each) by

introducing PBS into medium channels. Finally, the medium channels were filled with pre-warmed growth medium to feed the cells while being imaged. The stained microvessels were imaged by a confocal microscope. Imaging set-ups are summarised in **Table 2.3**.

Table 2.3: Confocal imaging set-up.

Confocal Imaging Set-up		
Objective	Z-step (µm)	Number of Slices
10X	10	21
20X	3	17
60X	1	30

2.2.8 Impact of FBs Density on Vascularisation

In line with answering what would happen to the networks if ECs were co-cultured with a lower number of FBs, we juxtacrine co-cultured ECs with 1 M/mL FBs (final concentration). The set-up was called JCC 4X (X is the ratio of the total number of ECs to the total number of FBs in the system.) The microvessels formed in JCC 4X were then compared to JCC 2X microvessels (control) in terms of vascular topology and vascular function, including perfusability.

2.2.9 Statistical Methods

Two-tailed student t-test was used to do statistical analysis. Each experiment was repeated at least 3 times. The number of repeats along with p values have been reported in both the main text and figure captions throughout the thesis.

2.3 Results

2.3.1 Impact of FBs on Vascularisation – 7–channel platforms

To investigate the impact of FB presence (paracrine signalling) and EC-FB physical interaction on microvessels formation, 7-channel microfluidic devices were seeded with different conditions, MC, PCC-1, and JCC (**Fig 2.15 a**). Over the course of one week, dramatic morphological changes were observed among different conditions. The initially rounded and mono-dispersed ECs began to spread out and extended protrusions, resulting in sheet-like clusters by day 4 in MC device. The clusters then began to regress. By day 7, some scattered and regressed sheet-like clusters remained in the EC channel (**Fig 2.15 b**). ECs paracrine co-cultured with FBs (PCC-1) formed sheet-like structures which lasted over one week of culture (**Fig 2.15 b**). While ECs failed to form microvessels in MC and PCC-1 devices, they succeeded in developing connected, thin, and well-defined functional microvessels by day 7 when juxtacrine co-cultured with FBs (**Fig 2.15 b**). The microvessels formed persisted through approximately three weeks. The bar chart in **Fig 2.15 c** compares JCC viability with MC and PCC-1. It is worth mentioning that by functional microvessels we mean permeable and perfusable microvessels throughout the current study.

*(**Fig 2.15** continued on next page. Legend follows)*

b

Day 1   Day 4   Day 7

MC

PCC-1

JCC

150 µm

c

Microvessel Viability
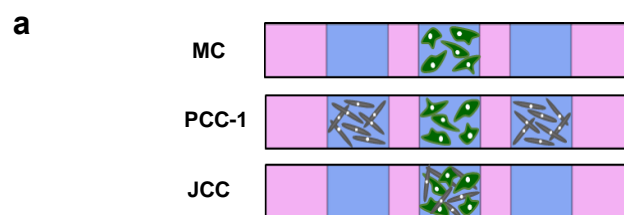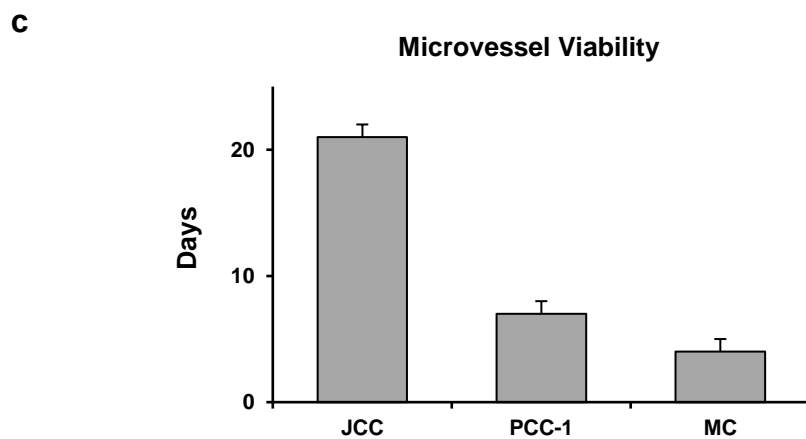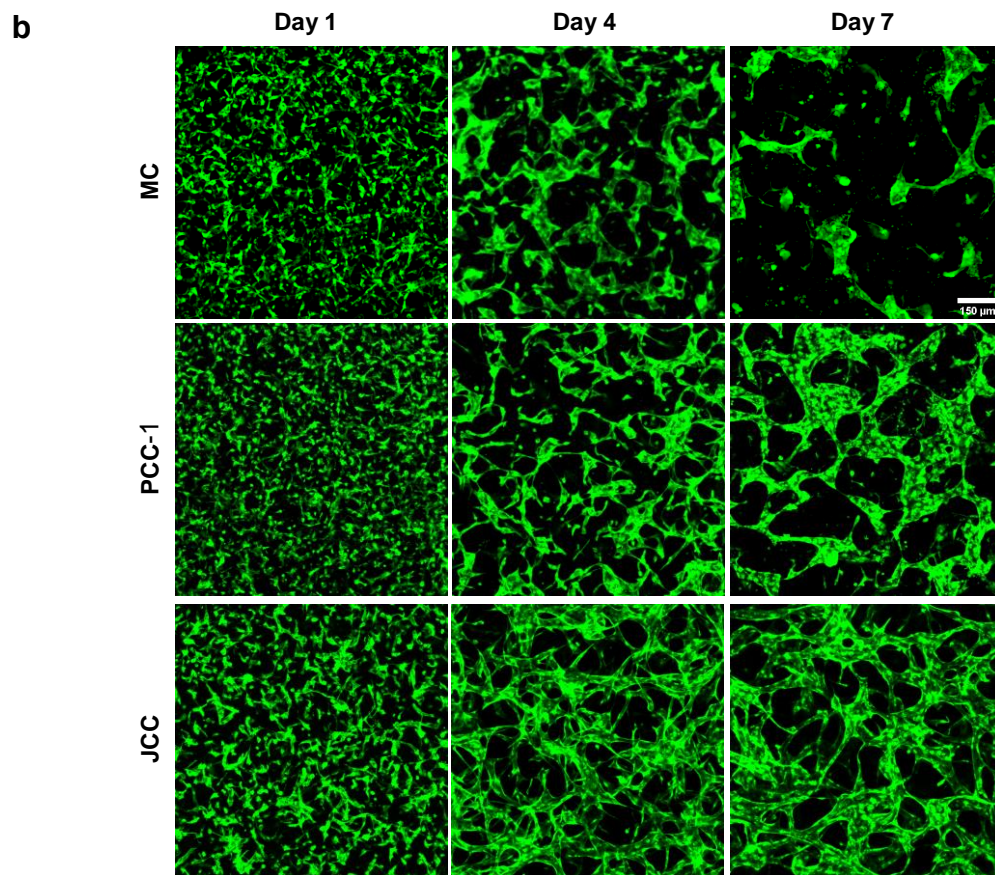
Fig 2.15: Microvessels formation comparison. a) Schematics of MC, PCC-1 and JCC. b) Comparison of microvessel formation in MC, PCC-1 and JCC condition over the course of 1 week. Scale bar 150 µm. c) Bar chart comparing JCC viability with MC and PCC-1. n=5.

68

The function of structures formed in different conditions was investigated by perfusion of a fluorescent tracer dye (dextran 70 kDa, **Fig 2.16 a**) using equation 2.1.

$$Perfusability\ (\%)= \frac{Area\ of\ vessels\ filled\ with\ dextran}{Total\ area\ of\ vessels} \times 100 \qquad \textbf{(Eq: 2.1)}$$

The bar chart in **Fig 2.16 b** compares MC, PCC-1, and JCC in terms of perfusability. Confocal images showed that unlike JCC microvessels through which dextran moved quickly, within a few seconds, and reached the other inside the medium channel, in MC and PCC-1 devices, dextran perfused to the EC channel via gel, proving the fact that sheet-like structures formed in those devices were neither interconnected nor functional (**Fig 2.16 c**).

a

Direction of Dextran Flow

b
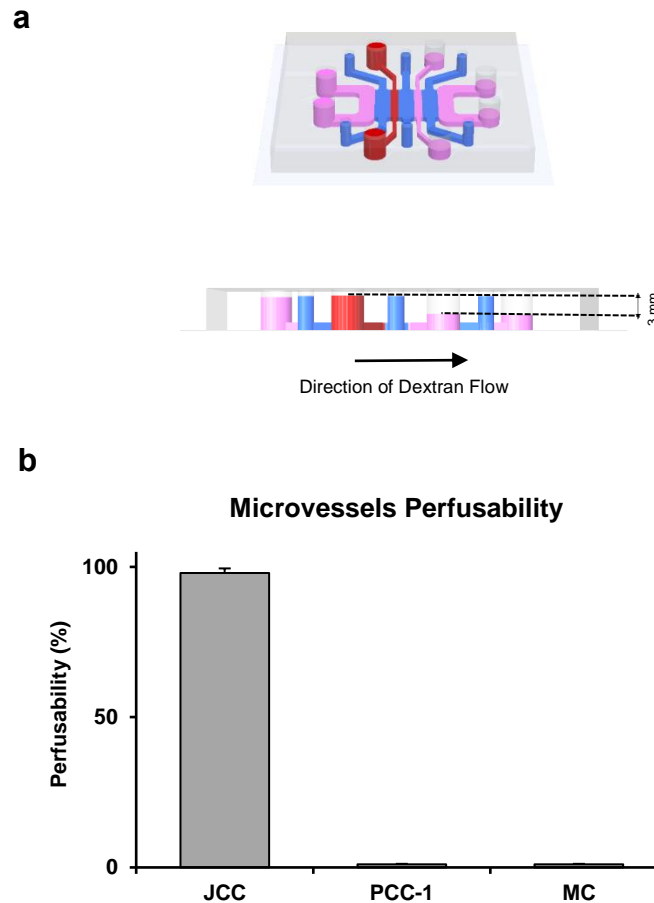
*(**Fig 2.16** continued on the next page. Legend follows)*
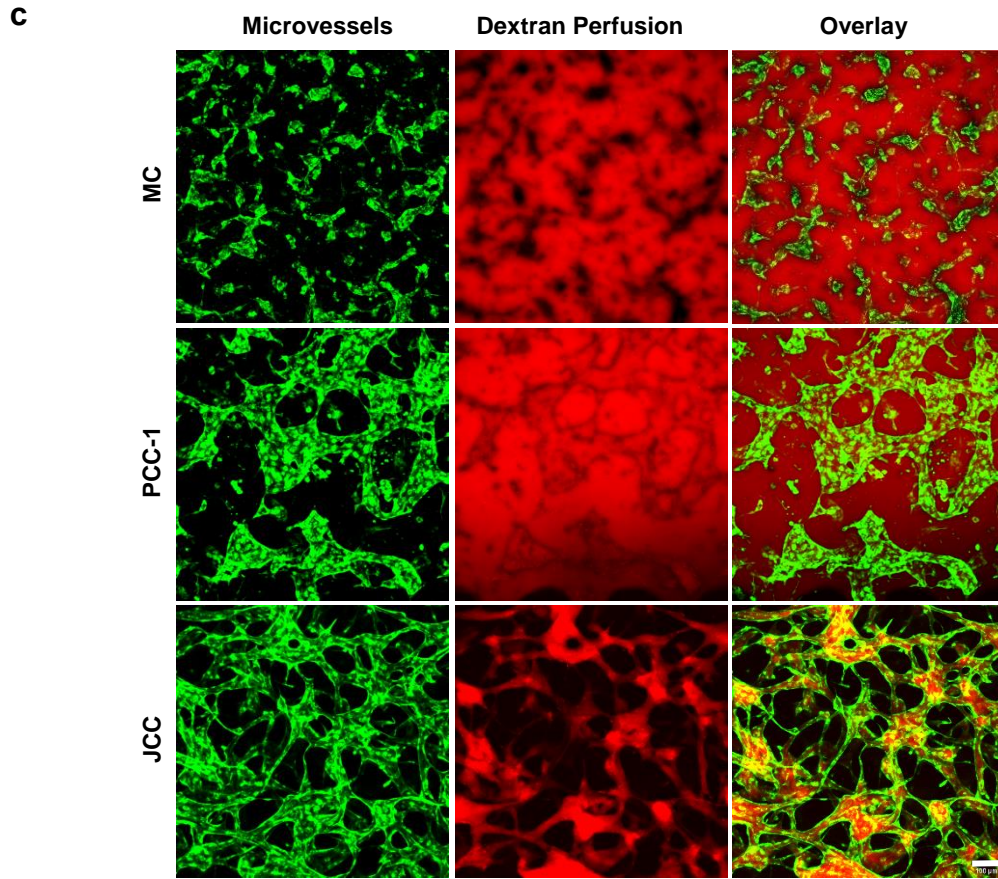
Fig 2.16: Perfusability visualisation. a) Schematic of perfusability set-up. b) Bar chart comparing microvessels perfusability, n=5. c) Confocal images showed that dextran perfused to EC channel through gel in MC and PCC-1 devices but it was confined within microvessels and moved through them within a few seconds in JCC device. Scale bar 100 µm.

2.3.2 Diffusion

Considering that the growth medium was replaced every 24 hours, we hypothesised that the lack of microvessel formation in PCC-1 devices might be due to not arrival of growth factors secreted by FBs to the EC channel because of their low diffusion rate. We measured the time that took 10 kDa fluorescent dextran to diffuse from outside medium channel to EC channel to examine this. Briefly, one of the outside medium channels was filled with dextran (**Fig 2.17 a**). No head pressure was applied to initiate dextran diffusion (**Fig 2.17 b**). Tracking dextran showed that it reached the middle of the EC channel (ROIs, **Fig 2.17 c**) about 30 minutes after the initiation of diffusion

70

(**Fig 2.17 d**). The non-smoothness seen in the curves at x=750 μm is due to stitching two adjacent ROIs.
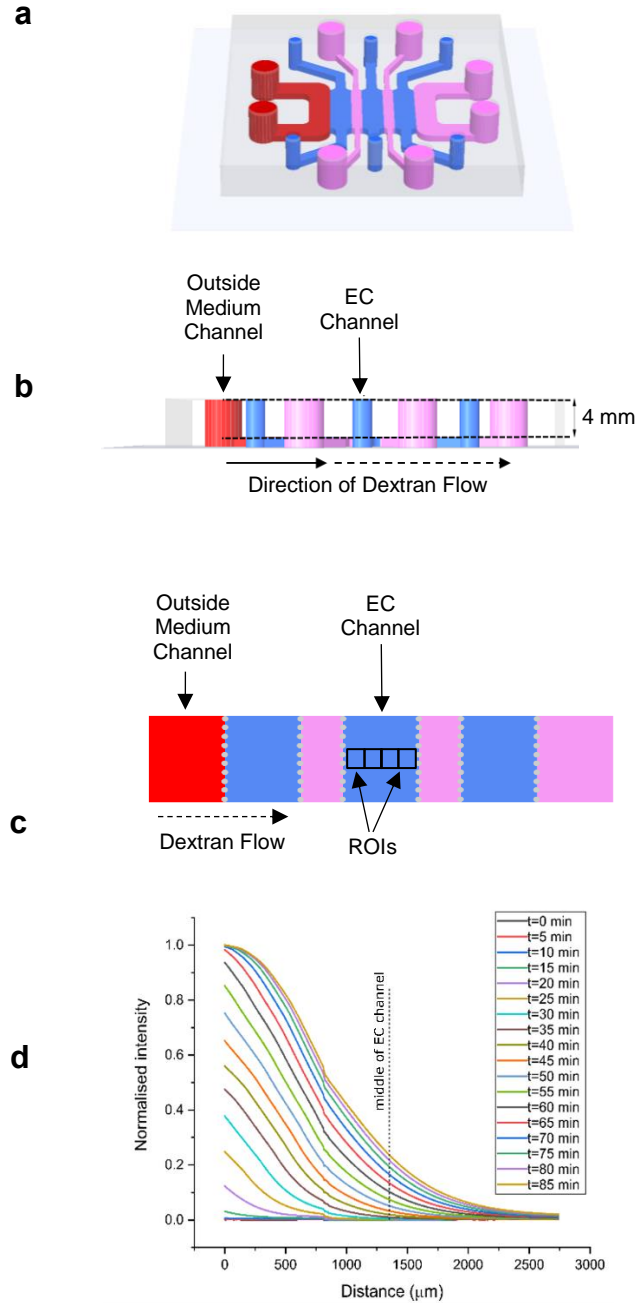
Fig 2.17: Diffusion. *a) Schematic of diffusion experiment set-up. b) Side view of the channels showing that no head pressure was applied to initiate dextran diffusion through the channels. c) Top view of the channels showing ROIs imaged to track dextran. d) Graph representing dextran diffusion to the gel over time. Normalised with respect to the intensity of the dextran at 85 minutes after diffusion.*

Since it took dextran about half an hour to reach the middle of the EC channel, 24 hours, the medium replacement intervals, should be sufficient for the growth factors to reach the EC channel. Thus, our hypothesis could be rejected that the lack of microvessel formation could be due to not arrival of growth factors secreted by FBs.

2.3.3 Impact of FBs on Microvessel Formation – 3-channel platforms

The results mentioned in section **2.3.1** showed that well-defined, interconnected, long-lasting, and functional microvessels formed when ECs were mixed co-cultured with FBs within one hydrogel channel (EC channel). Because one hydrogel channel was enough to form functional microvessels, to examine vascularisation in JCC condition further, we shifted to a 3-channel microfluidic device, consisted of two medium channels and one hydrogel channel, with the same dimensions (3 x 23 x 1 mm) as a 7-channel microfluidic device (**Fig 2.18 a**). The only difference is to increase the length of the device almost two times, from 10 mm to 23 mm. From here on, only 3-channel microfluidic devices were used to accomplish the experiments unless otherwise it is stated clearly in the text.

On the first attempt, we recapitulated vessel formation using a 3-channel microfluidic device. To fulfil that, ECs were seeded along with FBs within a fibrin matrix in the hydrogel channel (**Fig 2.18 b**). Initially, individually-scattered rounded ECs began to get elongated within the first few hours after co-embedding. By day 4, the cells formed nicely interconnected well-defined microvessels. This continued until day 7. **Fig 2.18 c** shows microvessel formation over the course of one week, and **Fig 2.18 d** is a confocal z-project that shows a large view of the microvessels formed homogeneously throughout the vascularisation channel by day 7. The microvessels formed lasted for approximately three weeks after culture.
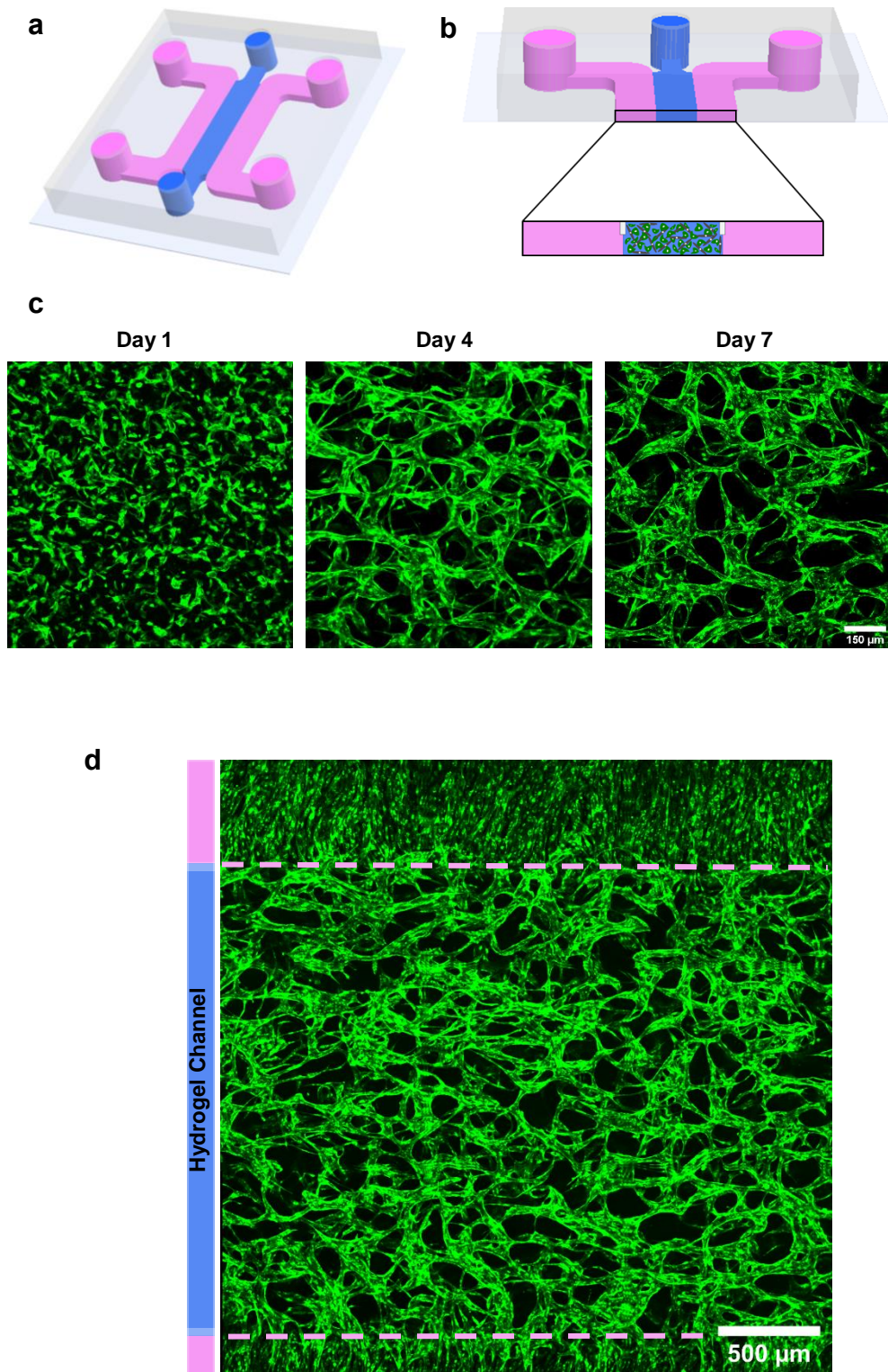
Fig 2.18: Microvessel formation in 3-channel microfluidic device. *a) 3D schematic of a 3-channel microfluidic device. b) ECs embedded along with FBs in a single hydrogel channel. c) Microvessel formation over one week. Scale bar, 150 μm. d) A large view of microvessels showing that the microvessels formed homogeneously throughout the hydrogel channel by day 7. Scale bar, 500 μm.*

2.3.4 Conditioned Medium Experiment

We hypothesised the formation of functional microvessels in JCC condition might be due to the production and secretion of some solutes produced and secreted due to direct interaction between ECs and FBs. To address this, we performed conditioned medium experiment. Conditioned medium is a harvested medium from cultured cells, in our case, from encapsulated cells within a fibrin matrix. Metabolites, growth factors, and extracellular matrix proteins secreted by the embedded cells can be found in the medium. Usually, as we did so, the medium harvested is diluted with fresh medium to replenish nutrients.

We employed 3-channel and 7-channel microfluidic devices to perform the experiment. 3-channel microfluidic devices were seeded with three different conditions, MC, JCC, and only FBs (**Fig 2.10 a**), while one 7-channel microfluidic device was seeded with PCC-2 (**Fig 2.10 b**). Conditioned medium was prepared by mixing the harvested growth medium from the cells embedded in fibrin gel with fresh medium. That dilutes growth factors in the harvested medium. The reason that ECs were paracrine co-cultured with ECs and FBs (PCC-2) was to make sure that the absence of microvessel formation in the devices fed with the conditioned medium was not due to dilution of growth factors because juxtacrine co-cultured ECs and FBs (in FB channels) would provide mono-cultured ECs (in EC channel) with the growth factors without any dilution. Confocal imaging of PCC-2 device and the devices fed with JCCCM and FBCM revealed that the conditioned media could not replicate the beneficial effects of actual juxtacrine co-culture. It is worth mentioning that microvessels formed in the JCC device fed with conditioned medium represented the microvessels formed in the JCC device fed with growth medium. This demonstrated that the lack of formation of microvessels in the devices fed with conditioned media was not due to deprivation of nutrients (**Fig 2.19**).
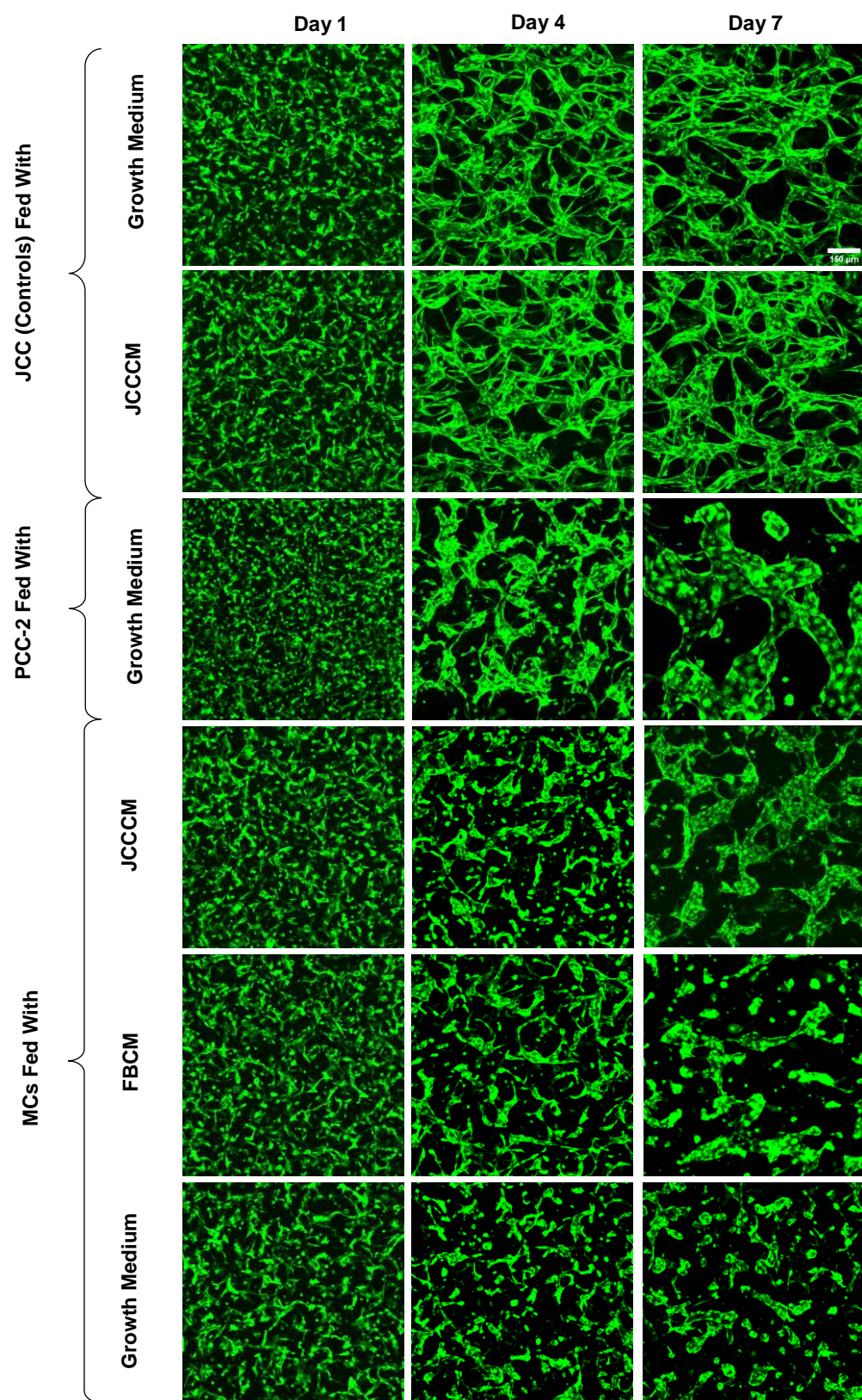
Fig 2.19: Conditioned medium experiment. *Confocal images of microvessel formation and development over one week under different feeding conditions. Scale bar, 150 μm.*

No significant increase was observed in the viability and coverage area when MC devices were fed with JCCCM and FBCM (P value >.05). However, we observed a significant increase in viability and coverage area of PCC-2 microvessels (***P value <.001, n=5), demonstrating that chemical interaction plays a vital role in microvessel formation (**Fig 2.20 a, b**). However, the microvessels formed did not represent features of microvessels formed in JCC devices proving that chemical interaction is not sufficient for the formation of well-connected, long-lasting, functional microvessels by itself.
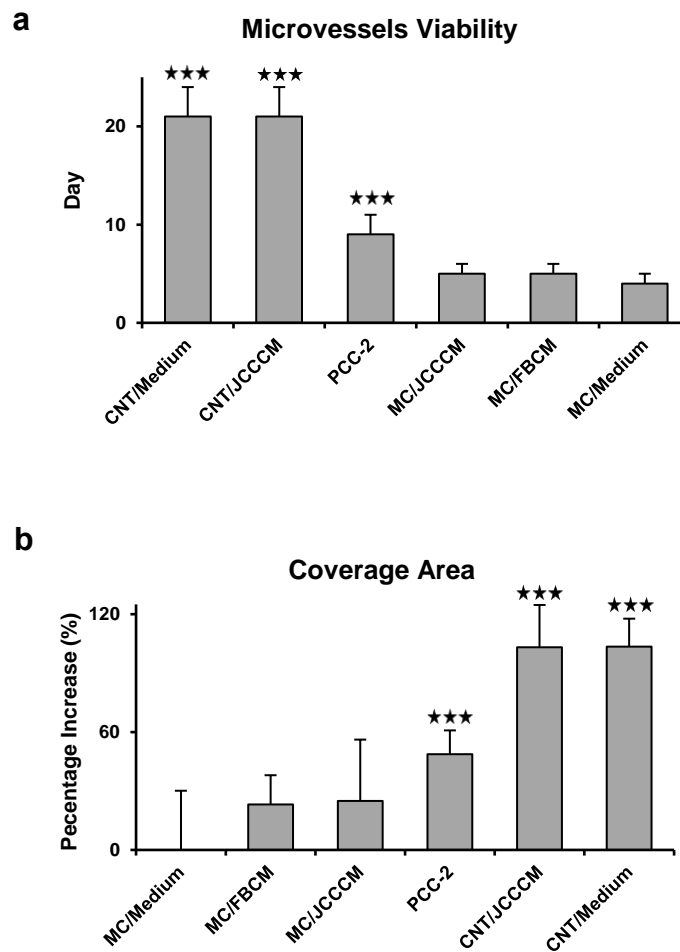
*Fig 2.20: Impact of conditioned medium on microvessels viability and coverage area. a) Bar chart representing microvessels viability in different conditions (***P value <.001). b) Bar chart comparing microvessel coverage area in different conditions (***P value <.001). Values normalised with respect to MC fed with growth medium on day 1. n=5.*

The function of the microvessels was then examined by dextran perfusion on day 7. **Fig 2.21 a, b** illustrates the set-up used to assess perfusability. Perfusion of dextran showed that unlike controls (JCC devices fed with growth medium and JCCCM), none of the structures formed in the devices fed with the conditioned medium was perfusable (**Fig 2.21 c**). Microvessels formed in PCC-2 condition were slightly perfusable (~ 3%) though compared to the perfusability of the controls (~ 98%), it was unremarkable (**Fig 2.21 d**).

The formation of functional microvessels in JCC device fed with JCCCM proves that the lack of formation of functional blood vessels in the devices fed with the conditioned medium was not due to a shortage of nutrients. However, the increase in coverage area in conditioned-medium-fed devices, as well as microvessel viability in PCC-2, showed that growth factors secreted by FBs are essential but not sufficient to stimulate the formation of functional blood microvessels.
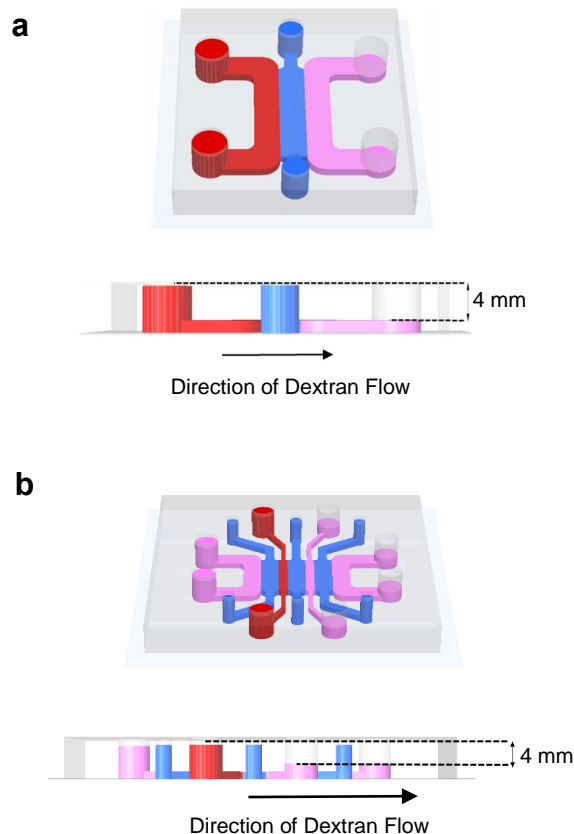
a

4 mm

Direction of Dextran Flow

b

4 mm

Direction of Dextran Flow

*(**Fig 2.21** continued on the next page. Legend follows)*

Microvessels   **Dextran Perfusion**   **Overlay**

*(**Fig 2.21** continued on the next page. Legend follows)*

78

d   **Microvessels Perfusability**
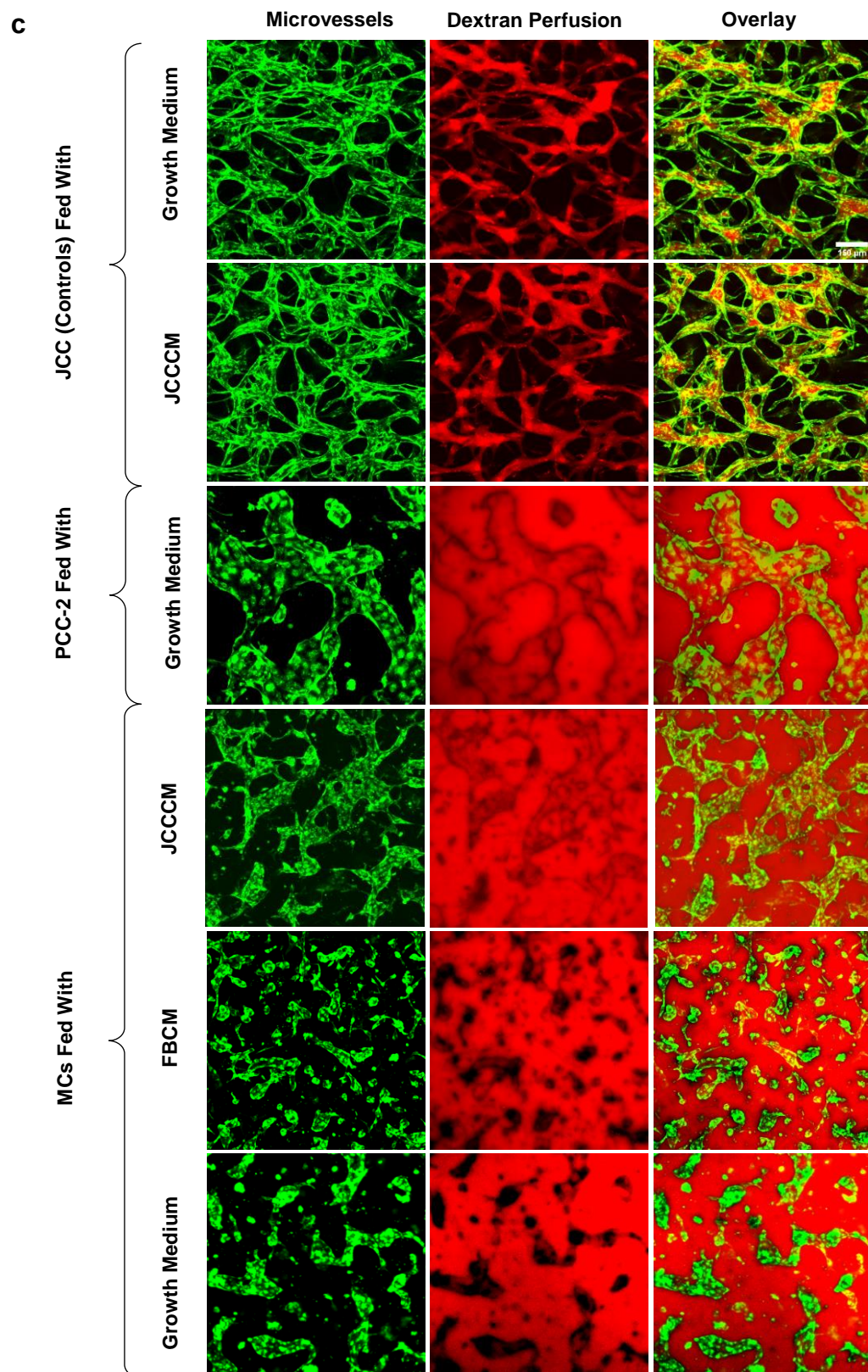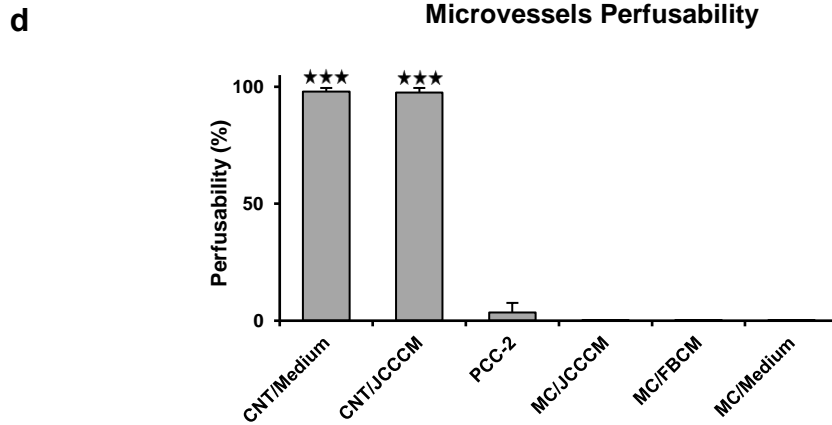
*Fig 2.21: Functionality of conditioned-medium-fed devices. a and b) Schematic representing experiment set-up. c) Unlike controls, dextran perfused into the bulk of hydrogel in the conditioned-medium-treated devices. Scale bar, 150 µm. d) Conditioned medium did not increase microvessels perfusability significantly compared to MC fed with growth medium (***P value <.001). n=5.*

2.3.5 3D Functional and Morphological Characterisation

Then, some methods were applied to accurately quantify some characteristics of JCC microvessels such as microvessel perfusability, permeability, length, diameter, coverage area, and topology on day 7 or over one week after culture. The microvessels were also stained for intercellular junctional molecular, VE-cadherin, and vascular EC adhesion molecule, PECAM-1.

2.3.5.1 Microvessels Perfusability

Perfusability was examined on days 1, 4, 7 post seeding. The schematics in **Fig 2.22 a** represent perfusability set-up. Perfusion of dextran showed that on day 1 dextran perfused into the hydrogel channel through the gel over 30 minutes because the cells had not formed microvessels yet. In contrast, on days 4 and 7, the tracer dye perfused into the hydrogel channel within a few seconds through microvessels and remained confined, proving that the microvessels were well-interconnected and well-defined. In other words, the microvessels were functional (**Fig 2.22 b**). Perfusability increased dramatically from day 1 to day 4 and peaked on day 7 (**Fig 2.22 c**).
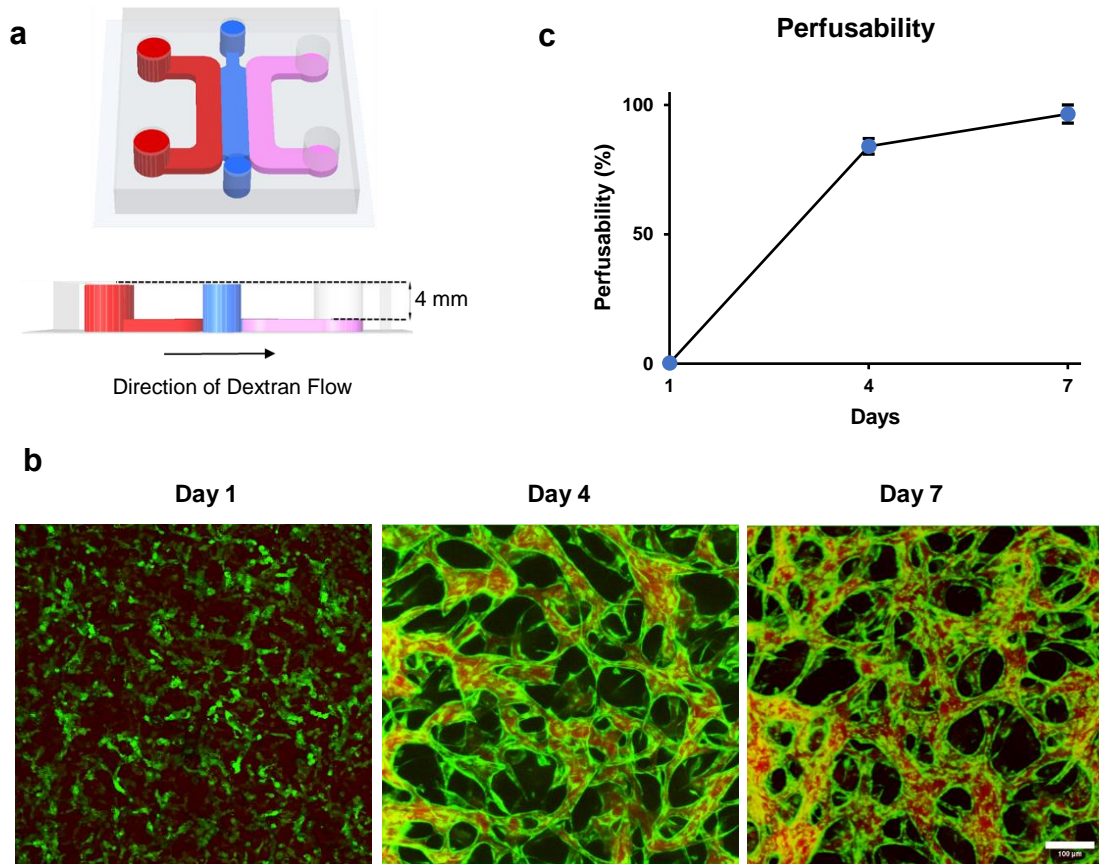
Fig 2.22: Perfusability of JCC microvessels. *a) Schematic of perfusability set-up b) Visualisation of dextran perfusion on day 1, 4 and 7 of culture. Scale bar, 100 µm. c) Graph showing perfusability over the course of one week calculated as percentage. n=9.*

2.3.5.2 Microvessels Permeability

To measure permeability, the average tracer intensity in both microvessels and interstitial space (voids) were calculated immediately after introducing the tracer (called T_0) and again after every 20 minutes for 1 hour, called T_1, T_2, and T_3, respectively (n=9).

It is worth mentioning that 3 days before permeability measurement, on day 4 after culture, ECs were seeded in the medium channels (**Fig 2.12**) to form a monolayer (**Fig 2.23 a, b**). This was to stop dextran perfusing to the hydrogel channel through the gel.

a

Blood Microvessels

EC Monolayer

b

Lip

EC monolayer

Blood Microvessels' Openings

Blood microvessels

ECs

Blood microvessel opening
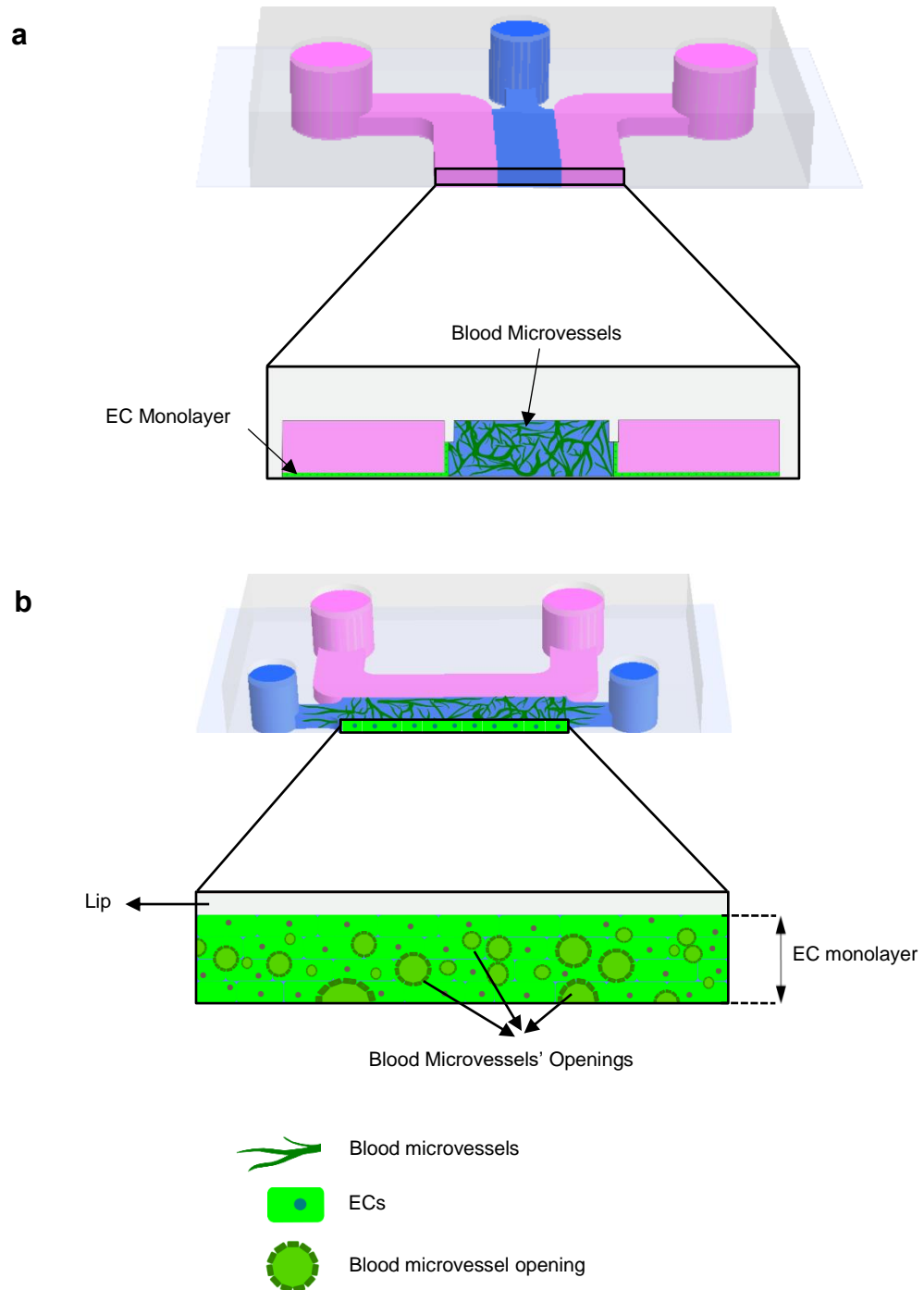
*Fig 2.23: **Formation of monolayer.** a) ECs formed a monolayer by day 7 in both medium channels for permeability experiments. This was to stop dextran perfusion to the vascularisation channel through the gel. b) Side view of the medium-hydrogel channel's edge representing the monolayer formed and openings.*

Fig 2.24 a, b represent permeability experiment set-up. **Fig 2.24 c** represents microvessels, voids, void area and perimeter. Equation **2.2** was used to calculate microvessel permeability coefficient (*P*).

$$P = \frac{I_{void}^{t_i} - I_{void}^{t_0}}{\bar{I}_{vessel} - \bar{I}_{void}} \times \frac{Area}{Perimeter} \times \frac{1}{t_i - t_0} \qquad \textbf{(Eq: 2.2)}$$

$$\bar{I}_{vessel} = \frac{I_{vessel}^{t_i} + I_{vessel}^{t_0}}{2}$$

$$\bar{I}_{void} = \frac{I_{void}^{t_i} + I_{void}^{t_0}}{2}$$

where $I_{void}^{t_i}$ and $I_{void}^{t_0}$ are the intensity of the tracer dye within the void at the time of interest (t_i) and immediately after injection of the tracer (t_0), respectively. $\bar{I}_{vessel}$ and $\bar{I}_{void}$ stand for the average intensity of the tracer dye within the microvessels and voids, respectively.

Fig 2.24 d shows the initial intensity of the tracer dye within a void at T_0 and the intensity of dextran in the same void at T_3, one hour after the injection of the tracer. We measured the permeability of the microvessels to 10 kDa dextran to be 2.44E-07 cm/s (T_0-T_1), 2.60E-07 cm/s (T_0-T_2), and 2.68E-07 cm/s (T_0-T_3). We observed a slight increase in the permeability over time (**Fig 2.24 e**). However, the increase was not significant (*P* value >.05). The average permeability was measured to be 2.57E-0.7 ± 1.23E-08 (**Fig 2.24 f**).
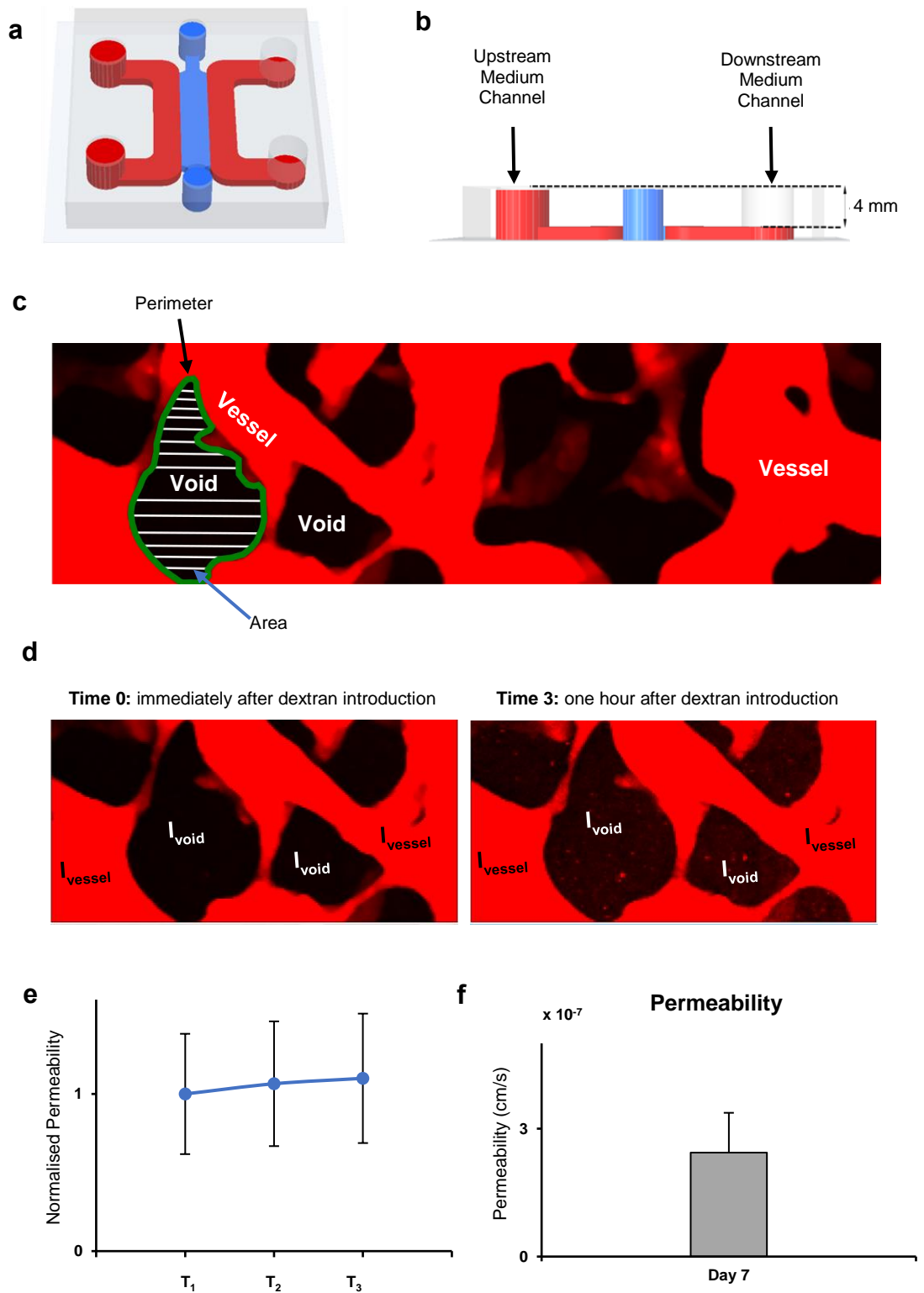
Fig 2.24: Permeability. *a) Schematic of permeability measurement set-up. b) Downstream medium channel was less filled to create a head pressure, needed to initiate dextran perfusion. c) Microvessels and voids visualisation. d) Intensity of dextran in voids increased over one hour. e) Bar chart representing permeability values over time. f) Bar chart representing permeability coefficient on day 7. n=9.*

2.3.5.3 Microvessel Length

The microvessels formed in our microfluidic device was composed of microvessels with a diverse range of lengths. We measured an average vessel length of 96 microns. Individual vessel lengths spanned a range of 10-540 microns. The histogram in **Fig 2.25** represents the frequency of different microvessel lengths (n=3).
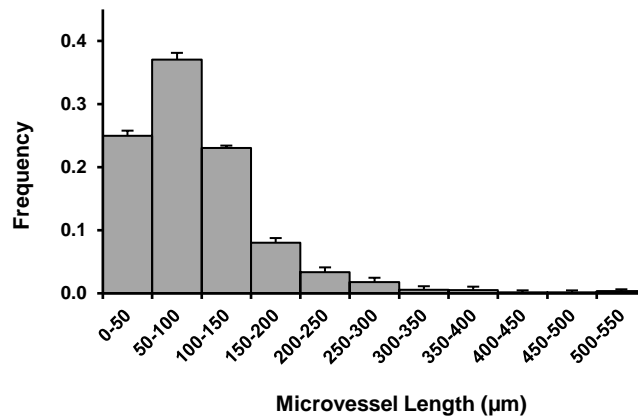
Fig 2.25: Microvessels length frequency. *Histogram representing the distribution of the microvessel lengths. n=5.*

2.3.5.4 Microvessel Diameter

As mentioned in the method section, the microvessel diameters were measured by drawing a line from one edge of a microvessel to the other edge (**Fig 2.26 a, b**). The results revealed that the JCC microvessels showed a heterogeneous range of diameters made up of capillaries (2-10 µm) and venules and arterioles (10-100 µm). It is worth mentioning that individual microvessel diameter spanned a range of 2-550 µm with an average of 30.15 µm (**Fig 2.26 c**).
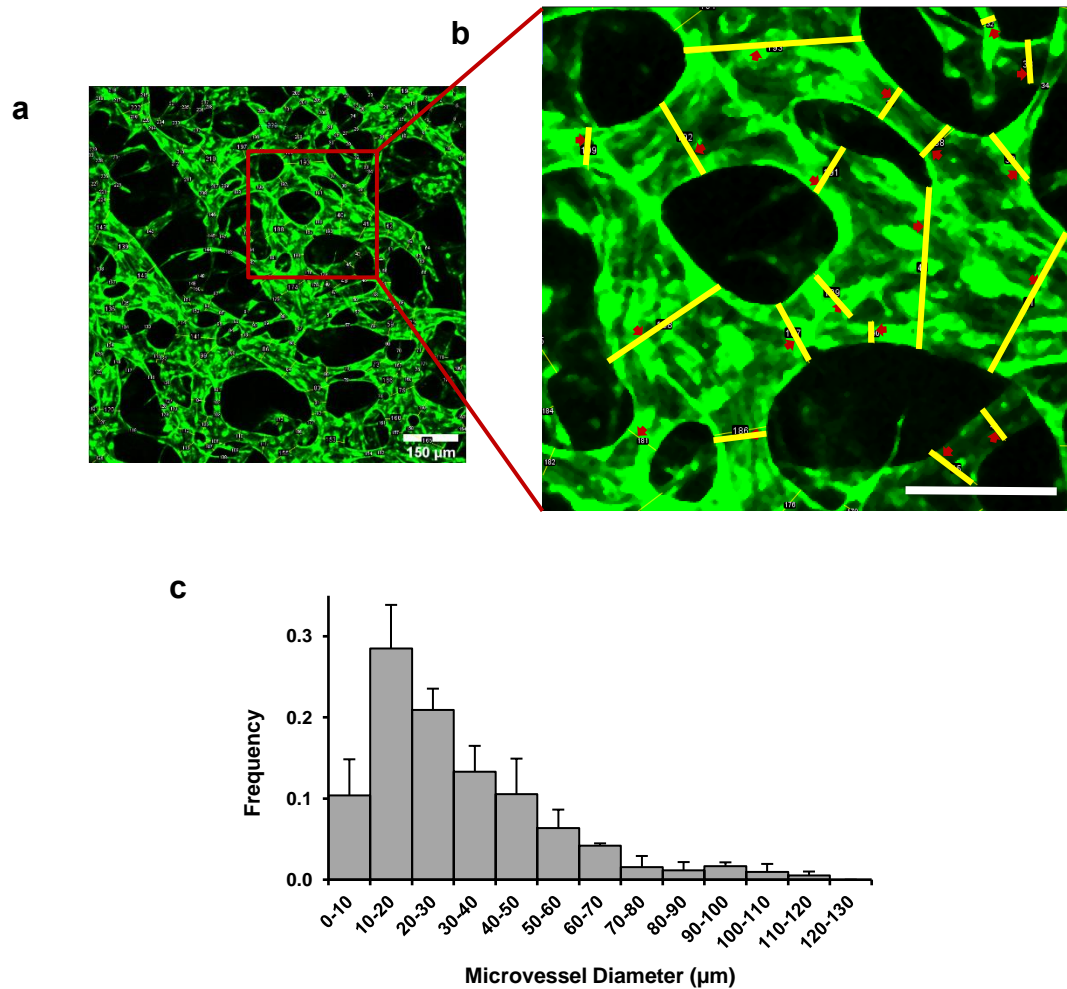
Fig 2.26: Microvessels diameter. *a) Diameter of the microvessels were measured at 534 points. Scale bar, 150 μm. b) Small arrows in red show some of the lines (in yellow) drawn to measure vascular diameter. Scale bar, 100 μm. c) Histogram representing the distribution of microvessel diameters. n=3.*

2.3.5.5 Microvessel Coverage Area

Microvessel coverage area was measured on day 1, 4 and 7. At the tissue level, the microvessel coverage area significantly increased from day 1 to day 4 and slightly increased over the next 3 days. **Fig 2.27** represents the microvessel coverage area over the course of one week.

85

Microvessel Coverage Area
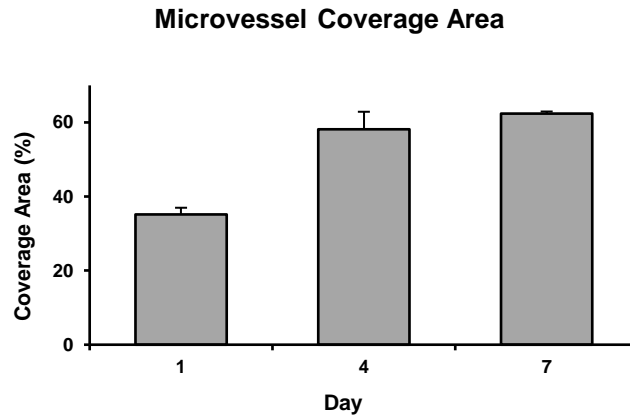
*Fig 2.27: **Microvessel coverage area.** Microvessel coverage area increased from day 1 to day 7. n=5.*

2.3.5.6 Microvessel Topology

We assessed microvessel topology, including microvessel branching, number of junctions, average branch length, and maximum branch length. We calculated the number of branches to be 653 ± 73 mm^{-2} (**Fig 2.28 a**) and the number of junctions to be 402 ± 35 mm^{-2} (**Fig 2.28 b**).

a   **b**
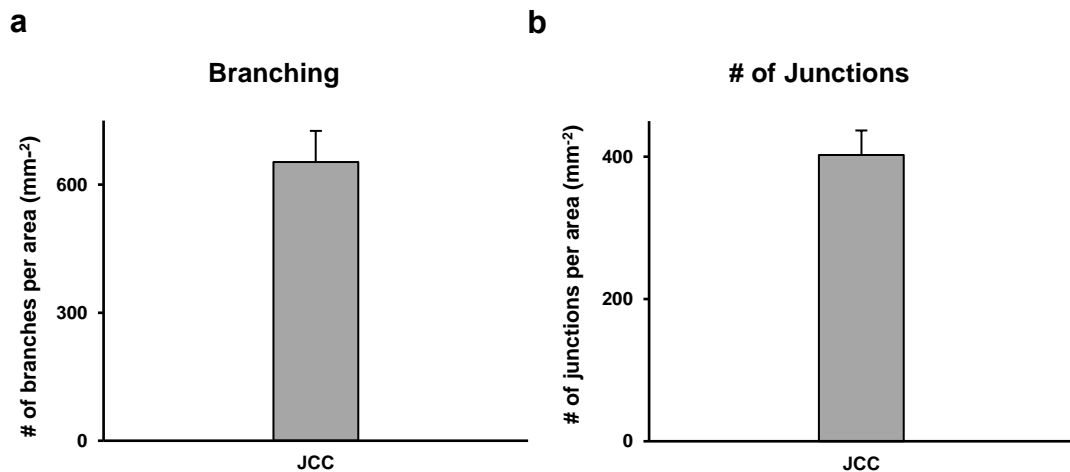
*Fig 2.28: **Microvessels topology.** a) Bar chart representing number of microvessels branches per area b) Bar chart representing number of junctions per area. n=9.*

As mentioned in section **2.3.5.3** microvessel average and maximum branch length were measured to be 96 and 540 μm, respectively.

2.3.5.7 Microvessel Staining

ECs are tightly connected to their neighbouring cells via VE-Cadherin located at junctions between two adjacent ECs. Being the major endothelial adhesion molecule, VE-cadherin plays a solid role in the regulation of cellular junctions, blood vessel formation, vascular permeability and leukocyte extravasation[156]. In addition to VE-Cadherin, PECAM-1, a heavily glycosylated transmembrane homophilic protein functions as a vascular EC adhesion molecule[156,157].

Apart from dextran's presence in microvessel to show the integrity and the presence of a tight endothelial barrier, which is one of the most important features of functional microvessels, the microvessels formed in the microfluidic device were immunostained with two antibodies that specifically targeted VE-Cadherin and PECAM-1. The immunostaining confirmed the presence of a tight endothelial barrier (**Fig 2.29**), demonstrating the microvessels' integrity.

a
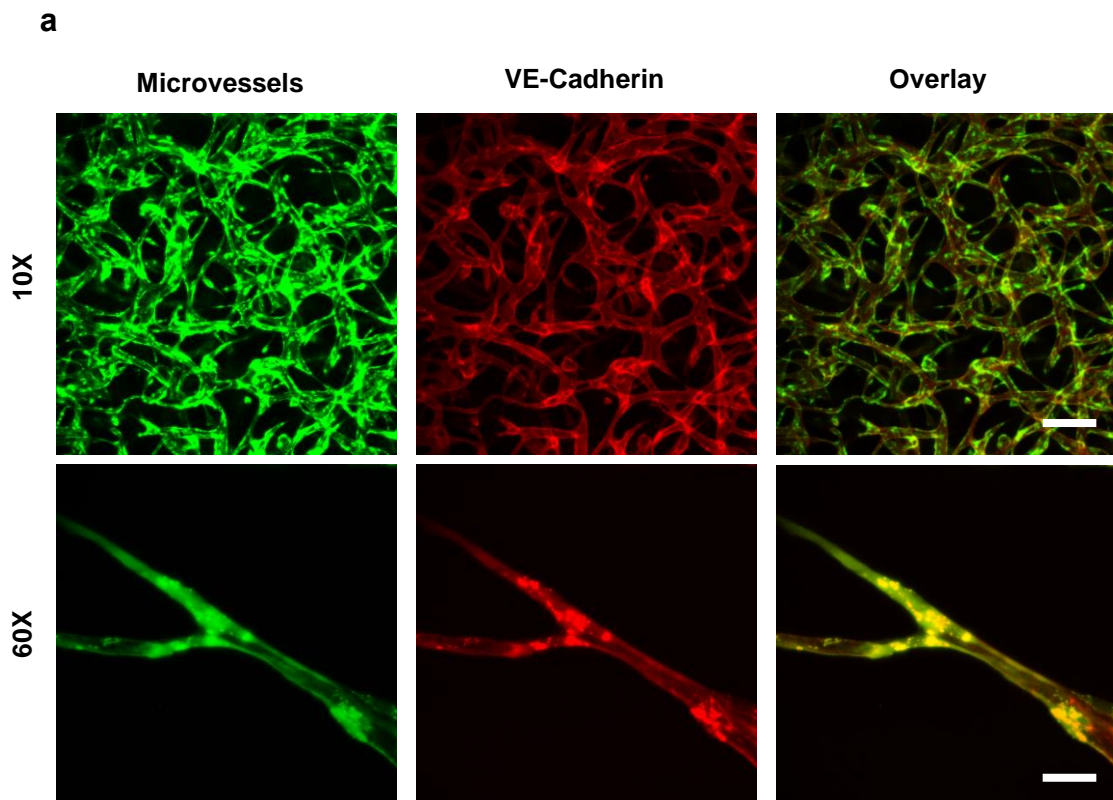
*(**Fig 2.29** continued on the next page. Legend follows)*
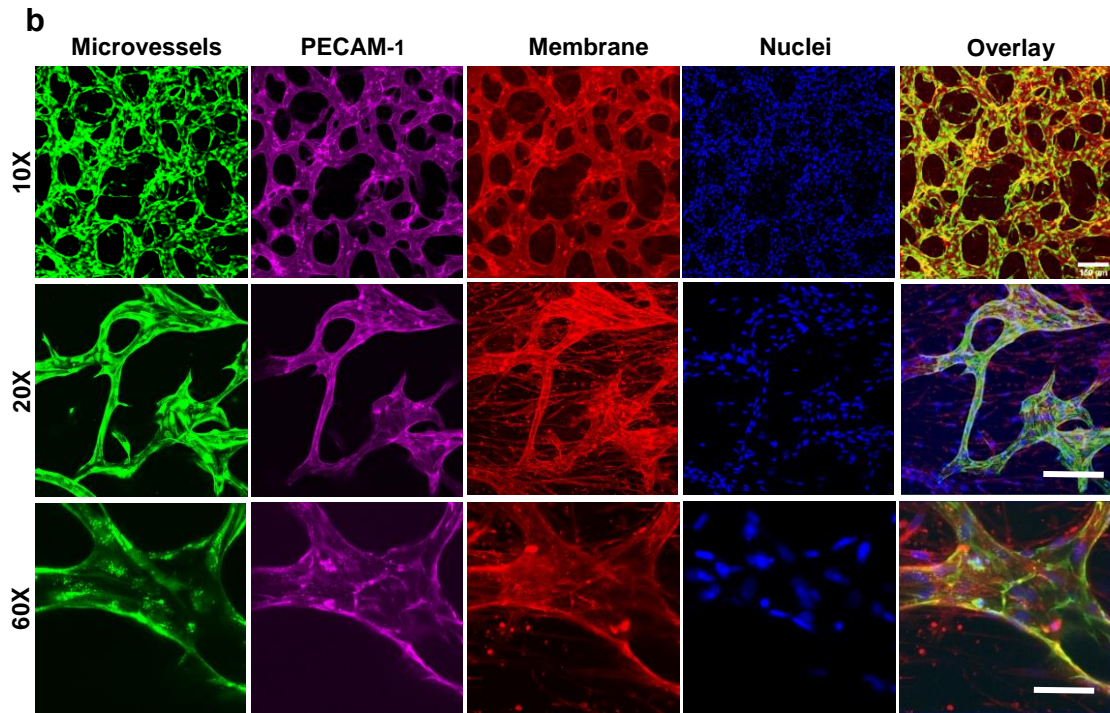
Fig 2.29: Engineered 3D microvessels characterised by immunostaining. *a)*
Immunostaining of the microvessels for VE-Cadherin (Red). Scale bars, 100 and 150 μm,
respectively. b) Immunostaining the microvessels for PECAM-1 (Magenta). Scale bars, 150,
150 and 50 μm, respectively.

2.3.6 Impact of FBs Density on Microvessels Formation

In fulfilment of assessing the impact of lower number of FBs on the networks,
we decided to co-seed ECs with a fewer number of FBs (JCC 4X). The 3D
confocal images showed that ECs were yet able to self-assemble and form
microvessels by day 7 in the presence of lower concentration of FBs. However,
the microvessels were remarkably different from JCC 2X in morphology (**Fig
2.30 a**). Characterising the microvessels showed that coverage area reduced
by ~53% ([***]*P* value <.001, n=4, **Fig 2.30 b**). Also, ECs co-cultured along with
a lower number of FBs tended to produce lumens with larger diameter ([***]*P*
value <.001, n=4, **Fig 2.30 c**).
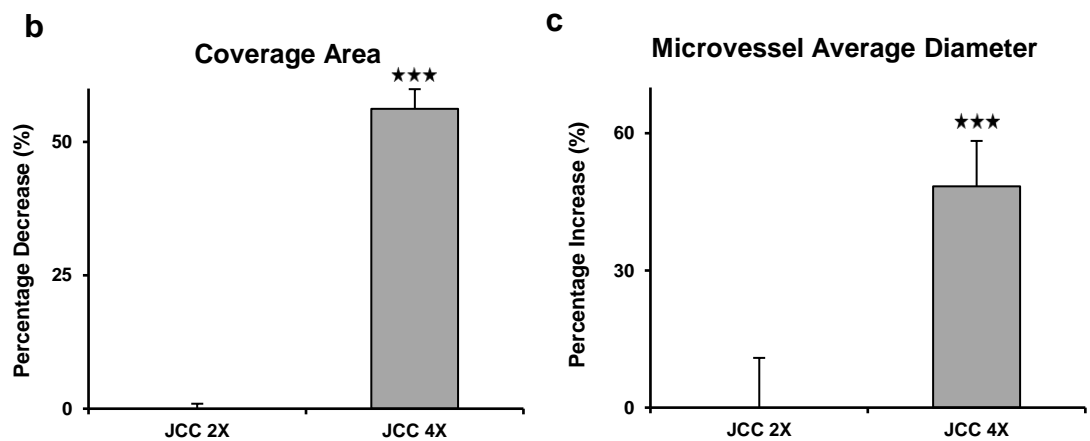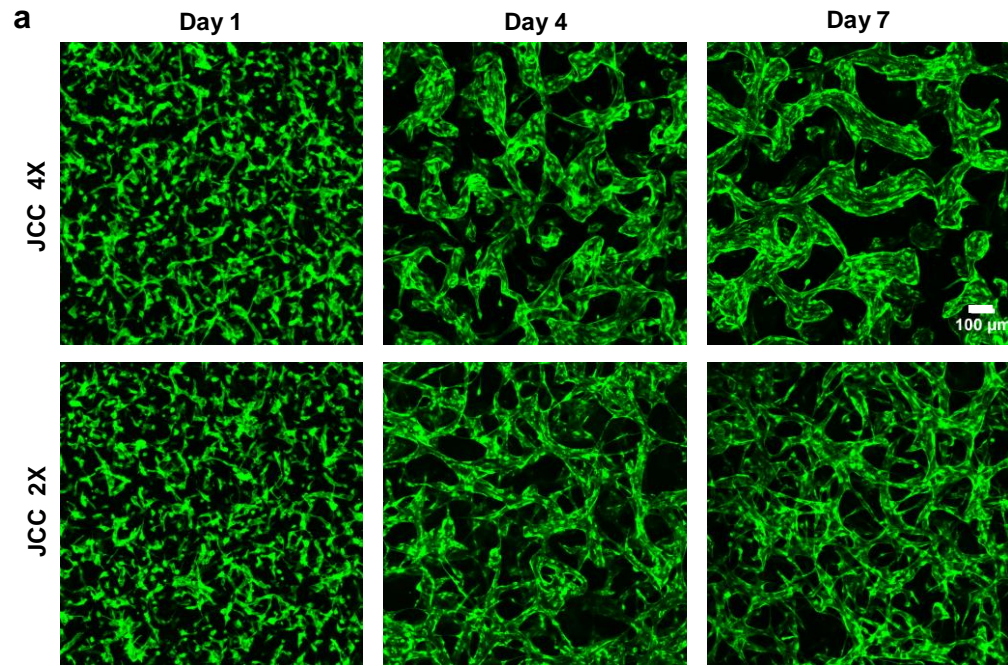
Fig 2.30: Impact of lower number of FBs on vascularisation. *a) Comparison of JCC 4X and JCC 2X microvessel formation and morphology over the course of 1 week. Scale bar, 100 µm. b) Bar chart comparing coverage area in JCC 2X and JCC 4X (***P value <.001) c) Bar chart comparing microvessel diameter in JCC 2X and JCC 4X (***P value <.001). n=4. Normalised with respect to control values.*

We also investigated the impact of the lower density of FBs on microvessel topology, including branching, the number of junctions, average and maximum branch length. The image data analysis showed JCC 4X microvessels were different from JCC 2X microvessels in morphology and topology. In such a way that a drastic decrease was observed in branching (**P value =.0012, n=4,

Fig 2.31 a) and the number of junctions ($^{***}P$ value <.001, n=4, **Fig 2.31 b**) whereas there was a significant increase in the average branch length of the microvessels ($^{*}P$ value =.043, n=4, **Fig 2.31 c**) and maximum branch length of the microvessels ($^{**}P$ value =.0019, n=4, **Fig 2.31 d**).
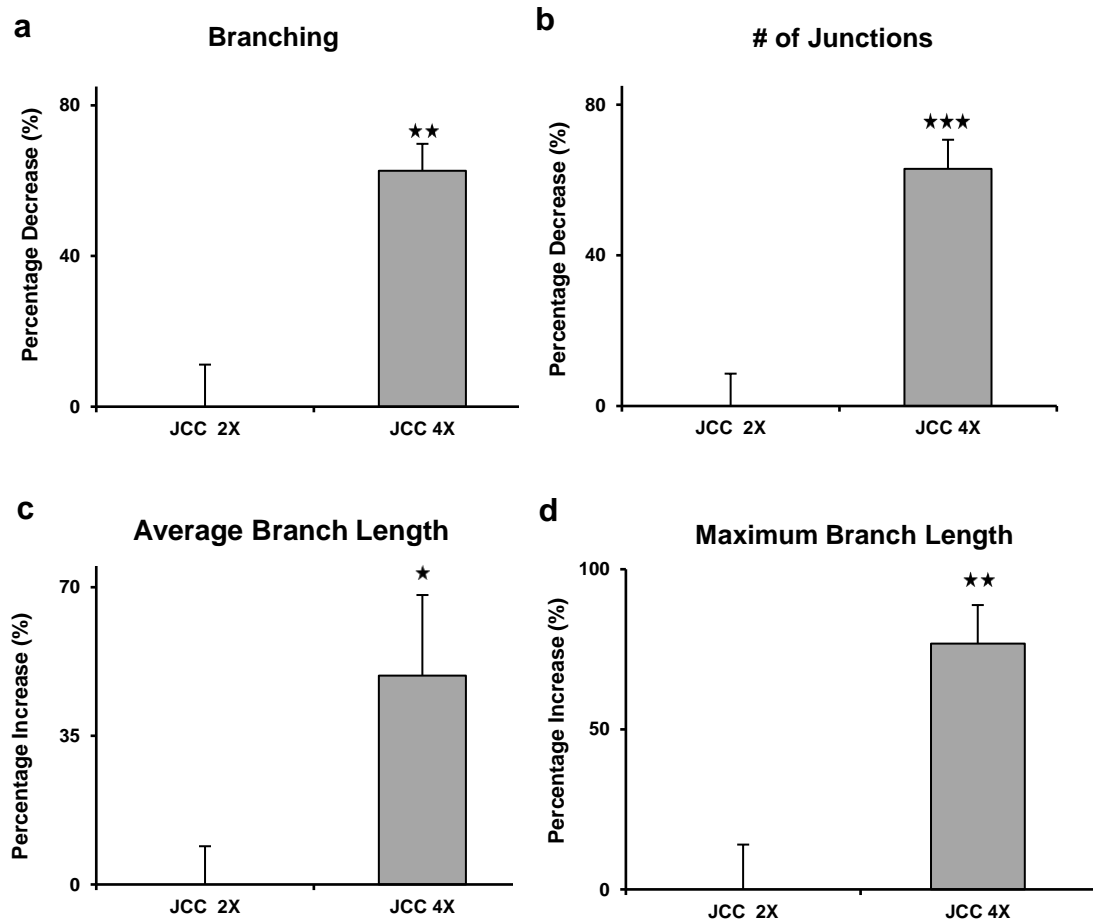
Fig 2.31: Comparison of microvessels topology and diameter in JCC 4X and JCC 2X. *a) Co-culturing ECs with a lower number of FBs resulted in reducing branching ($^{**}P$ value =.0012) and b) the number of junctions ($^{***}P$ value <.001), whereas that led to a significant increase in c) average branch length ($^{*}P$ value =.043) and d) maximum branch length ($^{**}P$ value =.0019), n=3. Normalised with respect to control values.*

Perfusion of the tracer dye revealed that in addition to the difference in microvessel morphology and topology, microvessels function decreased remarkably by reducing the number of FBs, as not all the microvessels formed

were perfusable ($^{***}P$ value <.001, n=5, **Fig 2.32 a**). Quantification of the data showed that the perfusability of the microvessels in JJC 4X dropped by ~ 35% (**Fig 2. 32 b**).
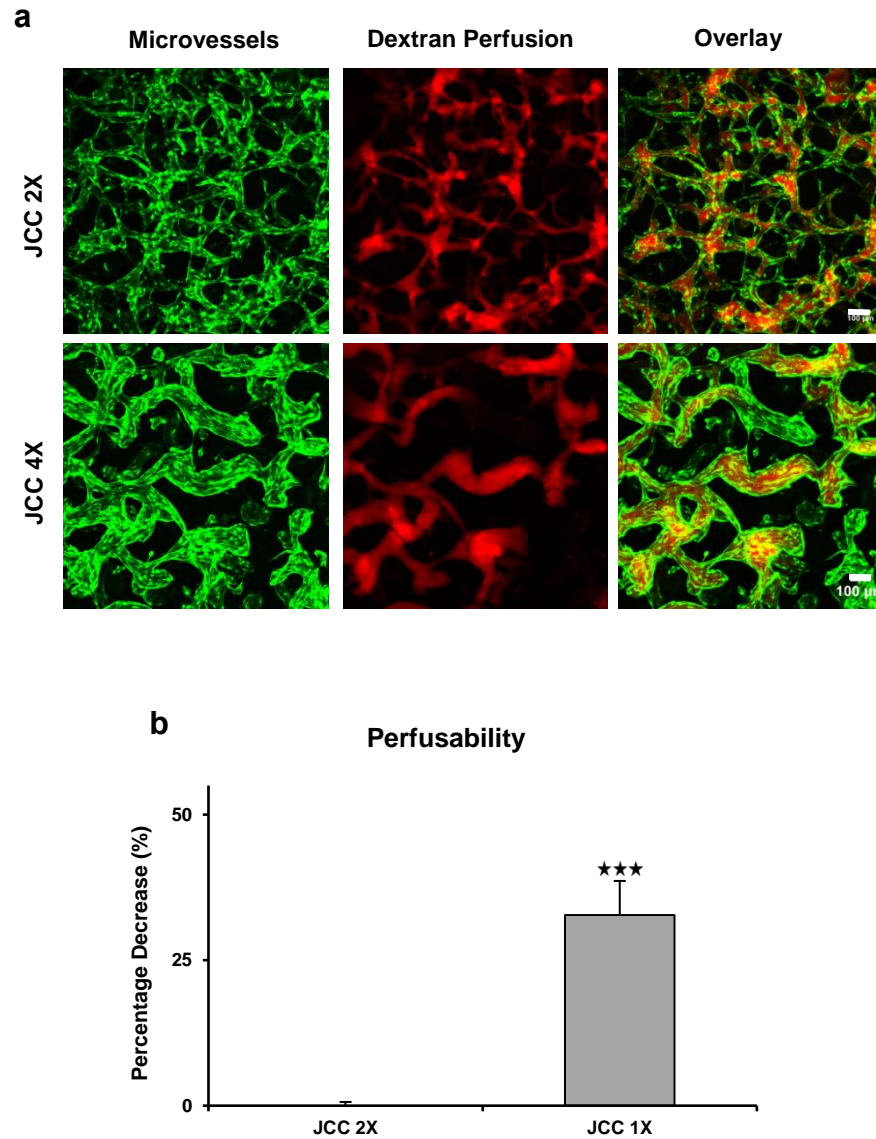
Fig 2.32: Impact of FBs density on microvessel function. *a) Not all the microvessels formed in JCC 4X were perfusable. Scale bar, 100 µm. b) Perfusability decreased significantly by reducing the number of FBs ($^{***}P$ value <.001, n=5.) Normalised to control value.*

2.4 Discussion and Conclusion

Formation of new blood vessels occurs through either vasculogenesis in early embryonic development or angiogenesis during late embryonic development and adulthood. ECs, the most important participants in vasculogenesis and angiogenesis, self-assemble and form tubules. However, despite their ability to develop microvessels, the vessels regress within 2-3 days in the absence of heterotypic cell partners. Many studies have shown that the presence of FBs, as partners of ECs, is essential for vessel formation, mainly due to producing and secreting growth factors[12–17,105–107,158,159]. Consistent with these studies our findings show that the physical interaction between ECs and FBs is essential for forming functional microvessels, as unlike juxtacrine co-cultured ECs and FBs, mono-cultured ECs and paracrine co-cultured ECs with FBs fail to form functional microvessels.

Hypothesising that the formation of functional microvessels might be due to secretion of some solutes and growth factors produced due to direct interaction between ECs and FBs when ECs and FBs were juxtacrine co-cultured, we treated mono-cultured ECs with the different conditioned media, including conditioned medium from JCC condition. A slight increase in the microvessels coverage area indicates that while soluble factors are essential for microvessel formation, they are not sufficient to trigger ECs self-assembly into functional microvessels. This finding is consistent with several studies, demonstrating that conditioned medium alone fails to stimulate microvessel formation by different types of ECs[115,159,160]. Knowing that dilution of harvested medium with fresh growth medium to replenish nutrients would dilute soluble factors, paracrine mono-cultured ECs (in EC channel) were co-cultured with FBs and ECs (in FB channels, PCC-2) to provide ECs with soluble factors without any dilution. Despite this, ECs failed to form functional microvessels, demonstrating inability of soluble factors to encourage ECs to form functional microvessels. When a device seeded with JCC condition was treated with conditioned medium from another JCC device (JCCCM), ECs retained their

ability to form fully functional microvessels proving that the lack of microvessel formation in the devices fed with the different conditioned medium was not due to a shortage of nutrients. However, despite having several conditions, there might exist some known or unknown labile factors as important drivers of vasculogenesis that our PCC systems and conditioned media fail to provide mono-cultured ECs with.

Many research groups have used dextran perfusion to investigate microvessel functionality, perfusability and permeability[161–167]. We examined our microvessels' function both by dextran perfusion and tight junction staining. Dextran perfusion revealed that the microvessels were fully functional, and tight junction staining demonstrated their integrity. We measured microvessel permeability to 10 kDa dextran to be 2.57E-0.7 ± 1.23E-08 cm/s, similar to the *in vitro* value reported by Lee *et al.* (2.21 ± 1.96E-0.7 cm/s)[168] and *in vivo* value reported by Yaun *et al.* (2.4E-0.7 ± 0.1E-0.7 cm/s)[169].

Intriguingly, our results also demonstrate that a certain number of FBs is critical to lead ECs to form functional microvessels. We observed significant changes in microvessel morphology and a considerable decrease in the microvessel coverage area, number of branching, number of junctions, and perfusability when ECs were co-cultured with a fewer number of FBs. Additionally, the reduced FBs density correlates with increased vessel diameter. These findings are in good agreement with an earlier study by Chen *et al*. They assessed the impact of low and high FB density on vascularisation by co-culturing HUVECs and cord blood endothelial progenitor cell-derived ECs with FBs. Their results revealed that both ECs developed less inter-connected, less dense microvessels within four days in the presence of a lower density of FBs[170].

Altogether, our data shows that not only the presence of fibroblasts is crucial to the formation of microvessels but also the direct physical interaction between fibroblasts and endothelial cells is essential for the formation and stabilisation of functional blood microvessels.

3 Inhibition of Mechanotransduction Genes in FBs and ECs

3.1 Introduction

Our preliminary results proved that direct interaction between FBs and ECs (JCC) is essential for the formation and stabilisation of functional blood microvessels. RNAseq experiment done in Kamm's lab revealed that when juxtacrine co-cultured, ECs and FBs express different gene profiles. In such a way that some genes belonging to mechanotransduction and chemotransduction pathways are upregulated in both cell types (data not shown). Hence, we sought to investigate the impact of these genes on microvessel formation, morphogenesis, topology, and function. To that end, we perturbed our interest genes (YAP, Src, Wnt/β-catenin, RhoA, and FAK belonging to mechanotransduction pathway and IGF-1, EED, and TGFβ belonging to chemotransduction pathway) in both ECs and FBs by treating them with gene-specific small molecule inhibitors (chemical inhibition).

3.2 Methods

In this section, the methods used to achieve the goals of chapter 3 have been mentioned in detail.

3.2.1 Impact of Dimethyl Sulfoxide (DMSO) on Microvessels

JCC devices were treated with different DMSO concentrations (10, 15, and 20 µL/mL) for one week. On days 1, 4 and 7, z-stack confocal images were taken to track the formation of microvessels. The microvessels formed were characterised for topology and function.

3.2.2 Impact of DMSO on Cell Viability and Proliferation

- Cell seeding and DMSO treatment: To assess the impact of DMSO on cell viability and proliferation, ECs ($2 \times 10^{+5}$/well) were seeded in a rat tail collagen 1-coated 6-well cell culture plates and were fed with growth medium. The day after, DMSO (10, 15 and 20 µL/mL) was reconstituted in growth medium. The seeded cells were treated with DMSO-Medium. One well was fed with growth medium as control.

Notes: In all experiments performed to measure cell viability and proliferation:

- The inhibitors of interest were diluted in EGM2-MV to treat both ECs and FBs because when the cells were encapsulated in a fibrin matrix and injected in a microfluidic device to form microvessels, they were fed with EGM-2MV.
- When the cells were treated with Inhibitor-Medium, the medium was not replaced with fresh medium for 4 days to avoid losing dead cells.

- Cell viability and proliferation measurement: Four days after treating the cells with different concentrations of DMSO, the cells were dissociated, spun down and re-suspended in 1 mL of growth medium. Using a NucleoCounter machine (NC-3000-Chemometec/Denmark), cell viability and cell number were measured. In such a way, approximately 60 µL of cell suspension was

loaded into a specialised cell sampling and staining device, Via1-Cassette™ (Chemometec/Denmark). The device contains two immobilised fluorophores, acridine orange (AO) and 4′,6-diamidino-2-phenylindole (DAPI). AO stains all cells in the sample, both live and dead cells, thus providing a total count; DAPI stains the dead cells.

The same process was performed to assess the DMSO impact on FB viability and proliferation (No coated 6-well cell culture palates were used to culture FBs).

3.2.3 Impact of Small Molecule Inhibitors on Microvessels

In this step of the project, the impact(s) of several small molecule inhibitors were investigated on microvessel formation. The small molecule inhibitors either targeted genes belonging to the mechanotransduction pathways or genes belonging to the chemotransduction pathways. **Table 3.1** shows the small molecule inhibitors, pathways and genes targeted by them.

Table 3.1: List of small molecule inhibitors, pathways and their target genes.

Pathway	Small molecule Inhibitors	Gene of Target
Mechanotransduction Pathway	Verteporfin	Yes-Associated Protein (YAP)
	PF-573228	Focal Adhesion Kinase (FAK)
	XAV939	Wnt/β-catenin
	CCG-1423	RhoA
	PP2	Src
Chemotransduction Pathway	Picropodophyllotoxin	Insulin-Like Growth Factor 1 (IGF-1)
	SB-431542	Transforming Growth Factor Beta (TGFβ)
	A-395	Embryonic Ectoderm Development (EED)

3.2.3.1 Impact of Small Molecule Inhibitors on Cell Viability and Proliferation

To find the desired concentration(s), which did not affect the cells' viability and proliferation, at first, we treated both ECs and FBs with different concentrations of each small molecule inhibitor to measure their viability and proliferation after 4 days. **Table 3.2** summarises different concentrations of each small molecule inhibitor as well as the solvent in which the inhibitors were reconstituted.

Table 3.2: Solvents and different concentrations of small molecule inhibitors.

Small molecule Inhibitors	Solvents	Concentrations (µM)					
Verteporfin	DMSO	0.25	0.5	1	3	5	-
PF-573228	DMSO	0.1	0.5	1	5	10	-
XAV939	DMSO	10	20	30	40	-	-
CCG-1423	DMSO	1	3	5	10	20	-
PP2	DMSO	1	5	10	20	40	-
Picropodophyllotoxin	DMSO	0.25	0.5	1	3	5	10
SB-431542	DMSO	0.1	1	10	20	40	-
A-395	Water	0.1	0.5	1	5	10	-

The impact of small molecule inhibitors on cell viability and proliferation was assessed as described in section **3.2.2**. The difference was that we had two wells as controls, one treated with growth medium and the other one treated with Solvent-Medium (DMSO-Medium/Water-Medium).

3.2.3.2 Impact of Small Molecule Inhibitors on Microvessels

We treated JCC devices with the desired concentrations of small molecule inhibitors, summarised in **Table 3.3**, for one week. Two JCC devices were fed with growth medium and Solvent-Medium, respectively, as controls. On days 1, 4, and 7, z-stack confocal images were taken to track microvessel formation.

Table 3.3: Desired concentrations of small molecule inhibitors chosen to treat JCC devices.

Small Molecule Inhibitors	Concentrations (µM)		
Verteporfin	0.25	-	-
PF-573228	0.1	0.5	-
XAV939	10	20	-
CCG-1423	1	3	-
PP2	1	5	-
Picropodophyllotoxin	0.25	-	-
SB-431542	0.1	1	10
A-395	0.1	0.5	-

3.3   Results

3.3.1   Impact of DMSO on Microvessels

DMSO was used as the major solvent to reconstitute small molecule inhibitors. However, many studies have proved the toxic effects of this solvent on cells[171–173]. To investigate the impact of DMSO on microvessels and determine the highest DMSO concentration that did not affect microvessel formation and characteristics, we treated JCC devices with different DMSO concentrations (10, 15, and 20 µL/mL) over the course of one week.

3D confocal imaging showed that excluding 20 µL/mL of DMSO, in both growth medium-treated devices (control) and DMSO-treated devices, ECs retained their ability to form microvessels. As **Fig 3.1** represents, we observed no significant difference between the microvessels formed in the device treated with 10 µL/mL of DMSO and control in terms of morphology, coverage area, and microvessel diameter. However, the microvessels formed in the device treated with 15 µL/mL of DMSO were significantly different morphologically, so that when treated with 15 µL/mL of DMSO, ECs tended to form less dense and less branched microvessels with larger diameters (**Fig 3.1 a**). In other words, the microvessels coverage area decreased significantly ($^*P$ value =.012, n=5, **Fig 3.1 b**). In contrast, microvessel diameter increased remarkably ($^{***}P$ value <.001, n=3) in the device treated with 15 µL/mL of DMSO in comparison to control (**Fig 3.1 c**).

*(**Fig 3.1** continued on next page. Legend follows)*

b

Microvessels Coverage Area

c

Microvessels Average Diameter
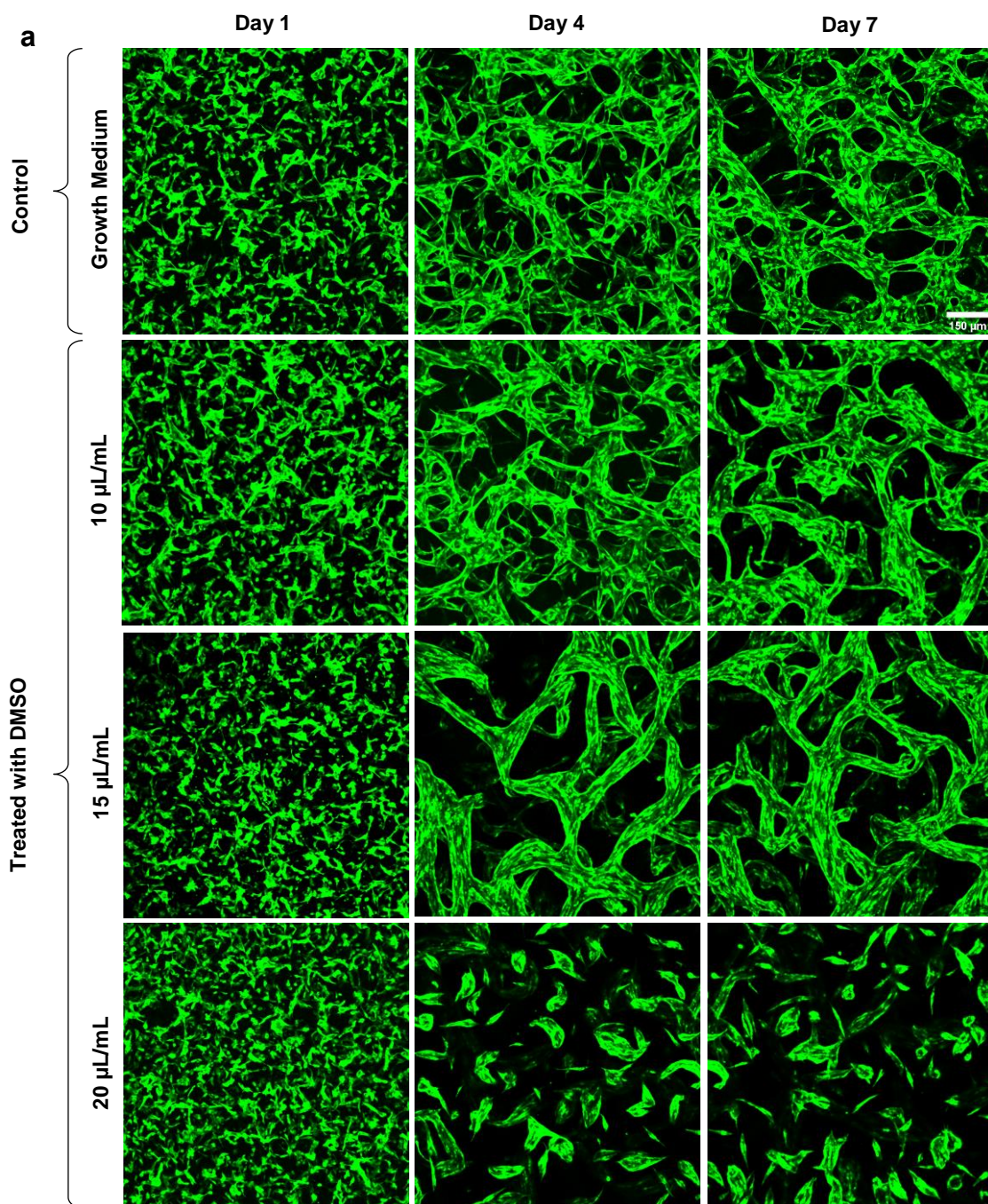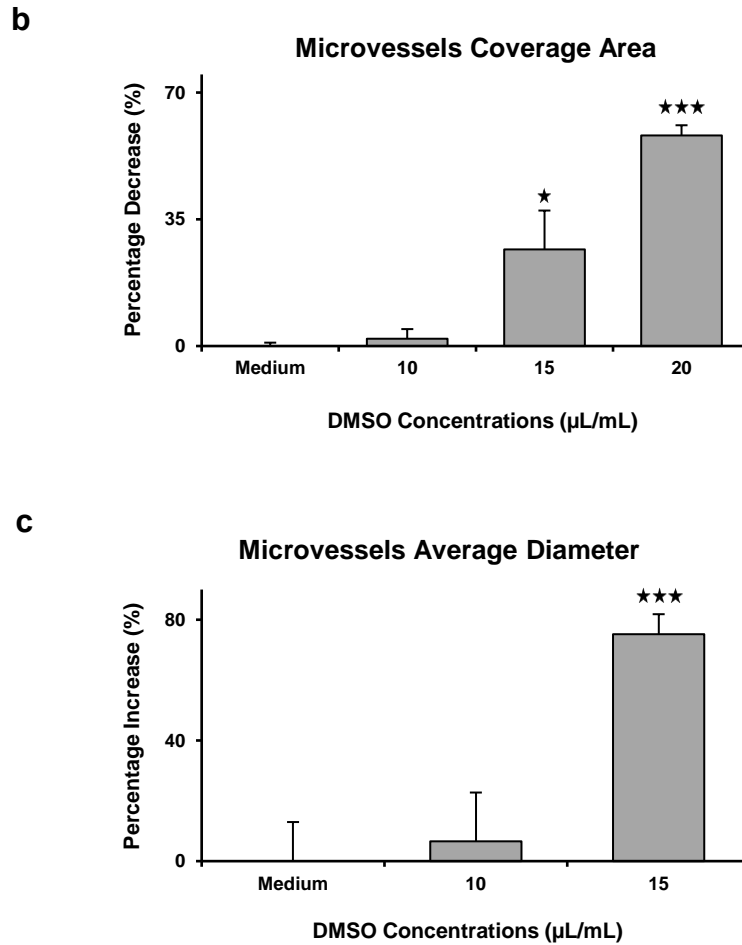
Fig 3.1: Impact of DMSO on microvessel formation. a) Confocal images of microvessel formation in different conditions over the course of one week. Scale bar, 150 µm. b) Bar chart representing changes in microvessel coverage area as a result of DMSO treatment. *P value = .012, and ***P value <.001, respectively. n=5. c) Bar chart comparing microvessel diameter in different conditions. ***P value <.001. n=3. Normalised with respect to control values.

We then analysed our image data to investigate the impact of DMSO on the topology of the microvessels. We measured microvessels branching, the number of microvessels junctions, average branch length, and maximum branch length. Similar to microvessels morphology, coverage area, and diameter, no significant difference was observed between the microvessels treated with 10 µL/mL of DMSO and control (P value >.05, n=5). Conversely, we found remarkable changes in the microvessels treated with 15 µL/mL of DMSO compared to control. There was a significant decrease in microvessel branching ($^{**}P$ value =.007, n=5) and the number of microvessels junctions ($^{**}P$

value =.005, n=5). At the same time, we observed a significant increase in average branch length (*P value =.029, n=5) as well as maximum branch length (*P value =.014, n=5) when the co-encapsulated cells were treated with 15 μL/mL of DMSO (**Fig 3.2**). We did not analyse our 3D confocal images for the device treated with 20 μL/mL of DMSO, as no microvessel formed in that condition.
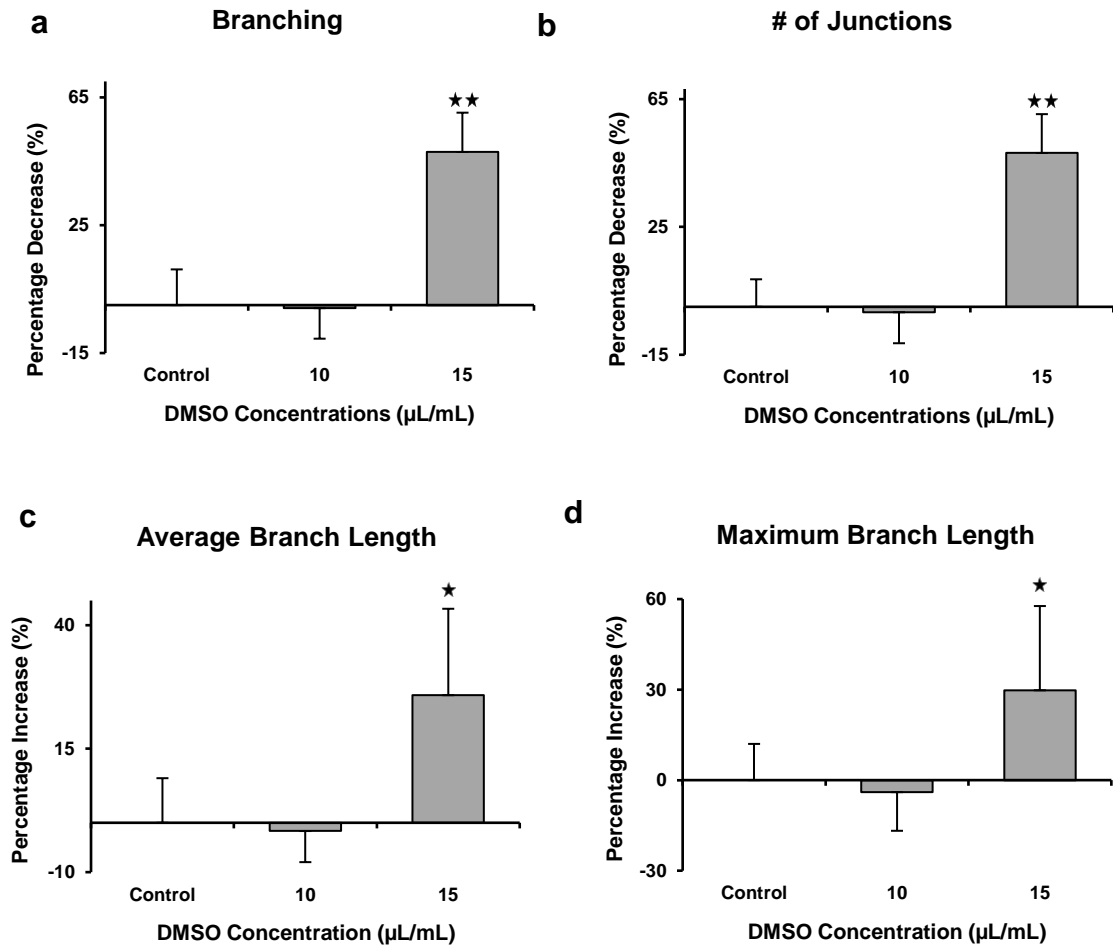
Fig 3.2: Impact of DMSO on microvessel topology. *Bar chart representing changes in a) microvessel branching (**P value =.007), b) number of microvessel junctions (**P value =.005), c) average branch length (*P value =.029) and d) maximum branch length (*P value =.014) as results of treatment with 10 and 15 μL of DMSO. n=5. Normalised with respect to control value.*

In efforts to characterise the DMSO-treated microvessels further, we investigated the impact of DMSO on the function of the microvessels, perfusability. To that end, the medium was replaced with a fluorescent tracer dye (Dextran 70 kDa) on day 7 of culture. 3D confocal imaging revealed that immediately after introduction, the tracer dye uniformly filled the microvessels and remained confined within them in all conditions, excluding 20 µL/mL of DMSO. Because no microvessels formed in such devices, the tracer dye perfused to the vascularisation channel through the gel (**Fig 3.3 a**). However, quantification of perfusability revealed that unlike the microvessels formed in the devices treated with 10 µL/mL of DMSO and control, which were fully perfusable (97 ± 2.5 %) to dextran 70 kDa, the microvessels formed in the device treated with 15 µL/mL of DMSO were not fully functional. We measured the perfusability of the latter microvessels to be 59.15 ± 2.1 percent ([***]P value <.001, n=5), demonstrating that the perfusability decreased by ~40% (**Fig 3.3 b**).

		Microvessels	Dextran Perfusion	Overlay
Control	Medium			
Treated with DMSO	10 µL/mL			
	15 µL/mL			
	20 µL/mL			

*(**Fig 3.3** continued on next page. Legend follows)*

106

b   **Microvessels Perfusability**
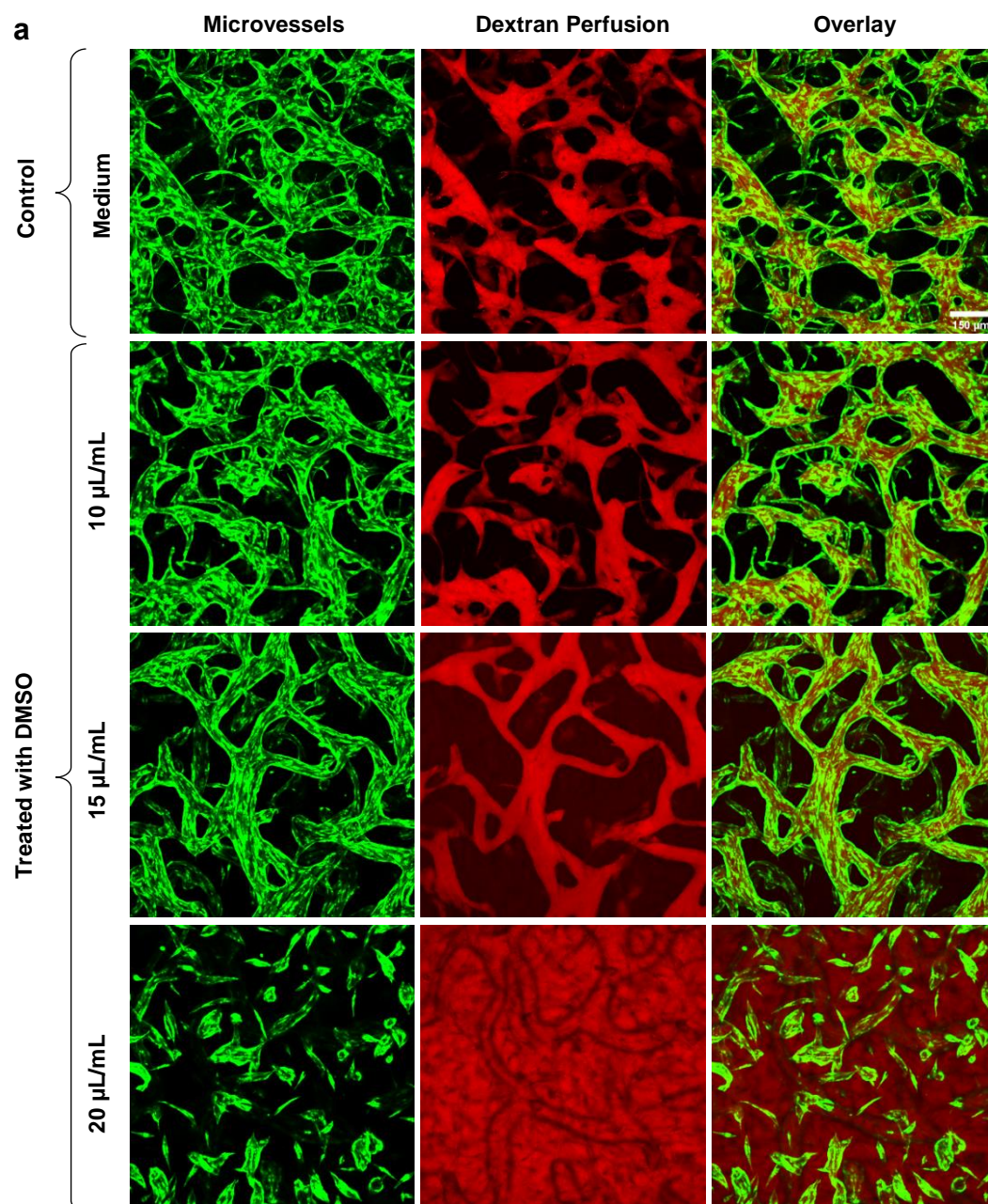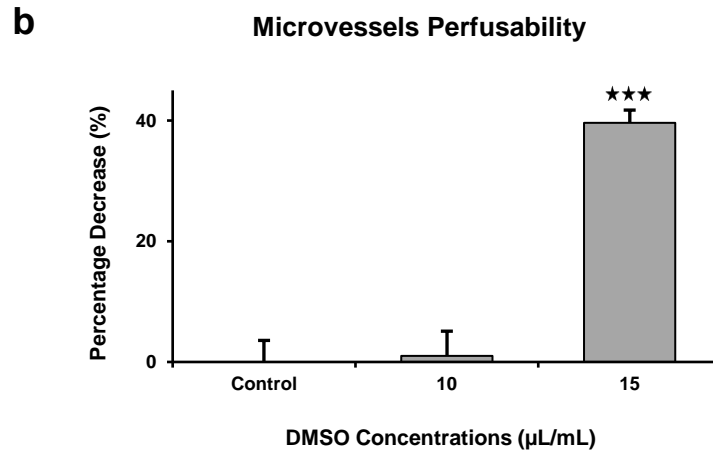
Fig 3.3: Impact of DMSO on microvessel function. a) Visualisation of dextran perfusion through microvessels formed under different conditions. Scale bar, 150 μm. b) Bar chart representing changes in perfusability (***P value <.001, n=5.) Normalised with respect to control value.

We hypothesised this could be due to the impact of high concentrations of DMSO on the viability of ECs and/or FBs and/or the proliferation of ECs and/or FBs. To test this, we seeded ECs and FBs in 6-well plates and treated them with different DMSO concentrations. The measurement of cell viability and cell proliferation demonstrated that DMSO had no significant impact on cell viability (**Fig 3.4 a**). In contrast, it affected cell proliferation in a dose-dependent manner (***P value <.001, n=3, **Fig 3.4 b**).
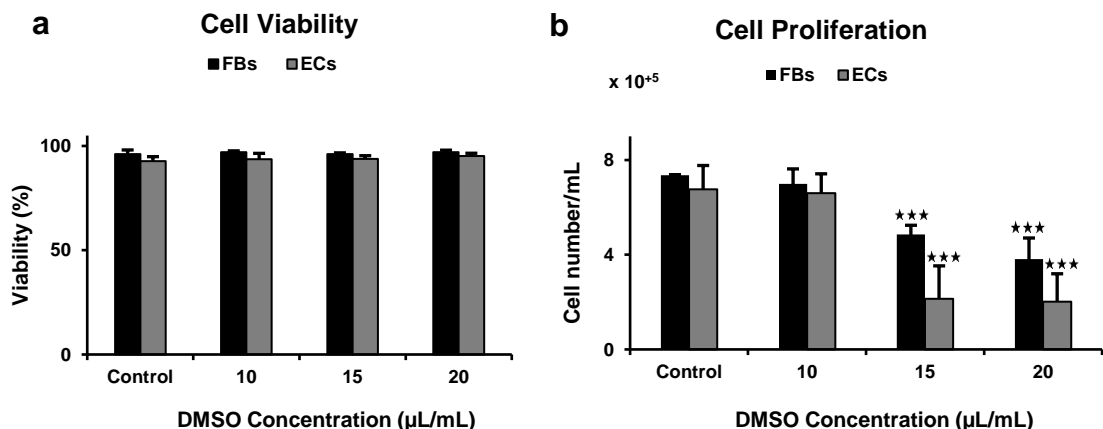
Fig 3.4: Impact of DMSO on the viability and proliferation of the cells. a) Bar chart representing impact of different concentrations of DMSO on FB and EC viability. b) Bar chart representing impact of different concentrations of DMSO on FB and EC proliferation (***P value <.001, n=3).

To summarise, in low concentration (10 µL/mL), DMSO had either no impact or negligible impact on the formation, morphology, characteristics, topology, and function of the microvessels. However, by increasing the concentration of DMSO, morphology, characteristics, topology, and function of the microvessels were affected (15 µL/mL), or the formation of microvessels was abolished entirely (20 µL/mL). Measuring cell viability and cell proliferation, we demonstrated that unlike cell viability, cell proliferation significantly reduced when treated with 15 and 20 µL/mL of DMSO. Reducing cell proliferation can explain the difference between the microvessels treated with different concentrations of DMSO. Altogether, our findings provide strong evidence that DMSO affects the formation of microvessels in a dose-dependent manner. It is worth mentioning that we kept the final DMSO concentration either under or at 10 µL/mL in all small molecule inhibitor treatment experiments to ensure the changes observed in microvessel formation, characteristics, topology, and/or function were not due to toxic effects of DMSO.

3.3.2 Impact of Mechanotransduction Inhibitors on Microvessels

3.3.2.1 Verteporfin, a YAP Inhibitor

To investigate the role of YAP in the formation and stabilisation as well as mechanical properties of the microvessels, we treated co-seeded ECs and FBs with verteporfin which is known to be a YAP inhibitor. Verteporfin binds to YAP and changes its conformation. The change in YAP conformation accelerates its cleavage by trypsin in a dose-dependent manner[147]. Before treating JCC devices with verteporfin, we performed cell viability and proliferation assay to determine the desired concentration(s) as verteporfin could kill cells[175]. The cell viability and proliferation assay revealed that both EC and FB viability and proliferation were extremely affected by verteporfin in a dose-dependent manner. However, the viability and proliferation of both verteporfin-treated cells and control were similar when the cells were treated with 0.25 µM of the inhibitor (**Fig 3.5 a, b**).

a Cell Viability

■FBs ■ECs

Viability (%)
100
50
0

Media DMSO 0.25 0.5 1 3 5

Verteporfin Concentrations (µM)

b Cell Proliferation

■FBs ■ECs

$\times 10^{+5}$

Cell Number/mL
8
4
0

Media DMSO 0.25 0.5 1 3 5

Verteporfin Concentrations (µM)
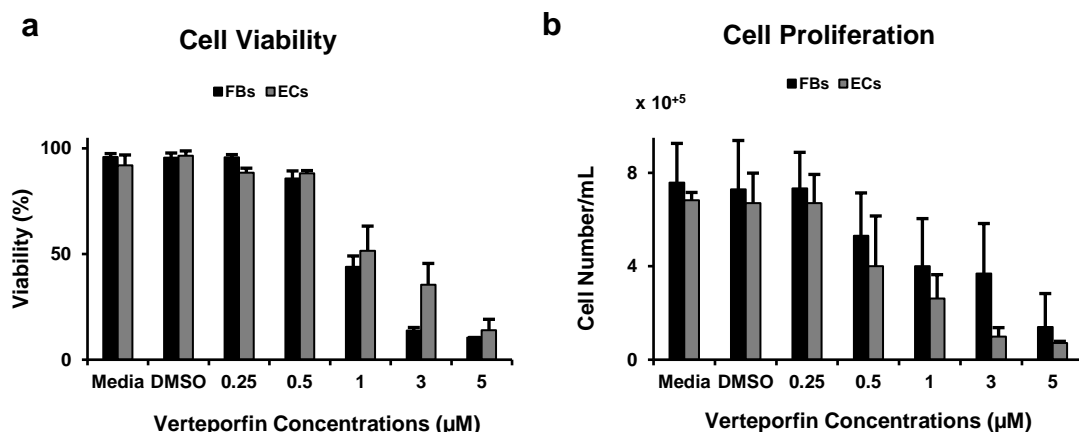
Fig 3.5: Determination of desired concentration of verteporfin. a and b) Both cell viability and proliferation were affected in a dose-dependent manner when the cells were treated with verteporfin. However, 0.25 µM was the threshold concentration, as both cell types preserve their properties – viability and proliferation – compared to control. n=3.

We next set out to assess the impact of YAP inhibition on the formation and stabilisation of microvessels. To this end, ECs and FBs were co-cultured and treated with 0.25 µM of verteporfin. Confocal imaging of the treated cells over one week revealed, although rounded and mono-dispersed ECs initiated to get elongated on day 1 of culture as an attempt to self-assemble and form microvessels, verteporfin arrested their ability to develop microvessels by day 4. Unlike control devices in which well-interconnected microvessels formed, no microvessels formed in the device treated with 0.25 µM of verteporfin by day 7 of culture (**Fig 3.6 a**). We measured the coverage area of the YAP-inhibited device to be 6.4 ± 0.5 percent. In other words, the coverage area decreased by ~89% (***P value <.001, n=5, **Fig 3.6 b**). It is worth noting that we did not measure perfusability, as no microvessels formed in the verteporfin-treated device.

To conclude, the lack of formation of microvessels indicates that YAP contributes to vascularisation in a very early stage, meanly formation.

109

a

| | Day 1 | Day 4 | Day 7 |

Control — Medium, DMSO+Medium

Treated with Verteporfin — 0.25 µM

Scale bar: 150 µm

b

Microvessls Coverage Area
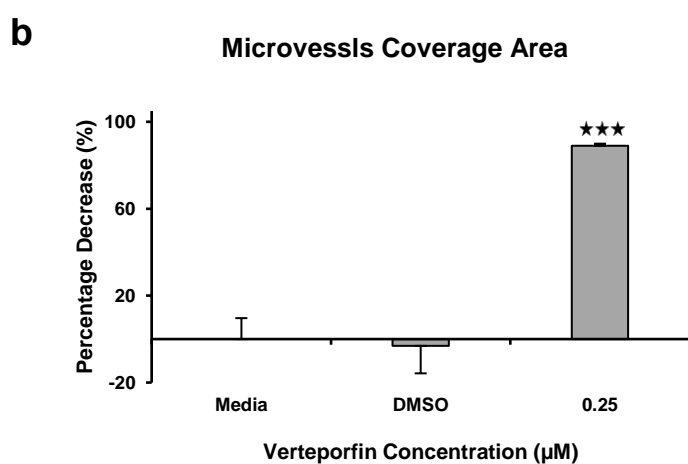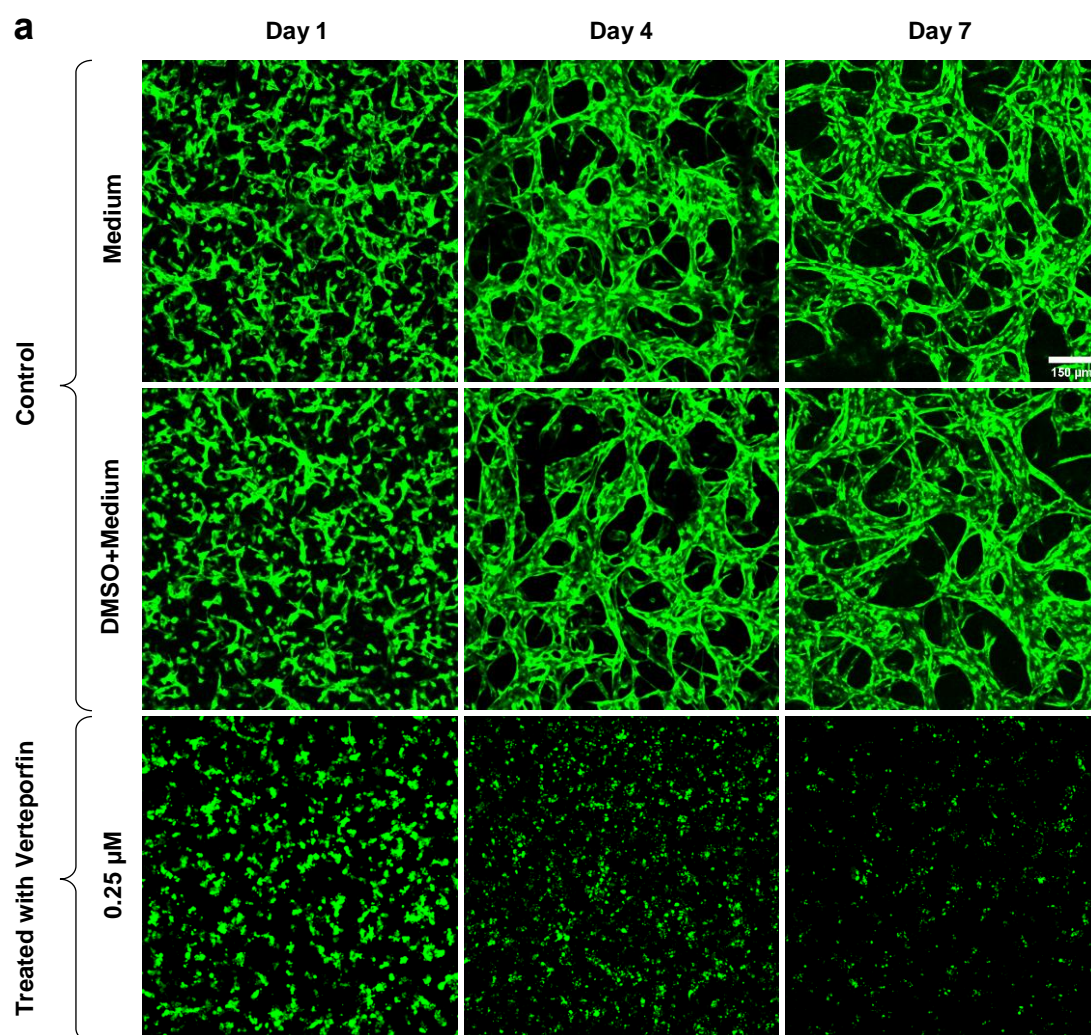
Fig 3.6: Impact of the inhibition of YAP on vascularisation. a) Treatment of the co-seeded cells resulted in arresting the formation of microvessels. Scale bar, 150 µm. b) A remarkable decrease was observed in coverage area in the verteporfin-treated device as a direct consequence of the lack of vascularisation (***P value <.001, n=5.) Normalised with respect to control value.

110

3.3.2.2 XAV939, a Wnt/β-catenin Pathway Inhibitor

We then investigated the contribution of Wnt/β-catenin pathway to the formation and stabilisation of microvessels. To this end, we treated JCC devices with different concentrations of XAV939, which is known to inhibit Wnt/β-catenin pathway by preventing β-catenin translocation from cytoplasm to the nucleus[176]. However, many research groups have shown that XAV939 is of cytotoxic effects on cells[177,178]. Therefore, as we did for verteporfin, we first determined the desired concentrations of the inhibitor, which exhibited no significant impact on the viability and proliferation of the cells. Cell viability and proliferation assay revealed that the viability of neither FBs nor ECs was affected by different concentrations of XAV939 (**Fig 3.7 a**). However, the inhibitor significantly impacted the proliferation of the cells at high concentrations (**Fig 3.7 b**). Consequently, we chose 10 and 20 µM of the inhibitor as the desired concentrations.
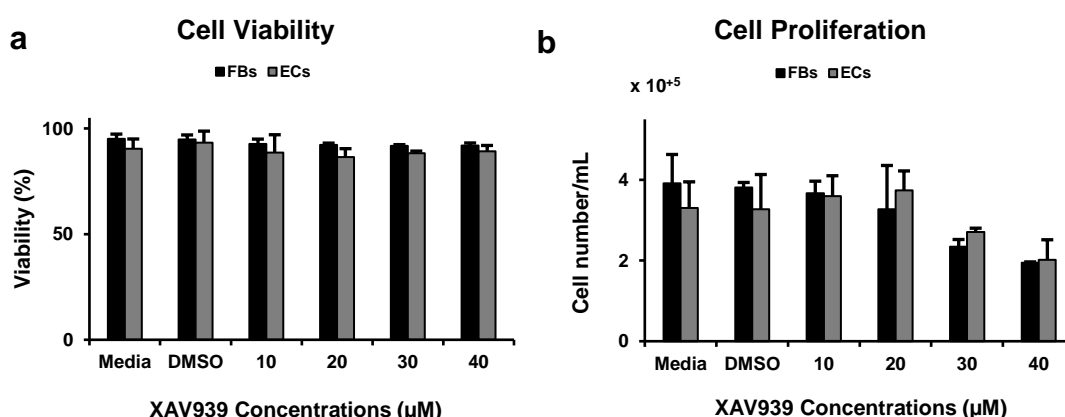
Fig 3.7: Determination of desired concentration of XAV939. *a) Bar chart representing the impact of Wnt/β-catenin inhibitor on the viability of both ECs and FBs. b) Bar chart showing the impact of Wnt/β-catenin inhibitor on the proliferation of both ECs and FBs. n=3.*

In efforts to investigate the contribution of Wnt/β-catenin pathway to vascularisation, we then treated JCC devices with two concentrations of XAV939 – 10 and 20 µM. 3D confocal imaging demonstrated that despite being treated with XAV939, ECs retained their ability to form microvessels by

day 4. However, we observed profound morphological differences between Wnt/β-catenin-inhibited microvessels and control microvessels. In such a way that Wnt/β-catenin-inhibited ECs tended to form thinner, less dense, and less branched microvessels than control (**Fig 3.8**).
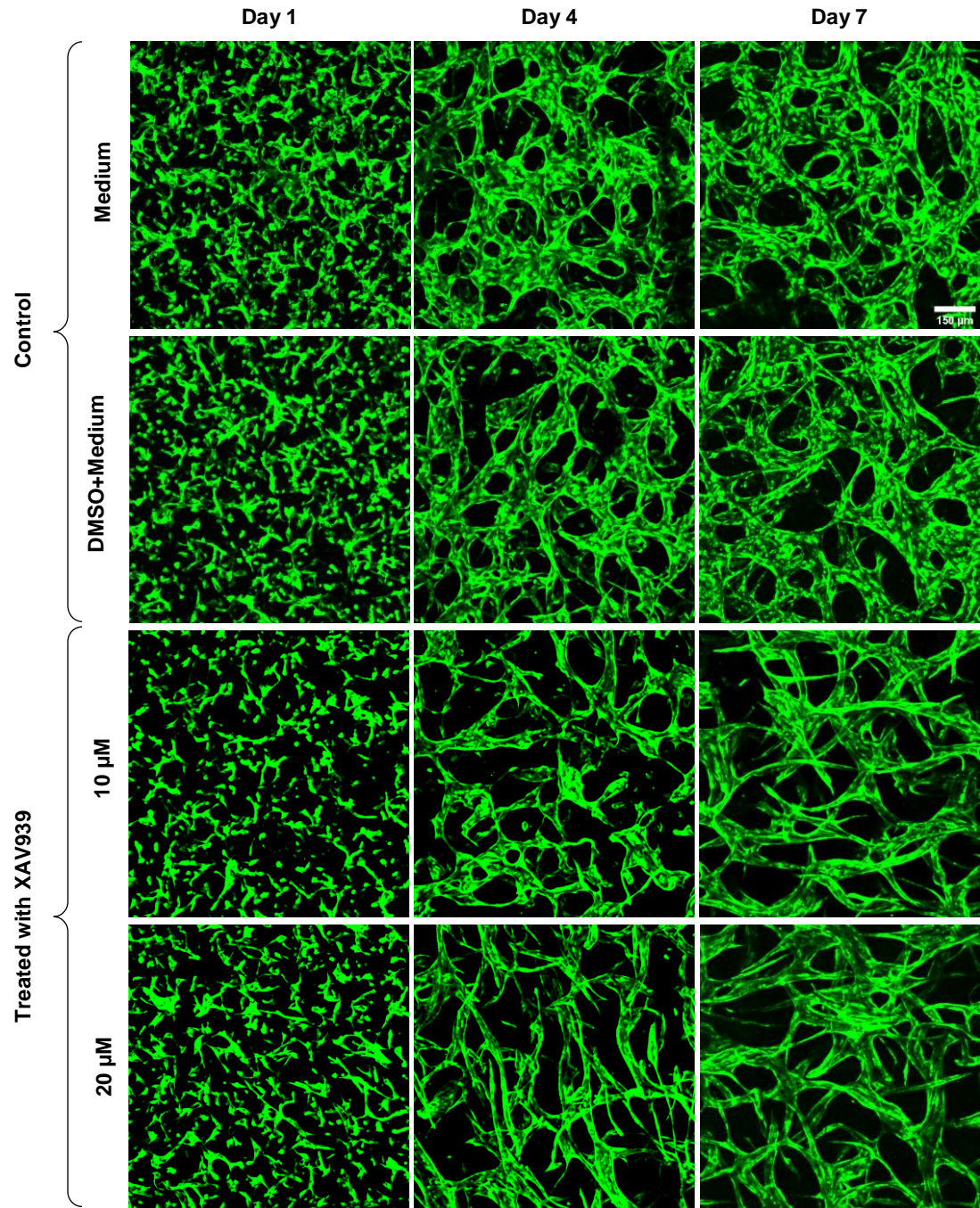
Fig 3.8: Impact of the inhibition of Wnt/β-catenin pathway on microvessel formation. *Confocal images of microvessel formation in Wnt/β-catenin-inhibited devices and controls over the course of one week. Scale bar, 150 µm.*

Further analysis revealed that microvessels coverage area decreased by 26.4 ± 4.5 percent in the devices treated with 10 µM of XAV939 and 30.6 ± 3.2 percent in the devices treated with 20 µM of XAV939 ([***]P value <.001 for both concentrations, n=3, **Fig 3.9 a**). We also observed a remarkable decrease in microvessels diameter in the treated devices in a dose-dependent manner ([***]P value <.001 for both concentrations, n=3, **Fig 3.9 b**).
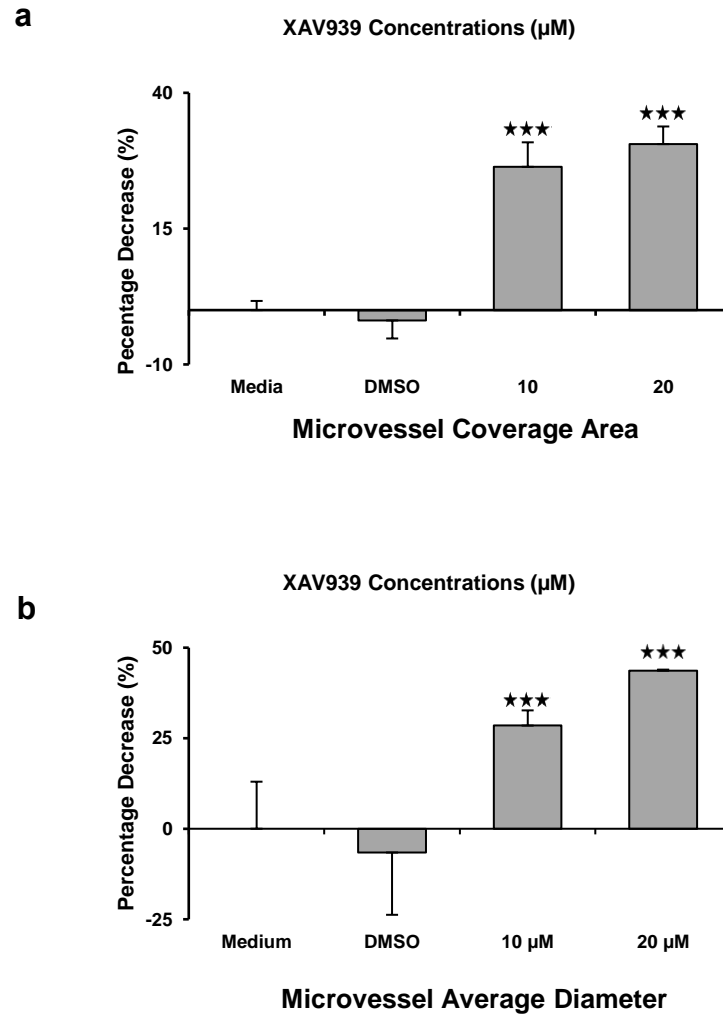
Fig 3.9: Impact of the inhibition of Wnt/β-catenin pathway on microvessel characteristics – coverage area and diameter. *As a result of inhibition of Wnt/β-catenin pathway a) microvessels were less dense ([***]P value <.001) and b) smaller in diameter ([***]P value <.001). n=3. Normalised with respect to control value.*

Topology analysis revealed that the Wnt/β-catenin-inhibited microvessels were significantly different from control microvessels in terms of topology too. For instance, we observed a significant decrease in branching ($^{**}P$ value =.0017 and $^{***}P$ value <.001 for 10 and 20 µM respectively, n=5, **Fig 3.10 a**) and the number of junctions ($^{**}P$ value =.005 and $^{**}P$ value =.004 for 10 and 20 µM respectively, n=5, **Fig 3.10 b**). Also, a significant decrease was observed in both average branch length ($^{*}P$ value =.044) and maximum branch length ($^{*}P$ value =.029, n=5) when the device was treated with 20 µM of the inhibitor (**Fig 3.10 c, d**).
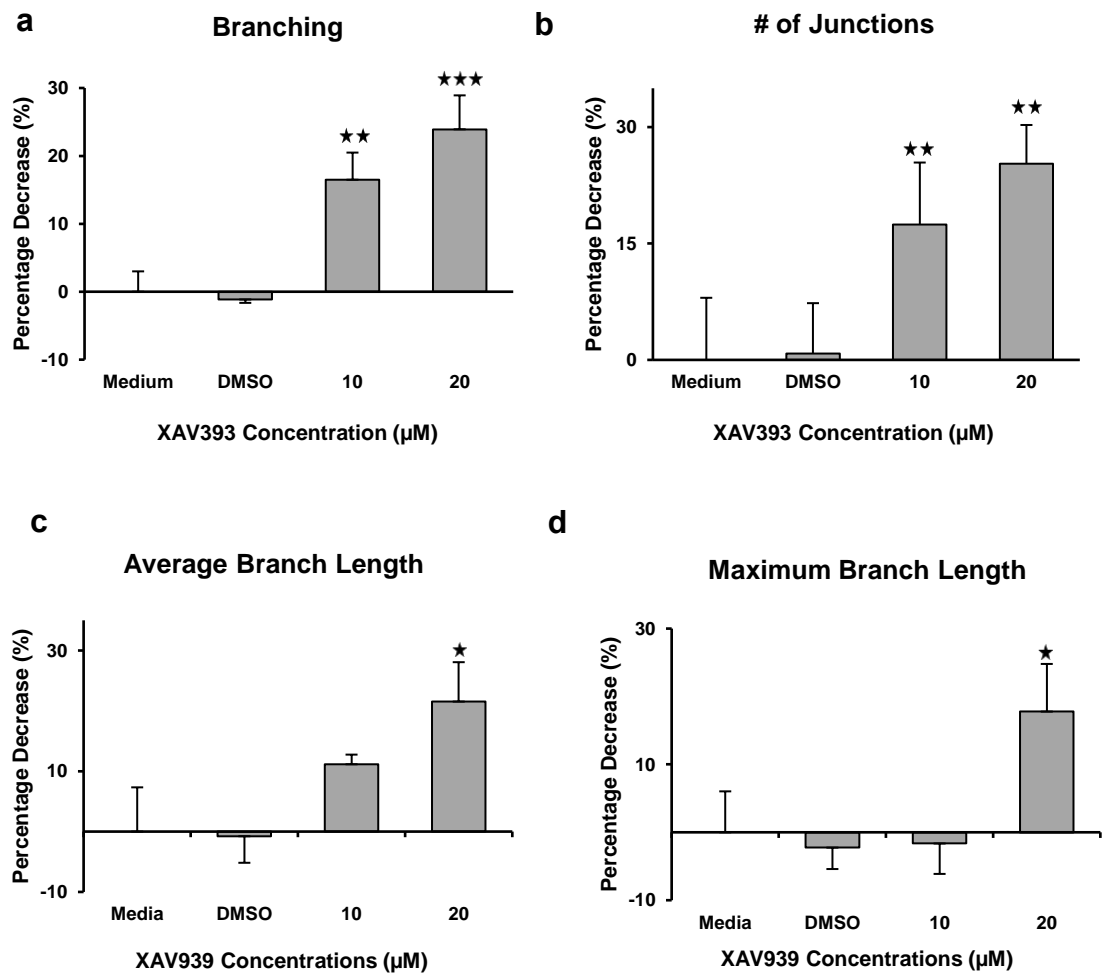
Fig 3.10: Impact of the inhibition of Wnt/β-catenin pathway on microvessel topology. Bar charts representing the impact of the inhibition of Wnt/β-catenin on a) producing branches ($^{**}P$ value =.0017 and $^{***}P$ value <.001 for 10 and 20 µM respectively), b) the number of junctions ($^{**}P$ value =.005 and $^{**}P$ value =.004 for 10 and 20 µM respectively), c) average branch length ($^{*}P$ value =.044), and d) maximum branch length ($^{*}P$ value =.029). n=5. Normalised to the control values.

Introducing the tracer dye on day 7 of culture, we investigated the impact of the inhibition of Wnt/β-catenin pathway on the function of microvessels – perfusability. 3D confocal images revealed that not all the microvessels formed in inhibitor-treated devices were perfused (**Fig 3.11 a**). The statistical analysis showed that the difference was significant ($^*P$ value =.022, and $^*P$ value =.016 for 10 µM and 20 µM respectively, n=5, **Fig 3.11 b**).

*(**Fig 3.11** continued on next page. Legend follows)*

b
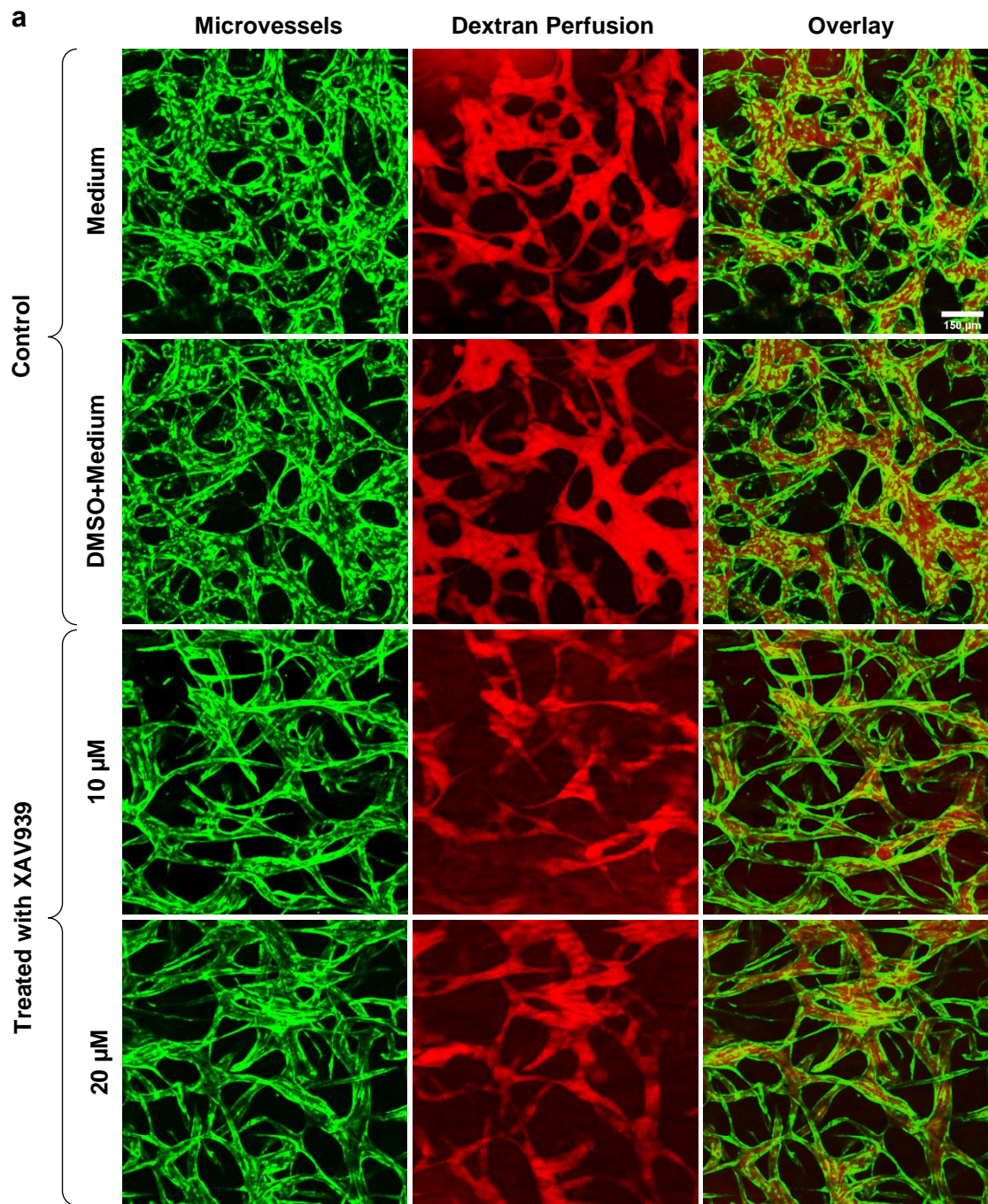
Microvessels Perfusability

Fig 3.11: Impact of the inhibition of Wnt/β-catenin pathway on microvessel function – perfusability. a) Visualisation of dextran perfusion through microvessels formed under different conditions. Scale bar, 150 μm. b) Bar chart comparing microvessel perfusability in different conditions (*P value =.022, and *P value =.016 for 10 μM and 20 μM, respectively. n=5). Normalised with respect to control value.

Wnt/β-catenin pathway is one of the most important genes belonging to mechanotransduction pathways. The inhibition of this pathway by an inhibitor – XAV939 – resulted in the formation of morphologically, topologically, and functionally different microvessels by ECs. This provides solid evidence that the gene plays an important role in vascularisation.

3.3.2.3 PF-573228, a FAK Inhibitor

Aiming to investigate FAK contribution to the formation and stabilisation of microvessels, we treated JCC devices with a FAK inhibitor, PF-573228. Being an ATP competitor, PF-573228 inhibits FAK function by binding to its kinase domain and decreasing FAK[397] phosphorylation[179,180]. However, to avoid the cytotoxic effect of the inhibitor on cell viability and/or proliferation[158], we first carried out an assay to determine the desired concentration(s) of the inhibitor. Measurement of the cell viability and proliferation treated with different inhibitor concentrations showed that neither cell property was affected by the inhibitor at two concentrations of 0.1 μM and 0.5 μM (**Fig 3.12 a, b**).
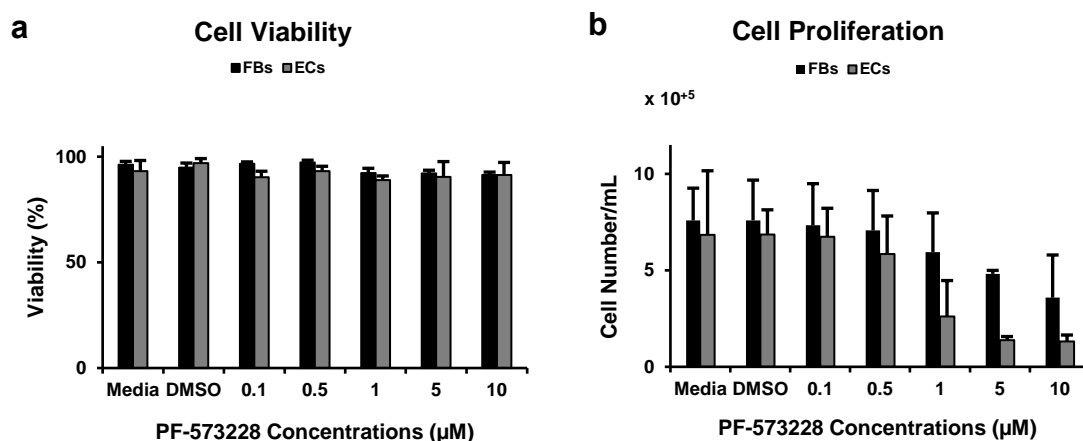
Fig 3.12: Determination of desired concentration of FAK-inhibitor – PF-573228. *a) Bar chart representing the impact of different concentrations of FAK inhibitor on the viability of both ECs and FBs. b) Bar chart representing the impact of different concentrations of FAK inhibitor on cell proliferation. n=3.*

We then set out to look over the impact of the inhibition of FAK on microvessels. To that end, we treated JCC devices with 0.1 µM and 0.5 µM of the inhibitor. We observed drastic differences in microvessel morphology of FAK-inhibited microvessels and control. When treated with 0.1 µM of the inhibitor, ECs initially retained their ability to self-assemble and form microvessels by day 4. However, the microvessels regressed by day 7. This could be either due to not being efficiently interconnected or/and lack of the formation of openings which made the flow of the growth medium to the vascularisation channel insufficient. Treatment of the co-seeded cells with 0.5 µM of the inhibitor arrested the formation of interconnected microvessels and some dispersed sheet-like clusters formed in the vascularisation channel by day 7 (**Fig 3.13**).
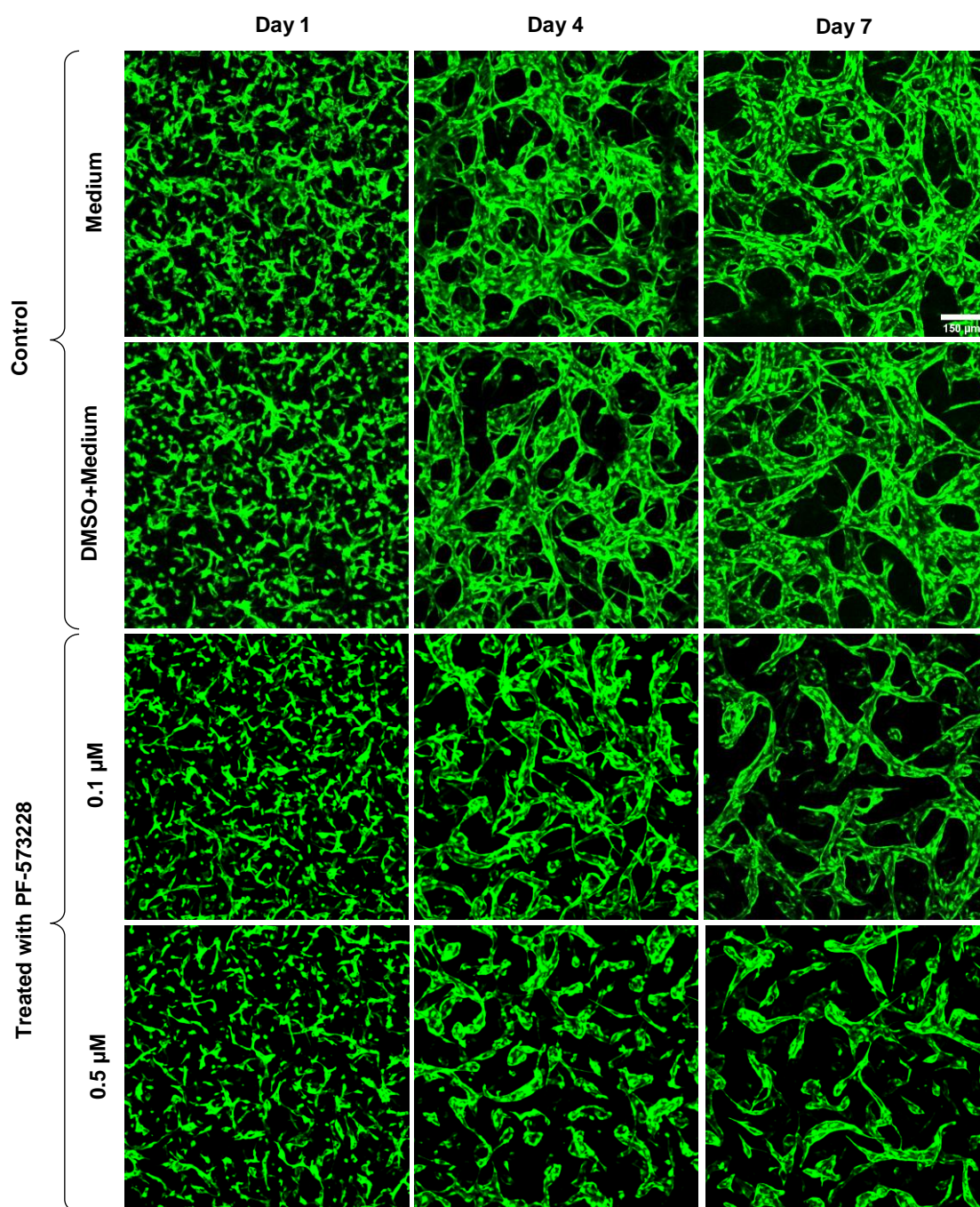
Fig 3.13: Impact of the inhibition of FAK on the formation of microvessels. *Confocal images of microvessel formation in FAK-inhibited devices and controls over the course of one week. Scale bar, 150 μm.*

Further characterisations revealed drastic differences between the FAK-inhibited microvessels and control. For instance, coverage area decreased by 29.9 ± 7.56 percent when the co-seeded cells were treated with 0.1 μM of the inhibitor ($^*P$ value =.032, n=3) and 46.9 ± 2.22 percent when the cells were treated with 0.5 μM of the inhibitor ($^{**}P$ value =.002, n=3, **Fig 3.14 a**). Besides, we measured the average diameter of the FAK-inhibited microvessels to be 31.08 μm for 0.1 μM condition, whereas it was measured to be 25.02 μm for control. We believe this would be due to either the regression of the microvessels with a smaller diameter and/or the lack of formation of such microvessels. **Fig 3.14 b** compares both treated microvessels and control in terms of microvessel diameters. The observed decrease in diameter was not statically significant.

a

Microvessel Coverage Area

b

Microvessel Average Diameter
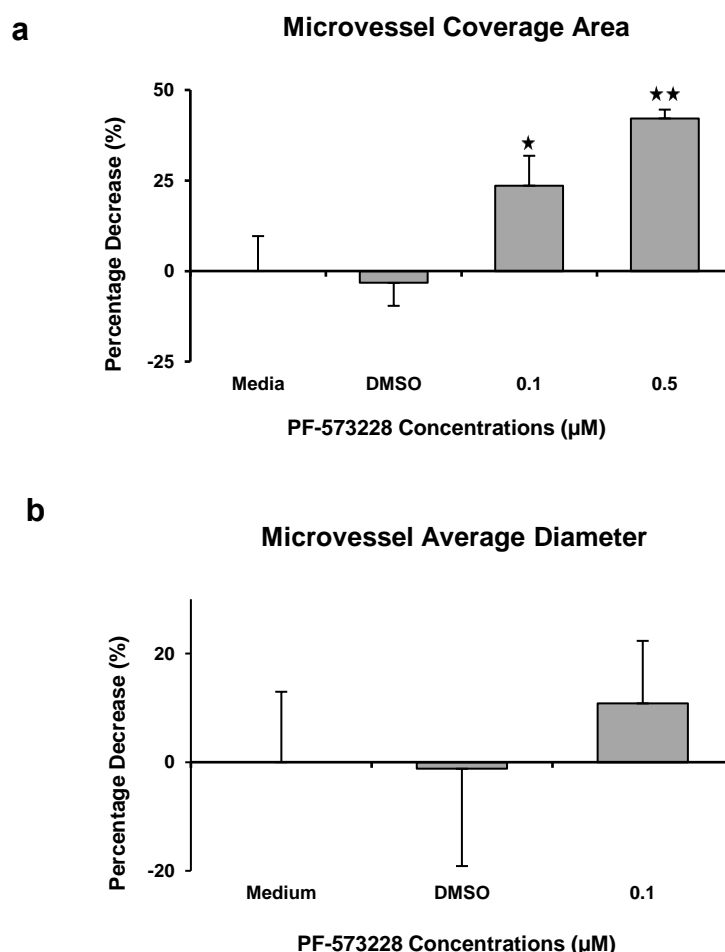
Fig 3.14: Impact of the inhibition of FAK on microvessel characteristics – Coverage area and diameter. a) Bar chart representing the impact of inhibition of FAK on microvessels coverage area ($^*P$ value =.032, $^{**}P$ value =.002) b) Bar chart comparing microvessel diameter in different conditions. n=3. Normalised with respect to control value.

We also observed notable differences between the FAK-inhibited microvessels and control in terms of topology. When FAK was inhibited, ECs formed less branched microvessels in a dose-dependent manner ($^*P$ value =.014, $^{**}P$ value =.007 for 0.1 µM and 0.5 µM respectively, n=5, **Fig 3.15 a**). Consequently, the number of junctions decreased significantly ($^{**}P$ value =.01, $^{**}P$ value =.005 for 0.1 µM and 0.5 µM respectively, n=5, **Fig 3.15 b**). When treated with 0.1 µM, there was a negligible increase in both average branch length and maximum branch length. However, both average branch length ($^*P$ value =.034, n=5) and maximum branch length ($^*P$ value =.042, n=5) increased when we treated the co-seeded cells with 0.5 µM of FAK-inhibitor (**Fig 3.15 c, d**).

a

Branching

b
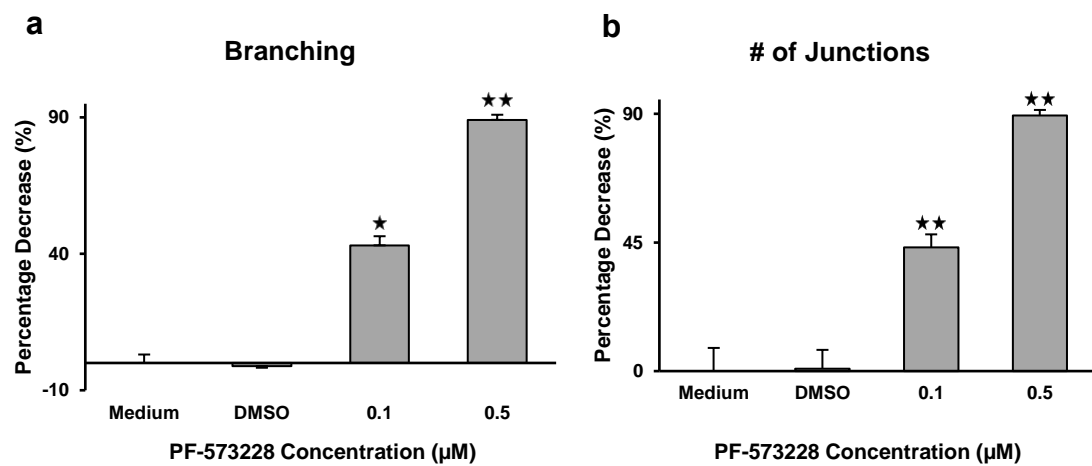
# of Junctions

*(**Fig 3.15** continued on next page. Legend follows)*
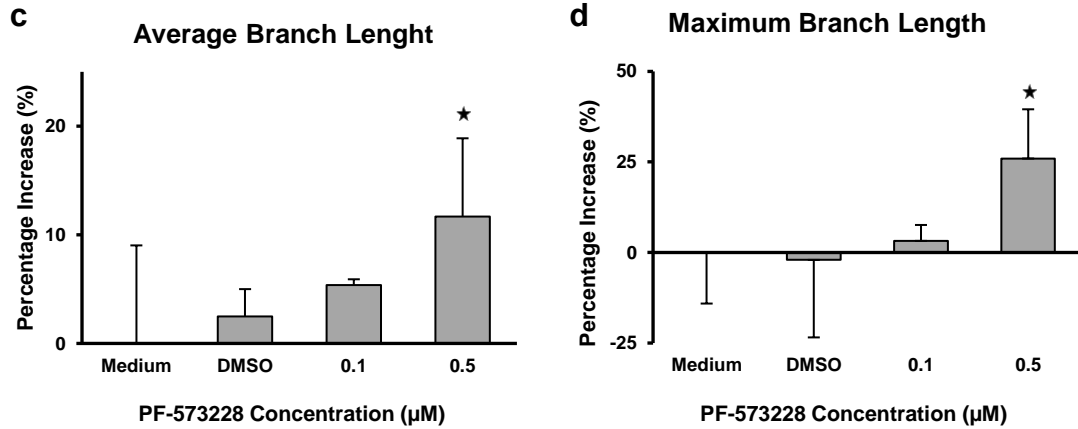
Fig 3.15: Impact of FAK-inhibitor, PF-573228, on microvessel topology. *a) Bar charts representing the impact of FAK inhibition on a) branching (*P value =.014, **P value =.007), b) the number of junctions (**P value =.01, **P value =.005), c) average branch length (*P value =.034) and d) maximum branch length (*P value =.042.) n=5. Normalised with respect to control values.*

Finally, dextran perfusion revealed that the FAK-inhibited microvessels were different from control microvessels not only in morphology and topology also in function. In such a manner that when the cells were treated with 0.1 µM of the inhibitor, perfusability was reduced by 16%, demonstrating that not all microvessels were perfusable (**P value =.002, n=5). Also, dextran perfused to the vascularisation channel through the gel when the co-seeded cells were treated with 0.5 µM of the inhibitor, indicating the lack of the formation of interconnected microvessels (**Fig 3.16 a**). **Fig 3.16 b** compares perfusability of the treated and untreated microvessels.

a

| | Vasculature | Dextran Perfusion | Overlay |

Control
- Medium
- DMSO+Medium

Treated with PF-573228
- 0.1 µM
- 0.5 µM

*(**Fig 3.16** continued on next page. Legend follows)*

122

b
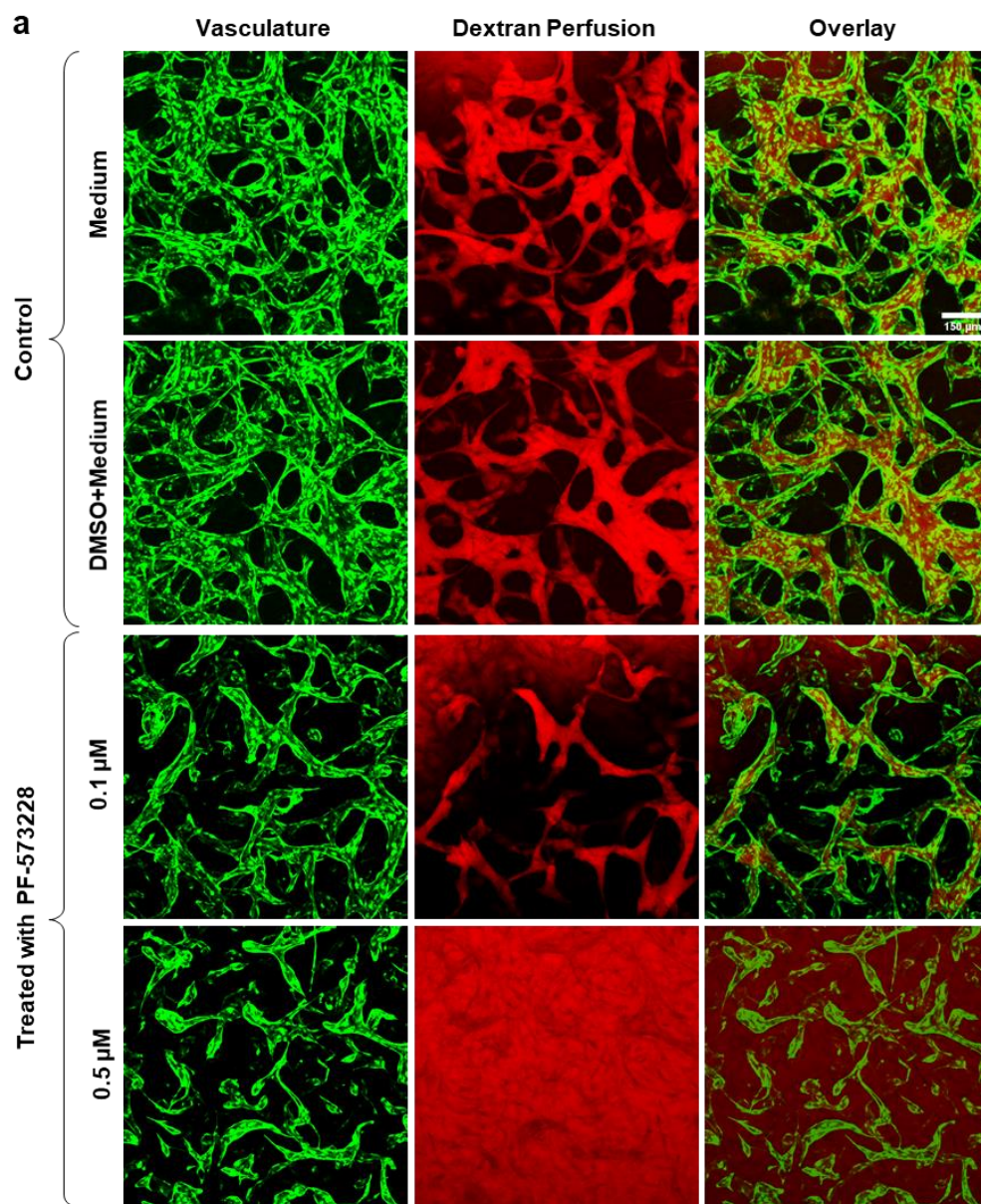
Microvessels Perfusability
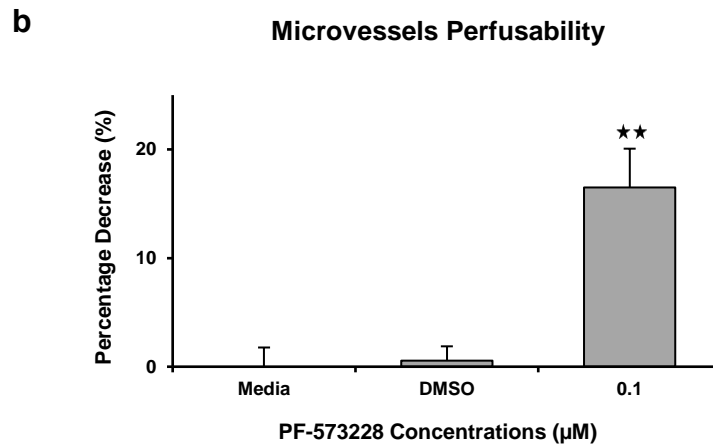
Fig 3.16: Impact of the inhibition of FAK on microvessel function - perfusability. a) Visualisation of dextran perfusion through microvessels formed under different conditions. Scale bar, 150 µm. b) Bar chart comparing perfusability of the treated microvessels with control (**P value =.002, n=5). Normalised with respect to the control value.

Drastic changes in microvessel formation, characteristics, topology, and function as results of FAK inhibition indicate the critical role of FAK in vascularisation.

3.3.2.4 CCG-1423, a RhoA Inhibitor

The contribution of RhoA to the formation and stabilisation of microvessels was assessed by treating the co-seeded cells with an inhibitor named CCG-1423. Acting downstream of RhoA, the inhibitor blocks a Rho-stimulated transcription, SRE.L-driven[181]. It has been shown that CCG-1423 could affect cell viability[181]. Aiming to determine the desired concentration(s) that did not affect cell viability and/or cell proliferation, we first treated ECs and FBs separately with different inhibitor concentrations. Cell viability assay and cell proliferation assay revealed that the inhibitor had no significant toxic effect on the cell viability and proliferation at the concentrations of 1 µM and 3 µM (**Fig 3.17 a, b**). This finding is consistent with earlier studies done by Kikuchi *et al.* and Barravecchia *et al.*[182,183].

a

Cell Viability

■FBs ▫ECs

b

Cell Proliferation

x 10^{+5}

■FBs   ▫Ecs
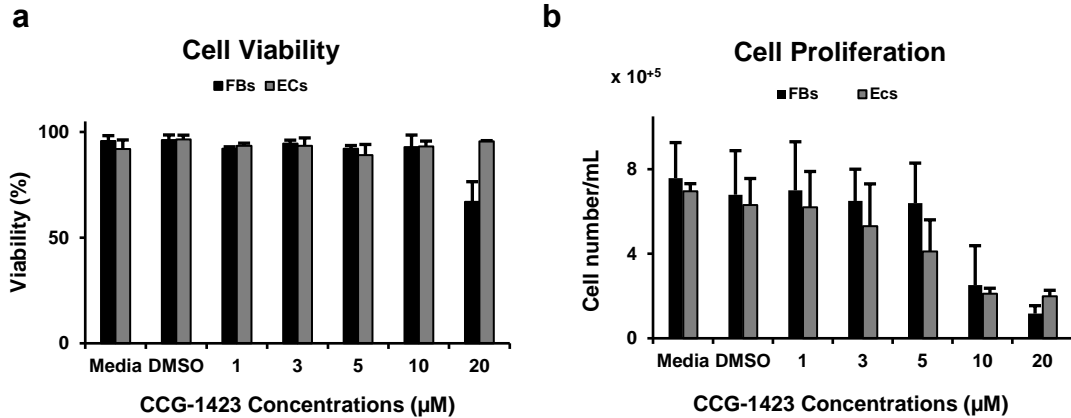
Fig 3.17: Determination of desired concentration(s) of RhoA inhibitor – CCG-1423. *a)*
Bar chart representing the impact of different concentrations of the inhibitor on cell viability. b)
Bar chart representing the impact of different concentrations of the inhibitor on cell
proliferation. n=3

We then set out to investigate the contribution of RhoA to vascularisation. In
doing so, we treated co-cultured ECs and FBs with 1 µM and 3 µM over the
course of one week. 3D confocal imaging showed that despite being treated
with 1 µM of the inhibitor, ECs retained their ability to form microvessels.
However, the microvessels were different from the control in terms of
morphology. When treated with 3 µM of the inhibitor, ECs initially got
elongated, self-assembled, and formed some small sheet-like structures by
day 4. However, the structures began to regress so that several dispersed
multicellular clusters remained in the vascularisation channel by day 7 of
culture (**Fig 3.18**).

124
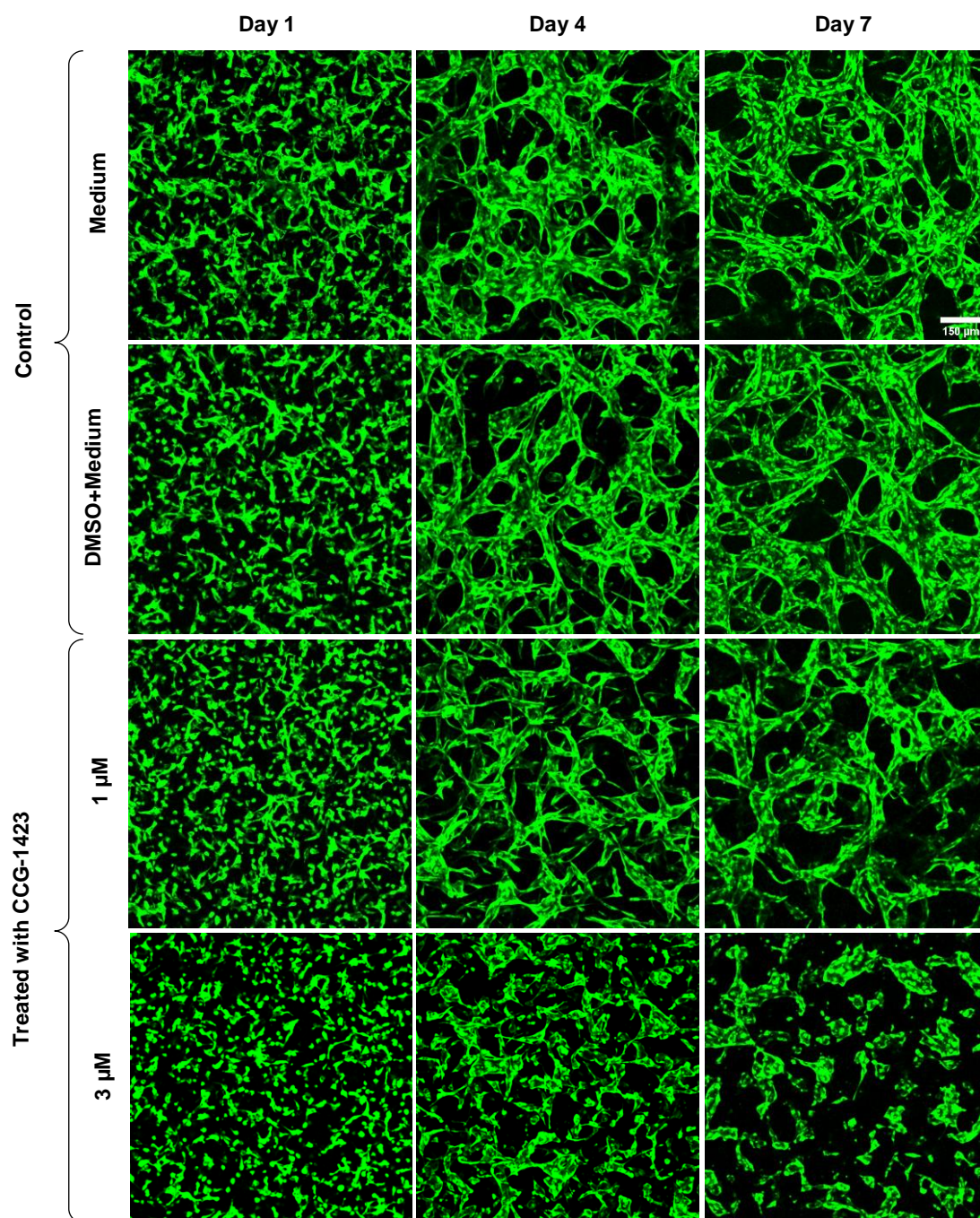
Fig 3.18: Impact of the inhibition of RhoA on microvessels formation and morphology. *Confocal images of microvessel formation in RhoA-inhibited devices and controls over the course of one week. Scale bar, 150 µm.*

Characterisation of the 3D confocal images revealed that the microvessels coverage area decreased by 50 percent when treated with 1 μM of the inhibitor ([***]P value <.001, n=3). There was also a 57 percent decrease in microvessels coverage area when the devices were treated with 3 μM of the inhibitor ([***]P value <.001, n=3, **Fig 3.19 a**). Conversely, there was an increase in microvessels diameter. However, the increase was not significant, demonstrating that the inhibition of RhoA had no considerable effect on microvessels diameter (**Fig 3.19 b**).
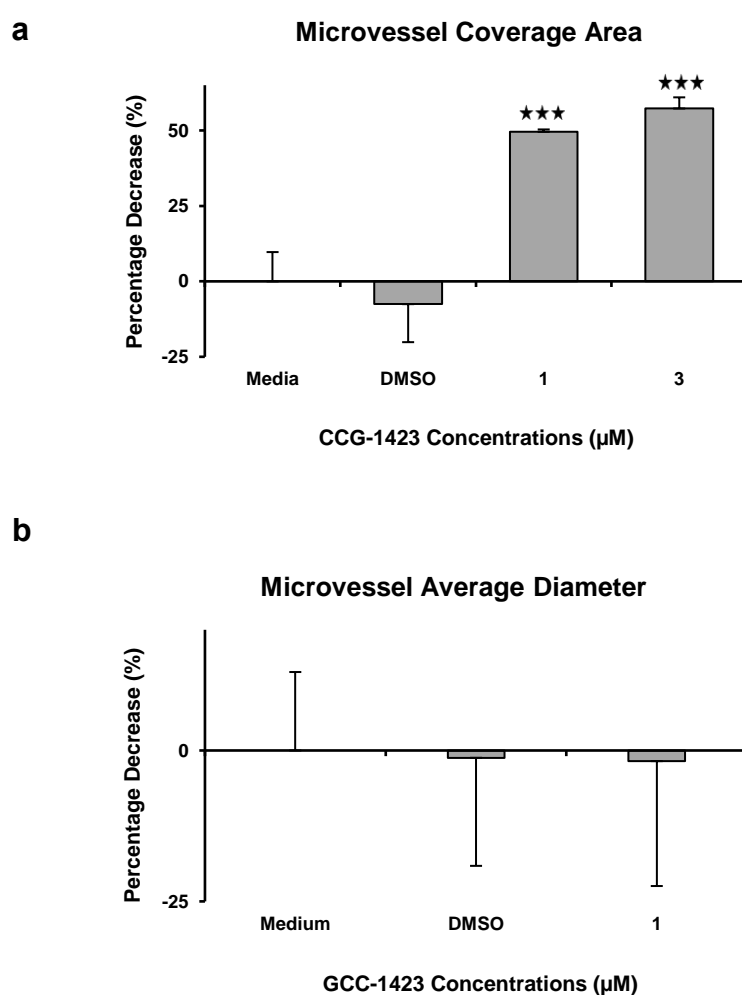
Fig 3.19: Impact of the inhibition of RhoA on microvessel characteristics. *a) Bar chart representing the impact of the inhibition of RhoA on microvessels coverage area ([***]P value <.001). b) Although a small increase was observed in the diameter of microvessels, it was not remarkable. n=3.*

We then investigated the impact of the inhibition of RhoA on the topology of the microvessels. As expected branching ($^{**}P$ value =.0014, n=5, **Fig 3.20 a**) and the number of junctions decreased notably ($^{**}P$ value =.003, n=5, **Fig 3.20 b**). A significant decrease was also observed in average branch length ($^{*}P$ value =.013, n=5) as well as maximum branch length ($^{*}P$ value =.033, n=5, **Fig 3.20 c, d**).
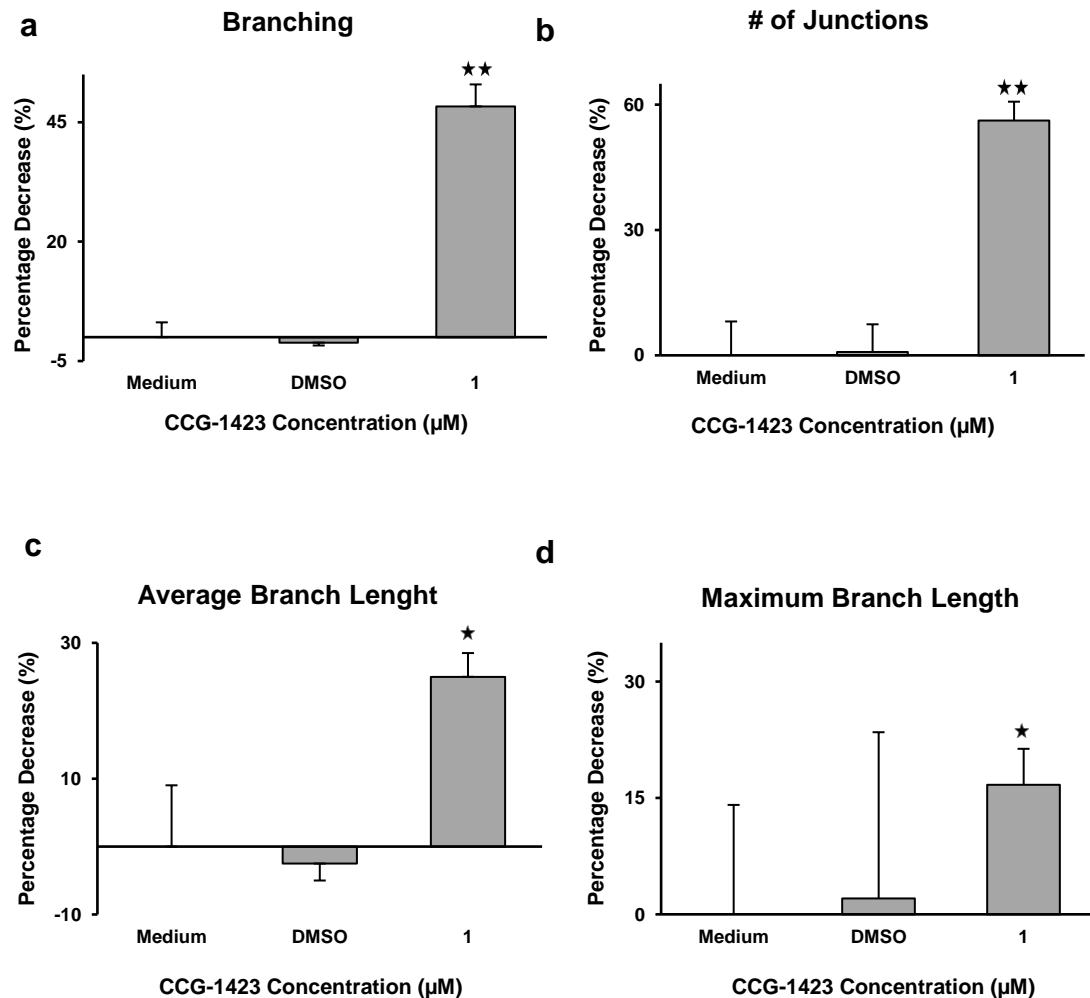
Fig 3.20: Impact of the inhibition of RhoA on microvessel topology. *Bar charts representing the impact of the inhibition of RhoA on a) branching ($^{**}P$ value =.0014), b) the number of microvessel junctions ($^{**}P$ value =.003), c) average branch length ($^{*}P$ value =.013) and d) maximum branch length ($^{*}P$ value =.033.) n=5. Normalised with respect to control value.*

In the end, assessing perfusability confirmed that not only the morphology, characteristics, and topology of the microvessels also their function was affected by the inhibition of RhoA, as perfusion of dextran revealed that not all

the microvessels formed were perfusable (**Fig 3.21 a**). We measured a decrease of 13 ± 6.2 percent in perfusability when the co-seeded cells were treated with 1 μM of the inhibitor (***P* value =.0045, n=5, **Fig 3.21 b**).

*(**Fig 3.21** continued on next page. Legend follows)*

b
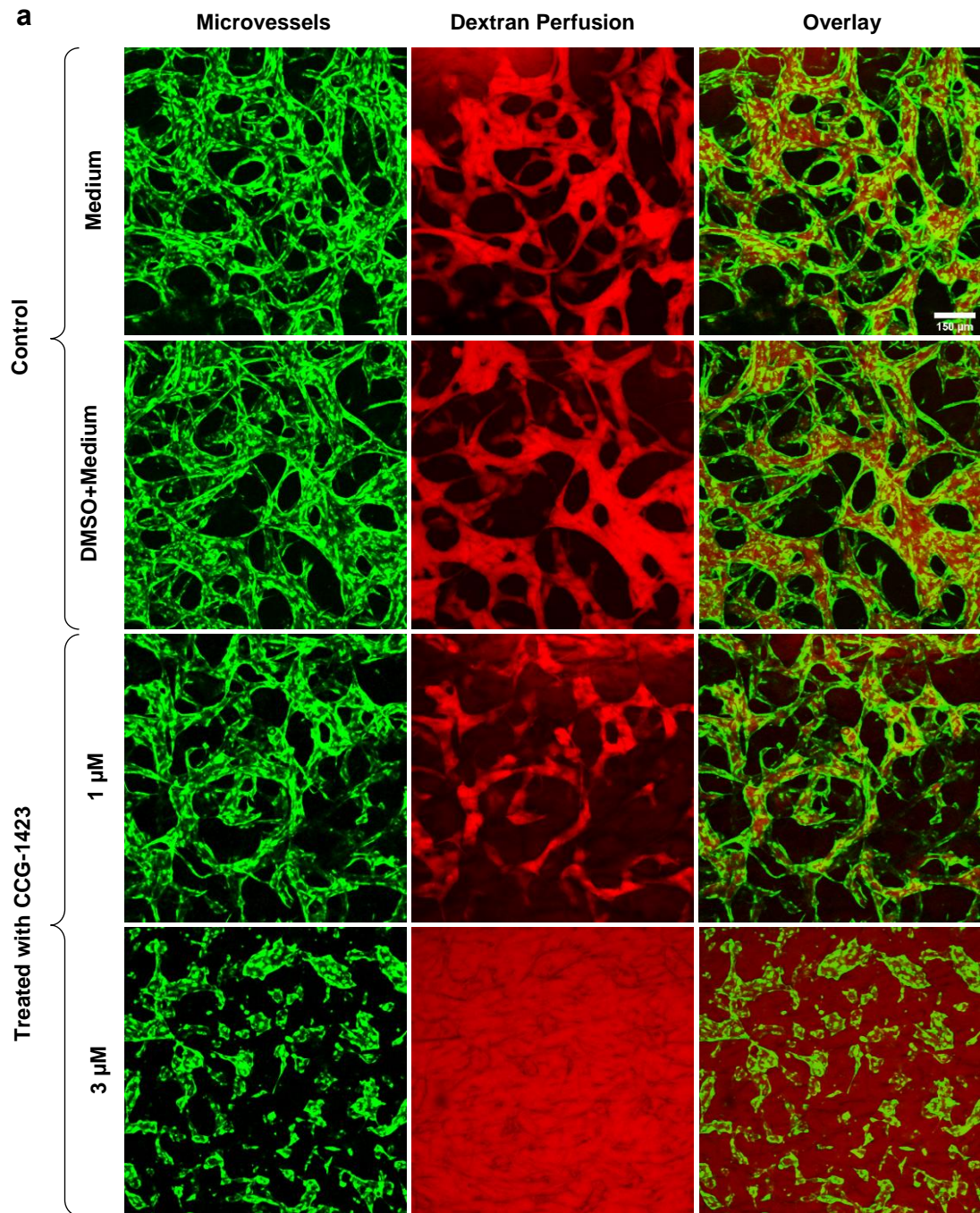
Microvessels Perfusability
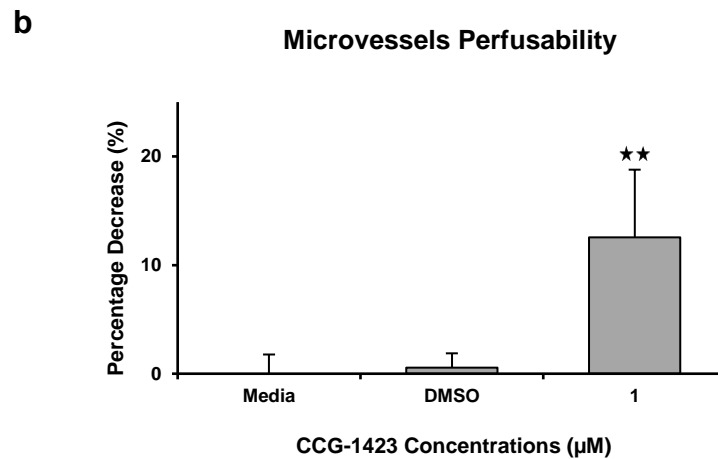
Fig 3.21: Impact of the inhibition of RhoA on microvessel function - perfusability. a) Visualisation of dextran perfusion through microvessels formed under different conditions. Scale bar, 150 µm. b) Bar chart comparing perfusability of the RhoA-inhibited microvessels with control (**P value =.0045, n=5). Normalised with respect to the control value.

RhoA is one of the most important genes belonging to the mechanotransduction pathway. The inhibition of this gene by an inhibitor – CCG-1423 – resulted in the formation of microvessels significantly different from untreated microvessels in morphology, topology, and function, demonstrating that the gene plays a solid role in the formation and function of the microvessels.

3.3.2.5 PP2, a Src Inhibitor

Src was the last gene belonging to the mechanotransduction pathway in which we were interested. Assessment of its contribution to the formation and stabilisation of microvessels was carried out by the inhibition of the gene, which was experimentally achieved by treating the co-embedded ECs and FBs with an inhibitor – PP2. PP2 selectively inhibits p56^{lck} and p59^{fynT}, the Src family kinases[184]. Knowing the inhibitor's potential ability to affect the viability and proliferation of the cells[184,185], we first set out to determine the inhibitor desired concentration(s), which did not exhibit any significant effects on the viability and proliferation of the cells while being effective. Measuring the

viability and the proliferation of the cells after 4 days of treatment, we found that concentrations of 1 µM and 5 µM of the inhibitor had no remarkable effect on cell viability and proliferation (**Fig 3.22 a, b**). which is consistent with the findings of Kong *et al.*[185].
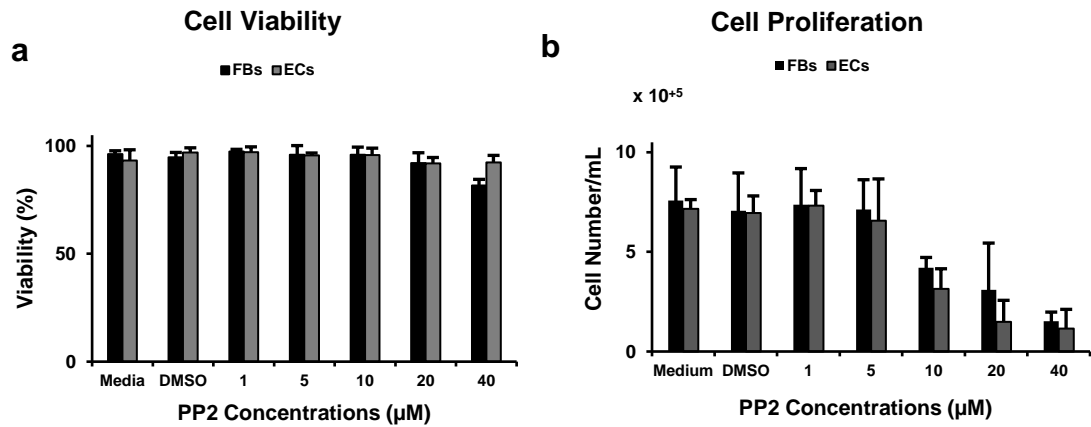
Fig 3.22: Determination of desired concentration of Src inhibitor – PP2. *a) Bar chart representing the impact of different concentrations of the inhibitor on cell viability. b) Bar chart representing the impact of different concentrations of the inhibitor on cell proliferation.*

We then set out to investigate the contribution of Src to the formation and stabilisation of microvessels. To this end, we treated co-cultured ECs and FBs with 1 µM and 5 µM of Src inhibitor for one week. When treated with different inhibitor concentrations, ECs retained their ability to form microvessels and by day 4. W could not recognise any particular difference between Src inhibited microvessels and untreated ones. However, surprisingly, we observed an obvious regression from day 4 to day 7 of culture so that some regressed, less-dense, less-interconnected, and morphologically different microvessels remained in the vascularisation channel of the inhibitor-treated devices by day7 (**Fig 3.23**). This could indicate that the gene plays a key role in the microvessel maturation rather than their formation.
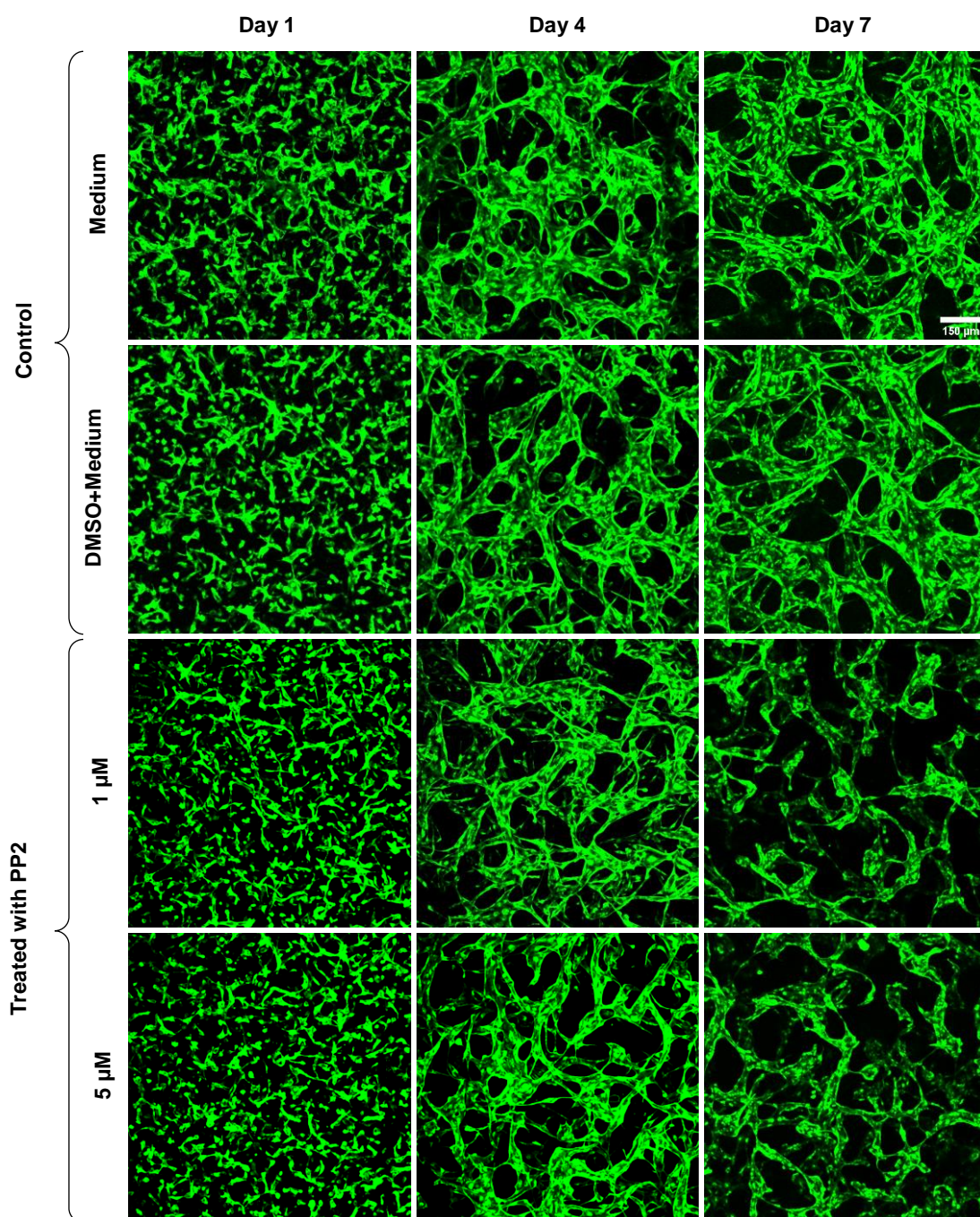
Fig 3.23: Impact of the inhibition of Src on the formation of microvessels. *3D confocal imaging revealed that the inhibition of Src had no obvious effect on microvessel formation by day 4. However, the microvessels treated with the inhibitor began to regress from day 4 leaving a less dense less interconnected microvessels by day 7. Scale bar, 150 µm.*

When we characterised the microvessels, we noticed that coverage area decreased by 23 ± 7 percent and 57 ± 1.6 percent when the co-seeded cells were treated with 1 µM (*P value =.018, n=5) and 5 µM (***P value <.001, n=5) of the inhibitor, respectively (**Fig 3.24 a**). We also observed a significant decrease in the diameters of the microvessels in the RhoA-inhibited devices (**P value =.006, **P value =.007 for 1 and 5 µM respectively, n=5, **Fig 3.24 b**).

a

b
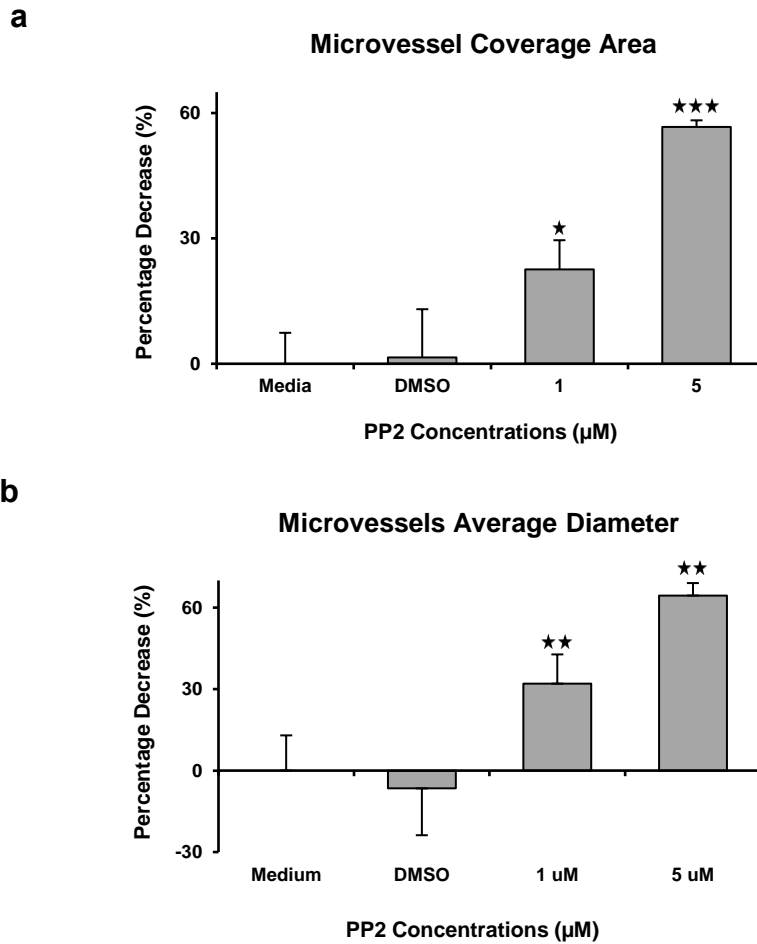
*Fig 3.24: Impact of the inhibition of Src on microvessel characteristics – coverage area and diameter. a) Bar chart comparing coverage area in treated and non-treated microvessels (*P value =.018, ***P value <.001). b) Bar chart comparing the diameter in treated and non-treated microvessels (**P value =.006, **P value =.007 for 1 and 5 µM, respectively). n=5. Normalised with respect to control values.*

Further analysis revealed that a part from microvessels formation, morphology, and characteristics, the topology of microvessels was also affected by the inhibition of Src. Both branch producing ([**]*P* value =.004, and [**]*P* value =.0067 for 1 µM and 5 µM respectively, n=5, **Fig 3.25 a**) and the number of microvessels junctions ([**]*P* value =.005 for both concentrations, n=5) decreased drastically when Src was inhibited (**Fig 3.25 b**). However, the changes observed in average branch length and maximum branch length were not significant (**Fig 3.25 c, d**).
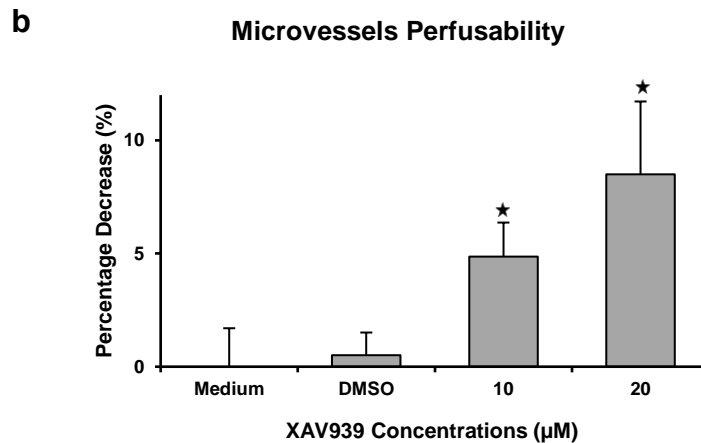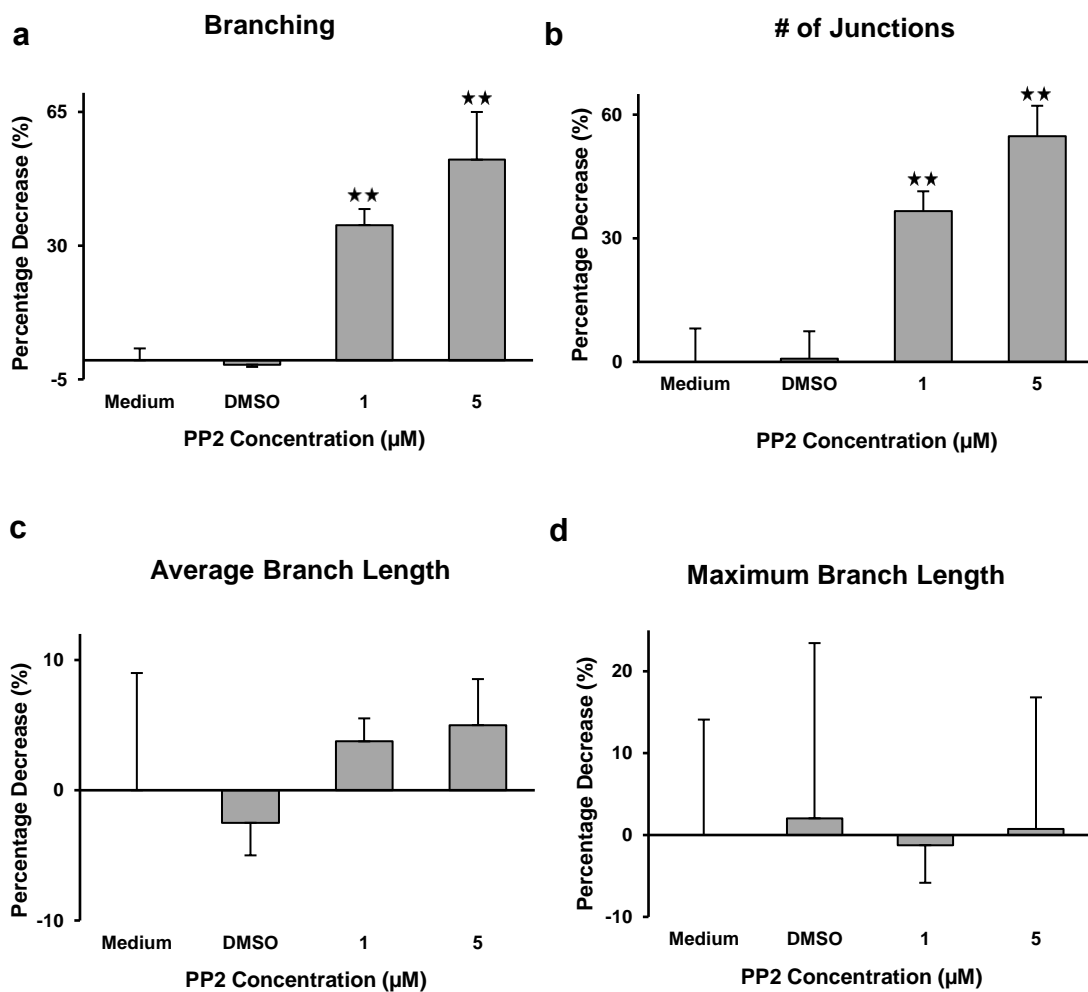

Fig 3.25: Impact of the inhibition of Src on microvessels topology. *a) Bar charts representing the impact of the inhibition of Src on a) producing branches ([**]P value =.004, and [**]P value =.0067 for 1 µM and 5 µM, respectively), b) number of junctions ([**]P value =.005), c) average branch length and d) maximum branch length. n=5. Normalised with respect to control values.*

Finally, perfusion of dextran showed that the function of the microvessels, perfusability, was also affected by the inhibition of Src, as we observed some non-perfusable microvessels (**Fig 3.26 a**). Quantification of perfusability confirmed our observation, as we calculated a decrease of 41.1 ± 10.6 percent for the microvessels treated with 1 µM of the inhibitor ([**]*P* value =.003, n=5) and a decrease of 41.5 ± 7.9 percent for the microvessels treated with 5 µM of the inhibitor ([***]*P* value <.001, n=5, **Fig 3.26 b**).

*(**Fig 3.26** continued on next page. Legend follows)*

134

b
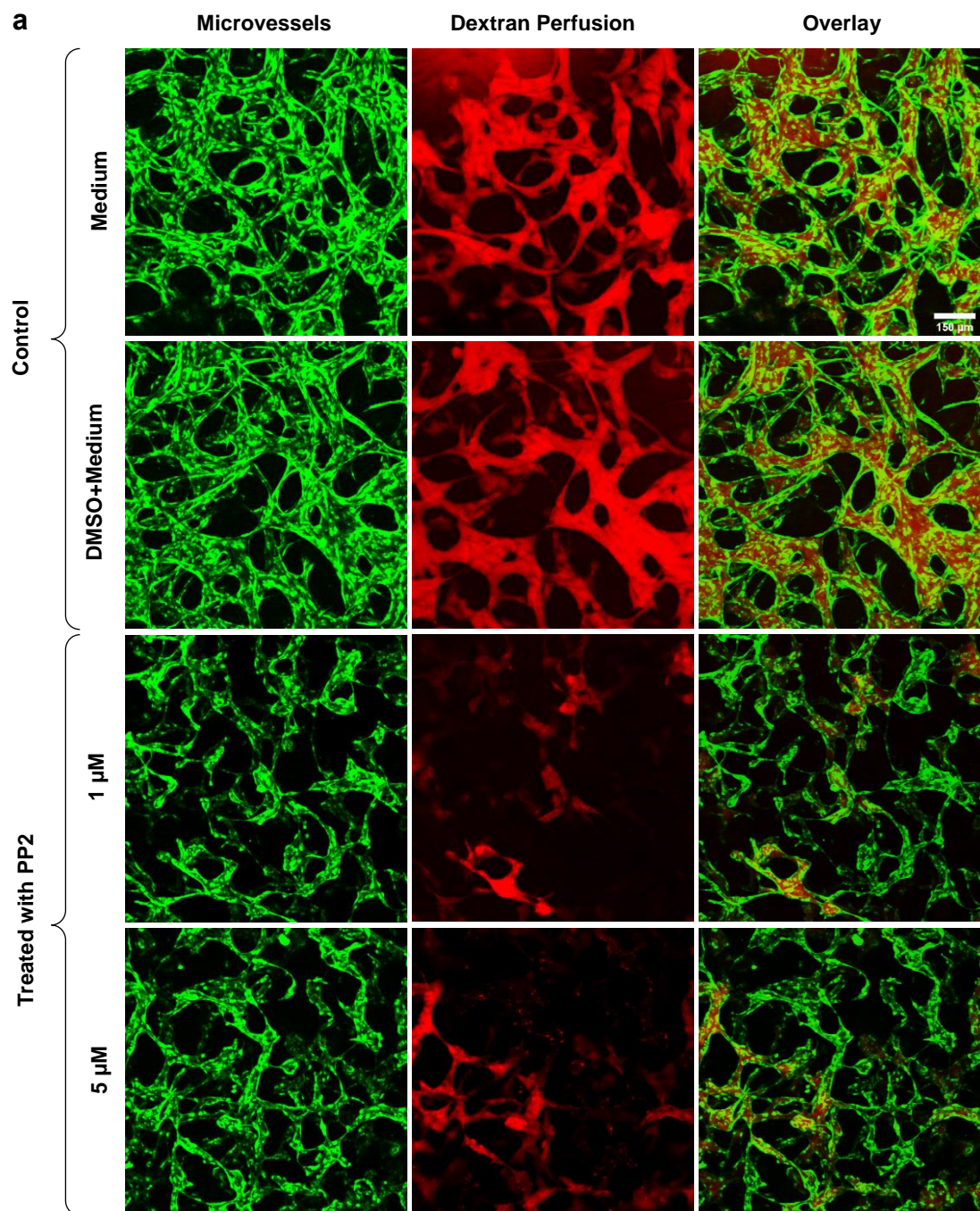
Microvessels Perfusability
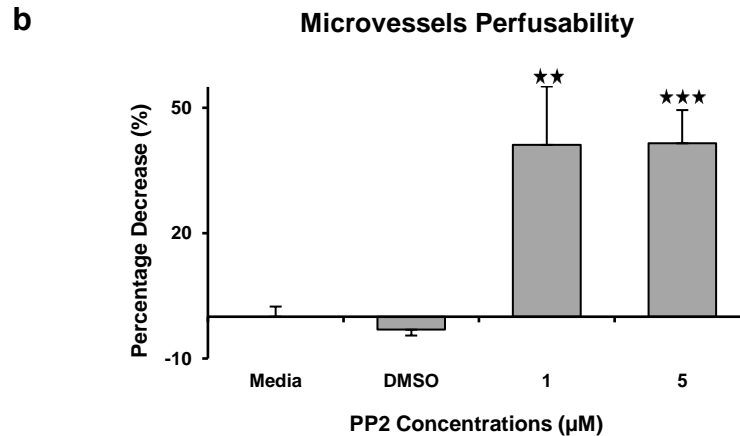
Fig 3.26: Impact of the inhibition of Src on the function of microvessels - perfusability. a) Visualisation of dextran perfusion through microvessels in different conditions. Scale bar, 150 µm. b) Bar chart comparing perfusability in Src-inhibited microvessels (**P value =.003, ****P value <.001, n=5.) and control microvessels. Normalised with respect to control value.*

The decrease in the coverage area, diameter, number of branches, and number of junctions of the microvessels when Src was inhibited provide solid evidence that Src contributes to the stabilisation, characteristics, topology, and function of microvessels.

3.3.3 Impact of Chemotransduction Inhibitors on Microvessels

3.3.3.1 Picropodophyllotoxin, an IGF-1 Inhibitor

IGF-1 was the first gene of this group that we investigated its contribution to vascularisation. To this end, we used an inhibitor, picropodophyllotoxin (PPP). The inhibitor is a specific inhibitor of IGF-1 pathway-mediated signalling. We first determined a concentration at which the inhibitor exhibited no toxic effect on the viability and the proliferation of the cells, as PPP is well-known to kill different cells via apoptosis-mediated mechanisms dose-dependently[186]. Cell viability assay revealed that the inhibitor had no significant effect on the cell viability (**Fig 3.27 a**). However, cell proliferation was affected remarkably by an increase in the inhibitor concentration (**Fig 3.27 b**). Nevertheless, we

determined 0.25 µM of the inhibitor as our desired concentration because neither cell viability nor cell proliferation was influenced at this concentration.
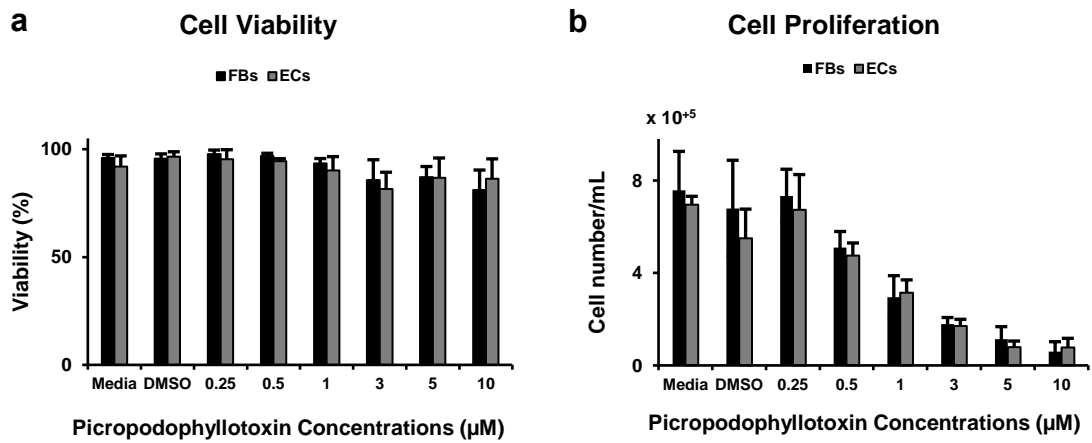
Fig 3.27: Determination of desired concentration of IGF-1 inhibitor - picropodophyllotoxin. *a) Bar chart representing the impact of different concentrations of IGF-1 inhibitor on the viability of the cells. b) Bar chart representing the impact of the inhibition of IGF-1 on the proliferation of the cells. n=3.*

Next, we treated co-cultured ECs and FBs with the desired concentration. The impact of the inhibition of IGF-1 was obvious from the beginning of culture. Unlike controls, ECs failed to form microvessels by day 4 of culture. On day 7, we observed drastic differences between controls and IGF-1-inhibited microvessels so that ECs produced a bunch of dispersed, disconnected, sheet-like clusters (**Fig 3.28 a**). Consequently, the microvessels coverage area decreased drastically ($^{**}P$ value =.007, n=3, **Fig 3.28 b**). Measurement of vascular diameter revealed that sheet-like structures were of quite larger diameter than controls ($^{***}P$ value <.001, n=3, **Fig 3.28 c**).

a

| | Day 1 | Day 4 | Day 7 |

Control — Medium

Control — DMSO+Medium

Picropodophyllotoxin — 0.25 μM

150 μm

b **Microvessels Coverage Area**

Percentage Decrease (%)

★★

Media   DMSO   0.25

Picropodophyllotoxin Concentration (μM)

c **Microvessels Diameter**

Percentage Increase (%)

★★★

Medium   DMSO   0.25

Picropodophyllotoxin Concentration (μM)
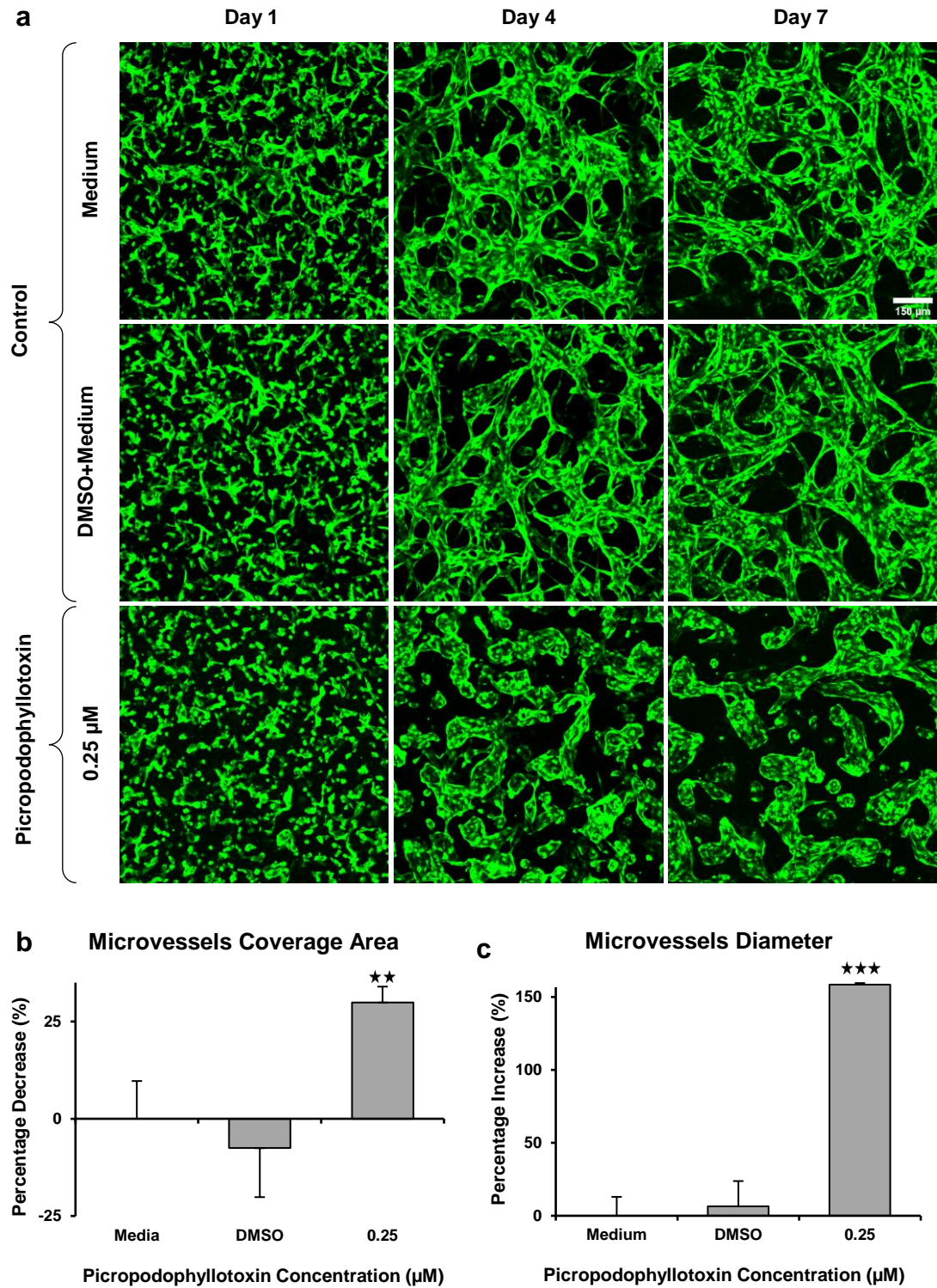
Fig 3.28: Impact of the inhibition of IGF-1 on vascularisation. *a) 3D confocal images visualising the impact of the inhibition of IGF-1 on microvessel formation over the course of 1 week. Scale bar, 150 μm. b) Bar chart comparing coverage area in IGF-1-inhibited microvessels and control microvessels (****P value =.007) c) Bar chart comparing diameter in IGF-1-inhibited microvessels and control microvessels (*****P value <.001.) n=3. Normalised with respect to control values.*

We analysed our 3D images further to investigate topological changes of the microvessels. Not surprisingly, both microvessels branching and the number of junctions reduced drastically ($^{**}P$ value =.002, n=5, for both features, **Fig 3.29 a, b**). Also, a notable decrease was observed in both average branch length ($^{**}P$ value =.003, n=5) and maximum branch length ($^{**}P$ value =.002, n=5, **Fig 3.29 c, d**).
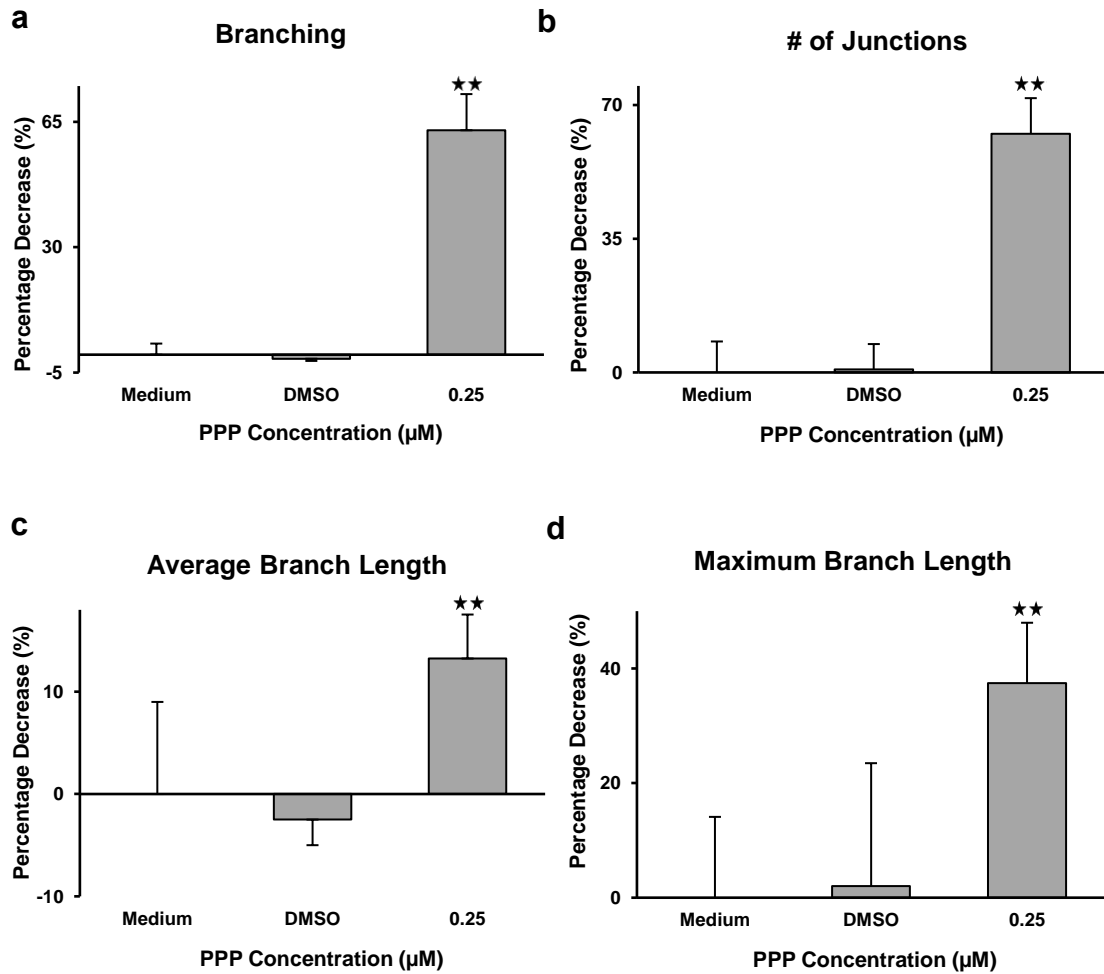
Fig 3.29: Impact of the inhibition of IGF-1 on microvessels topology. *Bar charts representing the impact of the inhibition of IGF-1 on a) microvessels branching ($^{**}P$ value =.002), b) the number of microvessels junctions ($^{**}P$ value =.002), c) average branch length ($^{**}P$ value =.003) and d) maximum branch length ($^{**}P$ value =.002.) n=5. Normalised with respect to control values.*

Similar to what we did for the former genes, we also investigated the impact of the inhibition of IGF-1 on the perfusability of microvessels by injecting the

tracer dye. As expected, perfusability decreased drastically, demonstrating that the sheet-like structures formed were neither interconnected nor intra-connected (***P value <.001, n=3, **Fig 30 a, b**).
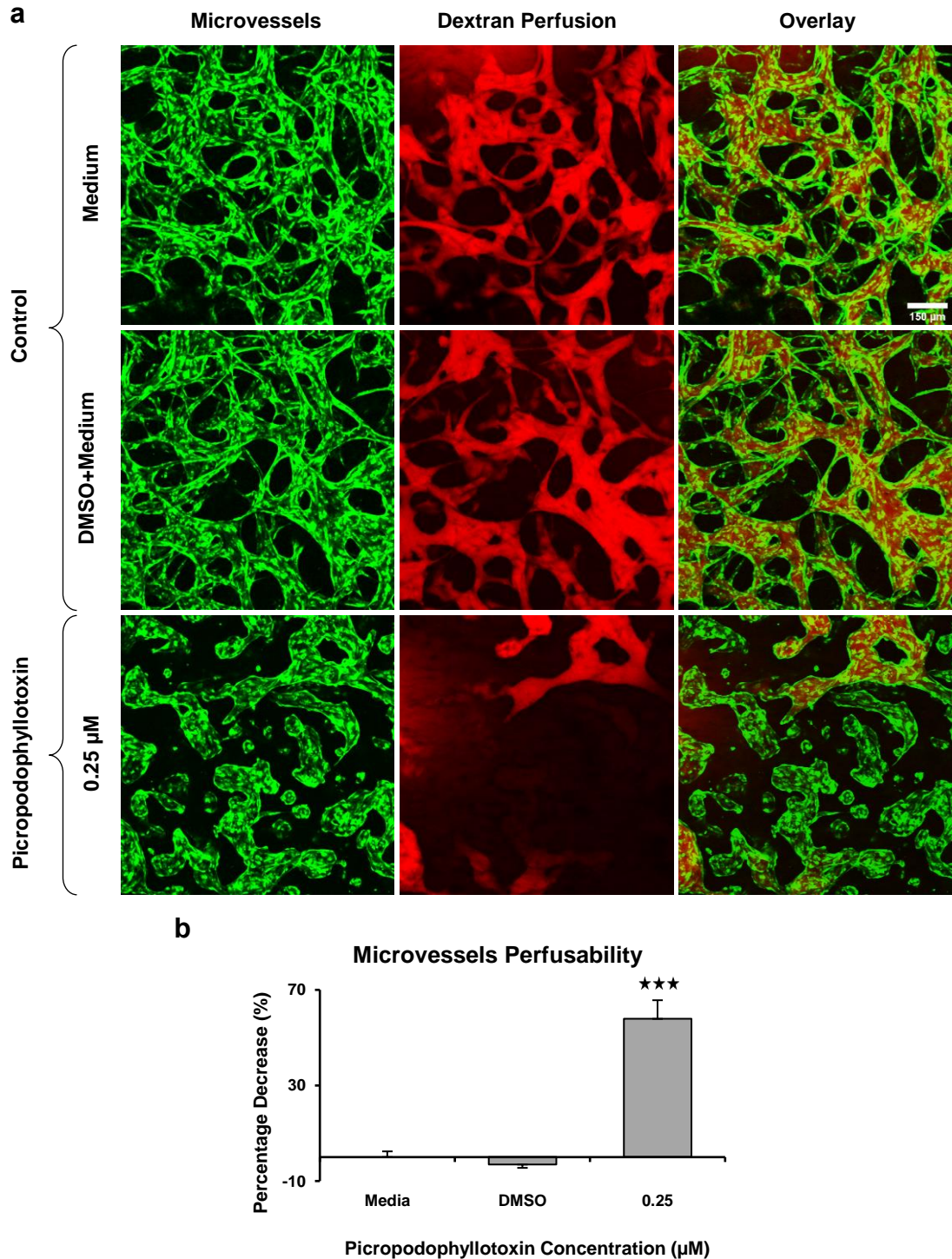
Fig 3.30: Impact of the inhibition of IGF-1 on the function of microvessels- perfusability.
*a) Visualisation of dextran perfusion through microvessels in different conditions. Scale bar, 150 μm. b) Bar chart comparing perfusability in Src-inhibited microvessels and control microvessels (***P value <.001, n=3.) Normalised with respect to control value.*

139

To wrap up, treated with PPP, ECs failed to self-assemble and produce functional microvessels. The lack of the formation of microvessels shows that IGF-1 contributes to vascularisation at an early stage.

3.3.3.2 SB-431542, a TGFβ Inhibitor

To assess the role of TGFβ in vascularisation, we inhibited the gene by an inhibitor, SB-431542. Blocking TGFβ type I receptor, the inhibitor prevents TGFβ function[187]. It also blocks the phosphorylation and nuclear translocation of the SMADs, intracellular mediators of TGFβ signalling, with decreased TGFβ-mediated transcription[188]. At first, we determined the desired concentration(s) of the inhibitor by treating ECs and FBs with different concentrations of SB-431542 as many research groups, including Hjelmeland *et al.* reported that SB-431542 inhibits cell proliferation[188]. Consistent with their findings, our assay showed that the inhibitor inhibits cell proliferation in a dose-dependent manner[188]. However, our cell viability and cell proliferation assays confirmed that neither features of the cells were affected significantly by three concentrations of the inhibitor, 0.1 µM, 1 µM, and 10 µM (**Fig 3.31 a, b**).
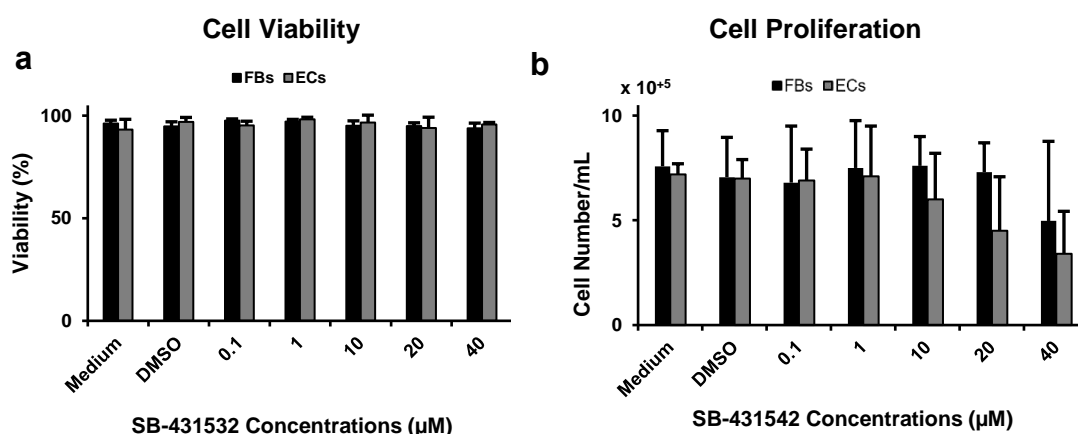
Fig 3.31: Determination of desired concentrations of TGFβ-inhibitor – SB-431542. a) Bar chart representing the impact of different concentrations of the inhibitor on the viability of the cells. b) Bar chart representing the impact of different concentrations of the inhibitor on the proliferation of the cells. n=3.

When treated with different concentrations of TGFβ-inhibitor, although ECs retained their ability to form microvessels, the microvessels formed were

drastically different from controls in terms of morphology and topology. The differences were visible from day 4. Compared to control microvessels, TGFβ-inhibited microvessels looked denser and much larger in diameter (**Fig 3.32**).
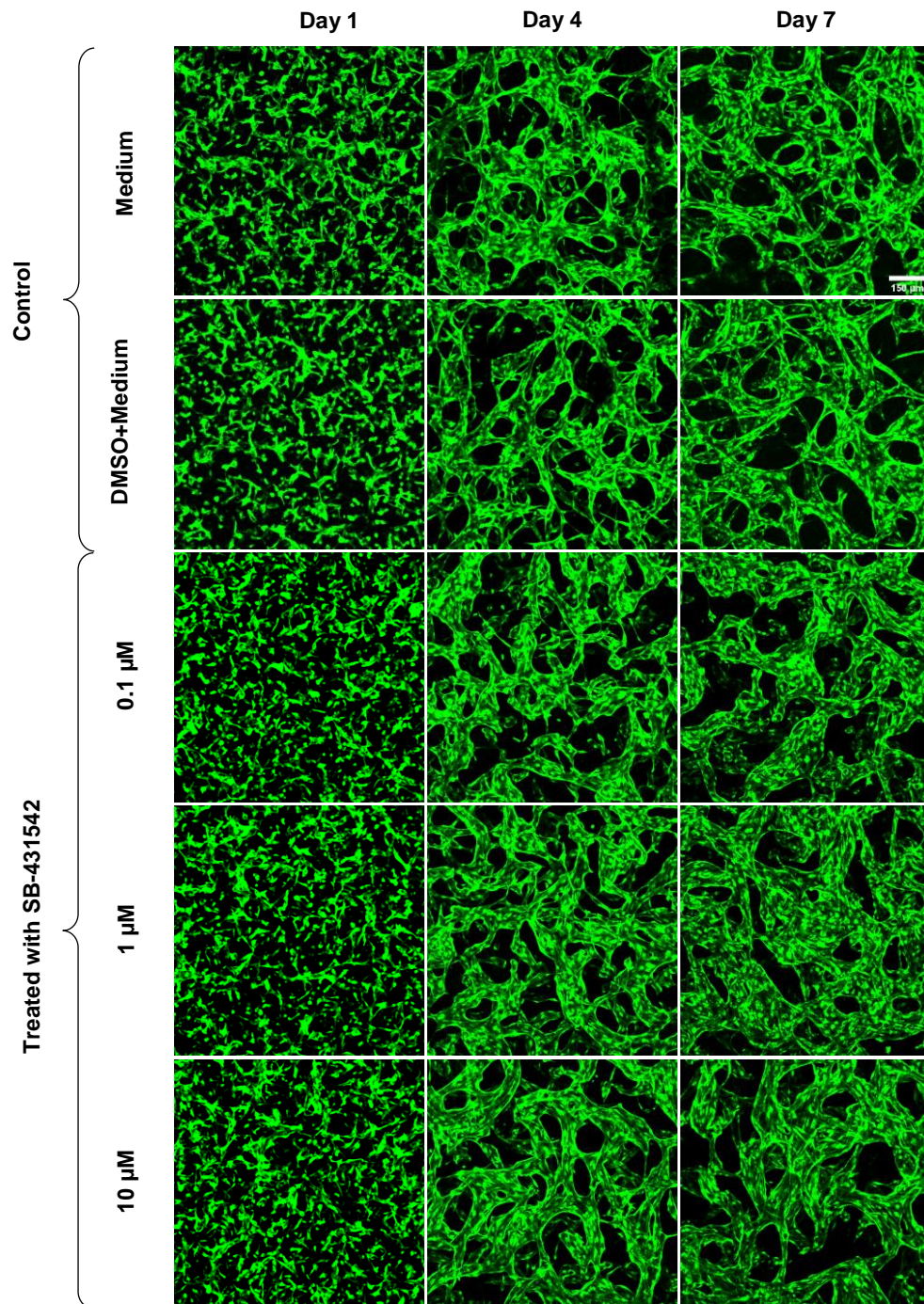
Fig 3.32: Impact of the inhibition of TFGβ on the formation of microvessels. *3D confocal images visualising the impact of the inhibition of TGFβ on microvessels formation and morphogenesis over the course of one week. Scale bar, 150 μm.*

Measurement of microvessel coverage area confirmed that the feature increased in a dose-dependent manner when the co-cultured cells were treated with the inhibitor ($^{***}P$ value <.001, n=5 for all concentrations of the inhibitor, **Fig 3.33 a**). We also observed a drastic increase in the microvessel diameter in a dose-dependent manner ($^{***}P$ value <.001, n=5 for all inhibitor concentrations). In other words, ECs tended to produce microvessels with much larger diameters when TGFβ was inhibited (**Fig 3.33 b**).
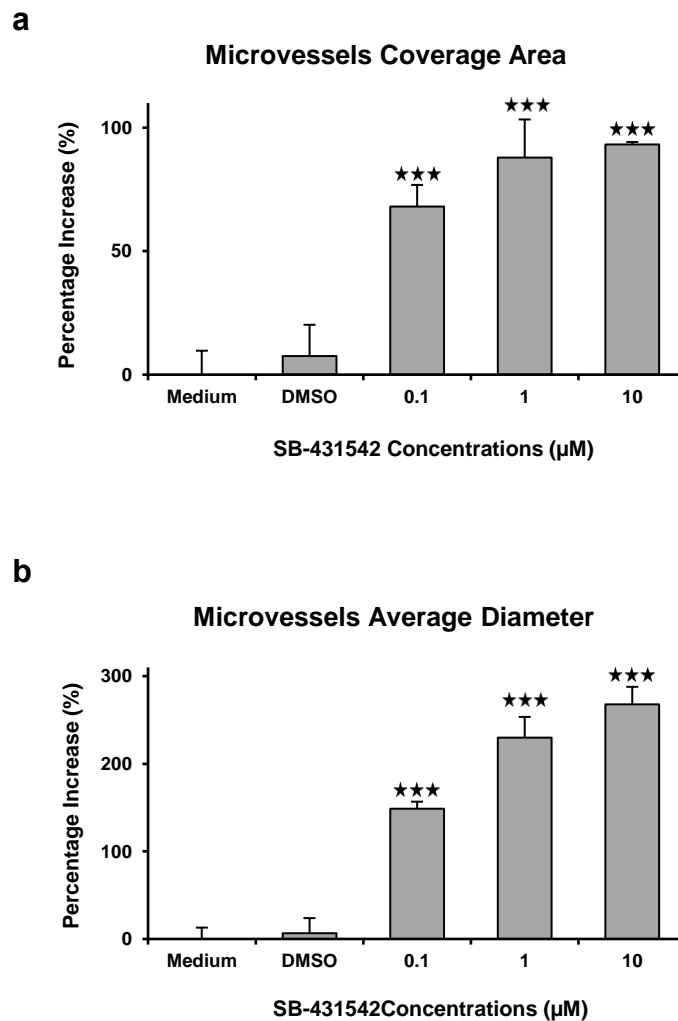
Fig 3.33: Impact of the inhibition of TGFβ on microvessel characteristics. *a) Bar chart representing the impact of the inhibition of TGFβ on microvessels coverage area ($^{***}P$ value <.001), b) Bar chart representing the impact of the inhibition of TGFβ on microvessels diameter ($^{***}P$ value <.001.) n=5. Normalised with respect to control values.*

Excluding the microvessels treated with 10 μM of the inhibitor, the observed increases in microvessels branching ($^{**}P$ value =.005, n=5, **Fig 3.34 a**) and the number of microvessels junctions ($^{**}P$ value =.007, n=5, **Fig 3.34 b**) were not significant. Interestingly, both average branch length ($^{**}P$ value =.005, for 0.1 μM and $^{***}P$ value <.001 for 1 μM and 10 μM of the inhibitor, n=5) and maximum branch length ($^{*}P$ value =.014, for 0.1 μM and $^{**}P$ value =.003 for 1 μM and 10 μM of the inhibitor, n=5) decreased significantly in the treated microvessels compared to control microvessels in a dose-dependent manner (**Fig 3.34 c, d**).
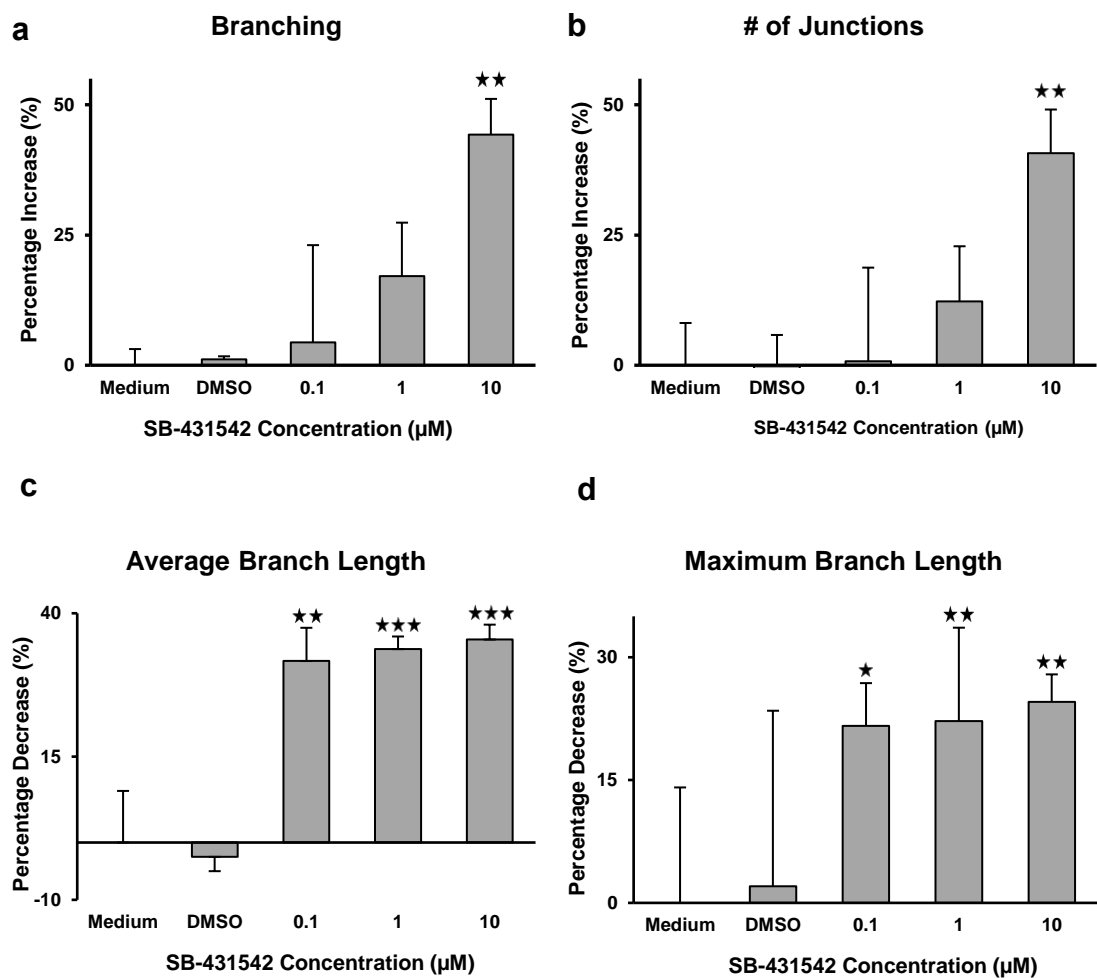
Fig 3.34: Impact of the inhibition of TGFβ on microvessel topology. *Bar chart representing the impact of the inhibition of TGFβ on a) branching ($^{**}P$ value =.005), b) number of microvessels junctions ($^{**}P$ value =.007), c) average branch length ($^{**}P$ value =.005, and $^{***}P$ value <.001), and d) maximum branch length ($^{*}P$ value =.014, and $^{**}P$ value =.003). n=5. Normalised with respect to control values.*

Perfusion of dextran revealed that the TGFβ-inhibited microvessels were perfusable indicating that the gene did not affect the function (perfusability) of the microvessels (**Fig 3.35 a, b**).
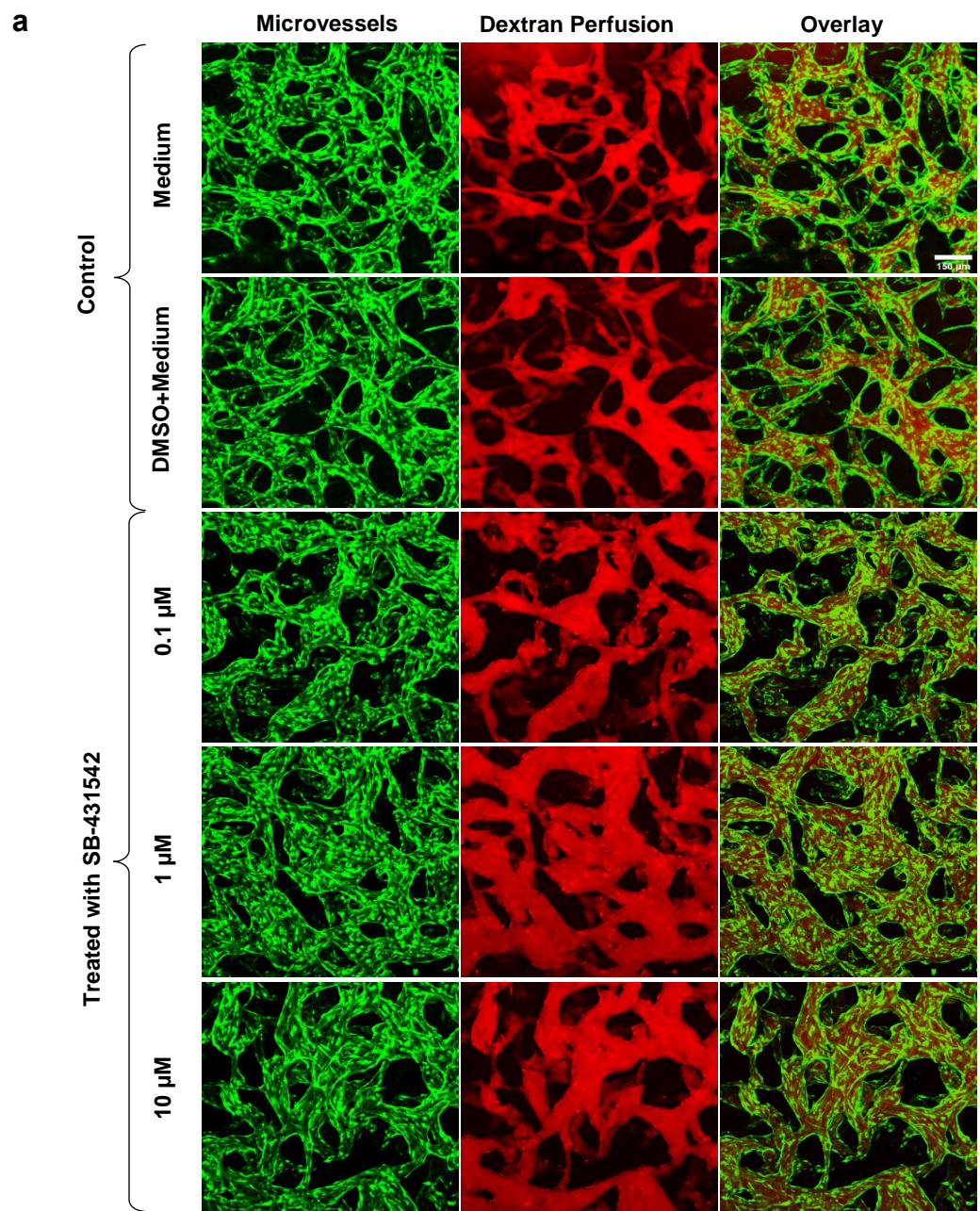
*(**Fig 3.35** continued on next page. Legend follows)*

b
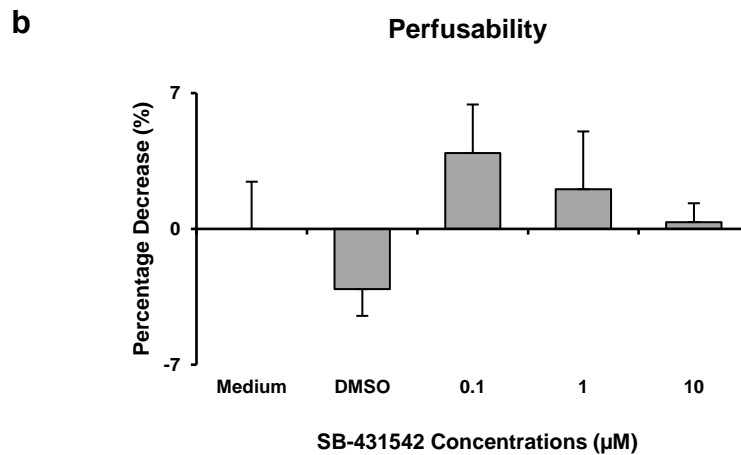
Perfusability

Fig 3.35: Impact of the inhibition of TGFβ on the function of microvessels. a) Visualisation of dextran perfusion through microvessels in different conditions. Scale bar, 150 µm. b) Bar chart representing the change in perfusability in different conditions. Normalised with respect to control value. n=5.

The formation of functional microvessels despite the inhibition of TGFβ demonstrates that TGFβ has no key role in the formation and function of microvessels. However, extreme increases in the coverage area, diameter, branching, and the number of junctions, and the remarkable decreases in microvessel average branch length and maximum branch length indicate that the gene contributes to the microvessel morphology and topology.

It is worth mentioning that TGFβ signalling can shift from being mostly angiostatic to pro-angiogenic. Although the process is not fully understood, this depends on the activation of the pro-angiogenic pathway which involves TGFβ type II receptor recruitment of the predominantly endothelial TGFβ type I receptor activin receptor-like kinase-1 (ALK1). The later, ALK1, initiates activation of the transcription factors SMAD1, 5 and 8, resulting in a proangiogenic phenotype. Several factors including TGFβ concentration, its bioavailability and the presence or absence of some factors including bone morphogenic proteins and accessory receptors such as endoglin and TGFβ type III receptor regulate this different signalling.

In a fascinating study Wang et al, introduced leucine-rich alpha-2-glycoprotein 1 (Lrg1) as a new regulator of TGFβ signalling which contributes to abnormal

145

vessel growth by activating a TGFβ switch. They showed that in the presence of TGFβ, Lrg1 triggers angiogenesis by inducing EC proliferation. Their findings also revealed that blockage of Lrg1 by an antibody results in the attenuation of angiogenesis. This new regulator regulates neovascularisation through TGFβ signalling meaning that TGFβ is one of the main mediators of neovascularisation[11,189]. Therefore, one could say that microvessels formed in our system despite being treated with SB-431542 because SB-431542 blocks TGFβ type I receptor while the other receptor, Lrg1, is still available to regulate TGFβ signalling.

3.3.3.3 A-395, an EED Inhibitor

The last gene we investigated its contribution to the vascularisation was EED which its inhibition was experimentally achieved by treating co-embedded ECs and FBs with different concentrations of an EED-inhibitor, A-395. Polycomb repressive complex 2 (PRC2) regulates cellular differentiation, development, and homeostasis[190,191]. EED protein is an essential subunit of PRC2. A-395 inhibits EED function by binding to it in its H3K27me3-binding pocket, subsequently PRC2[191]. Knowing the negative effect of A-395 on cell proliferation and viability[191], we treated our cells with different concentrations of the inhibitor to determine the desired concentration(s) that do not affect cell viability and proliferation. A-395 was first reconstituted in water. Although the amount of water used was negligible, to avoid any possible damages on the cells and subsequently on the microvessels, we assessed the impact of the extra water added to the growth medium on the cell viability and proliferation. We did so to determine the desired concentrations of the inhibitor too. Performing cell viability and proliferation assays, we showed that adding water exhibited no significant effect on both the cell types viability and proliferation. Also, we determined 0.1 and 0.5 µM as the desired concentrations of the inhibitor (**Fig 3.36 a, b**).

a **Cell Viability**

b **Cell Proliferation**
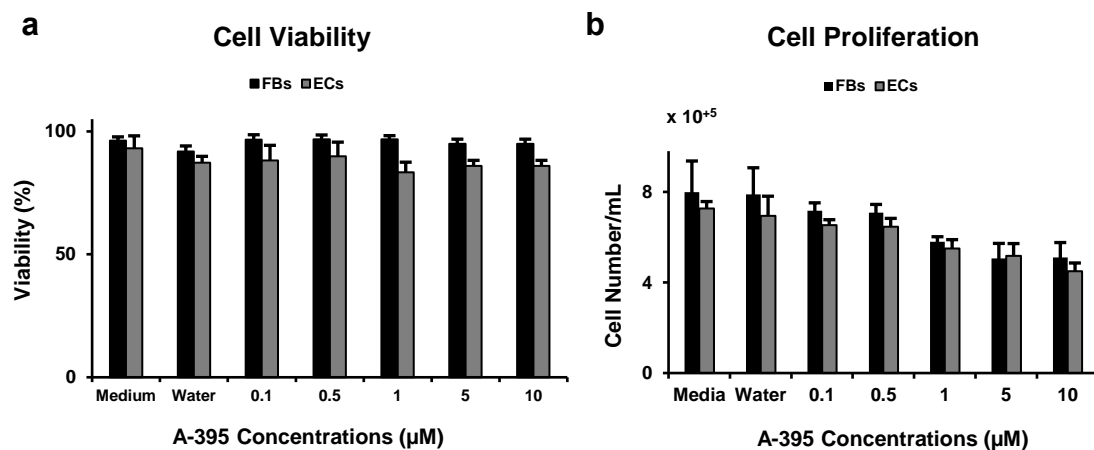
Fig 3.36: Determination of desired concentration of EED-inhibitor, A-395. *a) Bar chart representing the impact of different concentrations of EED inhibitor on the viability of the cells. b) Bar chart representing the impact of different concentrations of EED inhibitor on the proliferation of the cells. n=3.*

We next set out to investigate the contribution of EED to vascularisation by inhibiting it in co-embedded ECs and FBs. The inhibition was experimentally achieved by treating the cells with 0.1 µM and 0.5 µM of the inhibitor. When treated with EED inhibitor, ECs maintained their ability to form microvessels, demonstrating that the gene would not contribute to the formation of microvessels (**Fig 3.37**).
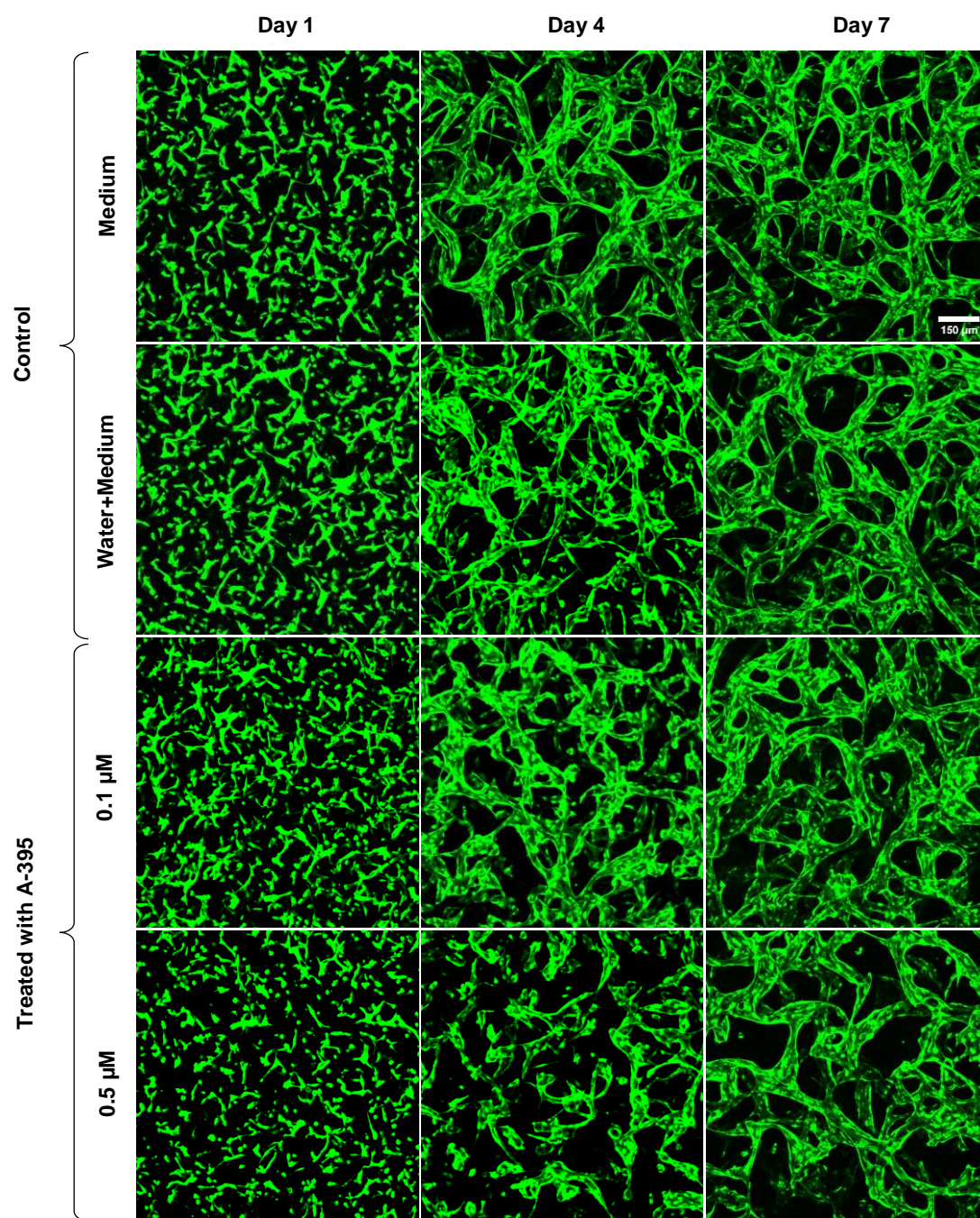
Fig 3.37: Impact of the inhibition of EED on microvessels formation. *3D confocal images visualising the impact of the inhibition of EED on the formation of microvessels. Scale bar, 150 μm.*

In efforts to characterise the microvessels, we quantified the microvessels coverage area. We observed some changes in the coverage area. However, the differences observed were not significant (**Fig 3.38 a**). Nevertheless, we noticed a significant increase in the diameters of the EED-inhibited microvessels ($^*P$ value =.039 and $^*P$ value =.044 for 0.1 µM and 0.5 µM of the inhibitor, respectively, n=3.) We measured the average diameter to be 32.4 ± 1.15 µm for the microvessels treated with 0.1 µM of the inhibitor ($^*P$ value =.039, n=3) and 32.26 ± 1.78 µm for the microvessels treated with 0.5 µM of the inhibitor ($^*P$ value =.044, n=3). **Fig 3.38 b** compares EED-inhibited microvessels and control microvessels in terms of diameter. The increase in microvessel diameter could explain why there was no significant change in the microvessel coverage area compared to the control microvessels despite a significant decrease in the number of branches.
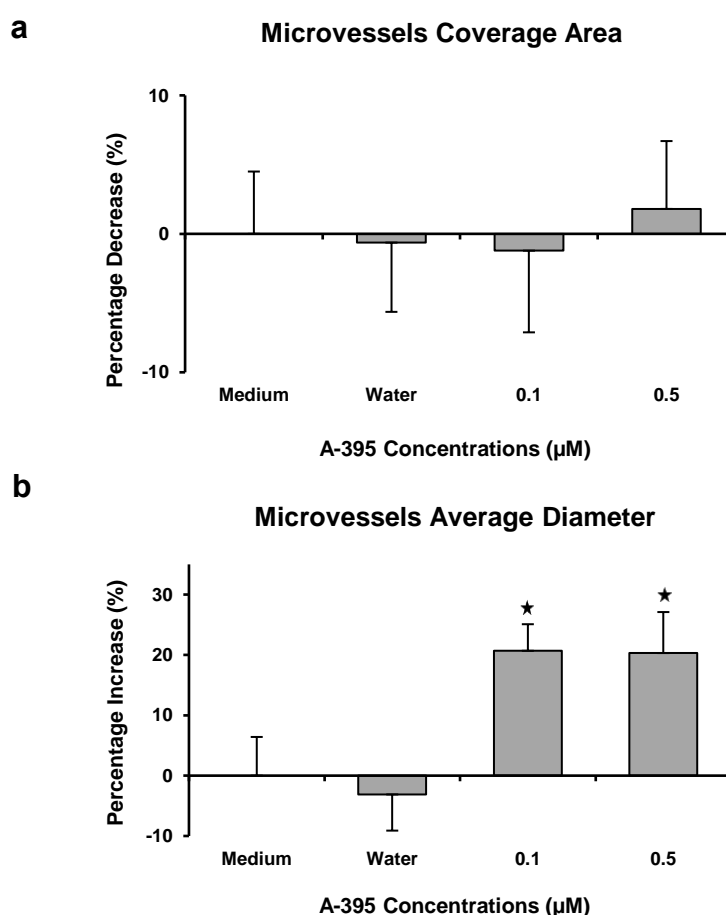
Fig 3.38: Impact of the inhibition of EED on microvessel characteristics. *Impact of the inhibition of EED on a) microvessels coverage area and b) microvessels diameters ($^*P$ value =.039 and $^*P$ value =.044 for 0.1 µM and 0.5 µM of the inhibitor, respectively, n=3.) Normalised with respect to control values.*

Assessment of topological changes revealed that both branching ($^{*}P$ value =.036, and $^{**}P$ value =.0016 for 0.1 µM and 0.5 µM respectively, n=5) and the number of junctions ($^{*}P$ value =.046, and $^{**}P$ value =.0019 for 0.1 µM and 0.5 µM respectively, n=5) decreased significantly in a dose-dependent manner (**Fig 3.39 a, b**). Also, we observed a significant decrease in the microvessel average branch length when the cells were treated with 0.5 µM of the EED inhibitor ($^{**}P$ =.0025, n=5, **Fig 3.39 c**). However, statistical analysis revealed that the changes observed in microvessel maximum branch length were not significant for any inhibitor concentrations (**Fig 3.39 d**).
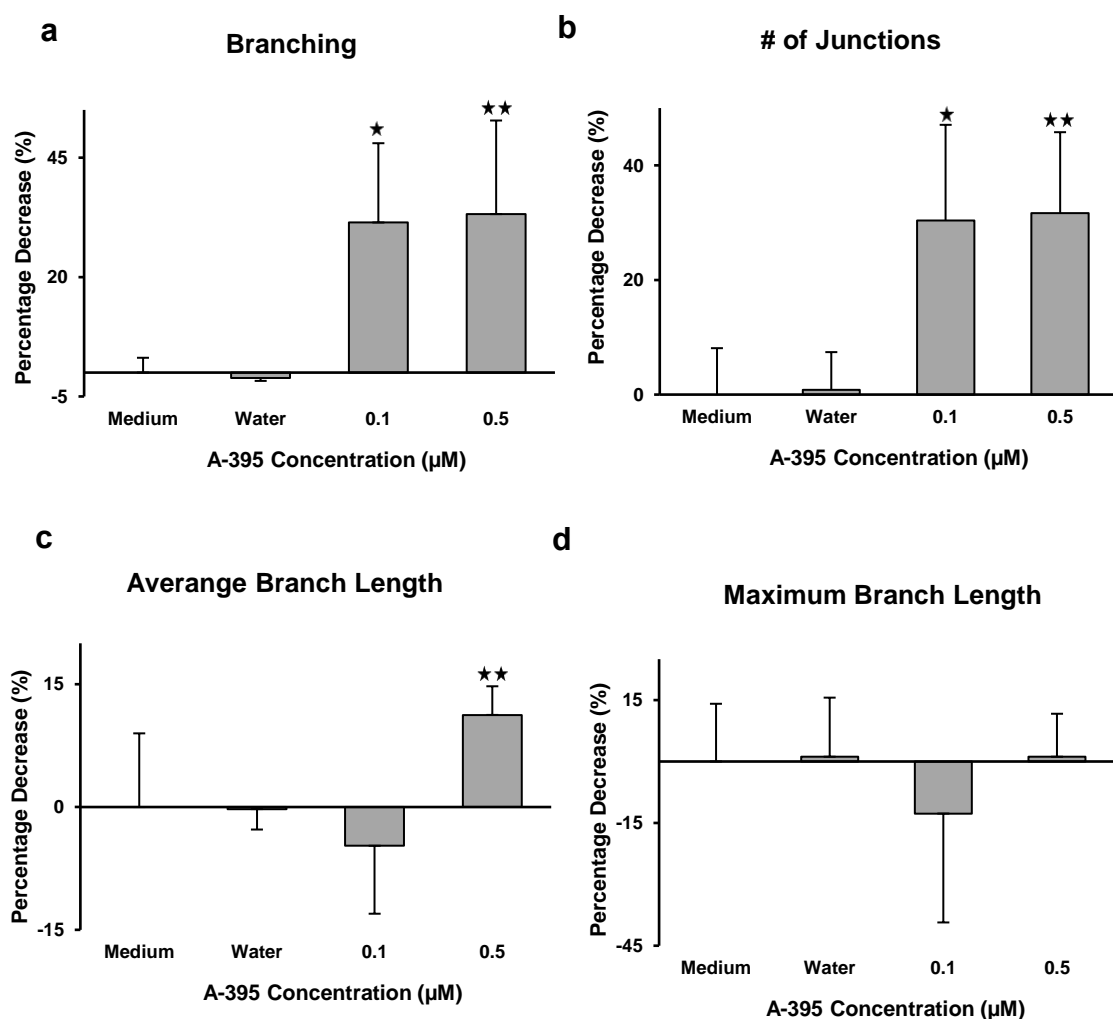
Fig 3.39: Impact of the inhibition of EED on microvessels topology. *Bar charts representing the impact of the inhibition of EED on a) producing branches ($^{*}P$ value =.036, and $^{**}P$ value =.0016) and b) the number of microvessels junctions ($^{*}P$ value =.046, and $^{**}P$ value =.0019), c) average branch length ($^{**}P$ =.0025), and d) maximum branch length. n=5. Normalised with respect to control values.*

Finally, the tracer dye's perfusion revealed that the EED inhibition also affected the microvessel function as the perfusability of the microvessels decreased significantly when the co-embedded cells were treated with 0.5 µM of the inhibitor ($^{**}P$ value =.002, n=5, **Fig 3.40**).
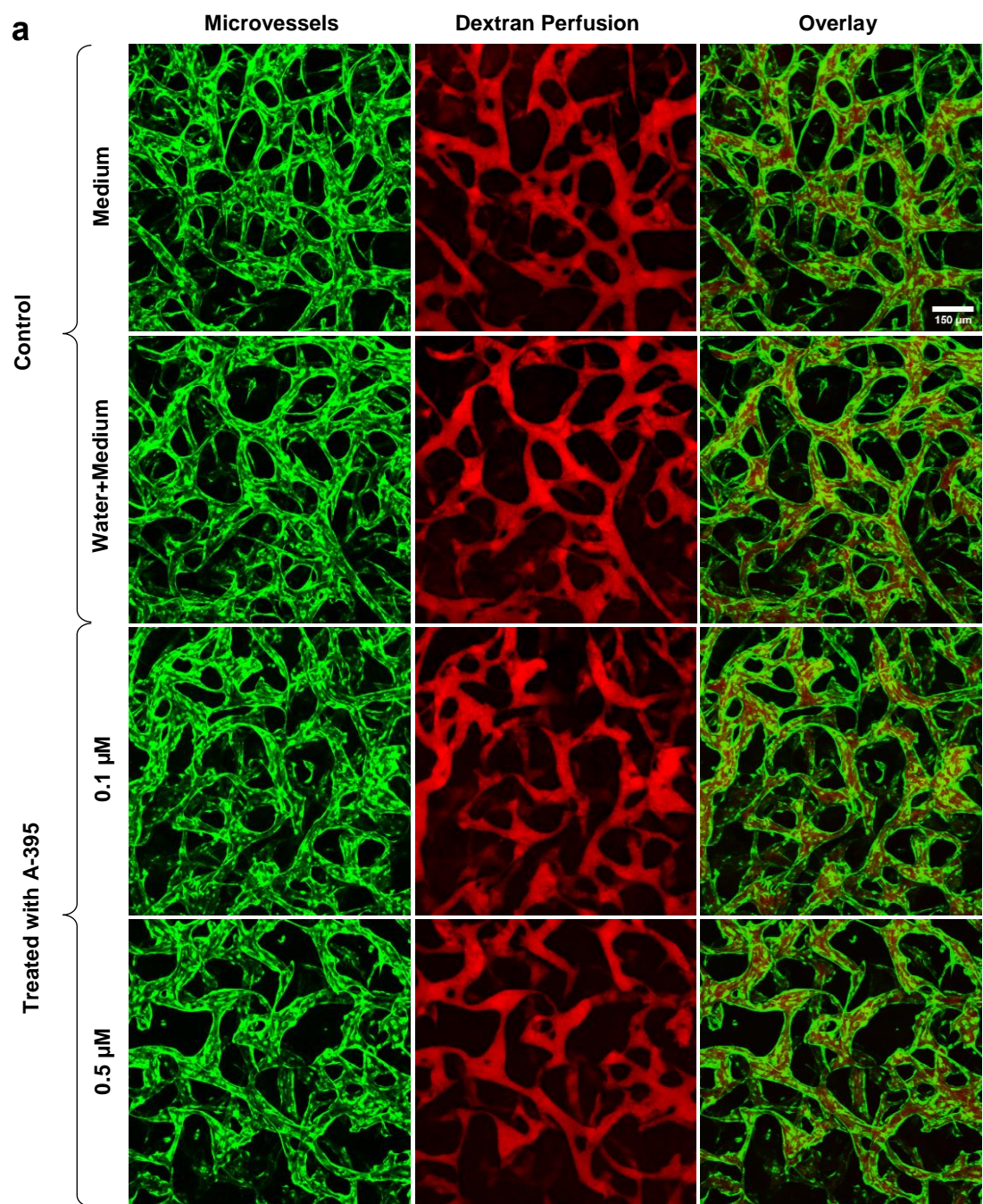
*(**Fig 3.40** continued on next page. Legend follows)*

b

Microvessels Perfusability
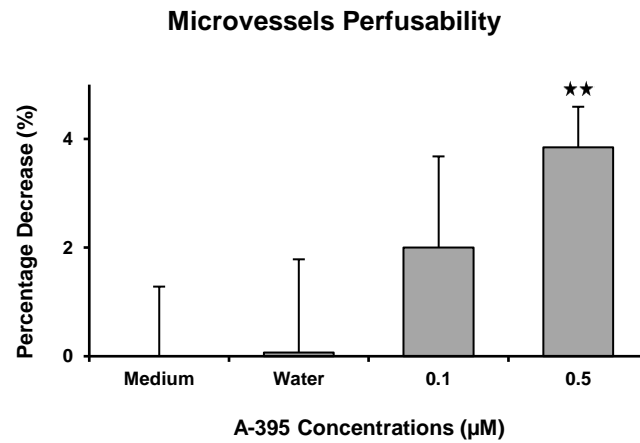
Fig 3.40: Impact of the inhibition of EED on the function of microvessels - perfusability. a) Perfusion of dextran showed that not all the microvessels treated with the concentrations of the EED were perfusable. Scale bar, 150 µm. b) Bar chart representing the impact of the inhibition of EED on the microvessels function (**P value =.002, n=5.) Normalised with respect to control value.

In the end, our data provide solid evidence that EED contributes to the microvessel topology and function but not the formation of microvessels.

152

3.4 Discussion and Conclusion

Some genes belonging to mechanotransduction pathways were chemically inhibited in both ECs and FBs to investigate their functions in vascularisation. Our chemical perturbation results are consistent with previous studies that found the critical role of several mechanotransduction pathways in vascularisation by mostly focusing on the perturbation of pathways in ECs only.

RhoA plays a crucial role in vascularisation by participating in cell motility and migration through actin fibre polymerisation[126]. The inhibition of RhoA, the master regulator of mechanotransduction pathways, by a high concentration of the inhibitor led to arresting microvessel formation in our system. It also resulted in less dense, less branched, enlarged microvessels at a low inhibitor concentration. Consistent with these findings, Amerongen *et al.* reported that RhoA or Rho kinase inhibition reduced EC migration and angiogenesis[192]. Designing a mouse skin model and embedding ECs in a collagen hydrogel, Hoang *et al.* also showed that the perturbation of RhoA inhibited microvessel formation in both *in vivo* and *in vitro* models[193]. Another study by Hashimoto *et al.* showed that the inhibition of RhoA by an inhibitor named Alendronate led to inhibition of tumour angiogenesis. This was due to a decrease in Rho activation, lack of actin stress fibres, and focal adhesion formation in HUVECs[127]. Using an exoenzyme, *Clostridium botulinum* C3 transferase, which suppresses explicitly Rho, Uchida *et al.* investigated the role of small GTPase Rho signal transduction pathway in angiogenesis *in vitro* and *in vivo*[126]. Their findings are in good agreement with our results and previously referred studies.

From a mechanical point of view, YAP and its coactivator, TAZ, play a pivotal role in vascular formation, sprouting angiogenesis, vascular barrier formation, and maturation by activating remodelling of the actin cytoskeleton which is critical for filopodia formation and junction assembly by ECs. Inhibition of YAP in our system resulted in the lack of microvessel formation, indicating that YAP

is a key player at the very early stage of vascularisation. Using animal models, Kim *et al.* showed that the deletion of YAP/TAZ in ECs in mice models resulted in tip cells with fewer and dysmorphic filopodia, less branched, less dense, and enlarged vessels, reduced and disarranged distributions of tight and adherent junction proteins, and decrease in choroidal neovascularisation. Injecting dextran (70 kDa) at a concentration of 25 mg/mL, they also revealed that perturbation of YAP/TAZ led to disrupted barrier integrity, increased permeability, and subsequent haemorrhage in the growing retina and brain vessels[194]. Zhu *et al.* also showed that YAP cooperating with signal transducer and activator of transcription factor 3 (STAT 3) regulates the proliferation, migration, and lumen formation of human retinal microvascular endothelial cells via VEGF signaling[195].

Although microvessel formation was not affected by Src inhibition in our JCC system, the microvessels were morphologically, topologically, and functionally different from control microvessels. These findings are consistent with an earlier study by Pyun *et al.* that demonstrated the Src family regulates angiogenesis and vascular permeability of ECs[141]. An interesting study showed that Src-inhibited fibroblasts fail to upregulate VEGF in hypoxia conditions indicating the role of Src in VEGF regulation and subsequently vascularisation[139]. Placing filter disks saturated with either bFGF or VEGF on a chick chorioallantoic membrane of 10-day-old chick embryos, Eliceiri *et al.* observed a 2-fold increase in Src activity. To examine the role of Src in angiogenesis, they then infected chick chorioallantoic membranes exposed to VEGF with the Src 251–containing retrovirus. This resulted in arresting angiogenesis in chick embryos, demonstrating that Src activity is required for VEGF-induced angiogenesis and EC servival[140].

FAK, a cytoplasmic tyrosine kinase, plays a pivotal role in integrin and growth factor mediated signalling and is a key player in angiogenesis. It is involved in vital processes for angiogenesis, such as cell migration and proliferation[196]. Aiming to study the role of FAK in vascularisation, we inhibited the gene in

both ECs and FBs with a specific inhibitor, which arrested the formation of functional microvessels in a dose-dependent manner. We also observed significant changes in microvessel characteristics, topology, and function, which are in good agreement with the findings of earlier studies. Treating ECs seeded on collagen I coated plates with increasing concentrations of FAK inhibitors, PF-573228 and FAK Inhibitor 14, Cabrita *et al.* demonstrated that the inhibition of FAK blocks lumen formation by ECs in a dose dependent manner[197]. Tavora *et al.* generated endothelial-specific tamoxifen-inducible FAK knockout mice to investigate the role of FAK in tumour angiogenesis. They observed that the endothelial FAK-deletion in adult mice inhibited tumour growth and reduced tumour angiogenesis, demonstrating the role of FAK in adult angiogenesis[196].

Microvessel formation was not affected by the deletion of Wnt/β-catenin in ECs and FBs in our JCC system. However, the microvessels were less dense, with a significant decrease in their diameters compared to controls. These observations, along with changes in microvessel topology and the decrease in their perfusability, provide concrete evidence that Wnt/β-catenin is an essential mechanotransduction gene in microvessel morphogenesis, topology, and function. Hu *et al.* utilised two Wnt antagonists to investigate the influence of Wnt on vascularisation. Their findings are in good agreement with our findings as they showed that the inhibition resulted in the reduction of vascular density and the number of lumens[198]. Consistent with these findings, using genetic mouse models, Stenman *et al.* found that the central nervous system (CNS) uses the canonical Wnt signalling pathway to promote the formation and CNS-specific differentiation of the organ's vasculature. In other words, canonical Wnt signalling in ECs is critical for CNS vascularisation[199].

We also inhibited three genes belonging to chemotransduction pathways, IGF-1, TFGβ and EED in our JCC system. Perturbation of IGF-1 and EED in both ECs and FBs in our system inhibited microvessel formation significantly. In contrast, knockdown of TGFβ did not affect microvessel formation. However,

the microvessels were morphologically, functionally and topologically different from control microvessels. Our results for chemically perturbing IGF-1, TGFβ, and EED are consistent with previous studies that found the critical roles of the above mentioned genes in vascularisation[200–202].

The findings of this chapter highlight that the formation, characteristics, topology, and function of blood microvessels are affected by the inhibition of mechanotransduction genes. Treating ECs co-cultured with FBs with different small molecule inhibitors of mechanotransduction pathways, we showed that EC ability to form blood microvessels is entirely or significantly arrested. In addition to microvessel formation, we observed significant differences between mechanotransduction pathway-inhibited microvessels and control microvessels as to characteristics, topology, and function, demonstrating the key roles of these pathways in different stages of vascularisation.

4 Perturbation of Mechanotransduction Genes in FBs

4.1 Introduction

The chemical inhibition of genes belonging to the mechanotransduction pathways in both ECs and FBs resulted in either the lack of formation of blood microvessels or formation of microvessels, which were drastically different from control microvessels in terms of morphogenesis, characteristics, topology, and function, demonstrating that these genes play solid roles in various stages of vascularisation. However, when treated with small molecule inhibitors, the genes of interest are inhibited in both FBs and ECs. This makes it a challenge to interoperate the results. Therefore, to investigate the mechanical contribution of FBs to the formation and stabilisation of microvessels we inhibited our interest genes by transfecting siRNA to FBs, followed by juxtacrine co-culturing them with ECs.

It is worth mentioning that a different Wnt family member, Wnt7b, was inhibited in replace of Wnt/β-catenin.

4.2 Methods

In this section, we will explain the methods by which we achieved the purposes of the chapter.

4.2.1 Inhibition of Mechanotransduction genes in FBs

Using siRNAs, purchased from Dharmacon/US, some genes belonging to mechanotransduction pathways, YAP, Src, RhoA, Wnt7b, and FAK, as well as one gene belonging to chemotransduction pathway, EED, were inhibited in FBs to assess the mechanical/chemical role(s) of these cells in the formation and stabilisation of microvessels.

4.2.1.1 Cell Plating

FBs were trypsinised, spun down, and counted. One hundred thousand cells were plated per well of a 6-well cell culture plate and were incubated at 37°C with 5% CO_2 overnight. The day after, when the cells were at 50% of confluence, transfection was performed.

4.2.1.2 Transfection

Concentration of all siRNA stocks and the final concentration of transferring siRNAs were 20 µM and 50 nM, respectively. The preparation of the transfection solution is summarised in **Table 4.1**. Briefly, the medium in wells was replaced with 1 mL serum-free medium to starve the cells for better efficiency of transfection. In tube A, 6 µL of siRNA stock and 94 µL of serum-free medium were mixed. In tube B, 5 µL of delivery reagent and 95 µL of serum-free medium were mixed. The contents of the tubes were given a quick mix (a few seconds) followed by incubation of both tubes at room temperature for 5 minutes. Then, the content of tube A was added to tube B and vortexed for a few seconds. The mixture was incubated for 20 minutes at room temperature. Finally, the transfection medium (200 µL) was added to each well drop by drop. After 6 hours, 1 mL of complete medium (containing serum) was added to each well. The cells were placed in an incubator for 72 hours. The

medium was not replaced over this period. Two controls, negative and death, were done for all experiments. The same process was followed for all types of siRNAs, YAP, Src, RhoA, Wnt7b, FAK and EED.

Table 4.1: Preparation of transfection solution. *After incubation for 5 minutes at room temperature, the contents of both tubes were mixed to make a transfection solution at 50 nM.*

Plating Format	Tube A		Tube B	
	Volume of siRNA (µL)	Volume of Medium (µL)	Volume of Delivery Reagent (µL)	Volume of Medium (µL)
6-Well Plates	6	94	5	95

4.2.1.3 Transfection Efficiency by Western Blot

For evaluation of transfection efficiency, western blot (WB) was performed. WB is a blotting technique by which the proteins of interest can be detected using antibodies. The method consists of four steps; protein extraction, separation, transferring, and immunostaining. Several buffers are needed to fulfil the steps. All buffers were made the day before expected use. It is worth mentioning all items required to perform WB were purchased from Bio-Rad/US. Also, protein efficiency assay was performed on day 3 (coincided with seeding devices – Day 0) and day 7 (coincided with Day 4 after seeding the devices) post transfection.

4.2.1.3.1 Buffer Preparation

Five buffers, as described below, were used to perform WB. All buffers except transfer buffer as well as blocking buffer were kept at room temperature. Two last buffers were kept in a fridge (4ºC). The volumes of the compounds used to make the buffers are summarised in **Table 4.2**.

160

Lysing buffer: To make lysing buffer 2-Mercaptoethanol and 4X Laemmli were mixed in a 1:10 ratio.

Running buffer: Running buffer, also known as loading buffer, was prepared by mixing Milli-Q water, Tris Glycine 10X (TG 10X), and Sodium dodecyl sulfate (SDS).

Transfer buffer: Milli-Q water, methanol, and Tris/Glycine/SDS 10X (TGS 10X) were mixed to prepare transfer buffer, also known as blotting buffer.

Blocking buffer: Milli-Q water, Tris Buffered Saline 10X (TBS 10X), Tween-20, and milk powder were mixed to make blocking buffer. The mixture was stirred on a stirrer for 30 minutes to be homogenised.

Wash buffer: Wash buffer was prepared by mixing Milli-Q water, TBS 10X, and Tween-20.

Table 4.2: Volumes of the compounds used to make the buffers.

Buffers	Compounds (mL for Liquids and gr for Powders)									
	2-Mercapto-ethanol	4X Laemmli	Milli-Q Water	Tris Glycine 10X	Sodium Dodecyl Sulfate	Methanol	Tris Glycine SDS 10X	Tris Buffered Saline 10X	Tween-20	Milk Powder
Lysing Buffer	0.1	0.9								
Running Buffer			900	100	1					
Transfer Buffer			700			200	100			
Blocking Buffer			900					100	1	50
Wash Buffer			900					100	1	

4.2.1.3.2 Protein Extraction

Seventy-two hours after transfection, the cells were dissociated, counted, and spun down. The supernatant was discarded, and the cells were re-suspended in lysing buffer to break their membrane down. The lysed cells were then heated up at 95°C for 9 minutes to denature proteins/make the proteins linear. The sample was spun down at 13,000 xg for 5 minutes.

4.2.1.3.3 Protein Separation

Proteins were separated by sodium dodecyl sulfate-polyacrylamide gel electrophoresis (SDS-PAGE), an electrophoresis technique separating proteins by mass.

A precast cassette gel (10%) was used to separate proteins except for FAK (8%). After assembling the loading chamber, the chamber was filled with running buffer. The samples (proteins extracted) were loaded 20 µL per well, gently avoiding tearing the gel or spreading the sample into the buffer. A pre-stained protein ladder was used as a reference. Once done, the gel was run for one and half an hour (80 volts for the first 10 minutes and then 100 volts for the next 80 minutes) to separate the proteins by their mass.

4.2.1.3.4 Protein Transferring – Wet Transfer

Since the gel is fragile and porous, it cannot be used for the next step, which is immunostaining as it may be torn or we may get false positive signals because of antibodies trapped into the gel's pores. Therefore, it is needed to transfer proteins from the gel to a nitrocellulose membrane. To do so, immediately after performing protein separation, transferring step was done.

First, the gel was activated in pre-cold transfer buffer (15 minutes). Pieces of nitrocellulose membrane, blotting papers, and fibre pads were pre-soaked in transfer buffer for 15 minutes. To make WB sandwiches, a tray was filled with pre-cold transfer buffer. A gel holder was placed in the tray with the black side down and immersed in the buffer. One piece of fibre pad was placed flat on

the black side of the gel holder. Next, a piece of blotting paper was laid on the fibre pad, avoiding any bubbles. The activated gel was then placed on the blotting paper very gently and carefully to avoid tearing it. Making WB sandwich was continued by applying a piece of nitrocellulose membrane squarely on the gel to blot the proteins. Any bubbles between the gel and the blotting paper were removed by a roller. One more piece of blotting paper and a fibre pad were then laid on the nitrocellulose membrane, respectively. The clear side of the gel holder was folded over the sandwich and was clamped to the black plastic side by a clip. The gel holder was inserted into the inner module. The inner module was then placed in the chamber. The chamber was filled with pre-cold transfer buffer. To keep the system cool, a frozen cooling unit was put inside the chamber. The power supplier was run at 20 volts for two and half an hour.

4.2.1.3.5 Protein Immunostaining

The proteins transferred to the nitrocellulose membrane were then stained with primary and secondary antibodies. To stain the proteins, first, the membrane was blocked with a blocking buffer. When the run was complete, WB sandwiches were opened, and the nitrocellulose membrane was immersed in 25 mL of blocking buffer for 15 minutes at room temperature on a rocking platform. The blocking buffer was discarded. Then, the membrane was incubated with primary antibodies diluted in fresh blocking buffer overnight at 4°C. **Table 4.3** shows the detail of antibodies, including the type of antibodies, the targets, molecular weight of the targets, host species, species reactivity, the concentrations, and the companies from where antibodies were purchased.

The next day, the primary antibody was discarded, and after washing the membrane with wash buffer (3X, 15 minutes each), the membrane was incubated with the secondary antibody at room temperature. Secondary antibodies act against the primary antibody. After one hour, the secondary antibody was poured off, and the membrane was washed with a wash buffer

3 times, for 15 minutes each. None of the antibodies used was fluorescently conjugated. For this reason, to reveal the protein bands, the stained membrane was exposed to the revealing reagent for 30 seconds. The reagent was then removed, and the membrane was squarely placed on a tray. The tray was placed inside the chamber of an imager machine (Amersham Imager 680/Cytiva) to image the bands.

Table 4.3: List of antibodies used.

Antibody Type	Target	Molecular Weight (kDa)	Concentration (μL/μL)	Host Species	Species Reactivity	Company and Country
Primary Antibodies	YAP-Associated Protein (YAP)	65	1:500	Mouse	Human	Insight Biotechnology/US
	Src	59.8	1:1000	Mouse	Human	Bioss Inc/US
	RhoA	22	1:5000	Mouse	Human	Proteintech/US
	Wnt/β-catenin	39	1:1000	Rabbit	Human	Abcam/UK
	Focal Adhesion Kinase (FAK)	125	1:500	Rabbit	Human	Sigma-Aldrich/US
	Embryonic Ectoderm Development (EED)	53	1:2000	Rabbit	Human	Abcam/UK
	B-Actin	42	1:3000	Mouse	Human	Sigma-Aldrich/US
Secondary Antibodies	Primary Antibody	-	1:3000	Goat	Mouse	Thermo Fisher Scientific/US
	Primary Antibody	-	1:3000	Goat	Rabbit	Thermo Fisher Scientific/US

4.2.1.3.6 Western Blot Quantification

WB data was quantified using ImageJ. The tracing tool was used to measure the percent of the band of interest. For calculation of the Protein/β-actin ratio, the value of the protein of interest was divided by the value of β-actin.

4.2.1.4 ECs JCC with Transfected FBs

ECs were juxtacrine co-cultured with transfected FBs. One device was seeded with ECs and non-transfected FBs as control. The microvessel formation was tracked by imaging the devices on days 1, 4, and 7.

4.2.1.5 3D Functional and Morphology Characterisation

On day 7, microvessels were characterised for some features such as perfusability, permeability, coverage area, diameter, topology, and elastic modulus of the gels (gel stiffness). As all features are described in chapter 2, we only mention and explain how the barrier function and elastic modulus were measured here.

Barrier Function: On day 7, after culture, the medium was removed from medium channels, followed by refilling them with the tracer dye (10 kDa dextran). The tracer's intensity in the voids (hydrogel) was measured one hour after dextran injection and used to calculate the barrier function. Barrier function is the inverse of dextran intensity in the interstitial area after one hour.

AFM Measurements: Elastic Modulus of the hydrogels was measured using Atomic Force Microscopy (AFM). To fulfil the goal above, on days 1, 4, and 7, PDMS was cut off around the vascularisation channel by a blade. The tissue was removed from the channel very carefully, leaving the tissue attached to the PDMS. This provided a supportive base as well as helped maintain the original geometry of the tissue. The tissue was then immersed in growth medium (CO_2 independent growth medium, consisting of Leibovitz's L-15 Medium without phenol red (Gibco Life Technologies/Ireland), and

supplemented with 10% FBS to keep the cells alive during stiffness measurement.

AFM force-distance measurements were acquired using a JPK Nanowizard Cellhesion 200 (JPK Instruments AG/Germany) placed on an inverted optical microscope (Zeiss Axiovert 200/Germany) with a manual xy-positioning stage. Tipples cantilevers (MLCT-O10, Bruker; nominal spring constant of 0.07 N/m) were modified by gluing 50 μm diameter glass microspheres (Cospheric/USA) to the tip of the cantilever via UV curing glue (ultraviolet curing, Loctite/Germany). Prior to gluing the beads, the spring constants of the cantilevers were determined using the thermal noise method of the AFM software (JPK SPM, JPK instruments). The stage was carefully moved to position the cantilever tip above the middle of the sample before approaching the tissue surface. No less than 50 force-distance curves were taken per sample by moving the stage manually (in ~0.5 mm steps) across the length of the tissue, with an approach speed of 10 μm/s and a set force of 30 nN.

Data analysis: Using JPK data processing software (JPK DP, JPK Instruments AG/Germany), the contact point and the force-indentation curve were extracted from the force-distance curve[203]. The apparent elastic modulus, $E/(1-\nu^2)$, was extracted by fitting the Hertz contact model, for a contact between a spherical tip and the planar hydrogel, to the measured force-indentation curve [204]. The reason for using Hertz model is that this model is the simplest model for describing the elastic response of a soft material indented by a spherical probe[205]. In AFM indentation measurements, the relation between the loading force *F* and the overall sample indentation *δ,* in the case of a spherical probe is as follows:

$$F = \frac{4}{3}\frac{E}{1-\nu^2}\sqrt{r}\delta^{3/2} \qquad\qquad (\textbf{Eq: 4.1})$$

where *E* is elastic modulus, *υ* is Poisson's ratio and *r* is the radius of the spherical probe[206].

Considering the size of the glass bead, the applied maximum force was chosen to apply sufficiently large indentations and probe the stiffness of the gels and vascular tissue constructs on a length-scale that is larger than the size of individual cells while also adhering to small strain conditions[207], thus providing the macroscopic level average elastic modulus of the constructs. Setting the maximum force to 30 nN resulted in average indentation depths δ ~7 µm and maximum of δ ~25 µm (for the softest samples such as cell-free fibrin gels). The average contact size was ~30 µm, and the analysis of force-indentation curves was limited to a maximum indentation depth of 10 µm. It should be noted that the increase observed in the apparent elastic modulus of the tissue-like constructs, is due to three factors; 1) the generation of a contractile pre-stress in the tissue by vasculature, 2) protein deposition by the cells, and 3) the cellular materials. Thus, to investigate the collective impacts of such factors on the tissue stiffness, for all the AFM experiments carried out on days 1, 4, and 7, the same amount of force (30 nN) was applied to the samples. The resulting displacements were normalised with respect to MC condition on day 1 to compare the values.

4.2.2 Investigation of FBs Interaction with ECs

In this step, the aim was to investigate FBs and ECs physical interaction. FBs purchased from Lonza were not fluorescently labelled. Thus, the cells were transduced first to express Red Fluorescent Protein (RFP) to fulfil the above goal.

4.2.2.1 Transducing FBs to Express Red Fluorescent Protein

FBs were transduced with a recombinant Lentivirus harbouring LifeAct®-TagRFP (Red Fluorescent Protein) transgene. All materials, including Lentivirus, delivery reagent, Polybrene, and antibiotic, Puromycin, were purchased from ibidi/Germany. The protocol consists of 4 steps; cell seeding, transduction, antibiotic titration, and selection of stable cells.

Cell seeding: The day before transduction, one well of a 6-well culture plate was seeded with $1 \times 10^{+5}$ FBs. The cells were fed with complete growth medium and incubated overnight.

Transduction: The cells exhibited 30% confluence after overnight incubation. To transduce the cells, Lentivirus particles were thawed over ice. Polybrene (11.4 µL) and growth medium (936.6 µL) were mixed. Lentivirus particles (50 µL) were then added to the Polybrene-medium mixture and mixed gently by pipetting up and down. The final concentration of Polybrene was 8 µg/mL. The medium was replaced with Polybrene-Lentivirus-medium mixture. The cells were incubated at standard cell culture condition. After 3 days, the cells were visualised under a fluorescent microscope for any LifeAct®-TagRFP signals.

Antibiotic titration: Puromycin needed to be added to the growth medium to select stable cells. To find the desired concentration of the antibiotic that killed all non-transduced FBs, Puromycin was titrated with non-transduced cells by adding different concentrations of the antibiotic to them. To achieve that, the day before, $1 \times 10^{+5}$ non-transduced FBs were seeded per well of a 6-well cell culture plate, fed with growth medium, and incubated overnight. The next day, different antibiotic concentrations, 0.1, 0.5, 1, 3, 5, and 10 µg/mL, were added to each well. Three days after adding antibiotic, cell viabilities were measured using a nuclei counter. The puromycin-containing medium was not replaced during incubation to save any dead cells.

Selection of the stable cells: For the selection of stable cells, three days after the transduction process, the growth medium was replaced with Puromycin-containing growth medium (1 µg/mL). The medium was replaced every 3 days until resistant cells were identified. After identifying resistant cells, the cells were expanded, frozen down, and kept in a liquid nitrogen tank (-196ºC).

4.2.2.2 ECs and RFP-FBs Interaction

Red Fluorescent Protein expressing FBs (RFP-FBs) were juxtacrine co-cultured with ECs in a 3-channel microfluidic device. The cell interaction was tracked by imaging the cells on days 1, 4, and 7 after seeding.

4.2.2.3 ECs and RFP-FBs^{-RhoA} Interaction

The inhibition of Rho expression was experimentally achieved by the transfection of siRNA molecules in RFP-FBs. RFP-FBs^{-RhoA} were then juxtacrine co-cultured with ECs in a 3-channel microfluidic device. The cell interaction was tracked by imaging the cells with a confocal microscope on days 0, 1, 4, and 7 post-seeding. For imaging set-up, please refer to **Table 2.3**.

Colocalisation analysis: Using ImageJ (JACoP plugin), Manders' coefficient, which shows the association of FBs with the lumens, was calculated automatically. Multiplying Manders' coefficient by 100, colocalisation percentage was calculated.

4.3 Results

4.3.1 Mechanical Role of FBs in Vascularisation

To investigate the mechanical role(s) of FBs in forming and stabilising microvessels, some genes belonging to mechanotransduction pathways such as RhoA, Src, YAP, FAK, and Wnt7b were perturbed in FBs by transfection of siRNAs. Inhibition of these the expressions of the genes resulted in FBs^{-RhoA}, FBs^{-Src}, FBs^{-YAP}, FBs^{-FAK}, and FBs^{-Wnt7b}. Also, EED, a gene belonging to the chemotransduction pathway, was inhibited in FBs, resulting in FBs^{-EED}.

WB was performed to examine the efficiency of the transfections on day 3 and day 7 after transfection. A four-day interval was considered, as it takes ECs four days to from microvessels after being co-cultured with FBs. WB results confirmed the efficient knockdown of the genes (**Fig 4.1 a**). Quantification of the data showed that the expression of all proteins of interest reduced significantly on both day 3 and remained inhibited until day 7 after transfection (**Fig 4.1 b, c**).

*(**Fig 4.1** continued on next page. Legend follows)*

b

Transfection Efficiency

Day 3

c

Transfection Efficiency
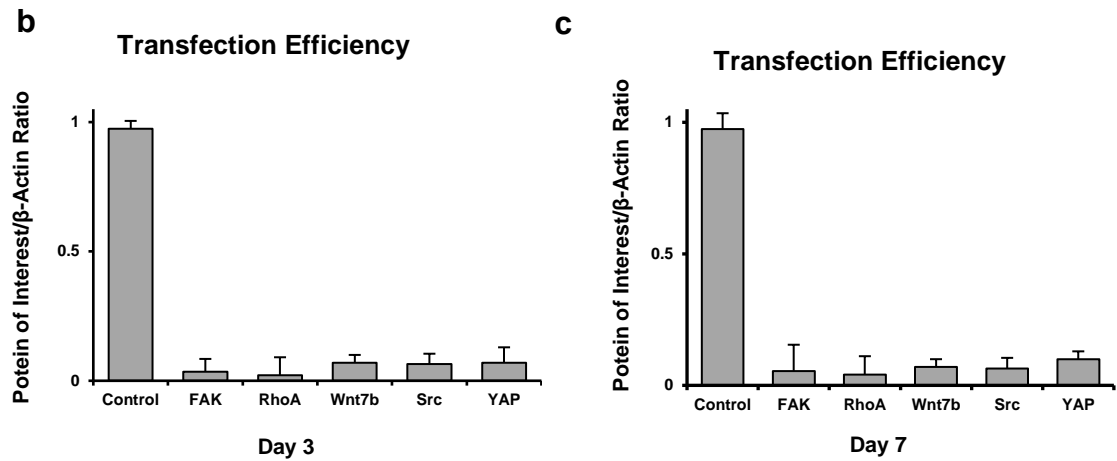
Day 7

Fig 4.1: Transfection efficiency. a) Performing WB confirmed the efficient inhibitions of the proteins' expressions. b and c) Graphs compare protein expression in control and siRNA-treated cells on day 3 and day 7 after transfection. Normalised to β-actin value at each day. n=3.

4.3.1.1 Microvessel Formation and Characterisation

Co-culturing ECs along with siRNA-treated FBs, we investigated the mechanical role of FBs in microvessels. 3D confocal images taken on days 1, 4, and 7 after seeding showed that ECs retained their ability to form microvessels when co-cultured with FBs^{-YAP}, FBs^{-FAK}, FBs^{-Wnt7b}, and FBs^{-Src}. However, RhoA inhibition in FBs resulted in arresting the formation of microvessels (**Fig 4.2 a**). Nevertheless, efforts to characterise the siRNA-treated microvessels and control microvessels showed that the microvessels were drastically different. For instance, the FAK inhibition resulted in a significant increase in the coverage area of the microvessels ($^{***}P$ value <.001, n=8). In contrast, the inhibition of YAP ($^{**}P$ value =.008, n=8), Src, and particularly RhoA led to a significant decrease in microvessels coverage area compared to control ($^{***}P$ value <.001, n=8, **Fig 4.2 b**). The diameter of microvessels decreased by the inhibition of Src ($^{**}P$ value =.004, n=3) and increased by the perturbation of Wnt7b, YAP, and FAK in FBs compared to control ($^{***}P$ value <.001, n=3, **Fig 4.2 c**).

171

a

| | Day 1 | Day 4 | Day 7 |

ECs Juxtacrine Co-Cultured With — untreated FBs

ECs Juxtacrine Co-Cultured with — FBs^{-YAP}, FBs^{-FAK}, FBs^{-Wnt7b}, FBs^{-Src}, FBs^{-RhoA}
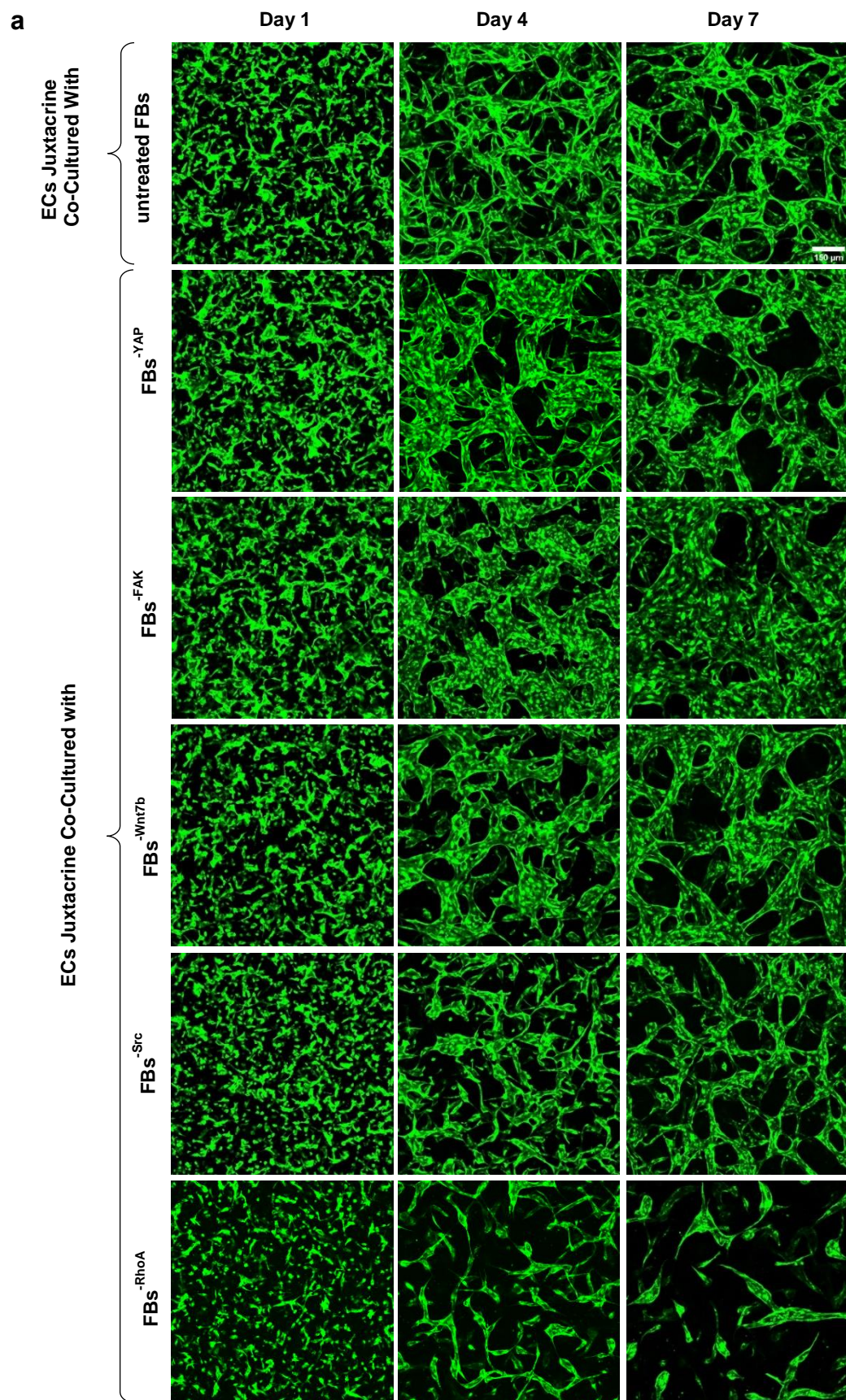
(*Fig 4.2* continued on next page. Legend follows)
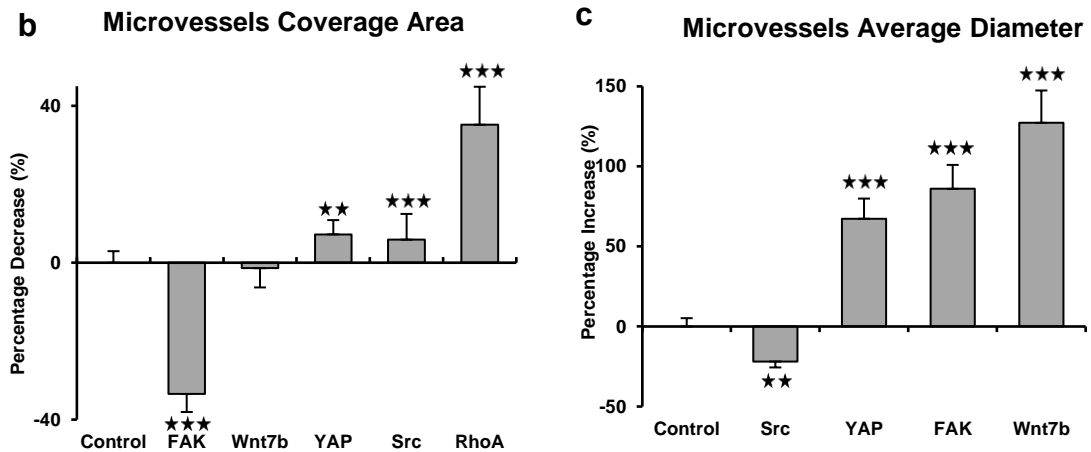
Fig 4.2: Impact of inhibition of genes belonging to mechanotransduction pathway on microvessels formation and morphogenesis. *a) 3D confocal images visualising the impact of the inhibition of YAP, Wnt7b, Src, RhoA and FAK in FBs on formation and morphogenesis of microvessels. Scale bar, 150 µm. b) Bar chart representing the impact of the inhibition of the genes in FBs on microvessels coverage area (**P value =.008, ***P value <.001, n=8.) c) Bar chart representing the impact of the inhibition of the genes in FBs on microvessel diameter (**P value =.004, ***P value <.001, n=3.) Normalised with respect to control value.*

4.3.1.2 Microvessel Function – Perfusability and Permeability

To characterise the microvessels further, we assessed microvessel primary functions – namely perfusability and permeability. To this end, a fluorescent tracer dye (Dextran 70 kDa) was introduced into the upstream medium channel. 3D confocal imaging revealed that the dye quickly and uniformly filled the microvessels formed in both siRNA-treated devices and control device, demonstrating that the microvessels were fully perfusable. However, the microvessel perfusability dropped by 14.3 ± 1.36 percent (***P value <.001, n=9) when ECs were co-cultured with FBs^{-Src}. Also, dextran failed to fill the dispersedly formed sheet-like structures in the RhoA-treated device, as they did not form any openings toward the medium channels (**Fig 4.3 a**). Excluding RhoA and Src-treated devices, the microvessels were statically unchanged with regard to perfusability (**Fig 4.3 b**).

a

| | Microvessels | Dextran Perfusion | Overlay |

ECs Juxtacrine Co-Cultured With — untreated FBs

ECs Juxtacrine Co-Cultured with — FBs^{-YAP}, FBs^{-FAK}, FBs^{-Wnt7b}, FBs^{-Src}, FBs^{-RhoA}
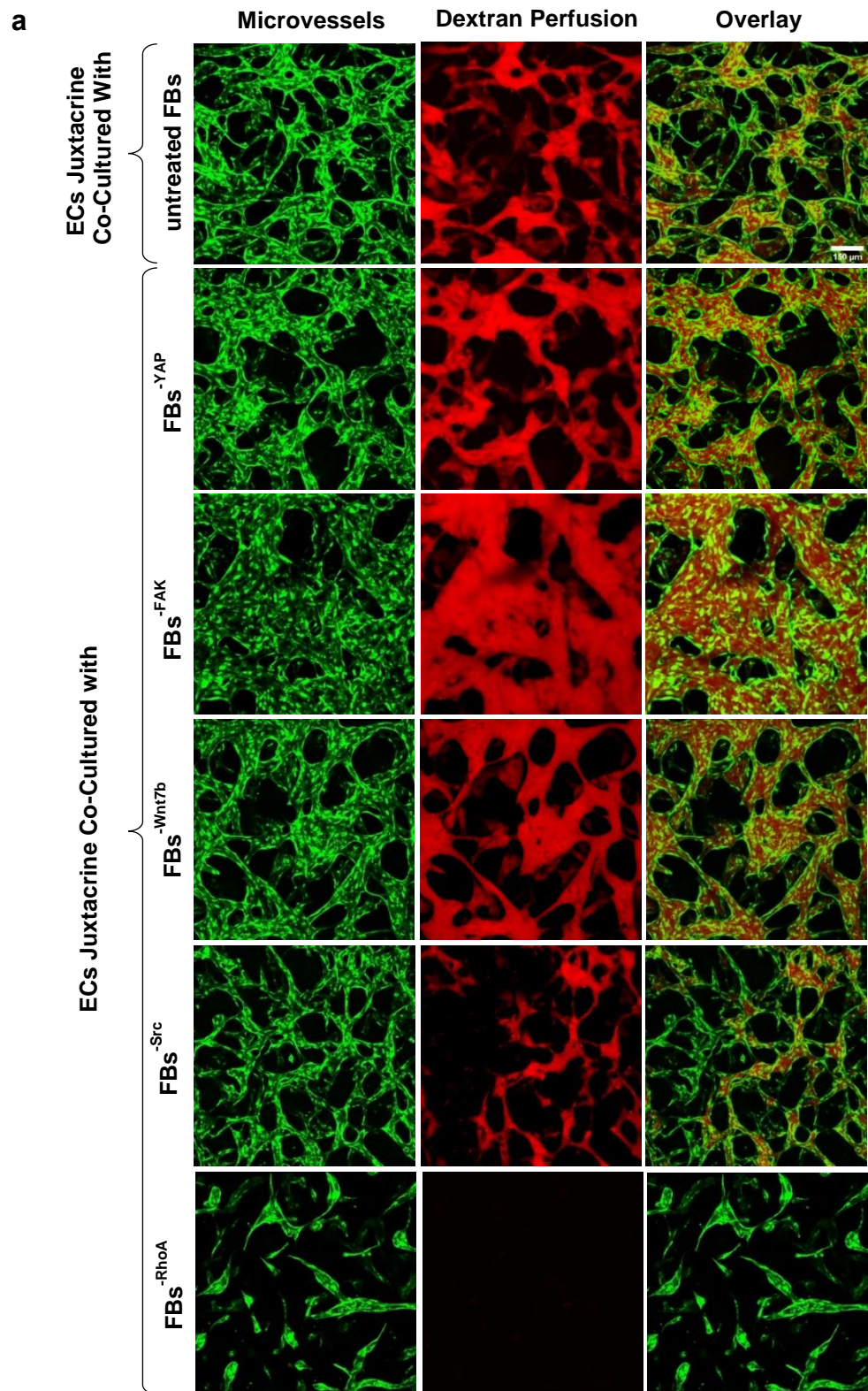
(***Fig 4.3*** *continued on next page. Legend follows)*

b
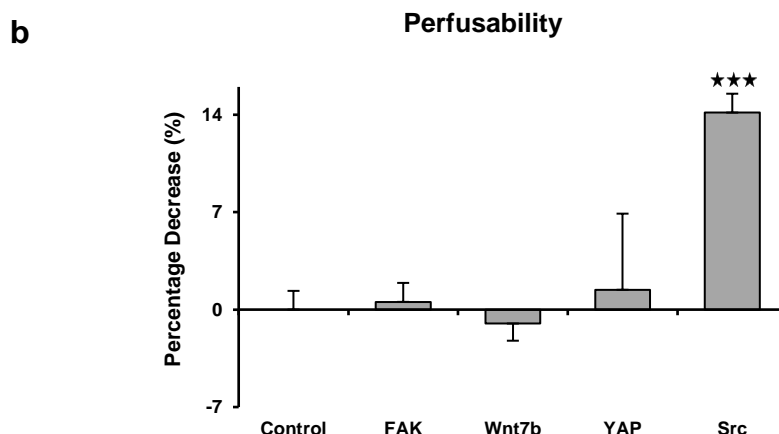
Perfusability

*Fig 4.3: siRNA-treated microvessel function comparison. a) 3D confocal images visualising the impact of perturbation of FAK, Wnt7b, YAP, Src and RhoA in FBs on microvessels function. Scale bar, 150 μm. b) Bar chart representing change in perfusability in different conditions (***P value <.001, n=9). Normalised with respect to control value.*

Although quantification of microvessels perfusability showed no significant difference between control and siRNA-treated microvessels, excluding Src and RhoA-treated ones, when we measured permeability of the microvessels to 10 kDa dextran, we observed a drastic difference between control and siRNA-treated microvessels. The permeability of control (untreated microvessels) was measured to be 2.4E-07 ± 9.33E-08 cm/s (n=21) whereas it was measured to be 4.8E-07 ± 1E-07 cm/s for YAP-treated microvessels (***P value <.001, n=18), 6.3E-07 ± 1.8E-07 cm/s for FAK-treated microvessels (***P value <.001, n=18), 7.2E-07 ± 2.7E-07 cm/s for Wnt7b-treated microvessels (***P value <.001, n=6) and 8.26E-07 ± 2.7E-07 cm/s for Src-treated microvessels (***P value <.001, n=6) (**Fig 4.4 a**). Continuing imaging the microvessels after introducing the tracer dye for 1 hour (~20-minute intervals) we showed that at all conditions, the values of permeability remained constant over time (**Fig 4.4 b**).

a

Permeability

b
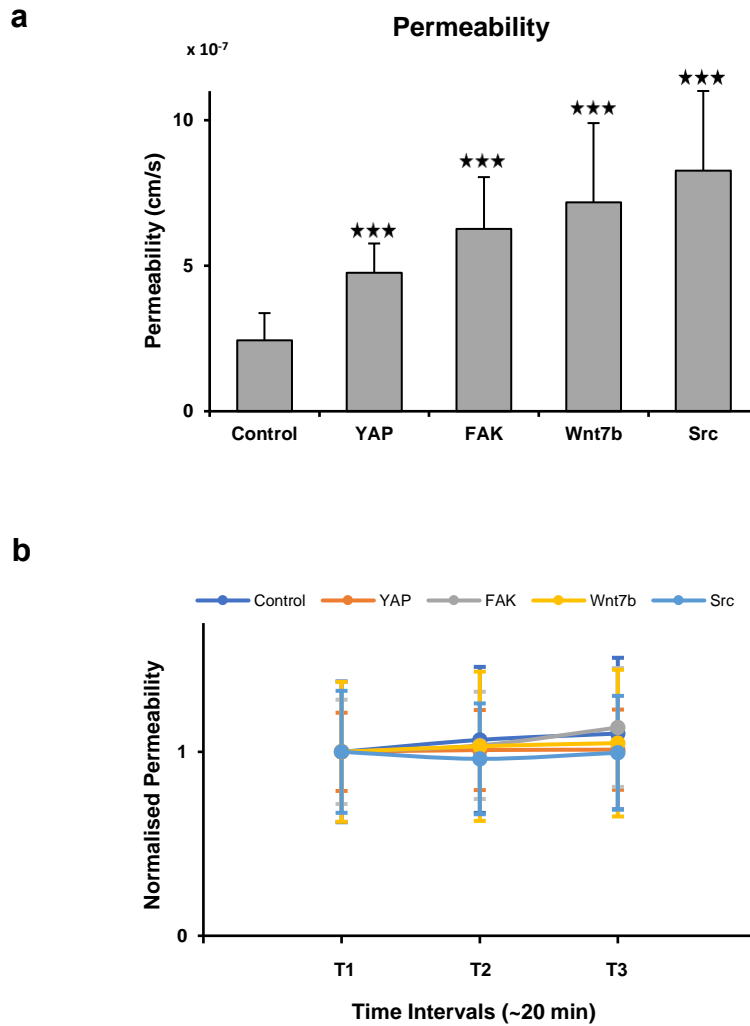
Fig 4.4: Impact of inhibition of mechanotransduction genes in FBs on microvessel permeability. *a) Bar chart representing the impact of the inhibition of YAP, FAK (***P value <.001, n=18), Wnt7b and Src (***P value <.001, n=6) in FBs on microvessels permeability. b) At all conditions, the values of permeability remained constant over time. Normalised with respect to control value.*

4.3.1.3 Microvessel Topology

We further investigated the impact of the inhibition of mechanotransduction genes on the topology of the microvessels, including branching, the number of junctions, average branch length, and maximum branch length. The analysis showed that ECs produced much fewer branches when co-cultured with siRNA-treated FBs (**P value =.005 for Src, **P value =.0017 for FAK, ***P value <.001 for Wnt7b and YAP, n=5, **Fig 4.5 a**). A significant reduction was also observed in the number of junctions when ECs were seeded along with

176

siRNA-treated FBs (**P value =.0041 for Src, **P value =.0034 for FAK, **P value =.0013 for YAP and ***P value <.001 for Wnt7b, n=5, **Fig 4.5 b**). However, perturbation of Wnt7b (**P value =.004), YAP (*P value =.028), and FAK (**P value =.006, n=5 for all conditions) in FBs resulted in a significant increase in average branch length (**Fig 4.5 c**). Maximum branch length also significantly increased when YAP was perturbed in FBs (*P value =.016, n=5, **Fig 4.5 d**).
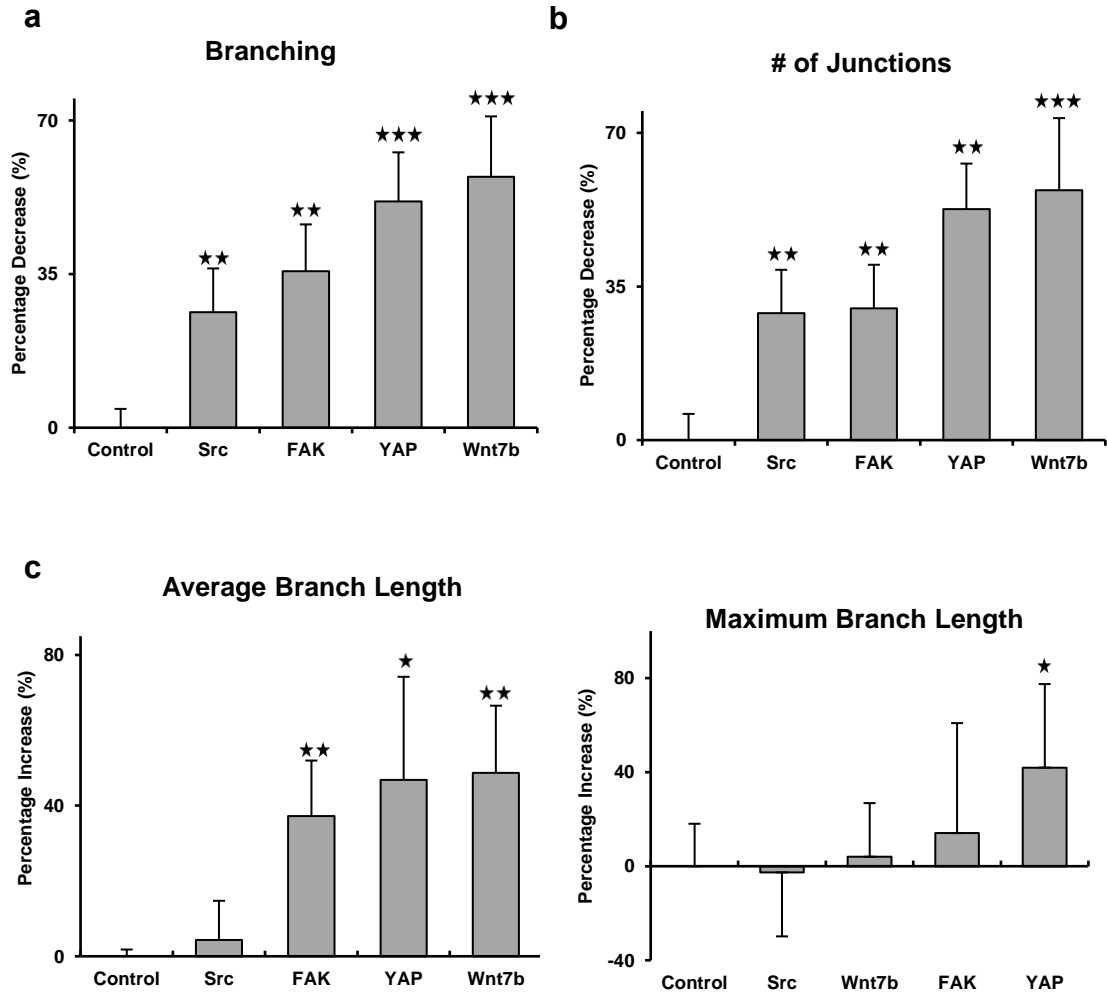
Fig 4.5: Microvessels topology comparison. *Bar charts representing the impact of perturbation of Src, Wnt7b, YAP and FAK on a) branching (**P value =.005 for Src, **P value =.0017 for FAK, ***P value <.001 for Wnt7b and YAP), b) the number of junctions (**P value =.0041 for Src, **P value =.0034 for FAK, **P value =.0013 for YAP and ***P value <.001 for Wnt7b), c) average branch length (**P value =.004 for Wnt7b, *P value =.028 for YAP, and **P value =.006 for FAK) and d) maximum branch length (*P value =.016). n=5. Normalised with respect to control values.*

Assessing microvessel length fold change on day 4 and day 7 of culture revealed that the difference between microvessels length of the siRNA-treated microvessels and control microvessels happened mostly from day 4 to day 7, and the difference was not significant by day 4 (**Fig 4.6**).
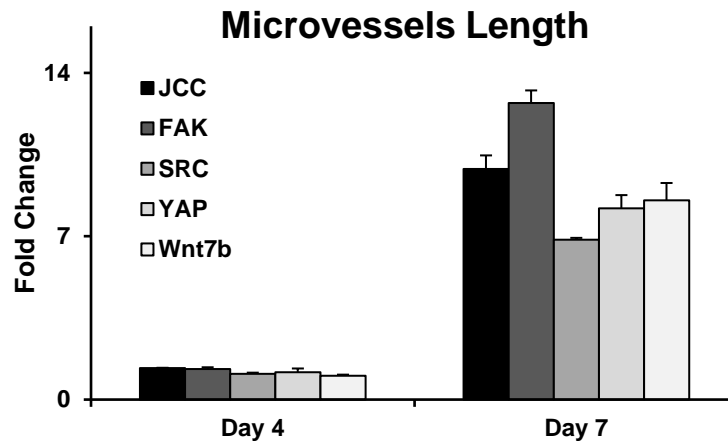
Fig 4.6: Microvessel length comparison on days 4 and 7 of culture. *Assessing microvessel length showed that the difference between microvessel length happens from day 4 to day 7 of culture. Microvessel length calculated as fold change, longest connected microvessel length, normalised to MC value at each day. n=5.*

To conclude, the inhibition of the mechanotransduction genes resulted in a decrease in branching and number of junctions and an increase in average branch length compared to control. This implies that genes play an important role in the morphogenesis and topology of microvessels.

4.3.1.4 Microvessel Openings

With the object of characterising the microvessels further, we assessed the microvessels openings, the conduits by which the networks were connected to the adjacent channels. The openings facilitate growth medium flow to the vascularisation channel. Also, their presence is essential for microvessels functions – perfusability and permeability. The confocal images revealed that the openings formed in different conditions were notably different from control openings in morphology (**Fig 4.7 a**). Further investigation revealed that in the presence of FBs^{-FAK}, FBs^{-Src}, FBs^{-YAP}, and FBs^{-Wnt7b}, ECs formed fewer

openings than control ([**]*P* value =.0012 for Src and [***]*P* value <.001 for the rest of conditions, n=6, **Fig 4.7 b**). Also, the average width of openings significantly decreased or increased when the genes were perturbed in FBs ([*]*P* value =.018 for YAP, and [***]*P* value <.001 for Src, Wnt7b, and FAK, n=6, **Fig 4.7 c**). In such a way that we measured an average width of the opening to be 27.1 ± 15.5 µm for control, 16.1 ± 10.6 µm for Src-treated microvessels, and 40.6 ± 22.4 µm for Wnt7b-treated microvessels and finally 54 ± 26.3 µm for FAK-treated microvessels.
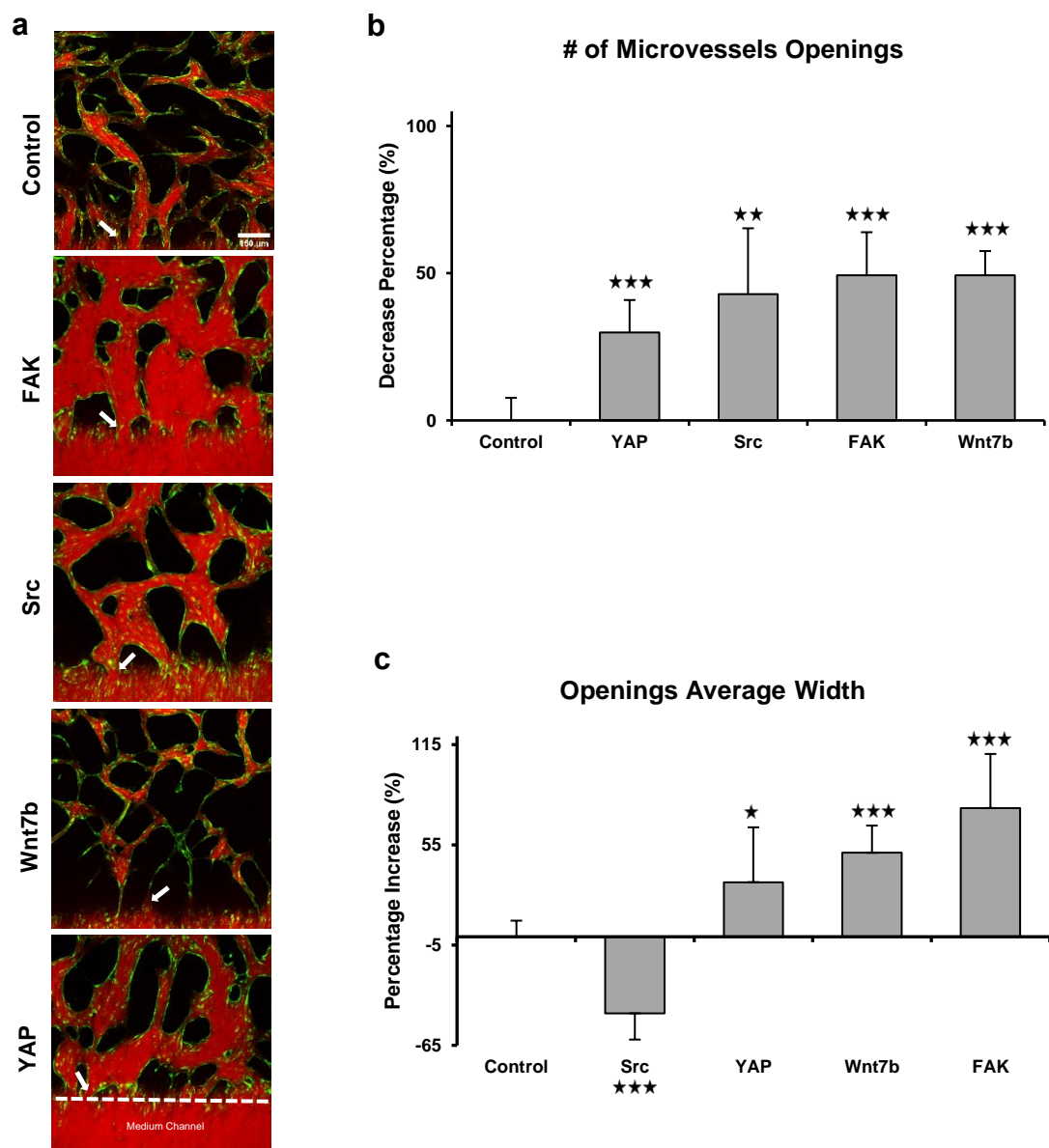
Fig 4.7: Impact of inhibition of mechanotransduction genes in FBs on microvessels openings. *a) Comparison of opening morphologies in different conditions. Scale bar, 150 µm.* White arrows denote openings. *b) Bar chart representing the impact of perturbation of Src ([**]*P value =.0012), YAP, FAK, and Wnt7b ([***]*P value <.001) on the number of microvessels openings. c) Bar chart representing the impact of perturbation of Src, YAP, Wnt7b and FAK ([*]*P value =.018, [***]*P value <.001) on the width of microvessel openings.* n=6. Normalised with respect to control value.

4.3.1.5 Barrier Function

The ECs form a confluent monolayer at the medium channel interface and vascularisation channel acting as a barrier to prevent dextran perfusion to the vascularisation channel through the hydrogel. This is called the barrier function. We investigated the impact of the inhibition of the mechanotransduction genes in FBs on forming the barrier by ECs. We observed the higher intensity of the tracer within hydrogel (interstitial area) in genes-inhibited conditions compared to control, demonstrating that the inhibitions of the genes in FBs lead ECs to form a leakier monolayer (barrier) ([***]P value <.001, n=9 for all conditions. **Fig 4.8**).
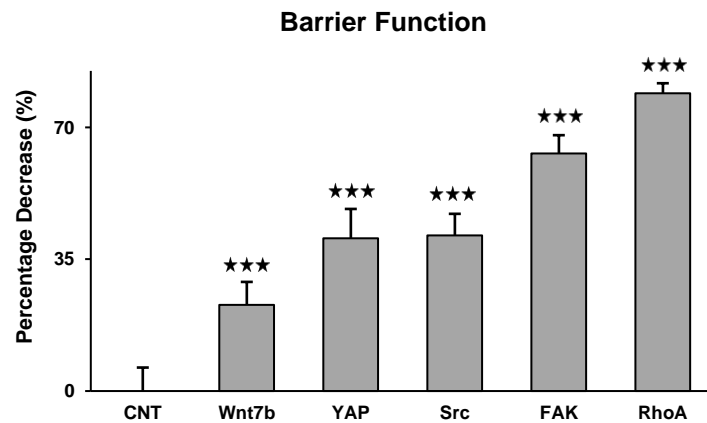
Fig 4.8: Impact of the inhibition of mechanotransduction genes in FBs on barrier function. Bar chart representing a significant decrease in barrier function as a result of gene inhibitions in FBs ([***]P value <.001, n=9).

4.3.1.6 Elastic Modulus

Kamm's lab has shown that the stiffness of the tissue-like constructs in JCC condition increases from 100 Pa to ~1000 Pa over the course of one week compared to cell-free gel, MC, and PCC-1 conditions. They have also shown that the observed increase is as results of 1) active stiffness which is defined as the generation of a contractile pre-stress in the tissue by vasculature (50%), 2) passive stiffness which is the results of cellular materials (20%) as well as 3) irreversible changes in the matrix (30%) which is the result of gel

remodelling and protein deposition by the cells (data not published). In this study, to investigate the impact of mechanotransduction pathways on tissue stiffening, stiffness measurements were performed for all conditions over the course of one week. We did not observe any significant difference between the stiffness of control and siRNA-treated conditions on day 1. However, there was a significant decrease in tissue stiffening between control and siRNA-treated conditions ($^{**}P$ value for Wnt7b =.0061, FAK =.0046, and YAP =.002, $^{***}P$ value for Src and RhoA <.001, n=3) on day 4. The decrease in tissue stiffness was also observed on day 7 ($^{*}P$ value for Wnt7b =.0261, $^{*}P$ value for FAK =.013 and YAP =.0039, $^{***}P$ value for Src and RhoA <.001, n=3). Overall, an increase in tissue stiffness was observed in all conditions from day 1 to day 4 and then from day 4 to day 7. However, the increase was much more considerable and higher for control compared to siRNA-treated conditions. In other words, the inhibition of mechanotransduction genes in FBs resulted in a significant decrease in tissue stiffness (**Fig 4.9**).
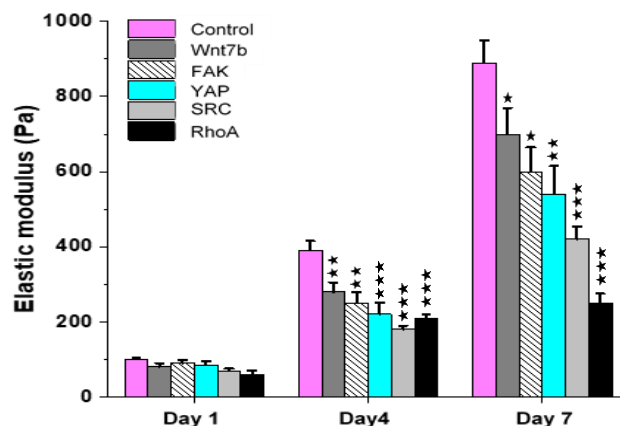
Fig 4.9: Tissue stiffening. Absolute stiffness measurements showed a significant decrease in tissue stiffening when ECs were co-cultured with siRNA-treated FBs on day 4 ($^{**}P$ value for Wnt7b =.0061, FAK =.0046, $^{***}P$ value for YAP, Src and RhoA <.001) and day 7 ($^{*}P$ value for Wnt7b =.0261, $^{*}P$ value for FAK =.013 and YAP =.0039, $^{***}P$ value for Src and RhoA <.001). n=3.

assessed. Visualisation of FBs was essential to fulfil the goal above. However, FBs purchased from the company were not fluorescently labelled. To label them fluorescently, FBs were transduced to express Red Fluorescent Protein. Titrating Puromycin with non-transduced cells, we found the desired

concentration, which killed all non-transduced cells (**Fig 4.10 a**). The transduced cells were then treated with Puromycin (1 µg/mL) to select stable cells. Transducing the cells resulted in Red Fluorescent Protein expressing FBs (RFP-FBs, **Fig 4.10 b, c**).

a

Cell Viability

b

c
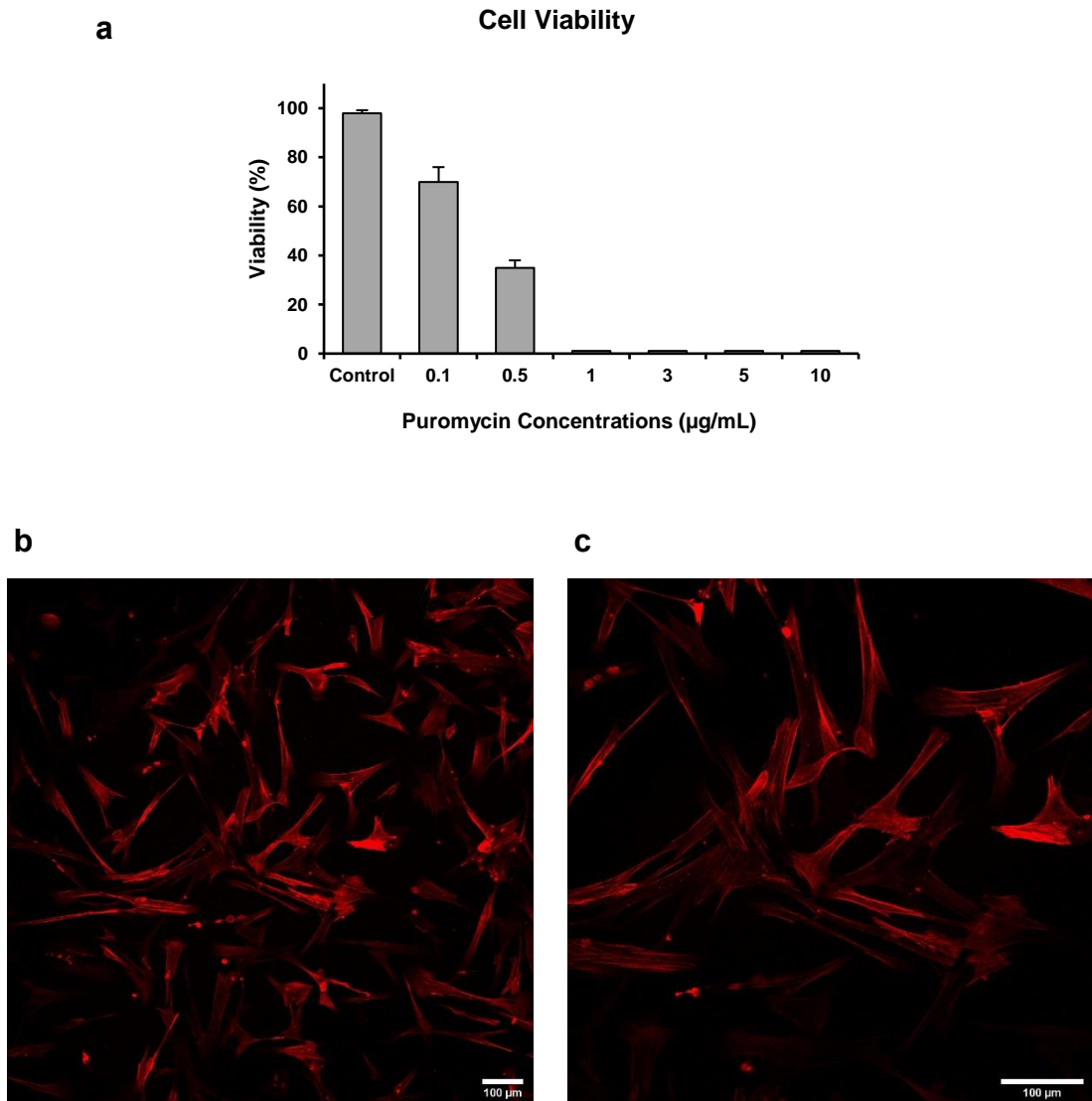
Fig 4.10: FBs expressing Red Fluorescent Protein. a) Measurement of cell viability showed that Puromycin was able to kill all non-resistant cells at concentration as low as 1 µg/mL. n=3. b and c) 3D confocal images visualising FBs expressing RFP. 10X and 20X objectives. Scale bar, 100 µm.

Imaging ECs co-embedded with RFP-FBs on days 0, 1, 4, and 7 of culture, we traced the progression of morphological changes and physical interaction of

the two cell types. 3D confocal Images showed that initially rounded and mono-dispersed ECs and RFP-FBs began to get elongated as early as a few hours after culture. ECs then self-assembled to form microvessels (**Fig 4.11**)
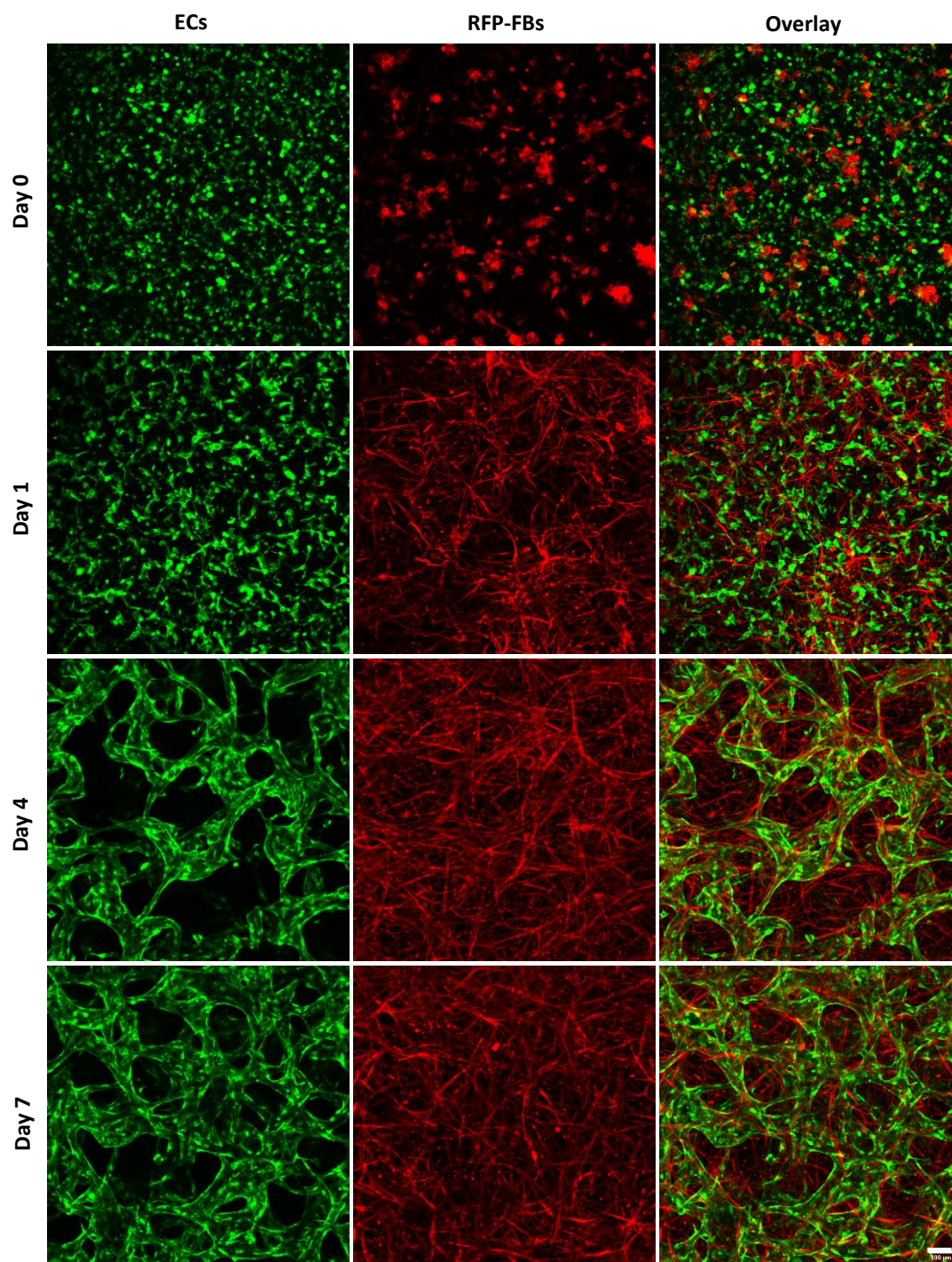
Fig 4.11: Progression of morphological changes in ECs and RFP-FBs during the course of one week. *Scale bar, 100 μm.*

High resolution 3D confocal imaging showed that RFP-FBs underwent considerable morphological changes and tended to be in close physical contact with the microvessels (**Fig 4.12**).
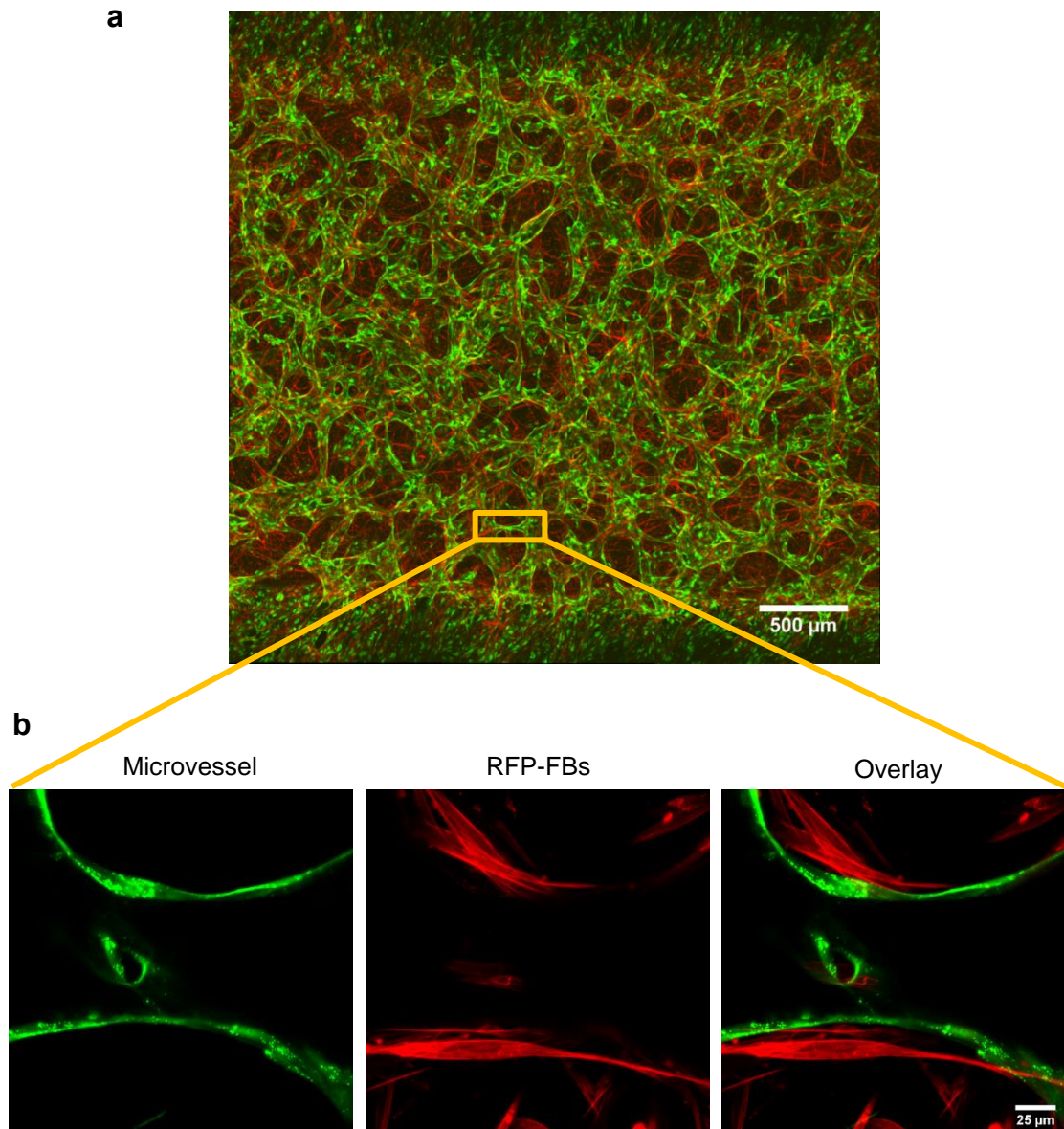
Fig 4.12: RFP-FBs and ECs interaction. *a) a big view of microvessels formed by co-culturing of ECs and RFP-FBs. Scale bar 500 μm. b) High resolution, 3D confocal images showing RFP-FBs elongating along the microvessels. 63X objective. Scale bar 25 μm.*

However, RhoA inhibition in FBs resulted in arresting the ability and preference of FBs^{-RhoA} to be close to the microvessels (**Fig 4.13**).

a

b

| Microvessel | RFP-FBs | Overlay |
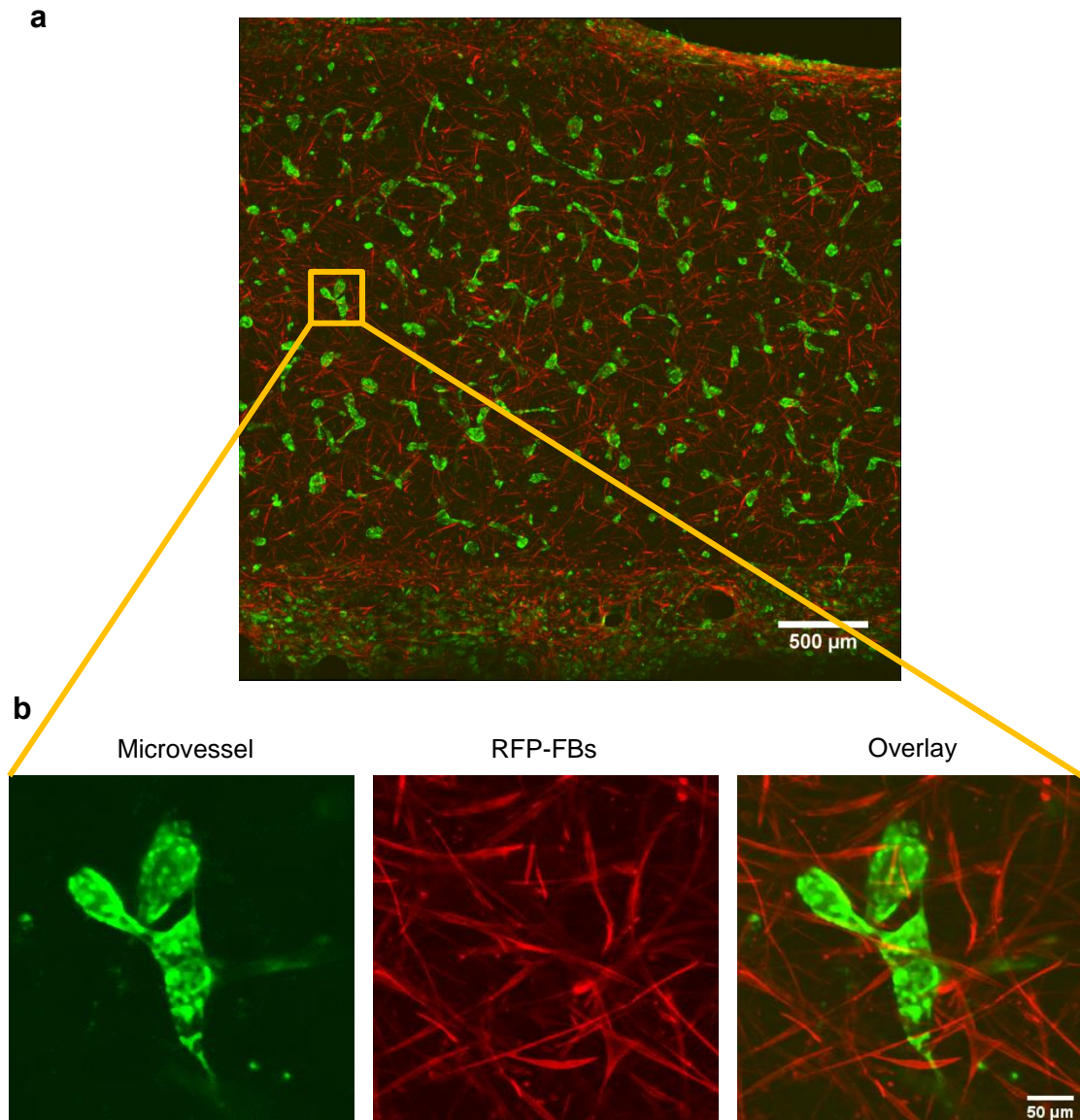
Fig 4.13: RFP-FB^{-RhoA} and ECs interaction. a) a big view of microvessels formed by co-culturing of ECs and RFP-FBs^{-RhoA}. Scale bar, 500 µm. b) Unlike RFP-FBs, RFP-FBs^{-RhoA} failed to be in close proximity of the lumens. Scale bar, 50 µm.

185

Quantification of the images on days 1, 4, and 7 also revealed that unlike control in which FBs and ECs colocalisation increased significantly from day 1 to day 4 and showed an upward trend by day 7, there was a slight increase in colocalisation of FBs^{-RhoA} with the microvessels, providing a proof that FBs lost their ability to concentrate around the microvessels when RhoA is inhibited in them ([***]P value <.001, n=3, **Fig 4.14 a**). Yellow locations in **Fig 4.14 b, c** represent colocalisation of FBs and FBs^{-RhoA} with the microvessels.
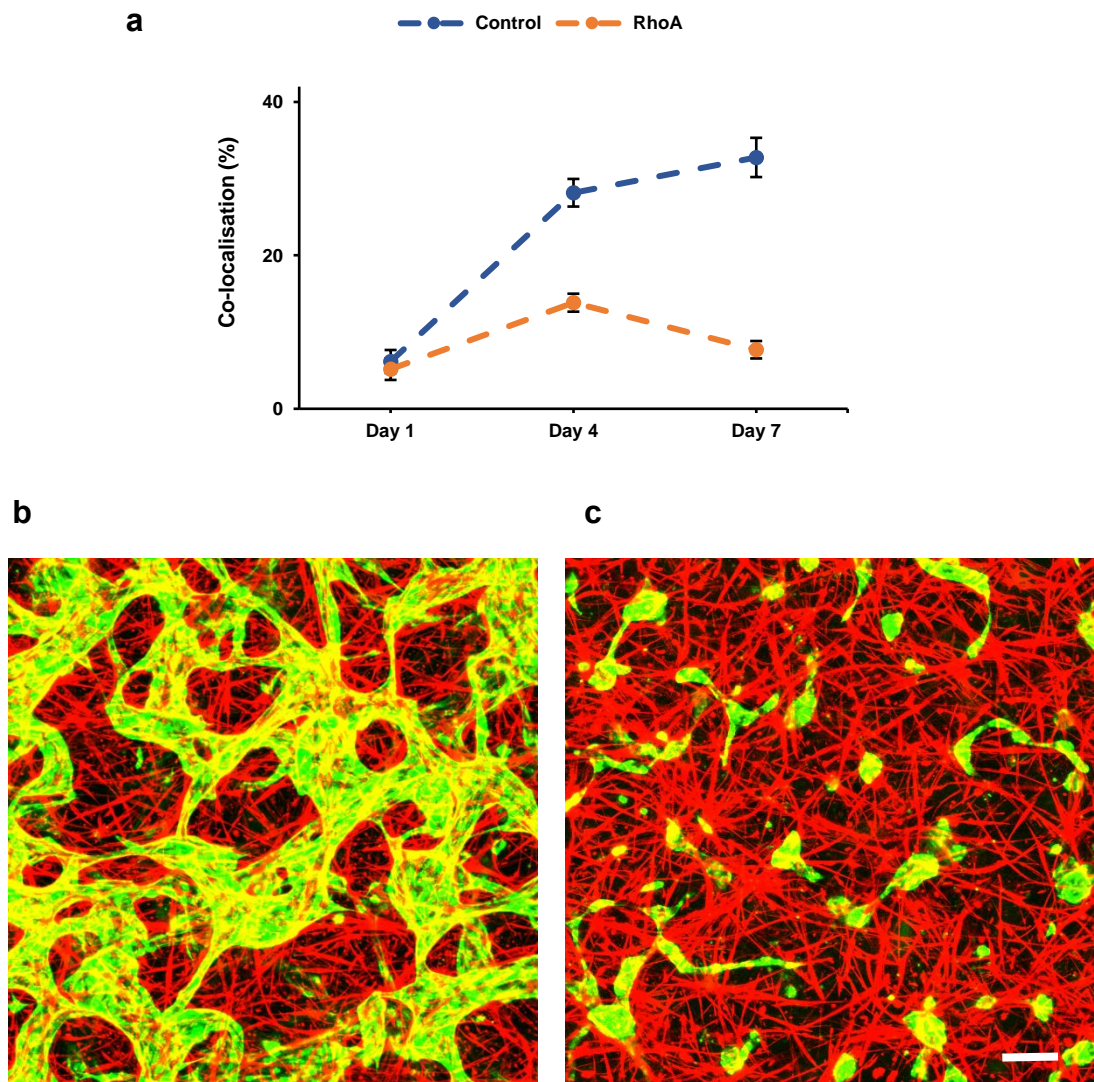
Fig 4.14: RFP-FB and ECs colocalisation. a) The graph represents changes in colocalisation of RFP-FBs and RFP-FBs^{-RhoA} with microvessels over the course of one week. ([***]P value <.001, n=3). Yellow areas show b) RFP-FBs and c) RFP-FB^{-RhoA} colocalisation with microvessels. Scale bar, 300 μm.

4.3.3 Role of EED in the Formation and Stabilisation of Microvessels

When ECs and FBs were juxtacrine co-cultured, one gene which got remarkably upregulated was EED. The gene does not belong to the mechanotransduction pathway. However, as EED got highly upregulated, we decided to investigate its contribution to microvessel formation and stabilisation. To this end, EED was inhibited in FBs, which was experimentally achieved by transfecting gene-specific siRNA. WB was then performed to examine the efficiency of the transfections on day 3 and day 7 after transfection (**Fig 4.15 a**). The data quantification showed that EED expression reduced significantly on day 3 and remained inhibited until day 7 after transfection (**Fig 4.15 b, c**).
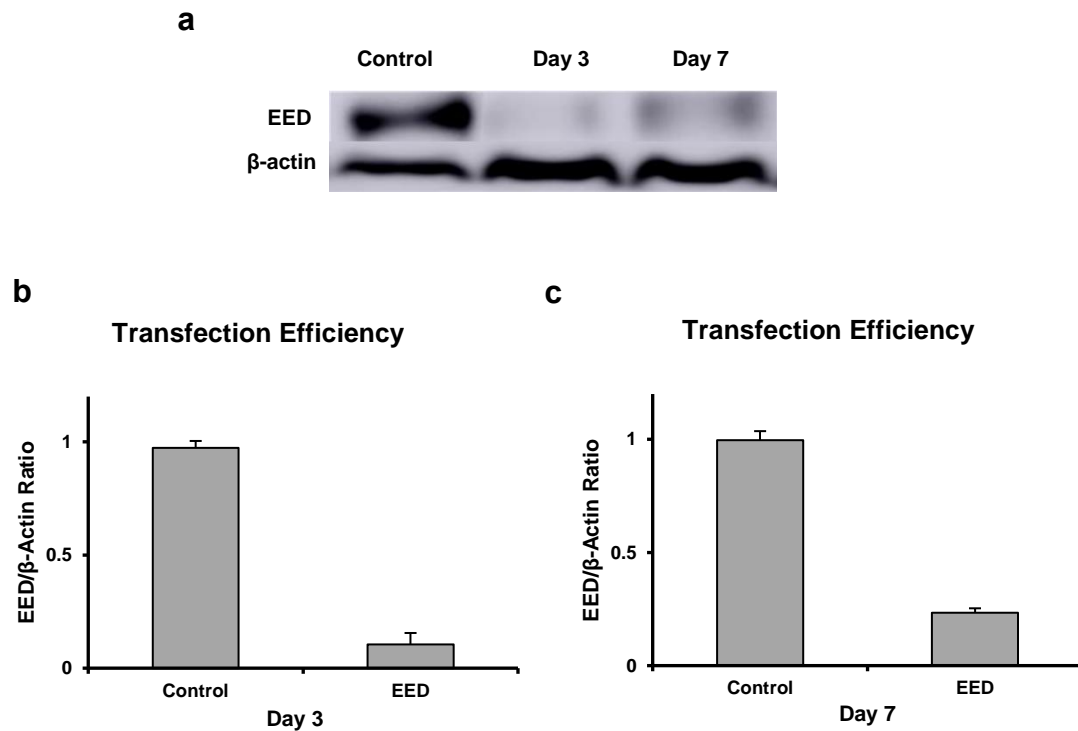
Fig 4.15: Transfection efficiency. *a) Performing WB confirmed the efficient inhibitions of EED expression. b and c) Graphs compare protein expression in control and EED-inhibited cells on day 3 and day 7 after transfection. Normalised to β-actin value at each day. n=3.*

EED-inhibited FBs were then co-embedded with ECs. 3D confocal images taken on days 2, 4, and 7 of culture revealed that ECs retained their ability to form microvessels. However, the microvessels were significantly different from the control in microvessel morphogenesis (**Fig 4.16 a**). Further characterisation of the microvessels revealed that EED-inhibited microvessels were different from control microvessels in terms of microvessels coverage area and microvessels average diameter, as we measured a significant decrease in the microvessels coverage area ($^{***}P$ value <.001, n=6, **Fig 4.16 b**) and a considerable increase in microvessels diameter ($^{***}P$ value <.001, n=3, **Fig 4.16 c**).
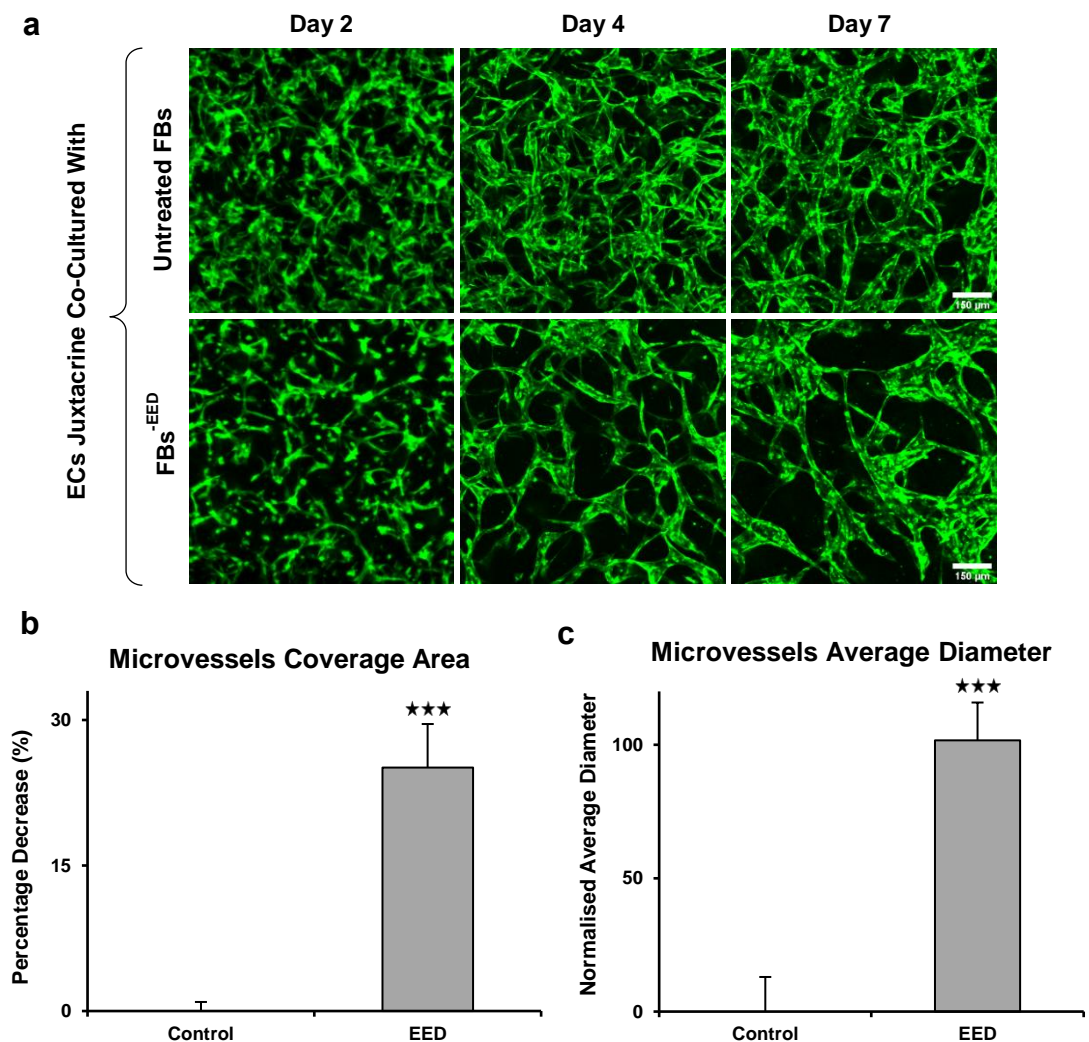
Fig 4.16: Impact of inhibition of EED on microvessel formation and morphogenesis. *a) 3D confocal images visualising the impact of inhibition of EED on microvessel formation and morphogenesis. Scale bar, 150 µm. Bar charts representing the impact of inhibition of EED on b) microvessels coverage area ($^{***}P$ value <001, n=6) and c) microvessels average diameter ($^{***}P$ value <001, n=3). Normalised with respect to control value.*

Topological characterisation showed that EED-inhibited microvessels and control were different in topology too. To such an extent, branching and the number of junctions produced by ECs considerably decreased when EED was inhibited in FBs (***P value <.001, n=5, **Fig 4.17 a, b**). On the other hand, we observed a significant increase in average branch length (*P value =.029, n=5, **Fig 4.17 c**). EED-inhibited microvessels were statically unchanged with regard to Maximum branch length (**Fig 4. 17 d**).
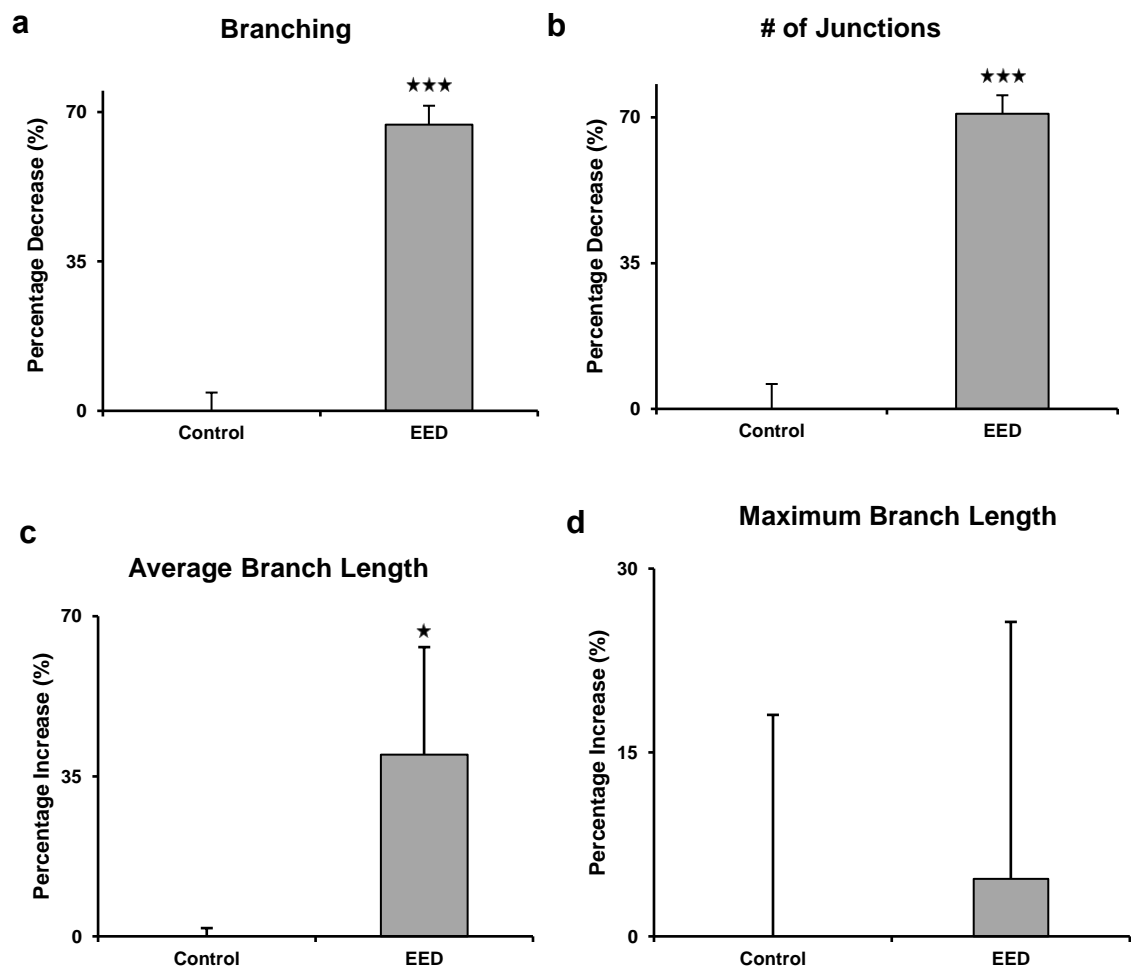
Fig 4.17: : Impact of inhibition of EED in FBs on microvessels topology. *Bar charts representing the impact of inhibition of EED on a and b) branching and number of microvessels junctions (***P value <.001) c) average branch length (*P value =.029) and d) maximum branch length. n=5. Normalised with respect to control value.*

To assess the impact of EED inhibition in FBs on microvessels function, we measured microvessels perfusability and permeability. The tracer dye injection

revealed that not all the microvessels formed by co-culturing ECs and FBs^{-EED} were perfusable (**Fig 4.18 a**). Quantification of 3D confocal images showed a significant decrease, ~40%, in perfusability of EED-inhibited condition compared to control ($^{***}P$ value <.001, n=6, **Fig 4.18 b**). The permeability of control to 10 kDa dextran was measured to be 2.4E-07 ± 9.33E-08 cm/s, whereas it was measured to be 5.18E-07 ± 7.6E-08 cm/s for EED-inhibited microvessels which demonstrates a three-fold increase (**Fig 4.18 c**).
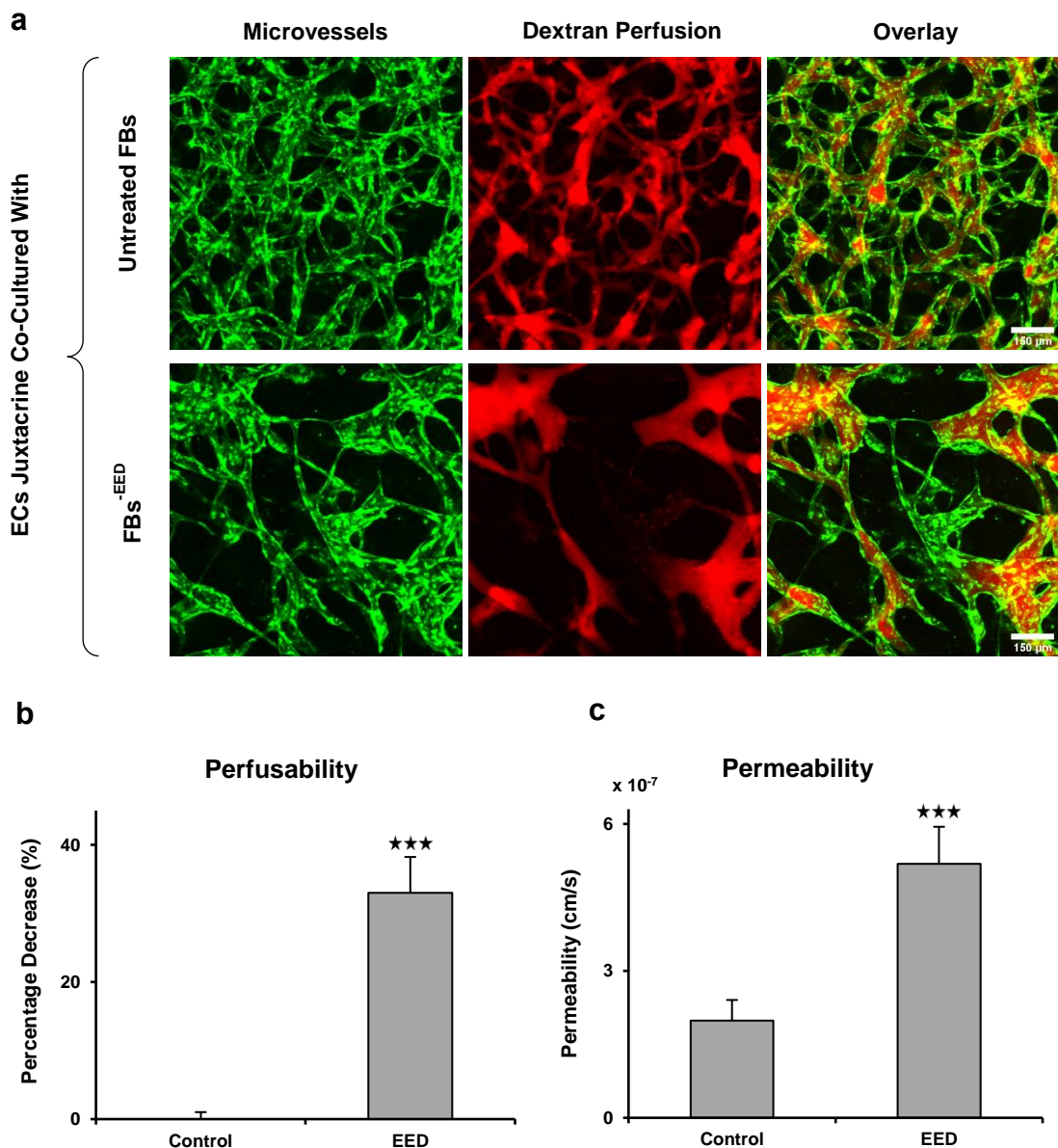
Fig 4.18: Impact of inhibition of EED in FBs on microvessels function. a) 3D confocal images visualising dextran perfusion through EED-inhibited microvessels and control. Scale bar, 150 µm. b) Bar chart representing change in perfusability of EED-inhibited microvessels and control c) Bar chart representing permeability values of EED-inhibited microvessels and control ($^{***}P$ value <.001), n=5. Normalised with respect to control value.

Comparison of microvessels openings revealed changes in the openings of EED-treated microvessels not only in terms of morphology (**Fig 4.19 a**) but also in terms of the number of openings as well as the width of openings. In such a way that we observed a remarkable decrease in the number of openings ([***]*P* value <.001, n=6, **Fig 4.19 b**) whereas a significant increase in the width of the openings compared to the control ([*]*P* value =.039, n=5, **Fig 4.19 c**).
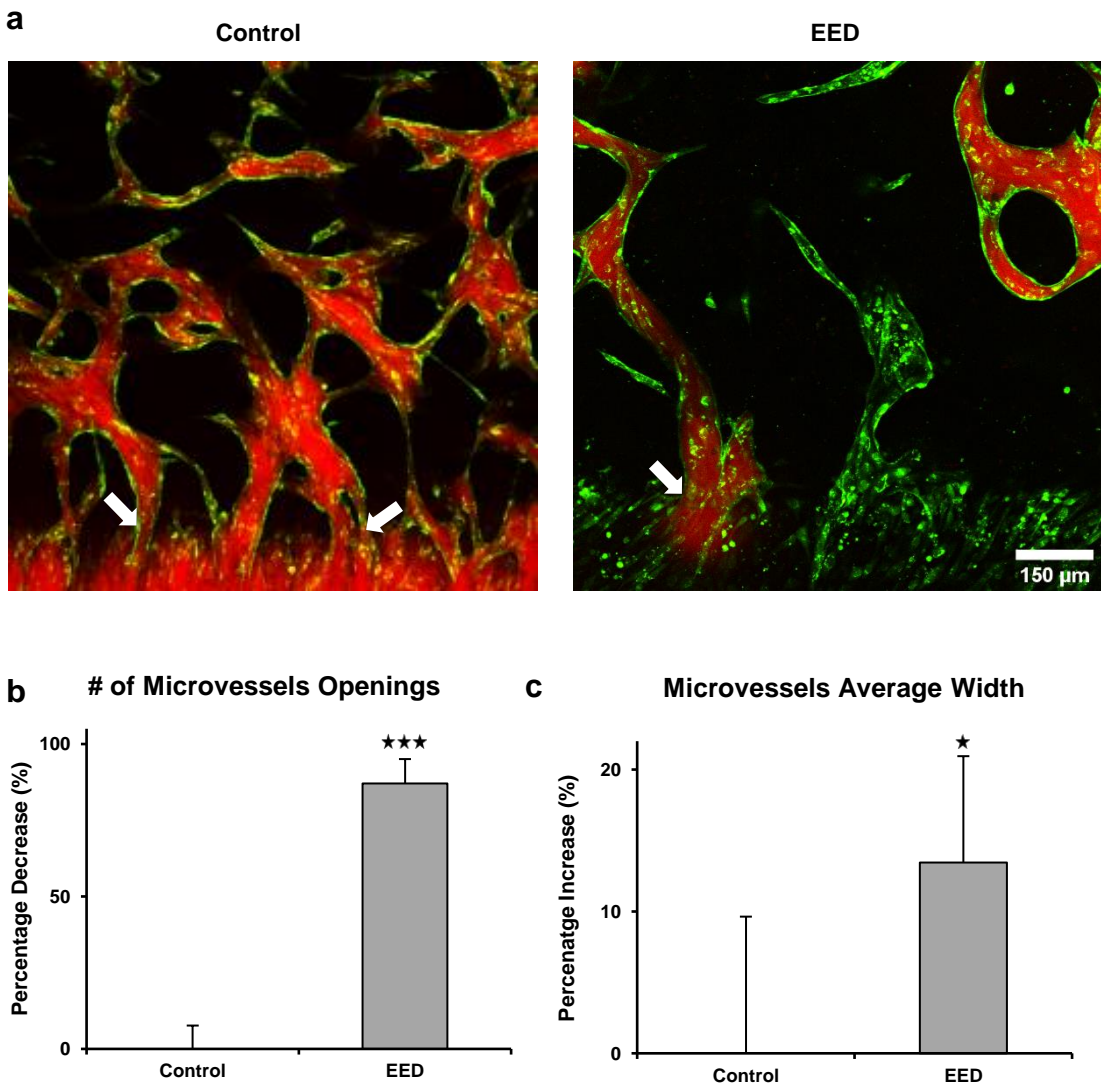
Fig 4.19: Impact of inhibition of EED in FBs on vascular openings. *a) Visualisation of morphology of EED-inhibited microvessels and control. Scale bar, 150 μm. b) Bar chart comparing the number of openings in EED-inhibited and control microvessels ([***]P value <.001, n=6). c) Bar chart comparing the average width of openings in different conditions ([*]P value =.039, n=5). Normalised with respect to control value.*

Taken together, our data provide strong evidence that EED contributes not only to the formation, morphogenesis, and characteristics of the microvessels also to their topology and function.

4.4 Discussion and Conclusion

In chapter 2, we showed that direct physical interaction between FBs and ECs is crucial to stimulate the formation of functional microvessels. Over the past few years, the mechanical role of FBs has gained increasing attention. Applying nanofibres, Hurley *et al.* investigated the dual role of FBs in regulating angiogenesis chemically and mechanically. They showed that FBs mediate angiogenesis via cell-mediated scaffold disruption, ECM deposition and ECM remodelling[112]. Other studies also showed that FBs regulate angiogenesis by altering the mechanical properties of ECM via deposition of matrix and metalloproteinase-mediated ECM remodelling[113,114]. Most of the studies about the mechanical role of FBs refer to ECM deposition and ECM stiffness. In good agreement with these findings, our study demonstrates a role for FBs mechanics in the development of vasculature using an *in vitro* assay of vasculogenesis. Our results demonstrate that FBs generate larger deformations within the ECM compared to MC and PCC conditions, which stimulate self-assembly of ECs into microvessels. However, the molecular mechanism underlying it has not been fully understood. We hypothesised that this process is mediated via mechanotransduction pathways including RhoA, YAP, SRC, Wnt7b and FAK. In chapter 3, chemically inhibiting mechanotransduction genes in both FBs and ECs, we successfully showed that mechanotransduction pathways play key roles in forming and stabilising microvessels plus their topology, characterisation and function. We then sought to investigate the mechanical role of FBs in a 3D *in vitro* assay of vasculogenesis by perturbing the same genes in FBs followed by co-culturing siRNA-inhibited FBs with ECs within a fibrin gel.

A recent study investigated FBs function by siRNA inhibition of some mechanotransduction genes such as ROCK, YAP, and Snail1 in cancer-associated fibroblasts (CAFs). Their results showed a significant decrease in vessel formation by ECs co-cultured with the ROCK, YAP or Snail1-inhibited CAFs[115]. Our results are in good agreement with these findings. When we

inhibited RhoA in FBs, ECs failed to form microvessels. This could be due to drastic changes in the FB cytoskeleton. Cytoskeleton is mechanical support for cells, which plays a vital role in maintaining cell shape, cell proliferation, and migration. It has three components; actin fibres, intermediate filaments, and microtubules. As the most important mediator for the cytoskeleton, RhoA regulates α-actin stabilisation, α-actin-myosin interaction necessary for cell contractility, and α-actin polymerisation. Inhibition of RhoA results in stopping some critical cell activities, including proliferation, migration, contractility, protein and growth factors secretion plus gel remodelling which facilitates ECs self-assembly. Therefore, when ECs are co-cultured with FBs^{-RhoA}, FBs^{-RhoA} fail to support lumen formation by ECs, and it is like there are no FBs, and ECs are mono-cultured. As mono-cultured ECs fail to form lumens, ECs co-cultured with FBs^{-RhoA} cannot create microvessels. Decellularisation of the ECM, and comparing gel deformation/remodelling with control needs to be done to answer the question.

Microvessel formation was not affected by the inhibition of YAP, Wnt7b, FAK, and Src in FBs, but it resulted in less dense microvessels by ECs for all conditions except FAK compared to the control. The formation of denser microvessels when FAK was perturbed in FBs could be due to the dramatic increase in microvessel diameter. The larger diameter in siRNA-inhibited conditions in particular FAK-deficient condition could be due to the lack of contractile forces which regulate microvessel diameter. FBs can acquire myofibroblasts phenotype, cells that secrete contractile proteins such as α-SMA, under mechanical stress such as changes in ECM[208]. Also, our findings show that FBs tend to concentrate around the lumens. This direct physical interaction exerts contractile forces to the lumens resulting in smaller diameters. Failing to migrate toward lumens leads to the lack of such forces, consequently increasing microvessel diameters. However, further investigation such as staining the FBs for αSMC in both siRNA-inhibited conditions and control could shed a light on biological mechanism underlying these observations.

In addition to increased diameters, the inhibition of mechanotransduction genes resulted in a significant change in microvessel topology, such as a remarkable decrease in the number of branches and the number of junctions and a significant increase or decrease in the average branch length and maximum branch length. This could result from a decrease in tissue stiffness in siRNA-inhibited conditions, as several research groups have reported that ECM stiffness regulates microvessels morphogenesis and topology[209,210].

Increased permeability in the microvessels formed in siRNA-inhibited conditions indicates that the integrity of the microvessels was affected by the inhibition of the mechanotransduction genes in FBs. Increase in the permeability of the siRNA-inhibited microvessels could be a consequence of changes in the tissue stiffness because ECM stiffness, along with other mechanical factors such as blood flow and the mechanical strain of the vessel, appears to play a key role in the control of endothelial permeability[211]. Also, distribution of VE-cadherin known as regulator of microvessels' permeability can be affected by tissue stiffness. This can consequently change vascular permeability. We observed lower stiffness in our system when mechanotransduction genes were perturbed in FBs. Consistent with our findings by culturing porcine aortic endothelial cells on polyacrylamide gels of varying stiffness Urbano *et al.* showed that substrate stiffness changes lead to changes in endothelial cells permeability via changes in VE-cadherin[212]. In future, that would be a good idea to assess the impact of perturbation of mechanotransduction genes on the expression and distribution of VE-cadherin in our system to shed light on how changes in tissue stiffening can change microvessel permeability.

Altogether the lack of formation of microvessels and the formation of microvessels that did not represent the features of control microvessels when ECs are co-cultured with mechanotransduction genes-inhibited FBs suggests that FBs promote and stabilise the microvessels mechanically.

Our work supports the hypothesis that FBs can enhance vascular formation and stabilisation through a vasculogenic process that is mediated, in part, by biomechanical forces and that the SRC, FAK, Wnt7b and Rho pathways as well as YAP signalling are involved. Although all of our studies were conducted in an *in vitro* assay, we believe this work correlates with *in vivo* work (done in partnership with Erik Sahai's group, data not shown, not published) describing the mechanical activity of FBs as it relates to YAP signalling. However, we believe that large mechanical deformations alone are insufficient to drive microvessel growth and stabilisation supported by stromal cells and that it is an important interaction between biomechanics and soluble signalling factors that ultimately directs vasculogenic processes.

At the end, it is worth mentioning that despite their unique advantages we are aware of some disadvantages of using microfluidic platforms and the current study. For instance, we recruited only one type of ECs (HUVECs) and FBs (NHLFs). It is obvious to generalise our findings we need to employ other types of ECs and FBs. Another limitation is that the system employed is a two-cell system which means many other parameters and factors such as cells including pericytes and chemical and mechanical cues like shear stress that play important roles in vasculogenesis are absent. Despite believing that this study is a valuable step towards mimicking *in vivo* models to study vasculogenesis we know there still exist a long journey to develop a platform which resembles *in vivo* models with their own unique complications.

Finally, several significant advantages such as providing the cells with an *in vivo*-like environment make this platform a promising and useful tool to develop organ-specific, disease-specific, and cancer-specific models by recruiting different cell types. This enhanced understanding of FB-mediated microvessel formation could also potentially provide alternative therapeutic strategies that focus on modulating the mechanobiology of FBs. Additionally, this information will help elucidate potentials for further developing vascularisation strategies for tissue engineering and regenerative medicine to

modulate the biomechanical behaviours of FBs that contribute to vascularisation.

5 General Conclusion, Preliminary Developments and Future Work

5.1 General Conclusion

In addition to chemical crosstalk, microvessel formation and function require tightly regulated mechanical signalling because cell migration and shape change inherently rely on mechanical force generation and the mechanical properties of the cellular environment. Furthermore, since cells are highly mechanosensitive, the mechanical properties of the vascular environment, such as stiffness, influence microvessel formation, morphogenesis, and function. The current study reveals direct physical interaction between ECs and FBs is essential for the formation of functional, long-lasting blood microvessels in large scale. We showed that the inhibition of mechanotransduction genes in both ECs and FBs led to either lack of microvessel formation or significant changes in microvessel morphogenesis, characteristics, topology and function. Fascinatingly, by the knockdown of mechanotrasduction genes in FBs, we showed that the emergence of the unique microvessel mechanical features such as stiffness, along with morphogenesis, topology as well as functions including perfusability and permeability are tightly interlinked with FBs mechanotransduction programs. For example, we demonstrated that during the course of microvessel formation tissue stiffness increased by over nine-fold. In contrast, perturbation of mechanotransduction genes in FBs resulted in a drastic decrease in tissue stiffness. Also, permeability increased due to mechanotransduction gene perturbation. Altogether, our research suggests that FBs are intrinsic mechanical promoters and stabilisers of microvessels.

5.2 Preliminary Findings and Future Work

Several significant advantages such as providing the cells with an *in vivo*-like environment, the ability to image vasculature in real-time and, the ability to quantitatively assess the formation, characteristics, and function of microvessels make this platform a promising and useful tool to develop organ-specific, disease-specific, and cancer-specific models by recruiting different cell types. This chapter offers preliminary findings and proposes future

directions for utilising the platform to develop organ-specific, disease-specific, and cancer-specific models.

5.2.1 Methods

Human Dermal Fibroblasts (HDFs) were grown in FGM-2, Human Lung Cancer-Associated Fibroblasts (HLCAFs) were cultured in DMEM supplemented with 1% insulin-transferrin-selenium (ITS, Invitrogen/USA) and 10% FBS (Thermo Fisher Scientific/USA), and Scleroderma-driven fibroblasts (provided by the Royal Free Hospital) were grown in DMEM supplemented with Glutamax (Gibco) and 10% FBS. The cells were frozen and stored in a nitrogen tank upon use. HDFs and Scleroderma-driven fibroblasts were used at passages 3 and 8, respectively. HLCAFs were used below passage 12. 3-channel devices were then seeded with ECs along with different FBs (JCC condition).

5.2.2 Results

5.2.2.1 Organ-Specific Model

It is known that every organ is of its specific vasculature. Hence, the development of *in vitro* organ-specific microvessels can be a useful tool to study features of any organ's specific vasculature. Vessel-specific ECs owe their specification to both inherited epigenetic modifications and local environmental cues such as the presence of stromal and mural cells. Knowing this, we replaced NHLFs with HDFs in our system to form blood microvessels mimicking skin microvessels. As expected, ECs co-seeded with HDFs successfully developed microvessels (**Fig 5.1**).

| Day 1 | Day 4 | Day 7 |
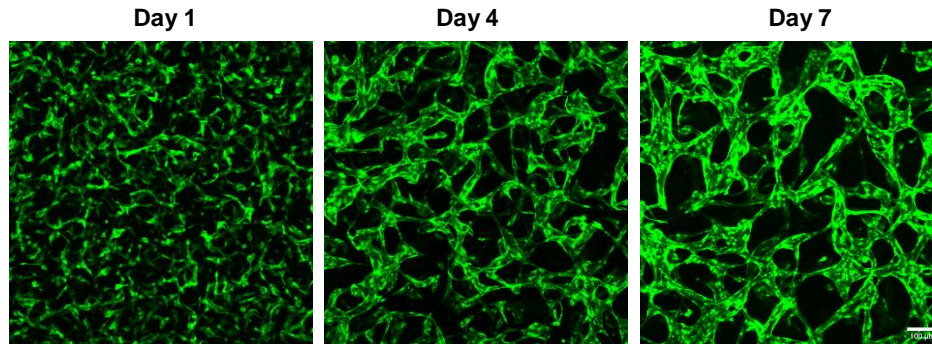
Fig 5.1: Microvessel formation by ECs in presence of HDFs. *Confocal images of microvessel formation by ECs when co-seeded with HDFs over the course of one week. Scale bar, 100 µm.*

Characterisation of the microvessels revealed that when co-seeded with HDFs, ECs created less dense vasculature with smaller diameters than NHLFs. We measured the microvessel coverage area to be 54.46 ± 0.74 percent (Fig 5.2 a) and the average diameter to be 20.2 ± 0.96 µm (Fig 5.2 b).
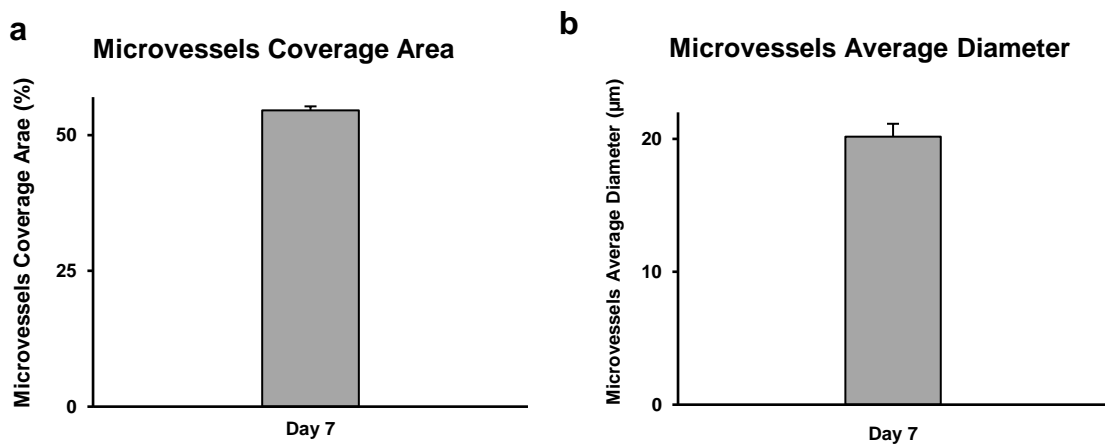
Fig 5.2: Characterisation of microvessels formed by co-culturing ECs and HDFs. *Bar charts representing a) microvessel coverage area and b) microvessel average diameter. n=3.*

Further characterisation revealed that co-culturing ECs with HDFs resulted in the formation of 70 ± 2.62 branches per unit area (Fig 5.3 a) and 38.3 ± 2.6 microvessel junctions unit area (**Fig 5.3 b**). We measured the microvessel

average branch length to be 86.8 ± 7.34 µm (**Fig 5.3 c**) and maximum branch length to be 404 ± 46.67 µm (**Fig 5.3 d**).
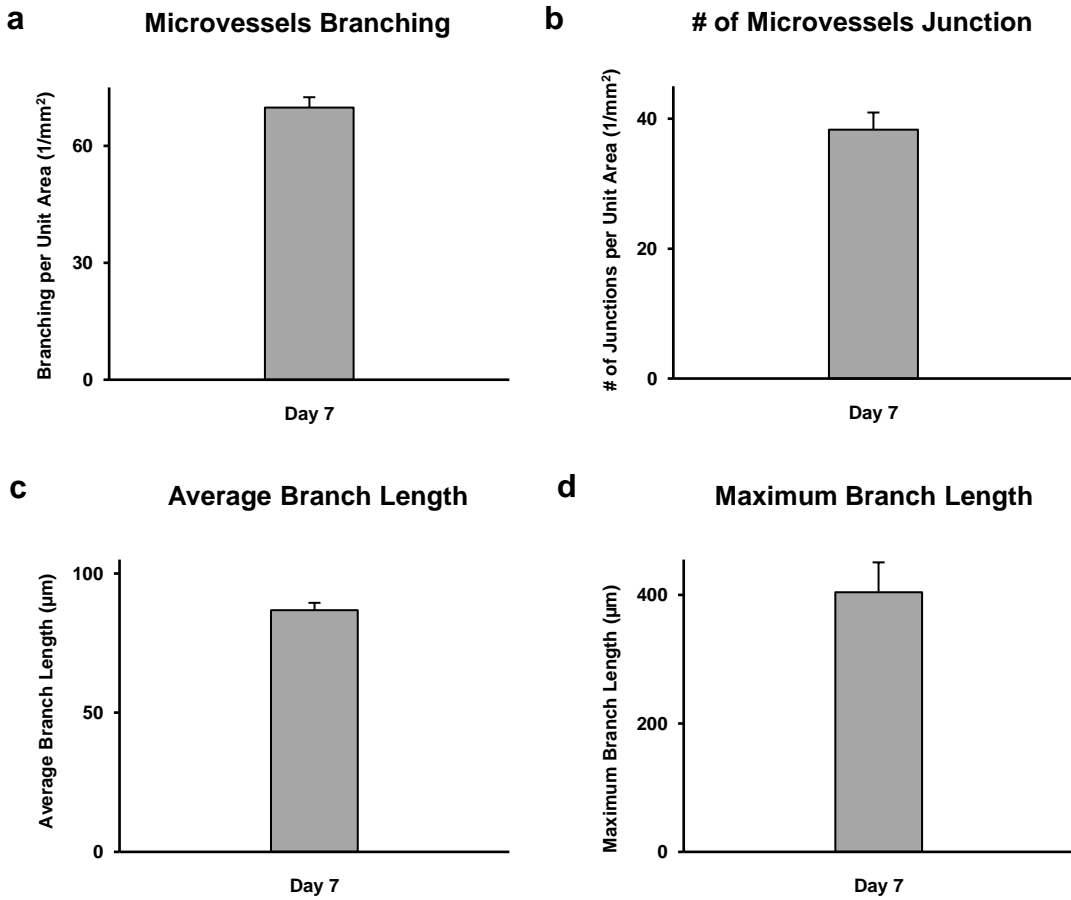
Fig 5.3: Topology of microvessels formed by co-culturing ECs and HDFs. *Bar charts representing a) branching b) junctions, c) average branch length and d) maximum branch length. n=3.*

We assessed the function of the microvessels by injecting dextran. Dextran uniformly filled the microvessels within a few seconds after injection and remained confined in the lumens demonstrating the microvessels were fully functional (**Fig 5.4**).

a microvesse ls Dextran perfusion Overlay

b Microvessels Perfusability
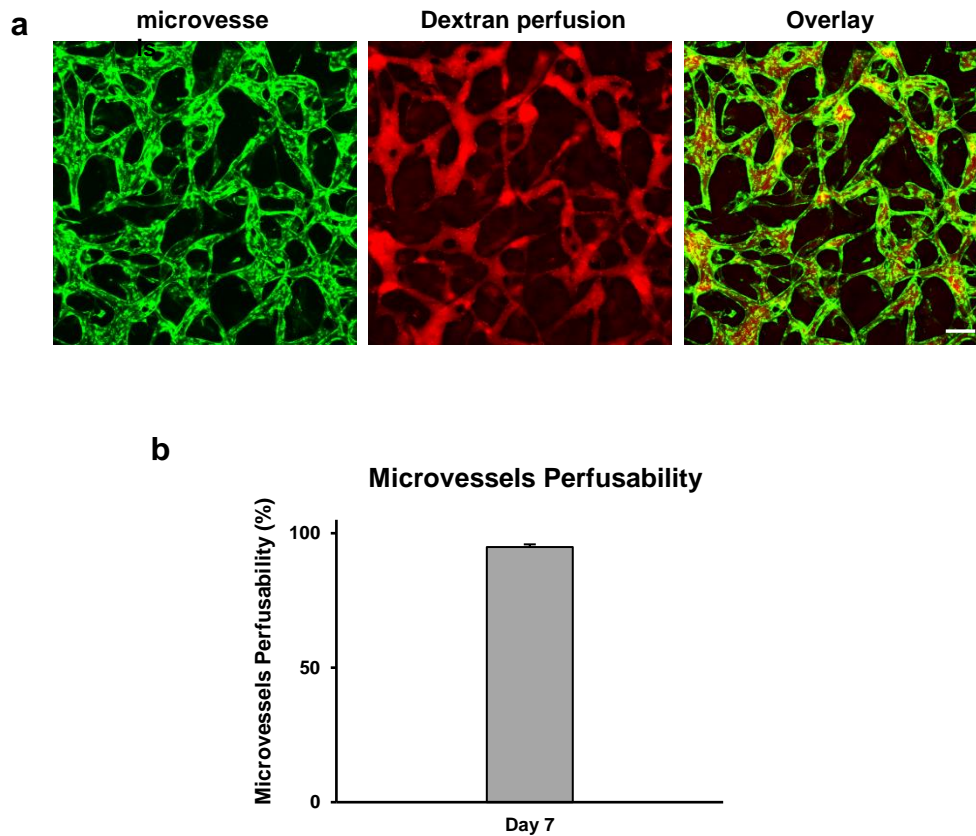
Fig 5.4: Function of microvessels formed by ECs and HDFs co-culturing. a) 3D confocal images visualising dextran perfusion through the microvessels. Scale bar, 100 µm. b) Bar chart representing quantified perfusability. n=3.

When co-seeded with HDFs, ECs formed functional microvessels different from the microvessels formed when co-embedded with NHLFs. This suggests that the presence of different FBs can lead to different microvessels. Altogether, one can hypothesise that the presence of organ-specific FBs can result in the formation of organ-specific microvessels. However, further analysis, such as permeability, is essential to prove the hypothesis.

5.2.2.2 Diseased-Specific Model

Blood vessels and FBs are affected by different diseases, including Scleroderma, a group of autoimmune diseases. Unlike NHLFs and HDFs, Scleroderma-driven fibroblasts failed to support ECs to form blood

microvessels, demonstrating the cells' dysfunction (**Fig 5.5**). Developing an *in vitro* model can be used to study fibroblast dysfunction and repair mechanisms and provide insight into the disease's molecular mechanisms.
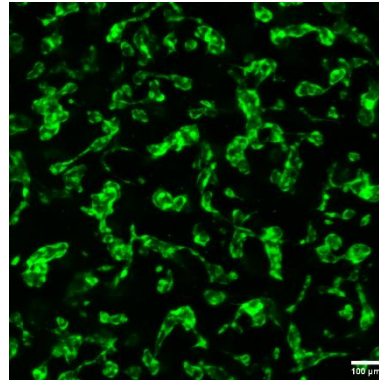
Fig 5.5: Scleroderma-driven fibroblasts failed to support microvessel formation. Scale bar, 100 μm.

5.2.2.3 Cancer-Specific Model

Formation of new blood vessels also occurs during cancer, where newly-formed vessels serve to feed the growing tumour and help the cancer cells escape from the primary tumour, find their way to the circulatory system, and reach a hosting tissue to form secondary tumours[213]. Stromal cells, FBs included help tumours to vascularise by producing and secreting proangiogenic factors[214]. CAFs are known to be a spy in the human body in tumourigenesis. They help cancer cells survive by providing them with nutrients and facilitating their invasion to the circulatory system by remodelling ECM[215]. Believing that this platform can be a useful tool to study the role of CAFs in tumour growth and cancer angiogenesis and metastasis, we replaced NHLFs with HLCAFs. Despite the need for optimisation, the formation of semi-functional microvessels (**Fig 5.6**) promises developing a useful platform to study the contribution of CAFs to tumour growth, cancer angiogenesis, and metastasis.

microvessels **Dextran perfusion** **Overlay**
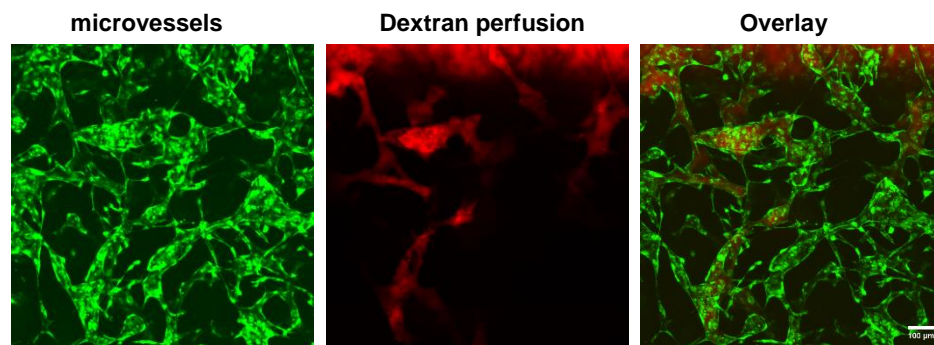
Fig 5.6: Microvessels formed by co-culturing ECs and HLCAFs. *Scale bar, 100 µm.*

Appendix

Appendix 1, Perfusability

```
Perfusability_Array = newArray();

//Input is a .tif confocal image stack with 2 channels: (1) HUVEC, (2) Dextran

//User is prompted to open folder containing multiple .tif image stacks for processing

dir = getDirectory("Choose a Directory ");

list = getFileList(dir);

for (j=0; j<list.length; j++) {

if (endsWith(list[j],"tif")) {

path = dir+list[j];

open(path);

run("Split Channels");

selectWindow("C1-" + list[j]);

rename("HUVEC");

selectWindow("C2-" + list[j]);

rename("Dextran");

//Process dextran channel, slice by slice

for (i=0; i<nSlices; i++) {

run("8-bit");

run("Subtract Background...", "rolling=1000 sliding slice");

run("Enhance Contrast", "saturated=5");

for(k=0; k<10; k++) run("Despeckle", "slice");

run("Gaussian Blur...", "sigma=3.0 slice");

//Threshold and Binarise

setAutoThreshold("Triangle");
```

```
setAutoThreshold("Triangle dark");

getThreshold(lower, upper );

setThreshold(lower, upper );

run("Convert to Mask", "only");

run("Next Slice [>]");}

//Reslice in XZ---plane

run("Reslice [/]...", "output=1.000 start=Bottom avoid");

rename("Dextran_Reslice");

//Process HUVEC channel, slice by slice

selectWindow("HUVEC");

for (i=0; i<nSlices; i++) {

run("8-bit");

run("Subtract Background...", "rolling=1000 sliding slice");

run("Enhance Contrast", "saturated=5");

for(k=0; k<10; k++) run("Despeckle", "slice");

run("Gaussian Blur...", "sigma=3.0 slice");

//Threshold and  binarise

setAutoThreshold("Triangle");

setAutoThreshold("Triangle dark");

getThreshold(lower, upper);

setThreshold(lower, upper);

run("Convert to Mask", "only");

run("Next Slice [>]");}

//Reslice in XZ---plane

run("Reslice [/]...", "output=1.000 start=Bottom avoid");
```

```
run("Invert", "stack");

rename("HUVEC_Reslice");

run("Set Measurements...", "area mean");

setSlice(1);

//Identify vessel outlines from HUVEC channel

run("Analyze Particles...", " show=Outlines include add stack");

//Measure binarised dextran pixel intensity within vessel outlines

selectWindow("Dextran_Reslice");

roiManager("measure");

Total_Area = 0;

Zero_Area = 0;

for (l=0; l<nResults; l++) {

b = getResult("Area", l);

Total_Area = Total_Area + b;

a = getResult("Mean", l);

//If no dextran from thresholded image is found within vessel region, that

region // is considered non---perfusable

if (a == 0) {

Zero_Area = Zero_Area + b;}}

Perfusability = (Total_Area - Zero_Area) / Total_Area;

Perfusability_Array  = Array.concat(Perfusability_Array,  Perfusability);

run("Close All");

selectWindow("Results");

run("Close");

roiManager("delete");}}
```

Array.show("Perfusability",Perfusability_Array)

//Perfusability is reported as a fraction of perfused volume divided by total
//vascular volume

Appendix 2, Diffusion

```
// StackProfileData

// This ImageJ macro gets the profile of all slices in a stack

// and writes the data to the Results table, one column per slice.

// Version 1.0, 24-Sep-2010 Michael Schmid

macro "Stack profile Data" {

if (!(selectionType()==0 || selectionType==5 || selectionType==6))

exit("Line or Rectangle Selection Required");

setBatchMode(true);

run("Plot Profile");

Plot.getValues(x, y);

run("Clear Results");

for (i=0; i<x.length; i++)

setResult("x", i, x[i]);

close();

n = nSlices;

for (slice=1; slice<=n; slice++) {

showProgress(slice, n);

setSlice(slice);

profile = getProfile();

sliceLabel = toString(slice);
```

```
sliceData = split(getMetadata("Label"),"\n");

if (sliceData.length>0) {

line0 = sliceData[0];

if (lengthOf(sliceLabel) > 0)

sliceLabel = sliceLabel+ " ("+ line0 + ")";}

for (i=0; i<profile.length; i++)

setResult(sliceLabel, i, profile[i]);}

setBatchMode(false);

updateResults;}
```

Appendix 3, Microvessel Length

```
dir = getDirectory("Choose a Directory ");

list = getFileList(dir);

networkLength = newArray();

for (j=0; j<list.length; j++) {

path = dir+list[j];

open(path);

//Perform image processing

run("Subtract Background...", "rolling=50");

run("Enhance Contrast...", "saturated=1");

run("Unsharp Mask...", "radius=100 mask=0.60");

setOption("BlackBackground", false);

//Binarise

run("Make Binary");

run("Dilate");
```

```
run("Dilate");

run("Dilate");

run("Dilate");

run("Dilate");

//Skeletonise

run("Skeletonise (2D/3D)");

//Analyze Skeleton

run("Analyze Skeleton (2D/3D)", "prune=none prune");

//run("Close All");

a = newArray();

//Calculate longest connected network

for (i=0; i<nResults; i++) {

b = getResult("# Branches",i)*getResult("Average Branch Length",i);

a = Array.concat(a,b);}

Array.getStatistics(a, min, max, mean, std);

networkLength = Array.concat(networkLength,max);

close("Results");

print(networkLength[j]);}

//Network length is the longest connected network for each image; if no units were

//stored in the original image properties, values will be reported in pixels.

run("script:Macro.ijm.ijm", "choose=F:/Test/");
```

Appendix 4, Microvessel Coverage Area

```
//Input is a .tif confocal image stack of vasculature filled with fluorescently labeled
```

//tracer. Only the tracer (dextran) channel should be used for this thresholding

//algorithm.

//User is prompted to open folder containing multiple .tif image stacks for processing.

dir = getDirectory("Choose a Directory ");

list = getFileList(dir);

VolFraction = newArray();

NumLumens = newArray();

for (j=0; j<list.length; j++) {

if (endsWith(list[j],"tif")) {

path = dir+list[j];

open(path);

//For each image stack:

//Process, threshold, and binarise – slice by slice

for (i=0; i<nSlices; i++) {

run("8-bit");

run("Subtract Background...", "rolling=1000 sliding slice");

run("Enhance Contrast", "saturated=10");

for(k=0; k<5; k++) run("Despeckle", "slice");

run("Gaussian Blur...", "sigma=3.0 slice");

setAutoThreshold("Triangle");

setAutoThreshold("Triangle dark");

getThreshold(lower, upper);

setThreshold(lower, upper);

run("Convert to Mask", "only");

run("Next Slice [>]"); }

```
//Identify vascular lumens for each slice in XZ---plane

//Calculate # lumens and vascularised area for each slice

run("Reslice [/]...", "output=1.000 start=Bottom avoid");

rename("lumens.tif");

run("Invert", "stack");

run("Set Measurements...", "area");

run("Analyze Particles...", "size=50-Infinity display summarise stack");

select Window("Results");

run("Close");

select Window("Summary of lumens.tif");

IJ.rename Results("Results");

a= new Array();

c = new Array();

//Retrieve % vascularised area for each XZ---slice

//Retrieve # lumens for each XZ---slice

for (i=0; i<n Results; i++) {

b = get Result("%Area",i);

a = Array.concat(a,b);

d = get Result("Count",i);

c = Array.concat(c,d);}

//Calculate average % vascularised area over all slices

Array.get Statistics(a, min, max, mean, std);

VolFraction = Array.concat(VolFraction,mean);

//Calculate average # lumens over all slices and normalise by crosssectional
area

Get Dimensions(width, height, channels, slices, frames);
```

```
Get Pixel Size(unit, pixelWidth, pixelHeight);

totalarea = (width*pixelWidth*height*pixelHeight)/1000000;

Array.get Statistics(c, minc, maxc, meanc, stdc);

NumLumens = Array.concat(NumLumens,meanc/totalarea);

Select Window("Results");

Save As("Text", path + "Morph_Quant.txt");

run("Close All");}}

Array.show("VolFraction",VolFraction)

Array.show("NumVessels",NumLumens)
```

Reference:

1. Pollet, A. M. A. O. *et al.* Recapitulating the vasculature using Organ-on-Chip technology. *Bioengineering* **7**, 1–18 (2020).

2. Sivaraj, K. K. *et al.* Blood vessel formation and function in bone. *Development (Cambridge)* **143**, 2706–2715 (2016).

3. Kolte, D. *et al. Vasculogenesis and Angiogenesis. Translational Research in Coronary Artery Disease: Pathophysiology to Treatment* (Elsevier Inc., 2016).

4. Herbert, S. P. *et al.* Molecular control of endothelial cell behaviour during blood vessel morphogenesis. *Nature Reviews Molecular Cell Biology* **12**, 551–564 (2011).

5. Chung, A. S. *et al.* Developmental and Pathological Angiogenesis. *Annual Review of Cell and Developmental Biology* **27**, 563–584 (2011).

6. Risau, W. Mechanisms of angiogenesis. *Nature* vol. 386 671–674 (1997).

7. Tahergorabi, Z. *et al.* A review on angiogenesis and its assays. *Iranian Journal of Basic Medical Sciences* **15**, 1110–1126 (2012).

8. Yoo, S. Y. *et al.* Angiogenesis and its therapeutic opportunities. *Mediators of Inflammation* **2013**, (2013).

9. Al-Abd, A. M. *et al.* Anti-angiogenic agents for the treatment of solid tumors: Potential pathways, therapy and current strategies – A review. *Journal of Advanced Research* **8**, 591–605 (2017).

10. Papagiannaki, C. *et al.* Development of an angiogenesis animal model featuring brain arteriovenous malformation histological characteristics. *Journal of NeuroInterventional Surgery* **9**, 204–210 (2017).

11. Wang, X. *et al.* LRG1 promotes angiogenesis by modulating endothelial TGF-β signalling. *Nature* **499**, 306–311 (2013).

12. Staton, C. A. *et al.* Current methods for assaying angiogenesis in vitro and in vivo. *International journal of experimental pathology* **85**, 233–48 (2004).

13. Bishop, E. T. *et al.* An in vitro model of angiogenesis: Basic features. *Angiogenesis* **3**, 335–344 (1999).

14. Velazquez, O. C. *et al.* Fibroblast-dependent differentiation of human microvascular endothelial cells into capillary-like, three-dimensional networks. *FASEB Journal* **16**, 1316–1318 (2002).

15. Han, S. K. *et al.* The Effect of Human Bone Marrow Stromal Cells and Dermal Fibroblasts on Angiogenesis. *Plastic and Reconstructive Surgery* **117**, 829–835 (2006).

16. Martin, T. A. *et al.* Regulation of angiogenesis and endothelial cell motility by matrix-bound fibroblasts. *Angiogenesis* **3**, 69–76 (1999).

17. Martin, T. A. *et al.* Matrix-bound fibroblasts regulate angiogenesis by modulation of VE-cadherin. *European Journal of Clinical Investigation* **31**, 931–938 (2001).

18. Cochrane, A. *et al.* Advanced in vitro models of vascular biology: Human induced pluripotent stem cells and organ-on-chip technology. *Advanced Drug Delivery Reviews* **140**, 68–77 (2019).

19. Choi, J. S. *et al.* Circumferential alignment of vascular smooth muscle cells in a circular microfluidic channel. *Biomaterials* **35**, 63–70 (2014).

20. Demir, R. *et al.* Vasculogenesis and angiogenesis in the early human placenta. *Acta Histochemica* **109**, 257–265 (2007).

21. Yancopoulos, G. D. *et al.* Vascular-specific growth factors and blood

vessel formation. *Nature* **407**, 242–248 (2000).

22. Singh, A. *et al.* Microscale technologies for cell engineering. *Microscale Technologies for Cell Engineering* 1–318 (2015).

23. Gurevich, D. B. *et al.* Live imaging of wound angiogenesis reveals macrophage orchestrated vessel sprouting and regression. *The EMBO Journal* **37**, 1–23 (2018).

24. Stenzel, D. *et al.* Endothelial basement membrane limits tip cell formation by inducing Dll4/Notch signalling in vivo. *EMBO Reports* **12**, 1135–1143 (2011).

25. Karagiannis, E. D. *et al.* Distinct modes of collagen type I proteolysis by matrix metalloproteinase (MMP) 2 and membrane type I MMP during the migration of a tip endothelial cell: Insights from a computational model. *Journal of Theoretical Biology* **238**, 124–145 (2006).

26. Potente, M. *et al.* Basic and therapeutic aspects of angiogenesis. *Cell* **146**, 873–887 (2011).

27. Betz, C. *et al.* Cell behaviors and dynamics during angiogenesis. *Development (Cambridge)* **143**, 2249–2260 (2016).

28. Zakirov, B. *et al.* Active perception during angiogenesis: Filopodia speed up Notch selection of tip cells in silico and in vivo. *bioRxiv* (2020).

29. Gianni-Barrera, R. *et al.* To sprout or to split? VEGF, Notch and vascular morphogenesis. *Biochemical Society Transactions* **39**, 1644–1648 (2011).

30. Gianni-Barrera, R. *et al.* Split for the cure: VEGF, PDGF-BB and intussusception in therapeutic angiogenesis. *Biochemical Society Transactions* **42**, 1637–1642 (2014).

31. Ylä-Herttuala, S. *et al.* Vascular Endothelial Growth Factors. Biology and

Current Status of Clinical Applications in Cardiovascular Medicine. *Journal of the American College of Cardiology* **49**, 1015–1026 (2007).

32. Ferrara, N. *et al.* The biology of VEGF and its receptors. *Nature Medicine* **9**, 669–676 (2003).

33. Nakatsu, M. N. *et al.* VEGF121 and VEGF165 Regulate Blood Vessel Diameter Through Vascular Endothelial Growth Factor Receptor 2 in an in Vitro Angiogenesis Model. *Laboratory Investigation* **83**, 1873–1885 (2003).

34. Giles, F. J. The vascular endothelial growth factor (VEGF) signaling pathway: a therapeutic target in patients with hematologic malignancies. *The oncologist* **6 Suppl 5**, 32–9 (2001).

35. Witmer, A. Vascular endothelial growth factors and angiogenesis in eye disease. *Progress in Retinal and Eye Research* **22**, 1–29 (2003).

36. Biology, C. Vascular Endothelial Growth Factor in Human Colon Cancer : Biology and Therapeutic Implications. **5**, 11–15 (2000).

37. Gille, H. *et al.* Analysis of biological effects and signaling properties of Flt-1 (VEGFR-1) and KDR (VEGFR-2): A reassessment using novel receptor-specific vascular endothelial growth factor mutants. *Journal of Biological Chemistry* **276**, 3222–3230 (2001).

38. Clauss, M. *et al.* The vascular endothelial growth factor receptor Flt-1 mediates biological activities Implications for a functional role of placenta growth factor in monocyte activation and. *Journal of Biological Chemistry* **271**, 17629–17634 (1996).

39. Tammela, T. *et al.* Lymphangiogenesis: Molecular Mechanisms and Future Promise. *Cell* **140**, 460–476 (2010).

40. Eklund, L. *et al.* Tie receptors and their angiopoietin ligands are context-

dependent regulators of vascular remodeling. *Experimental Cell Research* **312**, 630–641 (2006).

41. Fagiani, E. *et al.* Angiopoietins in angiogenesis. *Cancer Letters* **328**, 18–26 (2013).

42. Thurston, G. Role of Angiopoietins and Tie receptor tyrosine kinases in angiogenesis and lymphangiogenesis. *Cell and Tissue Research* **314**, 61–68 (2003).

43. Kim, I. *et al.* Angiopoietin-1 Regulates Endothelial Cell Survival Through the Phosphatidylinositol 3´-Kinase/Akt Signal Transduction Pathway. **1**, 24–29 (2000).

44. Park, Y. S. *et al.* Hypoxia and vascular endothelial growth factor acutely up-regulate angiopoietin-1 and Tie2 mRNA in bovine retinal pericytes. *Microvascular Research* **65**, 125–131 (2003).

45. Geevarghese, A. *et al.* Pericyte-endothelial crosstalk: Implications and opportunities for advanced cellular therapies. *Translational Research* (2014).

46. Mandriota, S. J. *et al.* Regulation of angiopoietin-2 mRNA levels in bovine microvascular endothelial cells by cytokines and hypoxia. *Circulation Research* **83**, 852–859 (1998).

47. Kullander, K. *et al.* Mechanisms and functions of Eph and ephrin signalling. *Nature Reviews Molecular Cell Biology* **3**, 475–486 (2002).

48. Triplett, J. W. *et al.* Eph and ephrin signaling in the formation of topographic maps. *Seminars in Cell and Developmental Biology* **23**, 7–15 (2012).

49. Caestecker, M. P. De *et al.* in Cancer. **92**, 420–425 (2000).

50. Marquardt, T. *et al.* Coexpressed EphA receptors and ephrin-A ligands

mediate opposing actions on growth cone navigation from distinct membrane domains. *Cell* **121**, 127–139 (2005).

51. Singh, B. *et al.* Dental Journal. *Dental Journal Of Advanced Studies* **1**, 12–26 (2013).

52. Diego, S. of a Fibroblast from Bovine Pituitary *. **260**, 2515–2520 (1975).

53. Johnson, D. E. *et al.* Structural and functional diversity in the fgf receptor multigene family. *Advances in Cancer Research* (1992).

54. Bikfalvi, A. *et al.* Biological Roles of Fibroblast Growth Factor-2 *. **18**, 26–45 (1997).

55. WAHL, S. M. *et al.* Macrophage Production of TGF-β and Regulation by TGF-β. *Annals of the New York Academy of Sciences* **593**, 188–196 (1990).

56. Wang Y, Z. S. Angiogenic Factors. *Vascular Biology of the Placenta* (2010).

57. Distler, J. H. W. *et al.* Angiogenic and angiostatic factors in the molecular control of angiogenesis. *The Quarterly Journal of Nuclear Medicine* **47**, 149–161 (2003).

58. Li, J. *et al.* Angiogenesis in wound repair: Angiogenic growth factors and the extracellular matrix. *Microscopy Research and Technique* **60**, 107–114 (2003).

59. Yang, E. Y. Transforming growth factor beta 1-induced changes in cell migration, proliferation, and angiogenesis in the chicken chorioallantoic membrane. *The Journal of Cell Biology* **111**, 731–741 (1990).

60. Merwin, J. R. Transforming growth factor beta modulates extracellular matrix organization and eell-eell junctional complex formation during in vitro angiogenesis. *Journal of Cellular Physiology* **161**, 149–161 (1996).

61. Enenstein, J. *et al.* Basic FGF and TGF-beta differentially modulate integrin expression of human microvascular endothelial cells. *Exp Cell Res* (1992).

62. Collo, G. *et al.* Endothelial cell integrin alpha5beta1 expression is modulated by cytokines and during migration in vitro. *Journal of cell science* **112 (Pt 4**, 569–78 (1999).

63. Roberts, A. B. *et al.* Transforming growth factor type beta: rapid induction of fibrosis and angiogenesis in vivo and stimulation of collagen formation in vitro. *Proceedings of the National Academy of Sciences* **83**, 4167–4171 (1986).

64. Wang, G. *et al.* Origin and differentiation of vascular smooth muscle cells. *The Journal of Physiology* **593**, 3013–3030 (2015).

65. Hewett, P.W. and Murray, J. C. Human microvessel endothelial cells: Isolation, culture and characterization. *In Vitro Cell. Dev. Biol.* 823–830 (1993).

66. Birbrair, A. *et al.* Pericytes at the intersection between tissue regeneration and pathology: Figure 1. *Clinical Science* **128**, 81–93 (2015).

67. Chistiakov, D. A. *et al.* Vascular smooth muscle cell in atherosclerosis. *Acta Physiologica* **214**, 33–50 (2015).

68. Lv, F. J. *et al.* Concise review: The surface markers and identity of human mesenchymal stem cells. *Stem Cells* **32**, 1408–1419 (2014).

69. Alberts, B. *et al. Molecular Biology of the cell. 4th edition. Amino Acids* (2002).

70. Garlanda, C. *et al.* Heterogeneity of endothelial cells: Specific markers. *Arteriosclerosis, Thrombosis, and Vascular Biology* (1997).

71. Aird, W. C. Phenotypic heterogeneity of the endothelium: I. Structure, function, and mechanisms. *Circulation Research* **100**, 158–173 (2007).

72. Mark B. Hampton, Anthony J. Kettle, and C. C. W. The Journal of The American Society of Hematology. *The Journal of The American Society ofHematology* **92**, 3007–3017 (1998).

73. Jaffe, E. A. *et al.* Culture of human endothelial cells derived from umbilical veins identification by morphologic and immunologic criteria. *J Clin Invest* **52**, 2745–2756 (1973).

74. Yamaguchi, T. P. *et al.* Flk-1, an Flt-Related Receptor Tyrosine Kinase Is an Early Marker for Endothelial Cell Precursors. *Development* **118**, 489–498 (1993).

75. Dore-duffy, P. *et al.* NIH Public Access. **82**, 18–27 (2012).

76. Crisan, M. *et al.* Purification and Long-Term Culture of Multipotent Progenitor Cells Affiliated with the Walls of Human Blood Vessels: Myoendothelial Cells and Pericytes. *Methods in Cell Biology* **86**, 295–309 (2008).

77. Sood, A. Role of pericytes in angiogenesis. *Antiangiogenic Agents in Cancer Therapy* 117–132 (2008).

78. Pallone, T. L. *et al.* Pericyte Regulation of Renal Medullary Blood Flow. *Nephron Experimental Nephrology* **9**, 165–170 (2001).

79. Soriano, P. Abnormal kidney development and hematological disorders in PDGF beta-receptor mutant mice. *Genes & Development* **8**, 1888–1896 (1994).

80. Hellström, M. *et al.* Lack of pericytes leads to endothelial hyperplasia and abnormal vascular morphogenesis. *Journal of Cell Biology* **152**, 543–553 (2001).

81. Bandopadhyay, R. *et al.* Contractile proteins in pericytes at the blood-brain and blood-retinal barriers. *Journal of Neurocytology* **30**, 35–44 (2001).

82. Peppiatt, C. M. *et al.* Bidirectional control of CNS capillary diameter by pericytes. *Nature* **443**, 700–704 (2006).

83. Von Tell, D. *et al.* Pericytes and vascular stability. *Experimental Cell Research* **312**, 623–629 (2006).

84. Armulik, A. *et al.* Pericytes regulate the blood-brain barrier. *Nature* **468**, 557–561 (2010).

85. Fischer, C. *et al.* Principles and therapeutic implications of angiogenesis, vasculogenesis and arteriogenesis. *Handbook of Experimental Pharmacology* (2006).

86. Raza, A. *et al.* Pericytes and vessel maturation during tumor angiogenesis and metastasis. *American Journal of Hematology* **85**, 593–598 (2010).

87. Basatemur, G. L. *et al.* Vascular smooth muscle cells in atherosclerosis. *Nature Reviews Cardiology* **16**, 727–744 (2019).

88. Meyer, H. S. Color Textbook of Histology. *JAMA: The Journal of the American Medical Association* (2007).

89. Yamashiro, Y. *et al.* The molecular mechanism of mechanotransduction in vascular homeostasis and disease. *Clinical Science* **134**, 2399–2418 (2020).

90. Metz, R. P. *et al.* Vascular smooth muscle cells: isolation, culture, and characterization. *Methods in molecular biology (Clifton, N.J.)* (2012).

91. Owns, G. K. Regulation of Differentiation of Vascular Smooth Muscle Cells. **75**, (1995).

92. Orlidge, A. Inhibition of capillary endothelial cell growth by pericytes and smooth muscle cells. *The Journal of Cell Biology* **105**, 1455–1462 (1987).

93. Hasan, A. *et al.* A multilayered microfluidic blood vessel-like structure. *Biomedical Microdevices* **17**, 1–13 (2015).

94. Ankrum, J. A. *et al.* Mesenchymal stem cells: Immune evasive, not immune privileged. *Nature Biotechnology* (2014).

95. Ghajar, C. M. *et al.* The effect of matrix density on the regulation of 3-D capillary morphogenesis. *Biophysical Journal* **94**, 1930–1941 (2008).

96. Sobrino, A. *et al.* 3D microtumors in vitro supported by perfused vascular networks. *Scientific Reports* **6**, 1–11 (2016).

97. Jeon, J. S. *et al.* Generation of 3D functional microvascular networks with mural cell-differentiated human mesenchymal stem cells in microfluidic vasculogenesis systems. *Integrative Biology* **100**, 130–134 (2012).

98. Kalluri, R. *et al.* Fibroblasts in cancer. *Nature Reviews Cancer* **6**, 392–401 (2006).

99. Hughes, C. C. W. Endothelial – stromal interactions in angiogenesis. *Current Opinion in Hematology* **15**, 204–209 (2008).

100. Chudzik, K. Final report " Generation of induced pluripotent stem cells from fibroblast cell lines and gene editing in pluripotent stem cell " By.

101. Tomasek, J. J. *et al.* Myofibroblasts and mechano: Regulation of connective tissue remodelling. *Nature Reviews Molecular Cell Biology* **3**, 349–363 (2002).

102. Parsonage, G. *et al.* Europe PMC Funders Group Europe PMC Funders Author Manuscripts A stromal address code defined by fibroblasts. **26**,

150–156 (2011).

103. Chang, H. Y. *et al.* Diversity, topographic differentiation, and positional memory in human fibroblasts. *Proceedings of the National Academy of Sciences* **99**, 12877–12882 (2002).

104. Simian, M. *et al.* The interplay of matrix metalloproteinases, morphogens and growth factors is necessary for branching of mammary epithelial cells. *Development (Cambridge, England)* **128**, 3117–3131 (2001).

105. Villaschi, S. *et al.* Paracrine interactions between fibroblasts and endothelial cells in a serum-free coculture model. Modulation of angiogenesis and collagen gel contraction. *Laboratory Investigation; a Journal of Technical Methods and Pathology* (1994).

106. Berthod, F. *et al.* Extracellular matrix deposition by fibroblasts is necessary to promote capillary-like tube formation in vitro. *Journal of Cellular Physiology* **207**, 491–498 (2006).

107. Costa-Almeida, R. *et al.* Fibroblast-Endothelial Partners for Vascularization Strategies in Tissue Engineering. *Tissue Engineering Part A* **21**, 1055–1065 (2015).

108. Sorrell, J. M. *et al.* Human dermal fibroblast subpopulations; Differential interactions with vascular endothelial cells in coculture: Nonsoluble factors in the extracellular matrix influence interactions. *Wound Repair and Regeneration* (2008).

109. Newman, A. C. *et al.* The requirement for fibroblasts in angiogenesis: fibroblast-derived matrix proteins are essential for endothelial cell lumen formation. *Molecular Biology of the Cell* **22**, 3791–3800 (2011).

110. Nakatsu, M. N. *et al.* Angiogenic sprouting and capillary lumen formation modeled by human umbilical vein endothelial cells (HUVEC) in fibrin

gels: The role of fibroblasts and Angiopoietin-1. *Microvascular Research* **66**, 102–112 (2003).

111. Kunz-Schughart, L. A. *et al.* Potential of fibroblasts to regulate the formation of three-dimensional vessel-like structures from endothelial cells in vitro. *American Journal of Physiology-Cell Physiology* **290**, C1385–C1398 (2006).

112. Hurley, J. R. *et al.* Complex temporal regulation of capillary morphogenesis by fibroblasts. *AJP: Cell Physiology* **299**, C444–C453 (2010).

113. Burbridge, M. F. *et al.* The role of the matrix metalloproteinases during in vitro vessel formation. *Angiogenesis* **5**, 215–26 (2002).

114. Spinale, F. G. MMP: Influence on Cardiac Form and Function. *Physiological reviews* **87**, 1285–1342 (2007).

115. Sewell-Loftin, M. K. *et al.* Cancer-associated fibroblasts support vascular growth through mechanical force. *Scientific Reports* **7**, 1–12 (2017).

116. Martino, F. *et al.* Cellular mechanotransduction: From tension to function. *Frontiers in Physiology* **9**, 1–21 (2018).

117. Lessey, E. C. *et al.* From mechanical force to RhoA activation. *Biochemistry* **51**, 7420–7432 (2012).

118. Shih, Y. R. V. *et al.* Matrix stiffness regulation of integrin-mediated mechanotransduction during osteogenic differentiation of human mesenchymal stem cells. *Journal of Bone and Mineral Research* **26**, 730–738 (2011).

119. Rizzo, M. T. Focal adhesion kinase and angiogenesis. Where do we go from here? *Cardiovascular Research* **64**, 377–378 (2004).

120. Wang, H. B. *et al.* Focal adhesion kinase is involved in mechanosensing during fibroblast migration. *Proceedings of the National Academy of Sciences of the United States of America* **98**, 11295–11300 (2001).

121. Ilić, D. *et al.* Reduced cell motility and enhanced focal adhesion contact formation in cells from FAK-deficient mice. *Nature* **377**, 539–544 (1995).

122. Mitra, S. K. *et al.* Intrinsic FAK activity and Y925 phosphorylation facilitate an angiogenic switch in tumors. *Oncogene* **25**, 5969–5984 (2006).

123. Mitra, S. *et al.* Focal adhesion kinase (FAK) activity promotes tumor growth and neo-vascularization via upregulation of angiogenic factors. *Cancer Research* **65**, 475 LP – 475 (2005).

124. Dudek, S. M. *et al.* Cytoskeletal regulation of pulmonary vascular permeability. *Journal of Applied Physiology* vol. 91 (2001).

125. Terry, S. J. *et al.* Spatially restricted activation of RhoA signalling at epithelial junctions by p114RhoGEF drives junction formation and morphogenesis. *Nature Cell Biology* **13**, 159–166 (2011).

126. Uchida, S. *et al.* The suppression of small GTPase Rho signal transduction pathway inhibits angiogenesis in vitro and in vivo. *Biochemical and Biophysical Research Communications* **269**, 633–640 (2000).

127. Hashimoto, K. *et al.* Alendronate suppresses tumor angiogenesis by inhibiting Rho activation of endothelial cells. *Biochemical and Biophysical Research Communications* **354**, 478–484 (2007).

128. Tang, Z. *et al.* A brief review: Some compounds targeting YAP against malignancies. *Future Oncology* **15**, 1535–1543 (2019).

129. Codelia, V. A. *et al.* Hippo signaling goes long range. *Cell* **150**, 669–670

(2012).

130. Wang, X. *et al.* YAP/TAZ Orchestrate VEGF Signaling during Developmental Angiogenesis. *Developmental Cell* **42**, 462-478.e7 (2017).

131. Chang, Y. C. *et al.* Hippo Signaling-Mediated Mechanotransduction in Cell Movement and Cancer Metastasis. *Frontiers in Molecular Biosciences* **6**, 1–7 (2020).

132. Dupont, S. Role of YAP/TAZ in cell-matrix adhesion-mediated signalling and mechanotransduction. *Experimental Cell Research* **343**, 42–53 (2016).

133. Dupont, S. *et al.* Role of YAP/TAZ in mechanotransduction. *Nature* **474**, 179–184 (2011).

134. Abuammah, A. *et al.* New developments in mechanotransduction: Cross talk of the Wnt, TGF-β and Notch signalling pathways in reaction to shear stress. *Current Opinion in Biomedical Engineering* **5**, 96–104 (2018).

135. Drenser, K. A. Wnt signaling pathway in retinal vascularization. *Eye and Brain* **8**, 141–146 (2016).

136. Reis, M. *et al.* Wnt signaling in the vasculature. *Experimental Cell Research* **319**, 1317–1323 (2013).

137. Cha, B. *et al.* Mechanotransduction activates canonical Wnt/β-catenin signaling to promote lymphatic vascular patterning and the development of lymphatic and lymphovenous valves. *Genes and Development* **30**, 1454–1469 (2016).

138. Kim, L. C. *et al.* Src kinases as therapeutic targets for cancer. *Nature Reviews Clinical Oncology* **6**, 587–595 (2009).

139. Mukhopadhyay, D. *et al.* Hypoxic induction of human vascular endothelial growth factor expression through c-Src activation. *Nature* **375**, 577–581 (1995).

140. Eliceiri, B. P. *et al.* Selective requirement for Src kinases during VEGF-induced angiogenesis and vascular permeability. *Molecular Cell* **4**, 915–924 (1999).

141. Pyun, B. J. *et al.* Capsiate, a nonpungent capsaicin-like compound, inhibits angiogenesis and vascular permeability via a direct inhibition of Src kinase activity. *Cancer Research* **68**, 227–235 (2008).

142. Matsui, H. *et al.* Src, p130Cas, and Mechanotransduction in Cancer Cells. *Genes and Cancer* **3**, 394–401 (2012).

143. Wang, Y. *et al.* Visualizing the mechanical activation of Src. *Nature* **434**, 1040–1045 (2005).

144. Boutahar, N. *et al.* Mechanical strain on osteoblasts activates autophosphorylation of focal adhesion kinase and proline-rich tyrosine kinase 2 tyrosine sites involved in ERK activation. *Journal of Biological Chemistry* **279**, 30588–30599 (2004).

145. Shimizu, T. *et al.* Dual inhibition of Src and GSK3 maintains mouse embryonic stem cells, whose differentiation is mechanically regulated by Src signaling. *Stem Cells* **30**, 1394–1404 (2012).

146. Akhtar, N. *et al.* The sponge / Matrigel angiogenesis assay. *Angiogenesis* 75–80 (2002).

147. Folkman, J. Tumor angiogenesis: A possible control point in tumor growth. *Annals of Internal Medicine* (1975).

148. Muthukkaruppan, V. R. *et al.* Tumor-induced neovascularization in the mouse eye. *Journal of the National Cancer Institute* **69**, 699–708 (1982).

149. Bogorad, M. I. *et al.* Review: In vitro microvessel models. *Lab on a Chip* **15**, 4242–4255 (2015).

150. Boussommier-Calleja, A. *et al.* Microfluidics: A New Tool for Modeling Cancer–Immune Interactions. *Trends in Cancer* **2**, 6–19 (2016).

151. Hsu, Y. H. *et al.* A microfluidic platform for generating large-scale nearly identical human microphysiological vascularized tissue arrays. *Lab on a Chip* **13**, 2990–2998 (2013).

152. Whisler, J. A. Engineered , Functional , Human Microvasculature in a Perfusable Fluidic Device by Doctor of Philosophy in Mechanical Engineering. (2017).

153. Mosesson, M. W. *et al.* The structure and biological features of fibrinogen and fibrin. *Annals of the New York Academy of Sciences* **936**, 11–30 (2001).

154. Ahmed, T. A. E. *et al.* Fibrin: A versatile scaffold for tissue engineering applications. *Tissue Engineering - Part B: Reviews* **14**, 199–215 (2008).

155. Nagy, J. A. *et al.* Vascular permeability, vascular hyperpermeability and angiogenesis. *Angiogenesis* **11**, 109–119 (2008).

156. Goncharov, N. V. *et al.* Markers and Biomarkers of Endothelium: When Something Is Rotten in the State. *Oxidative Medicine and Cellular Longevity* **2017**, (2017).

157. Lertkiatmongkol, P. *et al.* Endothelial functions of PECAM-1 (CD31). *Current opinion in hematology* **23**, 253–259 (2016).

158. Edgar, L. T. *et al.* Mechanical Interaction of Angiogenic Microvessels With the Extracellular Matrix. *Journal of Biomechanical Engineering* **136**, (2014).

159. Scott, R. A. *et al.* Regulation of neovasculogenesis in co-cultures of

aortic adventitial fibroblasts and microvascular endothelial cells by cell-cell interactions and TGF-β/ALK5 signaling. *Plos One* **15**, e0244243 (2020).

160. Evensen, L. *et al.* Mural cell associated VEGF is required for organotypic vessel formation. *PLoS ONE* **4**, (2009).

161. Kim, S. *et al.* Engineering of functional, perfusable 3D microvascular networks on a chip. *Lab on a Chip* **13**, 1489–1500 (2013).

162. Whisler, J. A. *et al.* Control of perfusable microvascular network morphology using a multiculture microfluidic system. *Tissue Engineering - Part C: Methods* **20**, 543–552 (2014).

163. Boussommier-Calleja, A. *et al.* The effects of monocytes on tumor cell extravasation in a 3D vascularized microfluidic model. *Biomaterials* **198**, 180–193 (2019).

164. Haase, K. *et al.* Pericytes Contribute to Dysfunction in a Human 3D Model of Placental Microvasculature through VEGF-Ang-Tie2 Signaling. *Advanced Science* **6**, (2019).

165. Moya, M. L. *et al.* In vitro perfused human capillary networks. *Tissue Engineering - Part C: Methods* **19**, 730–737 (2013).

166. Wang, X. *et al.* Engineering anastomosis between living capillary networks and endothelial cell-lined microfluidic channels. *Lab on a Chip* **16**, 282–290 (2016).

167. Phan, D. T. T. *et al.* A vascularized and perfused organ-on-a-chip platform for large-scale drug screening applications. *Lab on a Chip* **17**, 511–520 (2017).

168. Lee, S. W. L. *et al.* Modeling Nanocarrier Transport across a 3D In Vitro Human Blood-Brain–Barrier Microvasculature. *Advanced Healthcare*

Materials **9**, (2020).

169. Yuan, W. *et al.* Non-invasive measurement of solute permeability in cerebral microvessels of the rat. *Microvascular Research* **77**, 166–173 (2009).

170. Chen, X. *et al.* Rapid anastomosis of endothelial progenitor cell-derived vessels with host vasculature is promoted by a high density of cotransplanted fibroblasts. *Tissue Engineering - Part A* **16**, 585–594 (2010).

171. Chen, T. H. *et al.* Developmental exposures to ethanol or dimethylsulfoxide at low concentrations alter locomotor activity in larval zebrafish: Implications for behavioral toxicity bioassays. *Aquatic Toxicology* **102**, 162–166 (2011).

172. Galvao, J. *et al.* Unexpected low-dose toxicity of the universal solvent DMSO. *FASEB Journal* **28**, 1317–1330 (2014).

173. Trivedi, A. Ben *et al.* Toxicity of Dimethyl Sulfoxide as a Solvent in Bioassay System with HeLa Cells Evaluated Colorimetrically with 3-(4,5-Dimethyl thiazol-2-yl)-2,5-diphenyl-tetrazolium Bromide. *Agricultural and Biological Chemistry* **54**, 2961–2966 (1990).

174. Liu-Chittenden, Y. *et al.* Genetic and pharmacological disruption of the TEAD-YAP complex suppresses the oncogenic activity of YAP. *Genes and Development* **26**, 1300–1305 (2012).

175. Dong, L. *et al.* Verteporfin inhibits YAP-induced bladder cancer cell growth and invasion via hippo signaling pathway. *International Journal of Medical Sciences* **15**, 645–652 (2018).

176. Stakheev, D. *et al.* The WNT/β-catenin signaling inhibitor XAV939 enhances the elimination of LNCaP and PC-3 prostate cancer cells by prostate cancer patient lymphocytes in vitro. *Scientific Reports* **9**, 1–14

(2019).

177. Guo, W. *et al.* Wnt inhibitor XAV939 suppresses the viability of small cell lung cancer NCI-H446 cells and induces apoptosis. *Oncology Letters* **14**, 6585–6591 (2017).

178. Li, C. *et al.* XAV939 inhibits the proliferation and migration of lung adenocarcinoma A549 cells through the WNT pathway. *Oncology Letters* **15**, 8973–8982 (2018).

179. Kanteti, R. *et al.* Focal adhesion kinase a potential therapeutic target for pancreatic cancer and malignant pleural mesothelioma. *Cancer Biology and Therapy* **19**, 316–327 (2018).

180. Slack-Davis, J. K. *et al.* Cellular characterization of a novel focal adhesion kinase inhibitor. *Journal of Biological Chemistry* **282**, 14845–14852 (2007).

181. Evelyn, C. R. *et al.* CCG-1423: A small-molecule inhibitor of RhoA transcriptional signaling. *Molecular Cancer Therapeutics* **6**, 2249–2260 (2007).

182. Kikuchi, K. *et al.* Rho signaling inhibitor, CCG-1423, inhibits axonal elongation and dendritic complexity of rat cortical neurons. *Biochemical and Biophysical Research Communications* **492**, 474–479 (2017).

183. Barravecchia, I. *et al.* MICAL2 is expressed in cancer associated neo-angiogenic capillary endothelia and it is required for endothelial cell viability, motility and VEGF response. *Biochimica et Biophysica Acta - Molecular Basis of Disease* **1865**, 2111–2124 (2019).

184. Hanke, J. H. *et al.* Discovery of a novel, potent, and Src family-selective tyrosine kinase inhibitor: Study of Lck- and FynT-dependent T cell activation. *Journal of Biological Chemistry* **271**, 695–701 (1996).

185. Kong, L. *et al.* Src family kinase inhibitor PP2 efficiently inhibits cervical cancer cell proliferation through down-regulating phospho-Src-Y416 and phospho-EGFR-Y1173. *Molecular and Cellular Biochemistry* **348**, 11–19 (2011).

186. Kwak, A. W. *et al.* Picropodophyllotoxin, an epimer of podophyllotoxin, causes apoptosis of human esophageal squamous cell carcinoma cells through ROS-mediated JNK/P38 MAPK pathways. *International Journal of Molecular Sciences* **21**, 1–13 (2020).

187. Inman, G. J. *et al.* SB-431542 is a potent and specific inhibitor of transforming growth factor-β superfamily type I activin receptor-like kinase (ALK) receptors ALK4, ALK5, and ALK7. *Molecular Pharmacology* **62**, 65–74 (2002).

188. Hjelmeland, M. D. *et al.* SB-431542, a small molecule transforming growth factor-β-receptor antagonist, inhibits human glioma cell line proliferation and motility. *Molecular Cancer Therapeutics* **3**, 737–745 (2004).

189. Kallenberg, D. *et al.* A Humanized Antibody against LRG1 that Inhibits Angiogenesis and Reduces Retinal Vascular Leakage. (2020).

190. Huang, D. *et al.* Binding Modes of Small-Molecule Inhibitors to the EED Pocket of PRC2. *ChemPhysChem* **21**, 263–271 (2020).

191. He, Y. *et al.* The EED protein-protein interaction inhibitor A-395 inactivates the PRC2 complex. *Nature Chemical Biology* **13**, 389–395 (2017).

192. Van Nieuw Amerongen, G. P. *et al.* Involvement of RhoA/Rho kinase signaling in VEGF-induced endothelial cell migration and angiogenesis in vitro. *Arteriosclerosis, Thrombosis, and Vascular Biology* **23**, 211–217 (2003).

193. Hoang, M. V. *et al.* Rho activity critically and selectively regulates endothelial cell organization during angiogenesis. *Proceedings of the National Academy of Sciences of the United States of America* **101**, 1874–1879 (2004).

194. Kim, J. *et al.* YAP/TAZ regulates sprouting angiogenesis and vascular barrier maturation. *Journal of Clinical Investigation* **127**, 3441–3461 (2017).

195. Zhu, M. *et al.* YAP via interacting with STAT3 regulates VEGF-induced angiogenesis in human retinal microvascular endothelial cells. *Experimental Cell Research* **373**, 155–163 (2018).

196. Tavora, B. *et al.* Endothelial FAK is required for tumour angiogenesis. *EMBO Molecular Medicine* **2**, 516–528 (2010).

197. Cabrita, M. A. *et al.* Focal adhesion kinase inhibitors are potent anti-angiogenic agents. *Molecular Oncology* **5**, 517–526 (2011).

198. Hu, J. *et al.* Blockade of Wnt signaling inhibits angiogenesis and tumor growth in hepatocellular carcinoma. *Cancer Research* **69**, 6951–6959 (2009).

199. Stenman, J. M. *et al.* Canonical Wnt Signaling Regulates Organ-Specific Assembly and Differentiation of CNS Vasculature. *Science* **322**, 1247 LP – 1250 (2008).

200. Bid, H. K. *et al.* Potent inhibition of angiogenesis by the IGF-1 receptor-targeting antibody SCH717454 is reversed by IGF-2. *Molecular Cancer Therapeutics* **11**, 649–659 (2012).

201. Shigematsu, S. *et al.* IGF-1 regulates migration and angiogenesis of human endothelial cells. *Endocrine Journal* **46**, 59–62 (1999).

202. Darland, D. C. *et al.* TGFβ is required for the formation of capillary-like

structures in three-dimensional cocultures of 10T1/2 and endothelial cells. *Angiogenesis* **4**, 11–20 (2001).

203. Gautier, H. O. B. *et al.* Chapter 12 – Atomic force microscopy-based force measurements on animal cells and tissues. *Methods in Cell Biology* **125**, 211–235 (2015).

204. Lin, D. C. *et al.* Robust Strategies for Automated AFM Force Curve Analysis—I. Non-adhesive Indentation of Soft, Inhomogeneous Materials. *Journal of Biomechanical Engineering* **129**, 430 (2007).

205. Radmacher, M. Studying the Mechanics of Cellular Processes by Atomic Force Microscopy. *Methods in Cell Biology* **83**, 347–372 (2007).

206. Rheinlaender, J. *et al.* Cortical cell stiffness is independent of substrate mechanics. *Nature Materials* **19**, 1019–1025 (2020).

207. Moeendarbary, E. *et al.* The soft mechanical signature of glial scars in the central nervous system. *Nature Communications* **8**, 14787 (2017).

208. Chen, W. *et al.* Fibroblasts in post-infarction inflammation and cardiac repair. *Biochimica et Biophysica Acta - Molecular Cell Research* **1833**, 945–953 (2013).

209. Frye, M. *et al.* Matrix stiffness controls lymphatic vessel formation through regulation of a GATA2-dependent transcriptional program. *Nature Communications* **9**, 1–16 (2018).

210. Edgar, L. T. *et al.* Extracellular matrix density regulates the rate of neovessel growth and branching in sprouting angiogenesis. *PLoS ONE* **9**, 1–10 (2014).

211. Karki, P. *et al.* Substrate stiffness-dependent exacerbation of endothelial permeability and inflammation: mechanisms and potential implications in ALI and PH (2017 Grover Conference Series). *Pulmonary Circulation*

8, (2018).

212. Urbano, R. L. *et al.* Stiff Substrates Increase Inflammation-Induced Endothelial Monolayer Tension and Permeability. *Biophysical Journal* **113**, 645–655 (2017).

213. Bielenberg, D. R. *et al.* The Contribution of Angiogenesis to the Process of Metastasis. *Cancer Journal (United States)* **21**, 267–273 (2015).

214. Liang, W. *et al.* The complex role of Neutrophils in tumor angiogenesis and metastasis. *Cancer Immunology Research* **4**, 83–91 (2016).

215. Takebe, N. *et al.* Review of Cancer – Associated Fibroblasts and Therapies that Interfere with Their Activity. *Tumor Microenvironment and Therapy* **1**, 19–36 (2013).